DEVELOPMENT OF NIOBIUM-BORON GRAIN REFINER FOR ALUMINIUM-SILICON ALLOYS

A thesis submitted for the degree of Doctor of Philosophy (PhD)

by

Magdalena Nowak

Brunel Centre for Advanced Solidification Technology

(BCAST)

Brunel University

September 2011

To my mother and my late father...

Abstract

Aluminium castings with a large grain structure have poor mechanical properties which are primarily due to casting defects as opposed to fine grain structure. The grain refinement practice using chemical addition is well established for wrought alloys, however in the case of casting alloys, the practice of adding grain refiners and the impact on castability is not well established. The addition of well known Al-5Ti-B grain refiner to casting alloys with silicon (Si) content above 3 wt.% is not effective. This is believed to be due to the chemical reaction between Ti and Si. The current research aim is to find an alternative, but effective, chemical phase which can refine Al-Si alloy grains. Based on a crystallographic database search and intermetallic phases found in Aluminium–Niobium-Boron, there exists several iso-structural phases similar to those of Al_3Ti and TiB_2. We have selected a phase which exhibits chemical phase stability with Si (below 900 ^oC) and developed a potential novel grain refiner Nb-B for Al-Si cast alloys. Various Al-Si binary alloys and a commercial sourced LM6 (Al-10Si-Mg) cast alloys were cast after novel grain refiner addition to the melt. It is the first time that such fine grain structures were achieved for Al-Si alloys when Si >4wt.%. It is believed that Nb-B grain refiner enhances the heterogeneous nuclei in the melt. The effectiveness of this grain refiner under various cooling rate conditions is investigated to simulate various practical casting conditions. Due to increased heterogeneous nuclei density, a fine grain structure is also obtained at low cooling rates and the grain size is less sensitive to the cooling rate. The processing of high Si containing alloys for complex shaped castings with reduced defects, fine grain structure and improved mechanical properties are now possible.

Acknowledgment

It is a pleasure to thank those who made this thesis possible. I am thankful to my supervisor, Dr Hari Babu Nadendla, whose encouragement, guidance and support from the initial to the final level enabled me to develop an understanding of the subject for this thesis. He has been everything that one could want in an advisor.

I would like to thanks Isambard Research Scholarships for the financial support of my three years research and I would like to thank Prof. Z.Fan for providing casting facilities.

I which to thank Mr. A.R. Dennis from the Bulk Superconductivity Group at Cambridge University for measurements of the magnetic moment, Dr W. Kong from University of Sydney, for the TEM; also I would like to thank Dr K. Sundaram from Oxford University for SEM.

I am grateful to all my family specially my mother Bozena Nowak for her unending love and support. I am also very grateful to my brother Damian Nowak for encouragement. I would like to acknowledge my late father Slawomir Nowak for whom this PhD was completed.

I would like, also, to thank my boyfriend Adam Coventry for support over this last three years and help in reviewing this thesis.

I would like, also, to thank my friends, inside and outside of the studies who have been a constant source of intellectual generosity, personal support and leisurely relief.

I thank the members of BCAST for providing an intellectually and socially stimulating and well-organized environment.

Contents

Abbreviations

BCAST	Brunel Centre for Advanced Solidification Technology
bcc	Body-centered cubic
BF	Bright Field
CP	Commercial-purity
EDX	Energy Dispresive X-ray Spectrometer
fcc	Face-centered cubic
hcp	Hexagonal close-packed
HPDC	High Pressure Die Casting
HRTEM	High Resolution Transmission Electron Microscopy
NGR	Novel Grain Refiner
OM	Optical Microscope
PP	Plane Polarized Light
SEM	Scanning Electron Microscopy
SP	Super-purity
TEM	The transmission electron microscope
TP-1	Aluminium Association Test Procedure -1
UTS	Ultimate Tensile Strength
VH	Vickers Hardness
ZAF	Matrix Correction:
	Z - Element Number, A – Absorption, F- Secondary Fluorescence
BS	British Standards

List of symbols

A	Area of the sphere
a	Crystal unite cell lattice parameter
A_{ML}	Solid/mould interfacial area
A_{SL}	Solid /Liquid interfacial area
C	Composition of the liquid
c	Crystal unite cell lattice parameter
C_o	Initial composition
G_L^V	Free energy per unit volume of liquid
G_v^S	Free energy per unit volume of solid
K	Thermal conductivity
L_v	Latent heat of fusion per unit volume
m	Slop of the liquidus line
N_v^G	Number of grains per unit volume
N_v^P	Number of particles per unit volume
r^*	Critical radius for heterogeneous nucleation
$\dot{T}$	Temperature gradient
T_i	Interface temperature
T_L	Liquidus temperature
T_m	Melting temperature
T_{nucl}	Nucleation temperature
V	Volume of sphere
V_L	Volume of Liquid

V_s	Volume of solid sphere
γ_{ML}	Liquid-substrate interface
γ_{SL}	Solid-liquid interface
γ_{SM}	Crystal-substrate interface
ΔG_{het}	Heterogeneous nucleation
ΔG^{*}_{hom}	Homogeneous nucleation
ΔG_v	Volume free energy
ΔT	Undercooling

List of Figures

List of Tables

Chapter 1. Introduction

The production of aluminium alloys represents a significant proportion in worldwide light metal manufacturing. They have low density (2.7 gcm^{-3}) which is advantageous in many applications due to a high stiffness to weight ratio. As a result, aluminium is used in a variety of industries from food packaging to car manufacture. It is the most common metal and the third most abundant element on earth, comprising more than 8 percent of the earth's crust. Although aluminium is an extremely common and widespread element, the common aluminium minerals are not economic sources of the metal. Almost all metallic aluminium is produced from the bauxite ($AlO_x(OH)_{3-2x}$) ore. It was first isolated in 1825 by Örsted and its extraction from bauxite further developed resulting in the Hall-Héroult process. Since that time production has grown and Al is the second most used metal in the world after steel. Today the Al industry is well developed, however the demand from automotive industry for light metals is growing. The process improvement of aluminium alloys and their grain refinement is in the interest of foundries and casting companies. The aluminium alloys are divided into wrought alloys and casting alloys, the main difference between them is that wrought alloys need to be further processed after casting while casting alloys are cast to the desirable shape. Wrought alloys contain less than 10% of alloying elements whereas cast alloys can have up to 30%.

Metals and alloys usually solidify with coarse columnar grain structures under normal casting conditions unless the mode of solidification is carefully controlled. Over the centuries grain refinement through chemical additions has been an important technique for improving the properties of aluminium products. Castings with large grains have poor castability and mechanical properties compared to those with fine equiaxed grains. The commonly used grain refiner for aluminium alloys is 94wt%Al-5wt%Ti-1wt%B (Al-5Ti-B). Mechanisms for grain refinement during solidification of liquid Al melt are described in Chapter 2. The Al-5Ti-B master alloy development and its use as grain refiner is well established and the research has been intensively carried out for the last 50 years. Nevertheless there are chemicals that have similar structure and chemical properties to titanium and are in the same chemical elements

group, including molybdenum, niobium, tungsten and tantalum. However there is not much research carried out on their influence on aluminium alloys.

The aim of this thesis was to develop a new, but ***highly effective***, grain refiner for aluminium alloys. Chapter 4 describes the development of a novel grain refiner based on the current understanding of the Al-5Ti-B grain refiner alloy. The comparison of phase diagrams was the first step of the work. The Nb_3Al, $TaAl_3$, $MoAl_{12}$ and WAl_{12} have similar lattice parameters to the well known nucleation site of Al_3Ti. To assess the influence of Mo, Nb, W and Ta on grain refinement of aluminium, a series of experiments were carried out on pure Al. The process development for this new grain refiner is described in Chapter 5. The most commonly used second phase particles for grain refinement are Al_3Ti and TiB_2, which are intermetallic compounds in the Al-5Ti-B master alloy. Our research investigates the influence on grain refinement of different borides like NbB_2 and TaB_2, and the experiments show that Nb-B is a good grain refiner in pure aluminium. Chapter 4 describes the influence of the Nb-B addition to the pure aluminium and the results are compared with Al-Ti-B addition. Furthermore the research was concentrated on its applicability to Al-Si alloys. Aluminium-Silicon alloys are widely used as shape castings in automotive, rail, ship and construction engineering sectors. These alloys are easy to cast, have higher fluidity, low density and controllable mechanical properties. However, one of the *major problems associated with casting of aluminium-silicon alloys is large grain structure*. It is well established that Al-Ti-B does not work as a grain refiner for Al-Si alloy when the silicon addition is over 3%. At this concentration level of Si, the titanium is consumed by silicon and forms titanium silicides. There is a large interaction between titanium and silicon in both the liquid and α-Al. The strong interaction favours the formation of silicon and titanium containing phases TiSi and $TiSi_2$. Considering that most Al-Si casting alloys used in the transport industry contain 50-90 vol% of eutectic, and also that the eutectic reaction is the last major transformation during cooling, it is not unexpected that eutectic has a significant effect on mechanical properties. The addition of strontium to Al-Si alloys reduces the eutectic and changes its morphology. However, it is well known that modification with strontium is very difficult when the melt is solidified under slow cooling conditions (<3 ^{O}C/s). Addition of phosphorus is known to refine the primary Si particle size and morphology, but the refinement of primary Al phase remains a scientific challenge, to date. In Chapter 5, we describe the development of highly effective Nb-B grain refiner for Al-

Si alloys and show that Nb-B refines the primary Al phase, the primary Si phase and also promotes refinement of Si eutectic phase at wide range of cooling rates. Addition of phosphorous to the hypereutectic Al-Si alloys can refine the primary silicon particles at the expense of reducing fluidity. However, when Sr is added as an eutectic Si modifier, the refinement of primary Si is somewhat inhibited due to the neutralization of aluminum phosphate. The results shown in Chapter 5 are ***extraordinary.*** The microstructure analysis of Al-Si alloys with Si >4 wt% shows that Nb-B is highly effective in refining α-Al and decreasing eutectic Si. Chapter 5 describes the Nb-B influence on the grain sizes in binary Al-Si alloys from 1-10wt% of Si in comparison with Al-Si without any addition and with commercially used Al-5Ti-B.

The commercial Al-Si alloys have many other chemical additions like magnesium, manganese, cooper and nickel to improve the mechanical properties. We have investigated if the Nb-B novel grain refiner is chemically stable with the alloying elements. Chapter 5 describes the Nb-B addition to commercially used Al-Si alloys like LM6, LM13, LM25 and LM24. The investigation was carried out in Chapter 6 to check the influence of boron on the alloys and compared with the addition of Nb-B. Various moulds were used to achieve different cooling rates and thickness of the cast samples. The High Pressure Die Casting (HPDC) and gravity castings tensile samples were produced to test the mechanical properties of LM25 and LM6. The refined eutectic and grain sizes of α-Al are *observed to improve ultimate tensile strength and elongation by up to 30*%. This chapter explains the advantages of the Nb-B addition to commercial alloys. For practical applications, it is important to optimize the addition process to achieve the most effective grain refinement, e.g. finding the contact time with the highest grain refinement efficiency (critical contact time). If the contact time is too short, the finest grain size may not be achieved. On the other hand, if the contact time is too long, effectiveness of the grain refiner will be lowered. This lower effectiveness at excessive contact time is commonly referred to as fading. The experiments in Chapter 7 show that by gently stirring the melt prior to casting, the grain sizes are smaller even when the contact time is ~ 4 h. The results on fading studies proved that Nb-B has a slower dissolution rate than Al-Ti-B master alloy and we show that Nb-B can be used in process of castings with long holding times as well. In foundries and process industries, large amounts of scrap are generated and are commonly referred to as process scrap. Every time the process scrap is

recycled, it is a common process to add the Ti-B grain refiner. This results in unwanted TiB_2 inclusions and after several times of recycling, the composition of the alloy significantly deviates from the alloy specification. Hence, it is desirable to have a grain refiner that can retain its grain refinement characteristics even after several melt cycles. The recycling analysis was conducted for LM6 with the addition of Nb-B. The results show that the Al-Si alloys containing Nb-B can be recycled with the finest grain structure of up to two recycles, without needing to add Nb-B phase.

On an industry scale, when handling tons of liquid metal, it is not practical to add powder to the melt because these intermetallic particles are highly non-wettable with liquid melt. To overcome this problem, a master alloy containing the inoculant (seed) particles, is added to the liquid melt. When the master alloy dissolves into the melt, inoculant particles will be dispersed throughout the melt. Conventional Ti-B based grain refiner is an alloy with the composition of 94 wt% Al-5 wt% Ti- 1wt% B. This alloy is commonly referred as grain refiner alloy or grain refiner master alloys. We have also developed a process to produce master alloy of Al-Nb-B. Chapter 7 describes different attempts for manufacturing of the master alloy. The TEM and SEM analyses were conducted to investigate the potential nucleation sites that are responsible for the observed grain refinement. The influence of master alloy addition to aluminium and Al-Si alloys was also investigated.

The work presented in this thesis will be a step change for the Al cast industry. This grain refiner will enable the aluminium industry to produce lighter castings with less defects and more strength. As a result, this grain refiner will enable automotive industry to use much lighter structures. In addition, due to fine and uniform grain structure at wide cooling rates, high performance complicated shape castings can be produced. This is a major development in the history of Al-Si casting.

In summary, the thesis describes the development of Nb-B based effective grain refiner for Al-Si cast alloys. We show that the addition of Nb-B results in decreased undercooling and enhanced heterogeneous nuclei in the melt. We provide TEM evidence for coherent interface between the Al-phase and the Nb based inoculant phase. With this grain refiner, *for the first time*, Al-Si castings with fine, uniform cast structures with significantly improved strength and ductility have been produced.

Chapter 2. Literature Review

2.1 Introduction

In this chapter classical nucleation theory, proposed nucleation theories for Al-Ti-B grain refiner and solidification process are reviewed. Aluminium alloys classification and casting process for Al-Si cast alloys are also reviewed.

2.2 Solidification of Aluminium Alloys

Solidification is the transformation between liquid and solid states. It may be described as the nucleation and growth process. Nucleation is a formation of a new phase in a distinct region separated from the surroundings by a discrete boundary. During solidification, solid nuclei form in the liquid and subsequently grow until the whole of the volume is solid.

2.2.1 Classical Nucleation Theory

2.2.1.1. Homogeneous Nucleation

The classical theory of nucleation was developed by Volmer and Weber (Volmer M. and Weber A. 1926) and Becker and Döring (Becker R. 1935) for the condensation of a super saturated liquid. The subsequent theory of Turnbull, Fisher (Turnbull D. and Fisher J.C., 1948) and Hollman (Hollman J.H. 1953), for the liquid solid transformation was based on this earlier work. The theory is based on the free energy changes from liquid to solid. The maximum free energy change (or activation energy) for homogeneous nucleation to occur (ΔG^*_{hom}) may be expressed as,

$$\Delta G^*_{hom} = -V\Delta G_V + A\gamma_{SL} \quad \textbf{(2. 1)}$$

where V is the volume of a sphere, ΔG_v is the volume free energy, A is the area of a sphere and γ_{SL} is the surface free energy (Porter D.A. 1981)

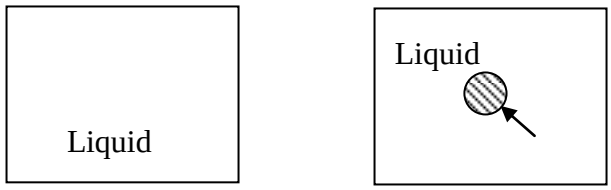

G_1 $G_2 = G_1 + \Delta G$

Figure 2.1 The graphic interpretation of free energy in homogeneous and heterogeneous system.

When the atoms of the liquid cluster gather together to form a small solid sphere (Figure 2.1) the free energy of the system will change to G_2.

$$G_2 = V_S G_V^S + V_L G_V^L + A_{SL}\gamma_{SL} \quad \textbf{(2. 2)}$$

Where V_S is the volume of the solid sphere, V_L the volume of liquid, A_{SL} is the solid/liquid interfacial area; $G^S{}_V$ and $G^L{}_V$ are the free energies per unit volume of solid and liquid respectively, and γ_{SL} the solid/liquid interfacial free energy. The free energy of system without any foreign particle present is given by:

$$G_1 = (V_S + V_L)G_V^L \quad \textbf{(2. 3)}$$

The formation of solid therefore results in a free energy change $\Delta G = G_2 - G_1$ where:

$$\Delta G = -V_S \Delta G_V + A_{SL}\gamma_{SL} \quad \textbf{(2. 4)}$$

and

$$\Delta G_V = G_V^L - G_V^S \quad \textbf{(2. 5)}$$

For an undercooling ΔT, ΔG_v is given by:

$$\Delta G_V = \frac{L_V \Delta T}{T_m} \quad \textbf{(2. 6)}$$

Where L_V is the latent heat of fusion per unit volume. Below T_m, ΔG_v is positive so that the free energy change associated with the formation of a small volume of solid has a negative contribution due to the lower free energy of bulk solid, but there is also a positive contribution due to the creation of a solid/liquid interface.

The excess free energy associated with the solid particle can be minimized by the correct choice of particle shape. The free energy ΔG is the difference between the interfacial energy γ_{SL} and volume free energy V_s, see Figure 2.2.

$$\Delta G = -\frac{4}{3}\pi r^3 \Delta G_V + 4\pi r^2 \gamma_{SL} \qquad \textbf{(2. 7)}$$

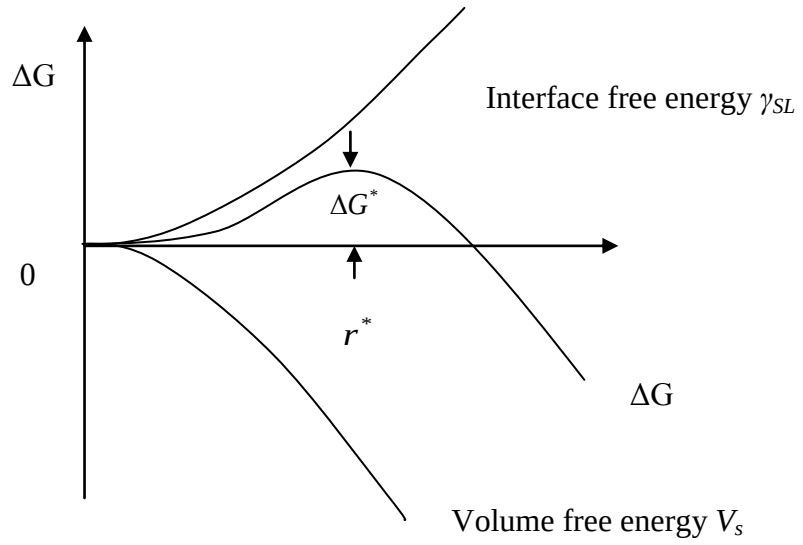

Figure 2.2 The free energy change associated with homogeneous nucleation of a sphere of radius *r*

Any embryos which form above T_m (melting temperature) will rapidly dissolve. However below T_m, the embryo reaches a critical radius r^*. If $r < r^*$ the system can lower it's free energy by dissolution of the solid, whereas when $r > r^*$ the free energy of the system decreases as the solid grows. Unstable solid particles with $r < r^*$ are known as clusters or embryos while stable particles with $r > r^*$ are referred to as nuclei- r^* is known as critical

nucleus size. Since ΔG = 0 when r = r^* the critical nucleus is effectively in (unstable) equilibrium with the surrounding liquid.

$$r^* = \frac{2\gamma_{SL}}{\Delta G_V} \quad \textbf{(2. 8)}$$

And

$$\Delta G^* = \frac{16\pi\gamma_{SL}^3}{3(\Delta G_V)^2} \quad \textbf{(2. 9)}$$

2.2.1.2. Heterogeneous Nucleation

The nucleation is considered to be heterogeneous when it takes places on the surface of the mould or on the particles presents in the system. Nucleation can occur on preferential sites. The theory has been developed by Turnbull (Turnbull D. 1950) then Volmer (Volmer M. 1952), for spherical cap of solid which form on a planar substrate. A critical factor is the wetting angle θ, which is the function of the surface energies of the liquid–mould interface γ_{SL}, the crystal-substrate interface γ_{SM} and the liquid-substrate interface γ_{ML} as shown on Figure 2.3. The wetting angle θ can be calculated from the equation:

$$\cos\theta = \frac{\gamma_{ML} - \gamma_{SM}}{\gamma_{SL}} \quad \textbf{(2. 10)}$$

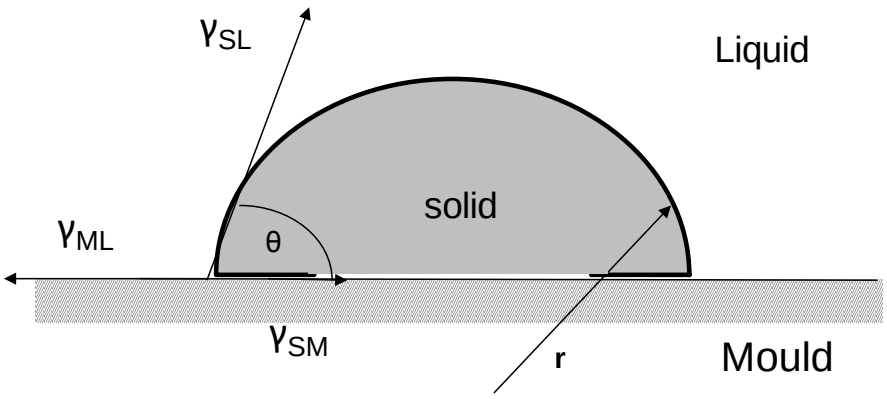

Figure 2.3 The schematic illustration of wetting angle between the mould and solid

The formation of embryo will be associated with an excess free energy given by

$$\Delta G_{het} = -V_S \Delta G_V + A_{SL}\gamma_{SL} + A_{SM}\gamma_{SM} - A_{SM}\gamma_{ML} \quad \textbf{(2. 11)}$$

Where V_s is the volume of the spherical cap, A_{SL} and A_{SM} are the areas of the solid/liquid and solid/mould interfaces, and γ_{SL}, γ_{SM} and γ_{ML} are the free energies of the solid/liquid, solid/mould and mould/liquid interfaces. The equation can be written in terms of wetting angle (θ) and the cap radious (r) (Porter D.A. 1981, Christian J.W. 1965, Ashby M.F. 1994) as:

$$\Delta G_{het} = \left\{ -\frac{4}{3}\pi r^3 \Delta G_V + 4\pi r^2 \gamma_{SL} \right\} S(\theta) \quad \textbf{(2. 12)}$$

Where

$$S(\theta) = (2 + \cos\theta)(1 - \cos\theta)^2 / 4 \quad \textbf{(2. 13)}$$

Equation 2.14 is the critical radius for heterogeneous nucleation (r^*) to occur. Equation 2.15 is the total free energy change or the critical activation energy (ΔG^*) to form a stable nuclei (i.e. at r^*_{het}) during heterogeneous nucleation.

$$r_{het}^{\ *} = \frac{2\gamma_{SL}}{\Delta G_V} \quad \textbf{(2. 14)}$$

and

$$\Delta G_{het}^{\ *} = \frac{16\pi\gamma_{SL}^3}{3(\Delta G_V)^2} S(\theta) \quad \textbf{(2. 15)}$$

A comparison of free energy of heterogeneous and homogeneous nucleation, can be seen in Figure 2.4.

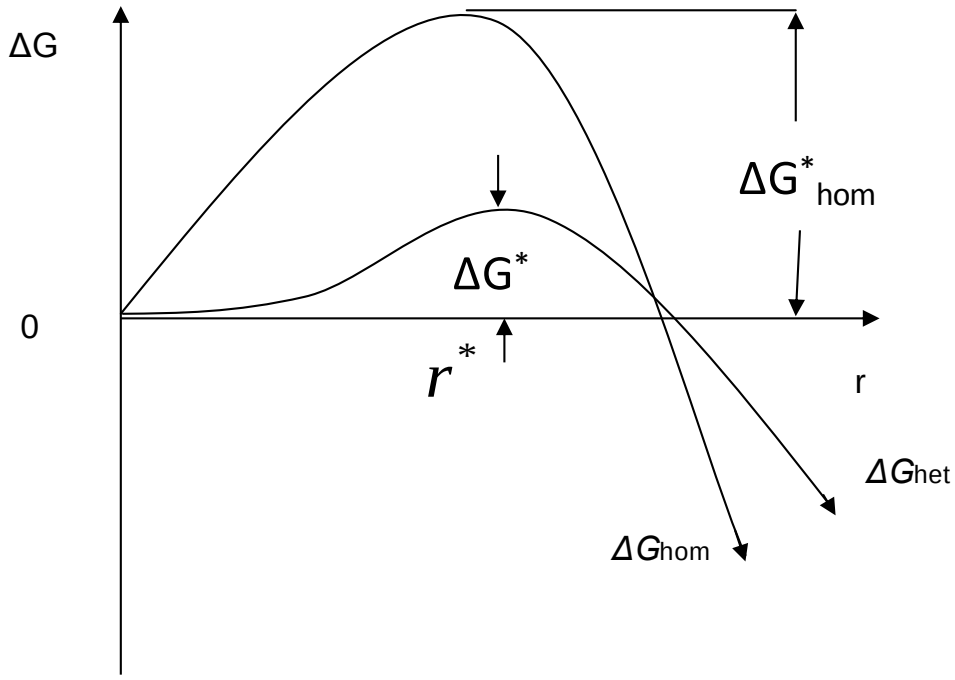

Figure 2.4 The diagram of energy barrier in heterogeneous nucleation.

The activation energy barrier against heterogeneous nucleation ΔG^*_{het} is smaller than ΔG^*_{hom} by the shape factor *S(θ).* In addition the critical nucleus radius (r^*) is unaffected by the mould wall and only depends on the undercooling.

$$\Delta G^*_{het} = S(\theta)\Delta G^*_{\text{hom}} \qquad \textbf{(2. 16)}$$

For systems where the wetting angle is small, it is clear that the barrier to nucleation is also small, and this can satisfactorily account for the low undercoolings. Turnbull and Vonnegut (B. Vonnegut and D. Turnbull 1952) related undercooling necessary for heterogeneous nucleation to the disregistry between the lattices of the crystal nucleus and substrate at the interface.

One of the most important technical aspects of casting is the control of nucleation. Grain size and grain shape together with segregation effects occurring during casting can have a significant influence on the physical, mechanical and chemical properties of the cast product.

Most commonly, control is exerted by the use of nucleating agents (inoculants). In this thesis this theory was used for development of Nb-B grain refiner.

2.2.2 Growth

After nucleation a first step is to consider the growth of nucleus. This requires an examination of the nature of the interface between the growing solid and the liquid. The structure and form of the interface influences both the microstructural morphology of the resultant solid and also the number and distribution of imperfections with the solid. It also has an effect on thermal and constitutional changes in the adjacent liquid, and the interaction between these effects, in turn lead to growth modifications. Growth plays an important role in solidification. Solidification can occur with a planar, cellular or dendritic interface (Jackson K.A, Hunt J.P. 1965) as shown on Figure 2.5.

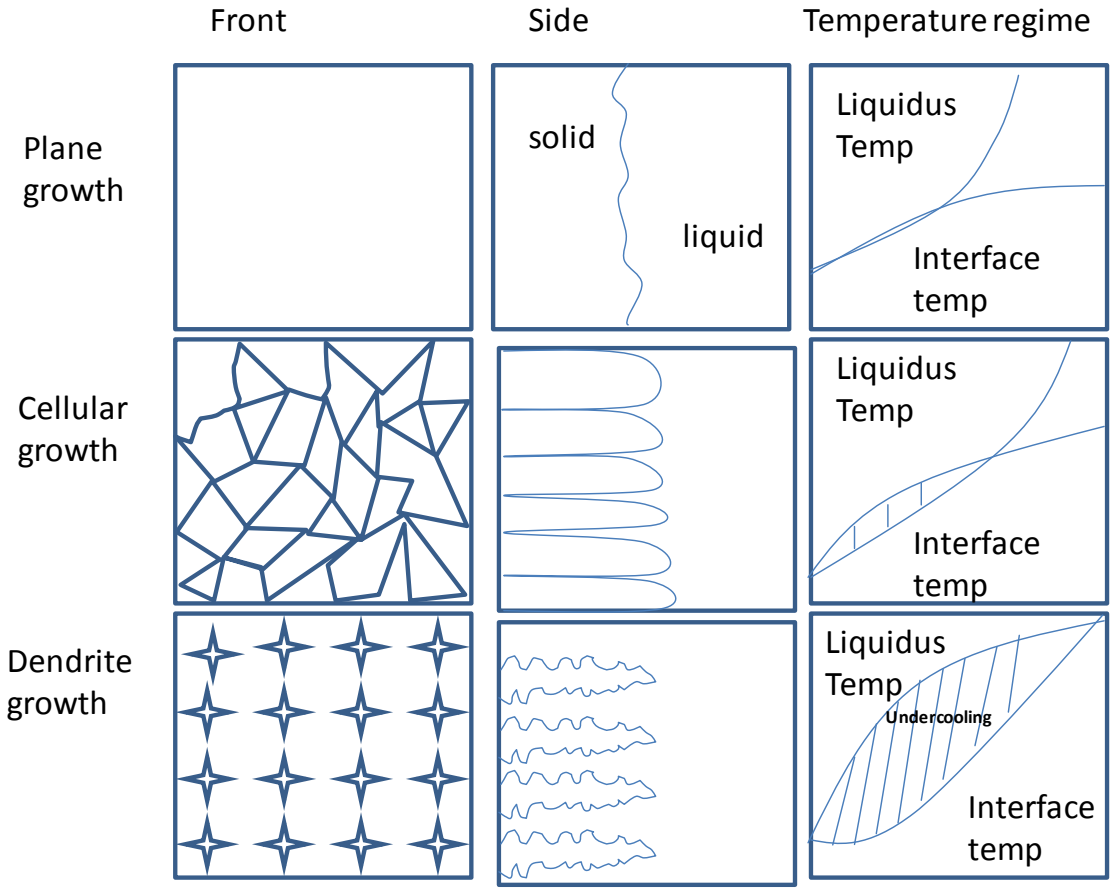

Figure 2.5 The comparison between different growths types: plane, dendrite and cellular.

2.2.2.1. Dendritic Growth

Trivedi (Triverdi R. 1994) gave the detailed overview about dendritic growth. If a state of metastability or instability is created near the growing interface by the occurrence of inverted gradient of free energy, the growth energy will break down and grow laterally and develop side branches. The interface thus degenerates and grows dendritically, Weinberg (Weinberg F., Chalmers B., 1951). Dendritic growth is strongly crystallographic. The primary arms and side branches have their arm parallel to specific crystallographic directions (the face-centerd cubic metals and alloys these are the <001> directions) (Weinberg F., Chalmers B., 1951, Hellawell A. and Herbert P.M., 1962). The growth forms are varied as each large branched dendrite grows from a single nucleus and has a single orientation. The structure is strongly anisotropic which can have deleterious effects on properties. The growth structure is determined by the type of undercooling (Winegard W.C. 1964) which may be produced by thermal means only or by temperature and compositional changes. It is also referred to as constitutional undercooling. It not only determines the internal structure of the grain but also controls the arrangement of the grains in the ingot. The undercooling must be large enough to cause nucleation within the melt. Morris and Winegard (Morris L.R. and Winegard W.C., 1967) show that the dendrite tip does not grow with constant shape but fluctuates periodically as it propagates into the melt as shown on The Figure 2.6. The heat is conducted away from the tip in three dimensions. If the solid is isothermal ($\dot{T}_S = 0$) the growth rate of the tip ν will be given by:

$$K_S \dot{T}_s = K_L \dot{T}_L + \nu L_\nu \qquad \textbf{(2. 17)}$$

Where K is thermal conductivity, $\dot{T}$ is the temperature gradient (dT/dx), the subscripts S and L stand for solid and liquid and L_ν is the latent heat of fusion per unit. It can be written as

$$\nu \cong \frac{K_L}{L\nu} \cdot \frac{1}{r}\left(1 - \frac{r^*}{r}\right) \qquad \textbf{(2. 18)}$$

It can be seen that the tip velocity tends to zero as $r \rightarrow r^*$ due to the Gibbs-Thomson effect and as $r \rightarrow \infty$ due to the slower heat conduction. The maximum velocity is obtained when $r = 2r^*$.

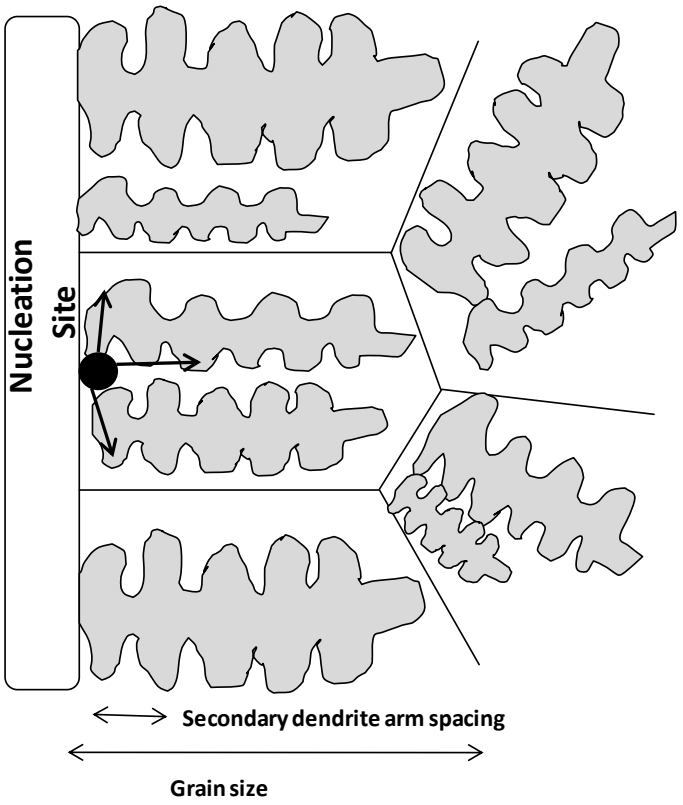

Figure 2.6 The schematic illustration of dendrites growth

2.5.2.2. Cellular Growth

The existence of zone of constitutional supercooling, and thus a negative gradient of free energy, ahead of the interface will make a initially planar interface unstable to perturbation in shape. Jakson and Hunt (Jackson K.A, Hunt J.P. 1965) suggested that at low degrees of supercooling a cellular interface develops from the planar interface.

The constitutional supercooling was analysed by Tiller *et al* (Tiller W.A. 1953). The liquidus temperature, T_L is given by:

$$T_L = T_m - mC \qquad \textbf{(2. 19)}$$

where T_m is the melting temperature of the pure metal and C is the composition of the liquid an m is the slope of the liquidus line. After calculation of steady-state solidification of an alloy with initial composition, Co, the interface temperature, T_i and for solute distribution, the equilibrium liquidus temperature will be

$$T_L = T_i + \frac{mC_0(1-k_0)}{k_0} 1 - \exp\left(-\frac{Rx}{D}\right) \quad \textbf{(2. 20)}$$

where k_0 is partition coefficient ($k_0=C_{SL}/C_{LS}$) , D diffusivity in the liquid. The actual temperature in the liquid is given by

$$T = T_i + T_g \quad \textbf{(2. 21)}$$

where T_g is the temperature gradient in the liquid ahead of the interface. The supercooling occurs during solidification and it is due to compositional changes and results in cooling liquid below the freezing point ahead of the solid-liquid interface Figure 2.7. The temperature distribution is essentially the same for $k_0 < 1$ and $k_0 > 1$, and is called constitutional supercooling. Low temperature gradients in liquid, fast growth rates, steep liquid lines and high alloy contents ($C_0 > 0.2\%$) are the conditions which will favour supercooling.

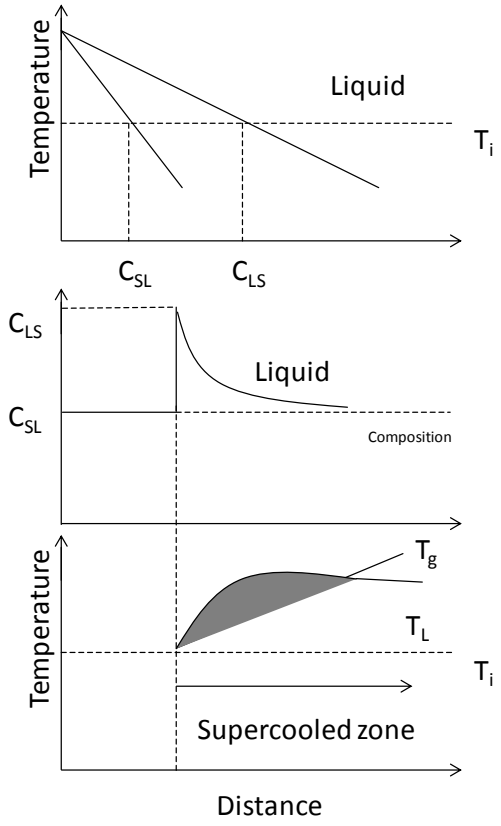

Figure 2.7 Constitutional supercooling occurs during solidification due to compositional changes C_{LS} and C_{SL} ahead of an interface. Temperature of liquid T_L is smaller than temperature of gradient T_g.

2.3 Lattice Mismatch

Crystals with low wetting angle reduce energy barrier for formation of stable nucleus (McCartney D.G. 1989). Thus crystals with good lattice match provide ideal nucleation sites.

2.3.1. Crystal Structure

The crystal structure is a unique arrangement of atoms or molecules in a crystalline liquid or solid. A crystal structure is composed of a pattern, a set of atoms arranged in a particular way, and a lattice exhibiting long-range order and symmetry. Patterns are located upon the points of a lattice, which is an array of points repeating periodically in three dimensions. The points can be thought of as forming identical tiny boxes, called unit cells, that fill the space of the lattice. The lengths of the edges of a unit cell and the angles between them are called the lattice parameters. The symmetrical properties of the crystal are embodied in its space group. The unit cells stacked in three-dimensional space describes the bulk arrangement of atoms of the crystal. The crystal structure has a three dimensional shape. The unit cell is given by its lattice parameters which are the length of the cell edges and the angles between them, while the positions of the atoms inside the unit cell are described by the set of atomic positions (x_i , y_i , z_i) measured from a lattice point. Most crystalline forms of metallic elements are body-centered cubic (bcc), face-centered cubic (fcc) shown on Figure 2.8 and hexagonal close-packed (hcp).

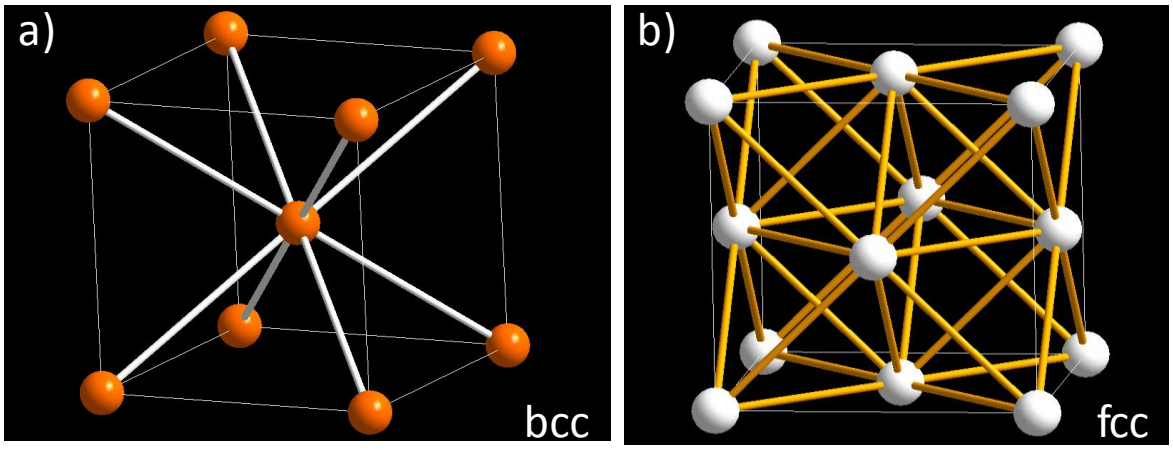

Figure 2.8 Lattice structures a) BCC -body centred cubic b) FCC-face centres cubic

The best nuclei are those with the lattice plane giving good atomic match with a lattice plane

in the nucleating solid (Bramfitt B.L. 1970).

Table 2.1 shows the lattice parameters of Mo, Nb, Ta and W.

The lattice mismatch f can be calculated using the following equation:

$$f = \frac{lattice\ constant\ of\ solid - lattice\ constant\ of\ substrate}{lattice\ constant\ of\ solid}$$

where *f* is lattice parameters mismatch.

Element	Lattice structure	Lattice constant parameter	Lattice parameters mismatch
Al	Face centered cubic	a = 4.050 Å	
Mo	Body-centred cubic	a = 3.147 Å	0.28
$MoAl_{12}$		a = 7.573Å	-0.46
Ta	Body-centred cubic	a=3.013 Å	0.34
$TaAl_3$	Tetragonal	a=3.84Å and c=8.53Å	0.05
W	Body-centred cubic	a=3.160Å	0.28
WAl_{12}		a=7.58 Å	-0.46
Nb	Body-centred cubic	a = 3.300 Å	0.22
$NbAl_3$	Tetragonal	a = 3.84 Å, c = 8.58Å	0.05
Ti	Hexagonal	a = 2.950 Å	0.37
$TiAl_3$	Tetragonal	a=3.849 Å, c=8.609 Å	0.05

Table 2.1 The lattice structures of various elements and compounds and their mismatch with Al

We can see that the lattice mismatch of Mo, W, Ta and Nb with Al is very similar to well known grain refiner, Ti. We can assume that these elements can be potential nucleation site.

2.4 Grain Refinement

2.4.1 Introduction

The grain refinement development is of scientific and practical significance in alloy casting as the fine and equiaxed grain structure is usually desirable. Fine, equiaxed grains are desirable in aluminium castings, whether of wrought or shape casting grades. The grain refinement influence on mechanical properties is discussed by many researchers (McCartney D.G. 1989, Rooy E.R. 1989, Granger D.A. 1998, Hunt J.D. 1984). The fine equiaxed grain structure imparts high yield strength, high toughness, good extrudability (Becker R. 1935), uniform distribution of second phase and micro-porosity on a fine scale resulting in improved machinability, good surface finish and resistance to hot tearing. The common grain refiner is titanium although there are potential grain refiners like Nb, V, Zr, Ta, W, Mo, Ce, that could be used for Al alloys and is reviewed by Murty *et al* (Murty B.S. 2002).

2.4.2 Grain Refinement by Al-Ti-B System

The phases present in the Al-Ti-B system and their effect on grain refinement can be understood by considering separate additions of Al-Ti and Al-B master alloys. Cibula (Cibula A. 1949-1950) showed that addition of small amounts of titanium into the melt can cause a drastic reduction in grain size, as little as 0.01 wt% has a significant effect. A peritectic reaction is present within the aluminium-titanium system at 665°C, Figure 2.9:

Liquid + Al_3Ti → α-Al (solid solution)

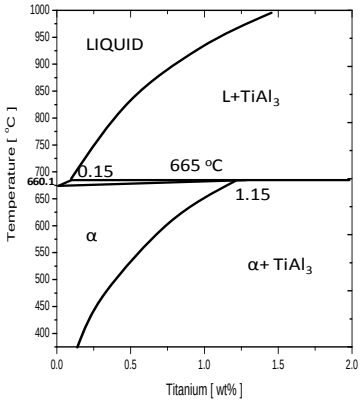

Figure 2.9 Peritectic reaction of Al-Ti

Al_3Ti has a tetragonal structure based on an ordered Cubic Closest Packed structure (Greer A.L. 2000) and it is stable in melts containing more than ~0.15 wt.% titanium (Mondolfo F. 1976). When an Al-Ti master alloy containing α-Al + Al_3Ti particles is added to the aluminium melt, the α-Al , which contains a very small amount of titanium, dissolves in the aluminium melt, while the Al_3Ti particles become suspended in the melt. The Al_3Ti particles are thought to contribute to presents of heterogeneous nucleation sites. Though rarely used, it is suggested that Al-B master alloys can refine cast alloys. This system exhibits a eutectic at 659.7°C and 0.022 wt. %B (Sigworth G.K. 1989) :

Liquid => AlB_2 + α-Al (solid solution)

The boride phase, AlB_2, is hexagonal: at 298 K, AlB_2 a = 0.3009 nm, c = 0.3262 nm (Arnberg L. 1982). The joint addition of both titanium and boron is responsible for a grain-refining effect larger than the addition of either element individually (Cibula A. 1949-1950); (Delamore G.W. and Smith R.W. 1971). Boride particles have been observed at long holding times within many dilute ternary alloys suggesting they are stable (Arnberg L. 1982, Johnsson M. and Jansson K., 1998, Cornish A.J. 1975, Johnsson M. and Backerud L. 1992, Guzowski M.M. 1987),

2.4.3 The Grain Refinement Theories

The grain refinement theories were developed to explain the phenomena of the grain refinement observed by Al-Ti-B addition to Al alloys.

2.4.3.1. The Nucleant Paradigm

The development of nucleant paradigm is based on two theories: the nucleant-particle theory and the phase diagram theory. These two theories are related to two types of particles present in the Al-Ti-B master alloy. The first theory suggests that the nucleation occurs on the borides present in master alloy (TiB_2, AlB_2 and (Ti, Al)B_2), while the second theory explains the grain refinement by nucleation on Al_3Ti, the hypoperitectic phase. The nucleant-particle theories were proposed by Cibula (Cibula A. 1949-1950). He suggested that nucleation happens on the borides or carbides when they are present. The nucleating behaviour of all the borides can be discussed concurrently, as TiB_2 and AlB_2 are known to be isomorphous and hexagonal, with the lattice parameters varying only slightly, being a = 0.30311 nm and c = 032291 nm and a =

0.3009 nm and c = 0.3262 nm, respectively (Mondolfo F. 1976). Boride particles are found in the centres of the grains which suggested that they nucleate α-Al. Nevertheless, Mohanty et al (Monthany P.S. 1994) have confirmed that borides are pushed to the grain boundaries and that no grain refinement is observed when there is no solute titanium present. That suggested that the borides are not so efficient nucleant like Al_3Ti. That is why the phase diagram theories were developed to explain how Al_3Ti could be the active nucleant in hypoperitectic composition. The phase diagram theories suggested that the grain refinement is caused by peritectic reaction on the primary particles, (Al_3Ti). Marcantonio and Mondolfo (Marcantonio J.A. 1971) suggested that there is a ternary eutectic, Liquid → (Al, Ti) B_2 + $TiAl_3$ + solid, at about 0.05 pct Ti, 0.01 pct B, and 659.5°C, but it is not proved by the direct experimental data. The main problem in phase diagram theory is that, at hypoperitectic concentrations, Al_3Ti is not present as nucleation sites except at very short holding times, and, hence the phase-diagram theories cannot explain grain refinement at hypoperitectic titanium concentrations. The nucleant-particle theory and phase diagram theory couldn't explain why the addition of Boron to Al-Ti system significantly improves grain refinement. Therefore, other theories have been developed, which combine those two theories or include other factors. One of the theories is the peritectic hulk theory, which was one of the most popular theories in the late 1980s and early 1990s, supported by Vader et al. (Vader M. 1991) and Backerud et al (Backerud L., Gustafson P., Johnsson M., 1991). The peritectic hulk theory proposes that the borides form a shell around the Al_3Ti and slow down their dissolution, as diffusion needs to proceed through the boride shell. The hypernucleation theory was proposed by Jones (Jones G.P. 1987), who suggested that very small amounts of titanium and boron make the fine grain size of aluminium. The duplex nucleation theory is the most recent in this paradigm. It was proposed by Mohanty *et al* (Mohanty P.S. and Gruzelski J.E., 1995), however Schumacher and Greer (Schumacher P. and Greer A.L. 1995) gave the most sensible evidence. They proposed that a layer of Al_3Ti forms at the boride-melt interface which in turn nucleates α-Al.

2.4.3.2. The Solute Paradgim Theory

The theory was suggested by Johnsson (Johnsson M. and Backerud L. 1992), who proposed that the addition of nucleant particles and amount of segregating elements, quantified by the growth restriction factor (GRF) are important in grain refinement. In this theory the effect of

the solute on the growth of dendrites and the constitutional undercooled zone in the front of the interface is equally important with nucleation. Maxwell and Hellewell (Maxwell I. and Hellawell A. 1975) have shown that the number of grains per unit volume N_v^G increases with number of particles per unit volume N_v^P, however only up to critical value and reaches a saturation beyond this point as shown in Figure 2.10. Beyond this critical value of N^P, all the particles added do not act as potent nucleating sites. Due to wide range of Al_3Ti and TiB_2 size distribution and clusters, only ~1% of total particles are known to be actively participating in the heterogeneous nucleation process (Quested T.E. and Greer A.L. 2004).

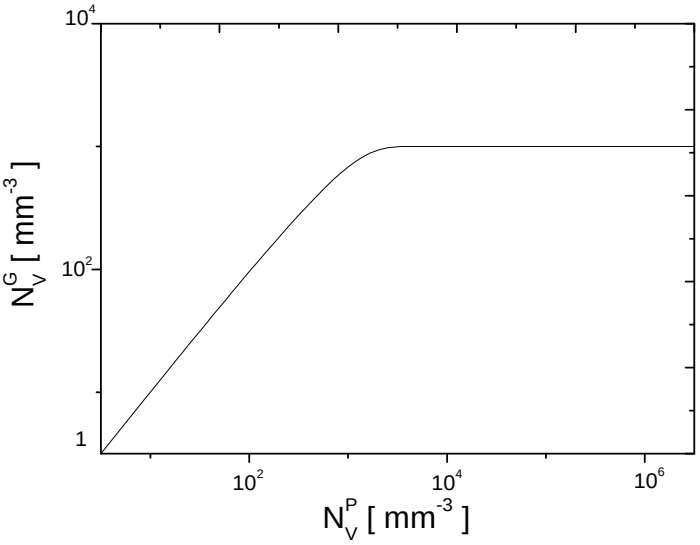

Figure 2.10 Numbers of grains per unit volume as a function of number of particles in the melt (Maxwell I. and Hellawell A. 1975)

The growth rate is inversely related to the constitutional supercooling parameter, $mC_o(k-1)$, where m is slope of liquidus, C_o is the concentration of the solute in the melt, and k is the equilibrium partitioning coefficient. The parameter with larger value of supercooling and small growth rate allows a large number of substrates to act as nucleating sites. It means that the critical value N^P depends strongly on the growth restricting factor. Pearson and Kearns (Pearson J. 1997) proposed that the grain size of aluminium decreases asymptotically with growth restriction factor.

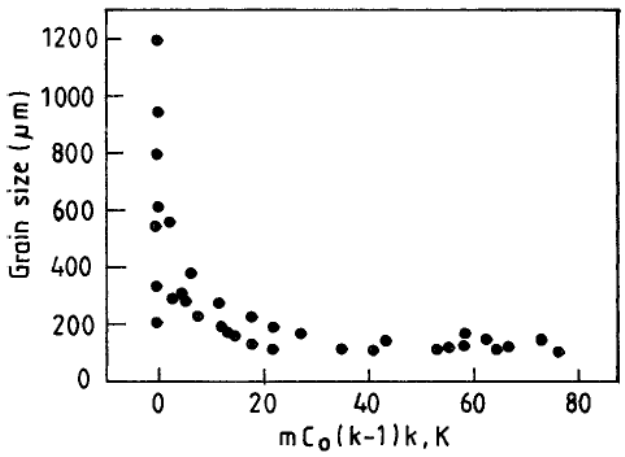

Figure 2.11 Grain size as a function of grain restriction factor (Pearson J. 1997)

In the alloys the growth restriction factor is measured by adding the constitutional supercooling parameter, $mC_o(k_0-1)$, of all individual elements. Johnson *et al* (Johnsson M., Backerud I., Sigworth G.K., 1993) and Maxwell and Hellawell (Maxwell I. 1975) argued that TiB_2 acts as a good nucleant once the melt has titanium, which provides sufficient undercooling for the TiB_2 to be a good substrate for aluminium.

2.5 Alloys Classification

The aluminium alloys can be put into two groups namely wrought alloys and casting alloys. The main difference between them is that the wrought alloys are 99% of Al plus another dilute addition where casting alloys can have more alloying elements. The freezing temperature range of wrought alloys is smaller than that of cast alloys. The wrought alloys are usually machined after casting and cast alloys are directly cast to the shape that is desired.

2.5.1 Wrought Alloys

In general, 75 to 80% of aluminium is used in wrought products, e.g. rolled plate (>6 mm thickness), sheet (0.15-6 mm), foil (<0.15mm), extrusions, tubes, rods, bars and wires. These are produced from large ingots, the structures of which are greatly changed by the various working operations and thermal treatments. Each class of alloys behaves differently, with composition and structure dictating the working characteristics and subsequent properties that are developed.

The alloys are divided as shown in Figure 2.12

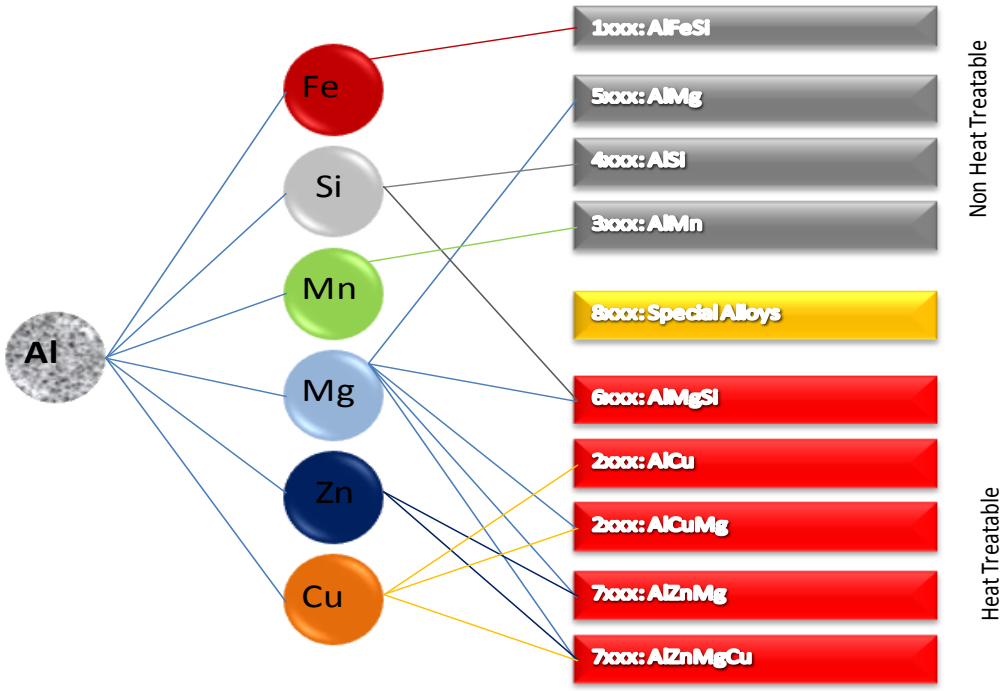

Figure 2.12 Series of wrought alloys classification

2.5.1.1. Production of wrought alloys (Polmear I.J. 1995)

Ingots are prepared for subsequent mechanical working by first melting virgin aluminium, and then adding alloying additions, usually in the form of a concentrated hardener or master alloy, in a suitable furnace. The main essentials in promoting ingot quality are a thorough mixing of the constituents together with effective fluxing, degassing, and filtering of the melt before casting in order to remove dross, oxides, gases and other non-metallic impurities. The production of a uniform ingot structure is desirable and this is promoted by direct-chill (DC), semi-continuous processes. Most commonly, ingots are cast by the vertical process in which the molten alloy is poured into one, or more fixed, water-cooled moulds having retractable bases. The process of solidification is accomplished in two stages: formation of solid metal at the chilled mould wall and solidification of the remainder of the billet cross-section by the removal of heat by the sub mould and spray cooling. Because a fine grain size is so desirable, it is usual to add small amounts of master alloys either Al-Ti, Al-Ti-C or Al-Ti-B to the melt before casting to promote further refinement. Al-Ti-B is the most widely used alloy with Ti:B ratios varying from 3:1 to 5:1, although Al-5Ti-lB is now the favoured composition. Now grain refiners used to be introduced to the melt in the form of tablets made from titanium and

boron salts. These grain refiners are prepared as small ingots that are added to the melt in the furnace, or as rods which are fed automatically into the launder and dissolved by the molten metal as it passes from the furnace to the casting station. This latter method is preferred because less time is available for the effects of the grain refiner to fade before the ingots have solidified.

The function of thermal treatment is to develop a desired balance of mechanical properties required for consistent service performance. It will be clear from the above considerations that such consistency presupposes attainment of a satisfactory uniformity of microstructure in the preceding stages of production of the wrought material.

2.5.1.2. Wrought alloys

Wrought alloys are classified into heat treatable and non heat treatable alloys.

A. Super-purity and commercial-purity aluminium (1 xxx series)

This group includes super-purity (SP) aluminium (99.99%) and the various grades of commercial-purity (CP) aluminium containing up to 1% of impurities or minor additions (e.g. 1145, 1200). The materials have been utilized as wrought products since the industry was first developed and the CP grades are available in most forms. Tensile properties are low and annealed SP aluminium has a proof stress of only 7-11 MPa. Applications include electrical conductors for which there are several compositions, chemical process equipment, foil, architectural products requiring decorative finishes, and lithographic plates.

B. Al-Cu alloys (2xxx series)

Although the complex changes that occur during the ageing of Al-Cu alloys have been studied in greater detail than any other system, there are actually few commercial alloys based on the binary system. Alloy 2011 (Al-5.5Cu) is used where good machining characteristics are required, for which it contains small amounts of the insoluble elements such as lead and bismuth that form discrete particles in the microstructure.

C. Al-Mn and Al-Mn-Mg alloys (3xxx series)

In general, 3xxx series alloys are used when moderate strength combined with high ductility and excellent corrosion resistance is required. Commercial Al-Mn alloys contain up to

1.25wt% manganese although the maximum solid solubility of this element in aluminium is as high as 1.82wt%. This limitation is imposed because the presence of iron as an impurity reduces the solubility and there is a danger that large, primary particles of Al-Mn will form with a disastrous effect on local ductility. The only widely used binary Al-Mn alloy is 3003, which is supplied as sheet. The presence of finer manganese-containing intermetallic compounds confers some dispersion-hardening, and the tensile strength of annealed 3003 is typically 110 MPa compared with 90 MPa for CP aluminium (1100), with corresponding increases in the work-hardened tempers.

This alloy is commonly used for foil, cooking utensils and roofing sheet. The addition of magnesium provides solid solution strengthening and the dilute alloy 3105 (Al-0.55Mn-0.5Mg), which is readily fabricated, is widely used in a variety of strain-hardened tempers. This alloy is used for manufacturing beverage cans, which is currently the largest single use of the metals aluminium and magnesium.

D. Al-Si (4xxx series)

4xxx series are low ductile alloys; due to the high silicon content of these alloys (up to 12 wt%), silicon is present in the form of intermetallic precipitates, but also as elemental silicon particles making the material brittle. These alloys have very low formability. They find only a limited number of applications as wrought product, for example, as cladding alloy on brazing sheet because of its lower melting point than the core alloys of the 3xxx or 6xxx series or as filler metal for welding.

E. Al-Mg alloys (5xxx series)

Aluminium and magnesium form solid solutions over a wide range of compositions and wrought alloys containing from 0.8% to slightly more than 5% magnesium are widely used. Strength values in the annealed condition range from 40 MPa yield and 125 MPa tensile for Al-0.8Mg (5005) to 160 MPa yield and 310 MPa tensile for the strongest alloy 5456. Elongations are relatively high and usually exceed 25%. Al-Mg alloys are widely used for welded applications. In transportation structural plate is used for dumper truck bodies, large tanks for carrying petrol, milk and grain, and pressure vessels, particularly where cryogenic storage is involved. Their high corrosion resistance makes them suitable for the hulls of small

boats and for the super-structures of ocean-going vessels. These alloys are also widely used for ballistic armour plate in light weight military vehicles.

F. Al-Mg-Si alloys (6xxx series)

Al-Mg-Si alloys are widely used as medium-strength structural alloys which have the additional advantages of good weldability, corrosion resistance, and immunity to stress-corrosion cracking. Just as the 5xxx series of alloys comprise the bulk of sheet products, the 6xxx series are used for the majority of extrusions, with smaller quantities being available as sheet and plate.

G. Al-Zn-Mg alloys (7xxx series)

The Al-Zn-Mg system offers the greatest potential of all aluminium alloys for age-hardening although the very high-strength alloys always contain quaternary additions of copper to improve their resistance to stress-corrosion cracking. There is, however, an important range of medium-stength alloys containing little or no copper which have the advantage of being readily weldable. These alloys differ from the other weldable aluminium alloys in that they age-harden significantly at room temperature. Moreover, the strength properties that are developed are relatively insensitive to the rate of cooling from high temperatures, and they possess a wide temperature range for solution treatment, i.e. 350 °C and above, with the welding process itself serving this purpose.

H. Miscellaneous alloys (8xxx series)

This series contains several dilute alloys, e.g. 8001 (Al-l.lNi-0.6Fe) which is used in nuclear energy installations where resistance to corrosive attack by water at high temperatures and pressures is the desired characteristic. Its mechanical properties resemble 3003. Alloy 8011 (Al-0.75Fe-0.7Si) is used for bottle caps because of its good deep drawing qualities and several other dilute compositions are included in the range of electrical conductor materials This alloy and other dilute compositions containing transition metal elements, such as 8006 (Al-l.6Fe-0.65Mn), are used for producing foil and finstock for heat exchangers In each of these alloys, the most important contribution to strengthening comes from dispersion hardening which commonly accounts for 30-40 MPa of the values for proof stress and tensile strength. Solid solution strengthening is the next most important factor providing estimated

increments of 2-10 MPa in proof stress of 5-20 MPa in tensile strength. Alloys such as 8280 and 8081 serve an important role as bearing alloys based on the Al-Sn system that are now widely used in motor cars and trucks, particularly where diesel engines are involved.

2.5.2 Casting Alloys

Cast aluminum-silicon alloys, especially hypoeutectic alloys are widely used in the aerospace and automotive industries due to the high mechanical properties and excellent foundry characteristics. The silicon content in standardized commercial cast aluminum-silicon alloys is in the range of 5 to 25 wt%. The structure of the alloys can be hypoeutectic (5-11 wt%), hypereutectic (13-25 wt%), or eutectic (11-13 wt%), as can be seen on the equilibrium phase diagram (Chapter 5, Figure 5.1). The properties of a specific alloy can be attributed to the individual physical properties of its main phase components (α-aluminum solid solution and silicon crystals) and to the volume fraction and morphology of these components.

2.5.2.1. Binary Al-Si Alloys

Binary Al-Si alloys up to the eutectic composition retain good levels of ductility, providing the iron content is controlled to minimize formation of large, brittle plates of the compound β-AlFeSi. In this regard, additions of manganese have been found to be beneficial because this element favours formation of the finer α-Al(FeMn)Si phase which has the so-called Chinese script morphology. An accepted rule in industry is that the Mn:Fe ratio needs to be at least 0.5:1 for β-AlFeSi to be suppressed, although the latter phase has been observed in alloys with Mn:Fe ratios as high as 1:1. However, such high levels of manganese can be a disadvantage since they may promote formation of greater volume fractions of intermetallic compounds than are present for the same levels of iron. This follows because α-Al(FeMn)Si contains a lower atomic percentage of iron so that it is possible for larger colonies of this phase to form than the β-AlFeSi . Thus the preferred strategy is to keep the iron levels as low as possible in the first place. If the silicon content is below 8%, modification of its eutectic morphology is not necessary to achieve acceptable levels of ductility because the primary aluminium phase is present in relatively large amounts. The eutectic composition, which has a high degree of fluidity and low shrinkage on solidification, has particular application for thin-walled castings. As a class, the alloys are used for sand and permanent mould castings for which strength is not

a prime consideration e.g. domestic cookware, pump casings and certain automobile castings, including water-cooled manifolds.

When as-cast alloys containing substantial amounts of silicon are subjected to elevated temperatures they suffer from growth due to the precipitation of silicon from solid solution. Dimensional stability can be achieved by heating for several hours in the temperature range 200-500 °C prior to subsequent machining or use, and tempers of the T5 (cooled from an elevated temperature shaping process and then artificially aged) or T7 (solution heat treated and then stabilized) types should be given to castings which are to be used at temperatures of 150 °C or above.

Grain refinement is one of the most important and popular melt treatment processes for aluminium silicon casting alloys. Grain refinement improves the quality of castings by reducing the size of primary α-Al grains in the casting, which generally will solidify with coarse columnar grain structure. It is well known that fine grains structure has uniform distribution of second phases and microporosity, improved feeding ability (McCartney D.G. 1989), high yield strength, high toughness and machinability (Spittle J.A. 1997). There are several methods of grain refiners depending on the alloy composition. The casting alloys can be refined by the use of heterogeneous nucleation promoted by the Al-B master alloys and Si particle size by the addition of Phosphorous and modification of eutectic Si shape and size by using Strontium. However it is very difficult to refine the high silicon alloys. Researchers (Johnsson M. 1994, Spittle J.A. 1997) showed that the Al-5Ti-1B master alloy poison the Al-Si alloys containing more than 3 wt% of Silicon. It is discussed in Chapter 5.

2.5.2.2. Selected Al-Si alloys

The Table 2.2 shows examples of the commercial alloys and their alloying elements in weight percent (wt%) used in this study.

GB	USA	Si	Mg	Mn	Cu	Ni	Zn	Fe
LM6	A413	10.0-13.0	0.1max	0.5max	0.1max	0.1max	0.1max	0.6max
LM13	336	10.0-13.0	0.2-0.4	0.5max	0.7-1.5	1.5max	0.1max	1max
LM24	A380	7.5-9.5	3max	0.5max	3.0-4.0	0.5	3	1.3max
LM25	A356	6.5-7.5	0.2-0.6	0.3	0.2	0.1	0.1	0.5
LM28	-	17-20	0.8-1.5	0.6	1.3-1.8	0.8-1.5	0.2max	0.7max
LM30	390	16-18	0.4-0.7	0.3	4.0-5.0	0.1	0.2	1.1

Table 2.2 Examples of the Al-Si commercial alloys and their composition of Aluminium casting alloys

A. LM6- Al-12Si

The aluminium-silicon alloys possess exceptional casting characteristics, which enable them to be used to produce intricate castings of thick and thin sections. Fluidity and freedom from hot tearing increases with silicon content and are excellent throughout the range. Their resistance to corrosion is very good, but special care is required in machining. In general, the binary alloys are not susceptible for heat treating; at elevated temperatures their strength falls rapidly. Although they possess medium strength, their hardness and elastic limit are low but they possess excellent ductility. LM6 is suitable for Marine 'on deck' castings, water-cooled manifolds and jackets, motor car and road transport fittings; thin section and intricate castings such as housing, motor casings and switchboxes; for very large castings, e.g cast doors and panels where ease of casting is essential; for chemical and dye industry castings, e.g pump parts; for paint industry, food and domestic castings. They are especially suitable for castings that are requiring welding.

B. LM13 (Al-12Si-1Cu)

LM13 alloy is used for pulleys for pistons for all types of diesel and petrol engines, and for other engine parts operating at elevated temperatures. It has the advantage of good resistance to wear, good bearing properties and a low coefficient of thermal expansion.

C. LM24 (Al-8Si-3.5Cu)

LM24 is essentially a pressure die casting alloy, for which it has excellent casting characteristics and is generally a little simpler to die cast than the higher silicon containing alloys. Die castings of LM24 are suitable for most engineering applications and have an advantage over an alloy such as LM6 when maximum mechanical properties are required. In practice LM6 is preferred to LM24 only for die castings in which a high resistance to corrosion is the primary requirement. Pouring temperatures for die castings depend on the machine and casting dimensions; pouring temperatures may vary between 630-710°C. The melt should not be allowed to stand at temperatures just above the freezing range as the bottom of the melt will become enriched in Iron and Manganese. It has very good fluidity as a result it is used for very thin sections without hot tears. It has poor weldability and brazeability.

D. LM25 (Al-7Si)

LM25 alloy is mainly used where good mechanical properties are required in castings of a shape or dimensions requiring an alloy of excellent castability in order to achieve the desired standard of integrity. The alloy is also used where resistance to corrosion is an important consideration, particularly where high strength is also required. This alloy has good weldability. Consequently, LM25 finds application in the food, chemical, marine, electrical and many other industries and, above all, in road transport vehicles where it is used for wheels, cylinder blocks and heads, and other engine and body castings. Its potential uses are increased by its availability in four conditions of heat-treatment in both sand and chill castings. It is, in practice, the general purpose high strength casting alloy, whose range of uses is increased by its availability in the as-cast and partially heat-treated condition as well. It is used in nuclear energy installations and for aircraft pump parts. LM25 may be superior for

castings, particularly in chill moulds, which are difficult to fabricate the required standard of soundness. This alloy offers better machinability and mechanical properties than LM6.

E. LM28 (Al–18Si-1.5Cu-1Mg-1Ni)

LM28 is used for pistons for high performance internal combustion engines where advantage can be taken of its low coefficient of thermal expansion and its high resistance to wear. Ths alloy has typical pouring temperature of 735°C minimum LM28 is refined with phosphorus containing agents, or Al-Cu-P to avoid the formation of coarse primary Silicon particles, the formation of which will cause problems in machining, segregation and brittleness. BS1490 permits a maximum primary silicon particle size of 70 microns for individual particles and an average of 40 microns for all silicon particles. To obtain the desired structure, a rapid rate of solidification is required, so permanent mould casting methods are preferable to sand casting. Prolonged degassing treatment may be necessary as at the high melt temperatures gas pickup is considerable. Oxidation will increase at these higher temperatures. Flux compositions must be free of sodium to avoid negating the modification process.

F. LM30 (Al-17Si-4.5Cu-0.5Mg)

Casting temperatures must be kept significantly above the liquidus temperature of 620-700°C. In order to prevent the formation of coarse Silicon particles, it is usual to refine melts with Phosphorus-containing agents, or Phosphor-Copper. The precipitation of primary silicon would result in a non-uniform structure having low properties and poor machinability. The pick-up of gas during melting must be kept as low as possible since prolonged degassing, with chlorine containing agents, will deplete magnesium and phosphorus. LM30 is a recently introduced alloy which was designed specifically for a die cast Aluminium automobile engine, operating without the usual iron cylinder liner. Potentially, its application extends to a wide range of castings where high wear resistance, associated with lightness, is required and especially where advantage can be taken of the economies of the die casting process, e.g., pumps, pulleys, brake shoes, and air compressors.

2.6 Casting Processes

The foundation of casting processes is the feeding of molten metal into cavity of the required shape, then cooling to manufacture a solid object (Rooy E.L. 2003). The difference in the

processes depends on the mould that the material to be cast. For example the sand moulds are made each time and then broken up to remove the casting. In the die casting the permanent mould is used repeatedly. The sand casting process has great flexibility, as the pattern made from the sand can have different shapes every time the metal is cast. The pattern is manufactured from the wood or other materials. The mould is made by packing the sand around the pattern forming two separate parts. After removing the pattern the melt can be poured into the mould cavity as seen in Figure 2.13. The sand is removed and the cast is ready for machining. The process is very simple and economical, can produce castings of wide range of sizes from few grams to several tonnes. The wastage of material is negligible as the sand can be reused. However the sand casting cannot be used for thin sections or complex shapes. Also the dimensional accuracy and surface finish are not excellent. In addition, there is a problem with the erosion of the mould - by the molten metal in very large castings.

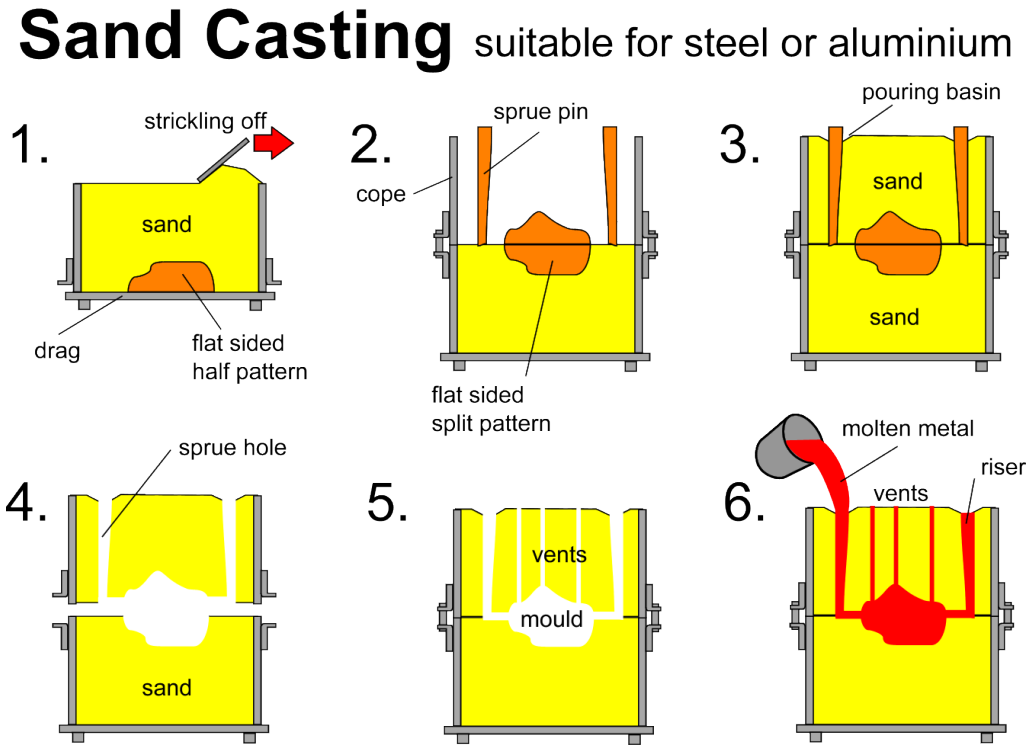

Figure 2.13 Sand casting mould (Warren Design and Technology)

The gravity die casting is the process where the molten metal is cast in the dies made from metal. The process is particularly suitable for the high-volume production of small, simple castings without complex undercuts. With the permanent moulds good surface finish and high

definition can be achieved. Pressure die casting differs from permanent mould casting as the pressure is applied on the metal in the mould during casting. For high pressure work there are two processes used: hot chamber die casting and cold chamber die casting. In hot chamber die casting the molten metal is maintained in a holding furnace which forms part of the machine. The melt is pumped into the mould. The process can be used only for lower melting point metals like zinc-based alloys. The cold–chamber die casting is used for high melting point metals like aluminium and magnesium alloys. The transfer chamber is loaded with molten metal and with the force it injects the metal to the die. The most commonly used process is the high pressure die casting, in which molten aluminium is injected at high pressure into a metal mould by a hydraulically powered piston. The machinery needed for the process can be very costly and this high pressure die casting is only economic when used for high volume production.

2.7 Defects in Castings

During the casting we can observe many defects such as shrinkage, gas porosity and oxide inclusions (Davies G.J. 1973). The main job with the alloys developments is to avoid them and produce castings which are defect free. The blowholes can arise from a number of causes like entrapment of air during solidification or by generation of gas by reaction with molten metal. To avoid blowholes the entrapped air needs to be removed by drying the moulds before casting. To avoid the gases form in chemical reactions the extra addition of degassing tablets is required.

2.7.1 Gas Porosity

Hydrogen solubility is low in solid aluminium, but causes molten aluminium to absorb hydrogen from moisture in the atmosphere and other sources (Davies G.J. 1973). This hydrogen gas is not naturally expelled and will stay in the grain structure during solidification and form pores in the solid castings. Gas porosity can have negative impact on casting quality and prevent castings from meeting high service requirements by reducing tensile, fatigue and impact properties and increasing hot tearing tendency. While atmospheric humidity may be the major source of hydrogen, moisture can come from many other sources, such as metal processing tools, improperly dried and cured crucibles, charge materials and furnace

combustion products. All tools used in contact with molten aluminium should be dry before usage. Another means to reduce porosity is through controlling melt temperature. Overheating the melt will increase the absorption of hydrogen dramatically. The aluminium oxide film on the surface of molten aluminium provides some inhibitor to gas, but turbulence during handling and pouring will break that oxide skin and increase the hydrogen absorption rate. Degassing is performed most often with an inert gas such as nitrogen, argon, freon or chlorine (or some combination), usually involving bubbling the purge gas into the bottom of the melt using a graphite lance. As the purge gas rise through the melt, it comes into contact with the hydrogen, absorbs it and carries it out to the surface.

2.7.2 Solidification Shrinkage

Shrinkage defects occur when feed metal is not available to compensate for shrinkage as the metal solidifies. Shrinkage metal can be split into two types: open shrinkage and closed shrinkage defects. Open shrinkage defects are open to the atmosphere, therefore as the shrinkage cavity forms air compensates. There are two types of open air defects: pipes and caved surfaces. Pipes form at the surface of the casting and burrow into the casting, while caved surfaces are shallow cavities that form across the surface of the casting. Closed shrinkage defects, also known as shrinkage porosity, are defects that form within the casting. The isolated pools of liquid form hot spots inside the solidified metal. The shrinkage defects usually forms at the top of the hot spots. They require a nucleation point, so impurities and dissolved gas can induce closed shrinkage (Campbell F.C. 2003)

2.8 Novel Grain Refiners

Improvement in the mechanical properties, ease of casting process and improvised cast structures are the driving force for the development of new grain refiners. By examining the lattice mismatch and phase stability with Al we have investigated few phases which could act as potential grain refiners for Al alloys. Chapters 4, 5, 6 and 7 describe the development of new grain refiner for aluminium alloys, in particular for Al-Si shape cast alloys.

Chapter 3 Experimental Procedures

3.1 Materials

3.1.1 Commercial Aluminium and Wrought Alloys

Commercially available aluminium was supplied by *Norton Aluminium Ltd., Staffordshire, UK* , and it was used for grain refinement experiments in the early stage of the grain refiner development. Table 3.1 shows the pure Al with it composition in weight percentage (wt%).

Al	Cu	Mg	Si	Fe	Mn	Zn	Ti	Cr	Ga
99.5	<0.001	<0.001	0.02	0.08	0.001	0.002	0.006	<0.001	0.005

Table 3.1 Chemical composition of commercial aluminium

3.1.2 Aluminium-Silicon Alloys

The binary alloys used for experiments were produced in the BCAST laboratory. The commercial aluminium was melted at 850 ^{o}C in an electric furnace and an Al-50Si alloy with required weight percentage was added to the melt to obtain the required chemical composition. Table 3.2 shows the list of binary Al-Si alloys produced to conduct further experiments.

Composition Alloys	Si	Mg	Fe	Mn	Ni	Zn	Cu	Ti	Al
Commercial pure Al	0.02	<0.001	0.07	0.001	0.001	0.002	<0.001	0.006	99.5%
Al-1Si	1±0.2	<0.001	<0.07	<0.001	<0.001	<0.002	<0.001	<0.006	remaining
Al-2Si	2±0.2	<0.001	<0.07	<0.001	<0.001	<0.002	<0.001	<0.006	remaining
Al-4Si	4±0.2	<0.001	<0.07	<0.001	<0.001	<0.002	<0.001	<0.006	remaining
Al-6Si	6±0.2	<0.001	<0.07	<0.001	<0.001	<0.002	<0.001	<0.006	remaining
Al-7Si	7±0.2	<0.001	<0.07	<0.001	<0.001	<0.002	<0.001	<0.006	remaining
Al-8Si	8±0.2	<0.001	<0.07	<0.001	<0.001	<0.002	<0.001	<0.006	remaining

Table 3.2 Chemical composition in wt% of Al-Si binary alloys

The commercial Al-Si cast alloys were also used in this study to ensure that the novel grain refiner can be used in industry. The alloys used for experiments are given in Table 3.3. Codes used in US industry for these alloys are also given in this table.

Alloy	USA	Si	Mg	Fe	Mn	Ni	Zn	Cu	Ti	Al
LM6	A413	10-11	0.3	0.6	0.5	0.1	0.1	0.01	0.1	remaining
LM24	A380	8.54	0.13	1.2	0.19	0.04	1.36	3.37	0.04	remaining
LM25	A356	6-8	0.3	0.5	0.005	--	0.003	0.003	0.11	remaining
LM13	336	10.5-13	0.8-1.5	1	0.5	1.5	0.5	0.7-1.5	0.1	remaining

Table 3.3 Chemical composition in wt% of commercial Al-Si alloys.

3.1.3 Metal Powders and Plates

The metal powders and plates used for the initial grain refining experiments were supplied by *Alfa Aesar, UK*. They were introduced to the molten alloy with different composition ranging from 0.01 to 5 wt%. Table 3.4 shows the particle size and purity of the powders used in the study.

Metallic Powder and Plate
• Niobium powder, -325 mesh, 99.8% (metals basis) • Molybdenum powder, -325 mesh, 99.9% (metals basis) • Tantalum plate, 6.35mm (0.25in) thick, 99.9% (metals basis) • Tungsten powder, -325 mesh, 99.9% (metals basis) • Potassium tetrafluoroborate KBF_4, 98% • Boron powder, crystalline, -325 mesh, 98% (metals basis) • Boron powder, amorphous, APS <5 micron, 94-96%, Mg nominal 1%

Table 3.4 Powders and plates used in experiments

The particle size of the powders is -325 mesh, which is equivalent to 44 μm. It is important to note that the smaller the particle sizes, the better for its dissolution into the Al melt.

3.2 Casting Processes

Various casting methods were used in order to examine the effect of grain refiners on the microstructure and mechanical properties of the commercial pure aluminium and aluminium alloys. The Aluminium Association Test Procedure-1 (TP-1) mould was used for casting with and without grain refinement. Commercial Al-Si alloys like LM24 and LM6 components were high pressure die cast for metallography study and mechanical property testing. Various steel moulds including steel and V-shape copper moulds were used for general microstructural observation.

3.2.1 Test Procedure-1 (TP-1 test) Mould

There are various factors that can affect the solidification microstructure of a given alloy but one of the important is the cooling rate. By keeping teh cooling rate constant we can examine the effect of heterogeneous additions on the grain size. The standard Test Procedure-1 (TP-1) mould technique was used, to maintain a constant cooling rate. The experimental steps followed in this casting process are:

a) The alloys were melted inside a crucible in an electrical resistance furnace at a preset temperature. The melt was held for 1 hour to homogenize.

b) The TP-1 mould ladle (Figure 3.1) was placed inside a furnace for preheating at 350°C.

c) The water flow rate of the TP-1 mould quench tank was set at 3.8 l/min. This flow rate resulted in 25 mm submersion from the bottom of ladle.

d) Sample preparation for Microstructural study: The test sample removed from the TP-1 conical mould was cut according to the standard procedure (38 mm above the base) as illustrated in Figure 3.1. The cooling rate at this position corresponds to 3.5 °C/s.

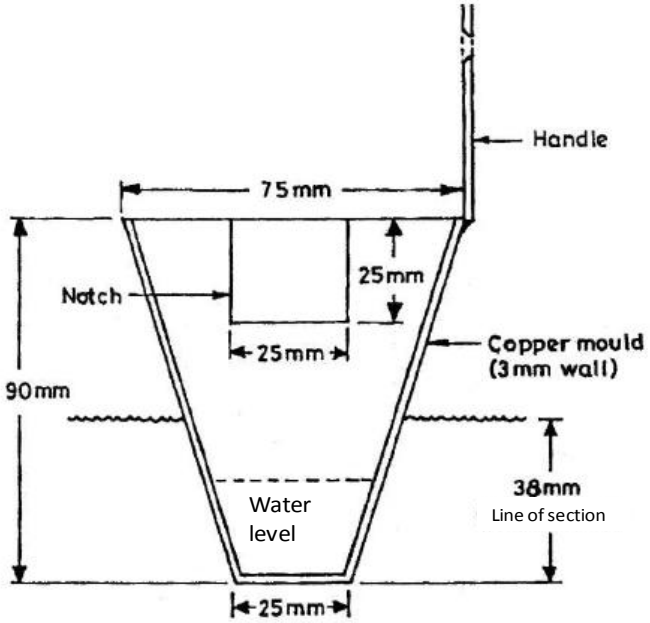

Figure 3.1 Schematic diagram of TP-1 grain refining test mould ladle [The Aluminium Association, 1990].

3.2.2 Cylindrical Moulds and Wedge-shape Moulds

In order to study the effect of cooling rate on grain size, the samples were produced with using different moulds. Two cylindrical moulds, a cone shape mould and a wedge-shaped mould were used to do the experiments. They were always preheated to 200 °C before casting to keep the same solidification conditions for grain size comparison. The cylindrical mould with 40 mm diameter shown in Figure 3.2 a, provides a cooling rate of about 1 °C/s to the melt during the solidification process. Whereas the cylindrical mould with 30 mm diameter (shown in the Figure 3.2b), provides a cooling rate about 2 °C/s. The solidified samples were cut, in the same place, at the middle to investigate the microstructure.

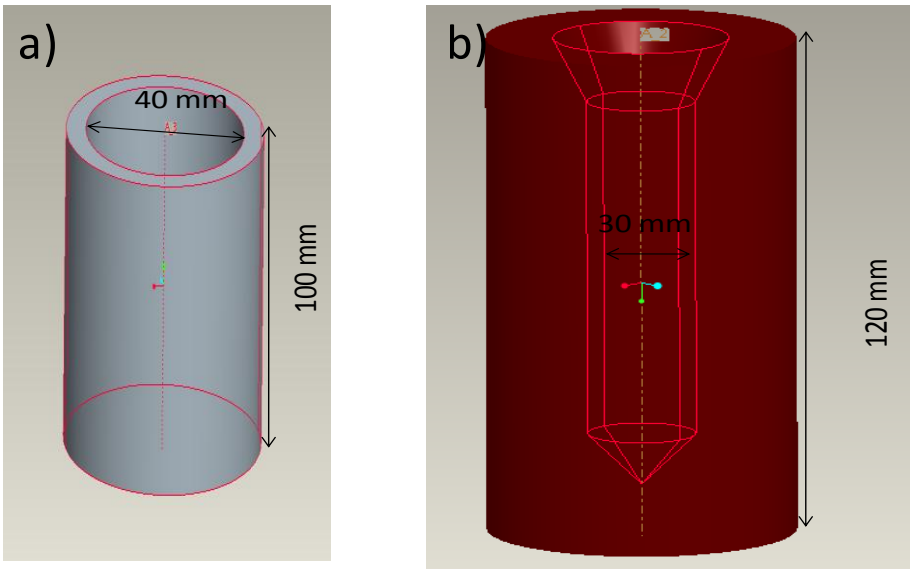

Figure 3.2 Schematic illustration of the cylindrical mould; a) with 40 mm b) 30 mm inner diameter. The wall thicknesses are 25 mm and 40 mm respectively.

The copper mould shown in Figure 3.3 has different cooling rates of 150, 50 and 20 °C/s for the lower, middle and upper positions, respectively (Suarez M.A. 2010). The samples were cut in the middle, along longitudinal direction, to compare the microstructures at various cooling rates.

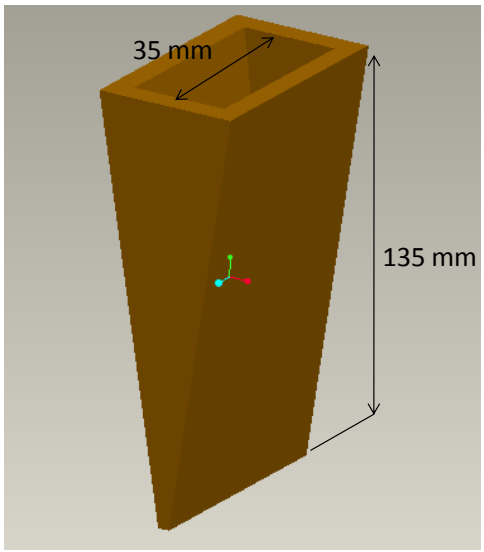

Figure 3.3 Schematic illustration of the wedge-shaped copper mould

Also a cone-shape mould (Figure 3.4) was used to provide slower cooling rate (~ 0.5 °C/s) for the Al-Si alloys with Al-Nb-B master alloy additions with different concentrations.

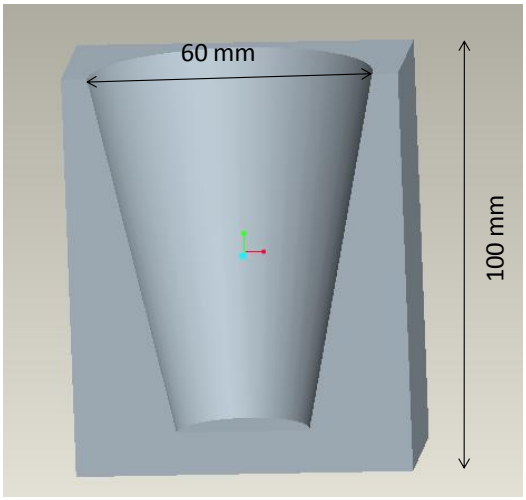

Figure 3.4 Schematic illustration of the cone-shape mould. The thickness of the wall is 25 mm at the top of the mould.

A mould with two cylindrical cavities, shown in Figure 3.5, was used to produce cylindrical bars for tensile test analysis. At first the alloys were cast into the mould then they were machined to appropriate tensile bar shape and dimensions.

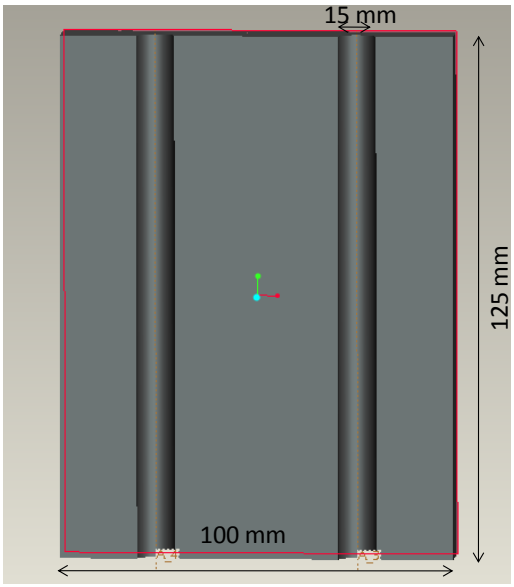

Figure 3.5 Mould for tensile bars preparation

3.2.3 The High Pressure Die-Casting (HPDC) Process

In order to study the microstructure of samples cast at high cooling rates, as well as being able to evaluate their mechanical properties, high pressure die casting was used to produce standard

mechanical property test samples. The HPDC process is well established and widely used as an effective manufacturing technique, especially in the automotive industry. A more detailed understanding of the process and its applications are given by Street (Street A.C. 1977). A standard cold chamber HPDC machine by *LK® Machinery Co. Ltd., Hong Kong* was used and a schematic illustration of the equipment is shown in Figure 3.6. The diameter of the plunger is 60 mm, and has a maximum accelerated shot speed of 6.22 m/s, with the maximum shot distance being 405 mm. The dies were clamped at a load of 280 tones and pre-heated using 8 cartridge heaters embedded symmetrically inside the two halves of the die-block maintaining a uniform temperature across the die-cavity. The settings used for producing LM24 and LM6 tensile bars were: the die temperature 180 °C; the distance of shot 200 mm with the trigger pressure of 70 bars.

The steps followed for the HPDC process are (Oscar Frech GmbH., 2010)

a) Carefully clean the die surfaces of any material left from previous castings and coat with 'Hotemp 2000' lubricant to aid ejection of cast samples.

b) Pour a pre-determined amount of melt at a pre-set temperature (650 ^{o}C) into the shot sleeve of the HPDC machine

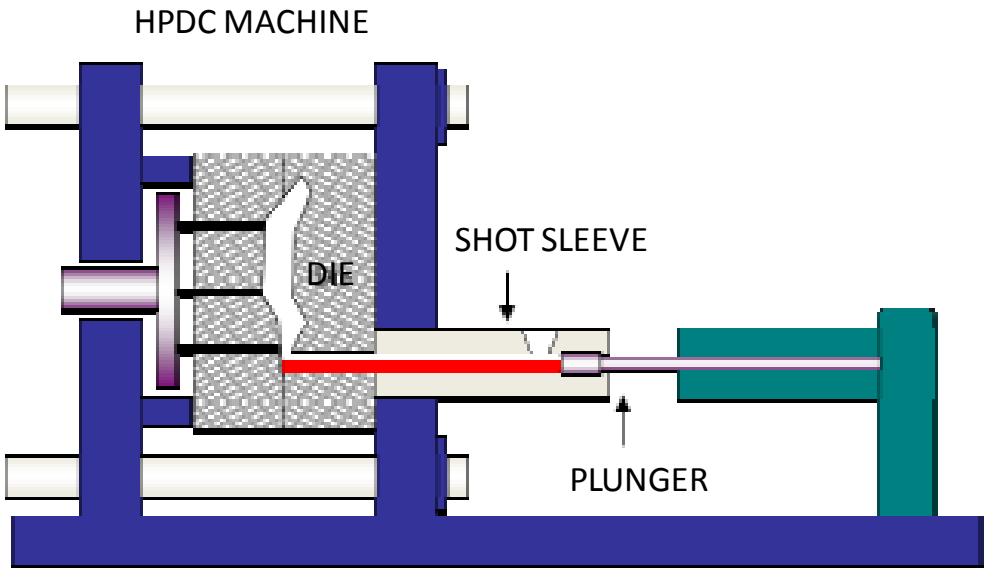

Figure 3.6 A schematic picture of the cold chamber high pressure die casting (HPDC) set-up at BCAST. (Tzamtzis S. 2011)

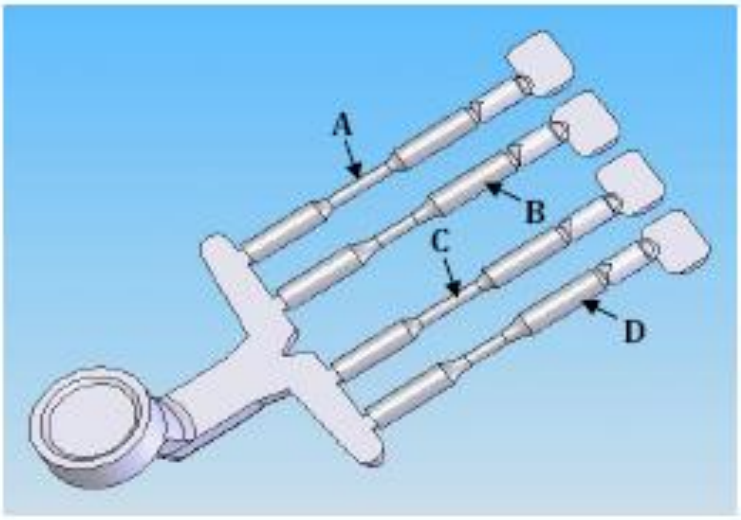

Figure 3.7 Schematic illustration of the samples produced using the die attached to HPDC, showing the two tensile test specimen (labelled A and C) and the two fatigue test specimen (labelled B and D). (Tzamtzis S. 2011) The tensile bars dimensions are as per the ASTM standard.

c) Activate the HPDC machine to apply the shot according to the set profile of the plunger speed, position and pressure. The machine automatically runs through the cycle of injection, intensification, dwelling (while the casting fully solidifies) and finally ejection of the cast component. The die used for the test samples consists of four cavities, two are tensile test samples (labelled A and C) and two are fatigue test samples (labelled B and D) as shown in Figure 3.7. The exact dimensions of the tensile test specimens and the fatigue test specimens are 6.4 and 6.3 mm in gauge diameter respectively, 25 mm in gauge length and 12 mm in diameter of grip section.

3.3 Microstructural Characterization

3.3.1 Metallographic Sample Preparation

Samples were cut from various locations of the final cast components for microstructural characterization. The specimens were prepared by the standard technique of mounting in Bakelite followed by grinding using 120, 500, 800, 1200, 2500 and 4000 grit SiC papers for Al-Si alloys and Mg alloys. The commercial aluminium samples were prepared with two different methods. First method with grinding till 4000 grit SiC paper and then electro-

polished. The electrolyte composition was perchloric acid ($HClO_4$) 20 ml dissolute in acetic acid (CH_3COOH) 80 ml. The sample was dipped in a cool bath and a 30 V (dc) voltage was applied for 2 min. The second method of polishing aluminium was manual using 2500 grit paper and then polishing on cloth sprayed with a paste that contained 3μm diamond suspended particles. Al-Si alloys were ground using - 120, 500, 800, 1200, 2500 and 4000 grit SiC papers and then cloth polished with a silica suspension. The microstructures were examined without etching to reveal primary α-Al grains, intermetallic particles and eutectic phases. In order to reveal grain boundaries, the samples of commercial Al and Al-Si alloys were etched in a solution of 70 ml ethanol, 10 ml water, 20 ml acetic acid and 4.2 grams picric acid for 2 minutes. An optical microscope with polarised light and x plate was used to obtain coloured grain boundaries. For macro-etching the ground samples are immersed in the Tucker's solution (HF 15 ml, HCl 45 ml, HNO_3 15 ml and H_2O 25 m) for10-20 seconds was used.

3.3.2 Optical Microscopy (OM)

A Carl Zeiss Axioskop 2 MAT optical microscope equipped with image analysis software, a camera and a computer was used for the OM observation and the quantitative measurements of microstructural features. A software application was used to acquire images from the camera and to perform image analysis. This microscope was fitted with 2.5, 10, 20 and 50 objective lenses and the corresponding magnifications were 25×, 100×, 200× and 500×. The grain sizes and intermetallics were measured from the images taken at various magnifications. In the bright field (BF) mode, polished surface shows bright in contrast and the surface irregularities such as grain boundaries and intermetallics appear dark in contrast. Plane polarized light (PP) is most commonly used for grain size measurements on colour etched surfaces. The typical micrographs of anodized sample and polished Al-Si alloys are presented in Figure 3.8.

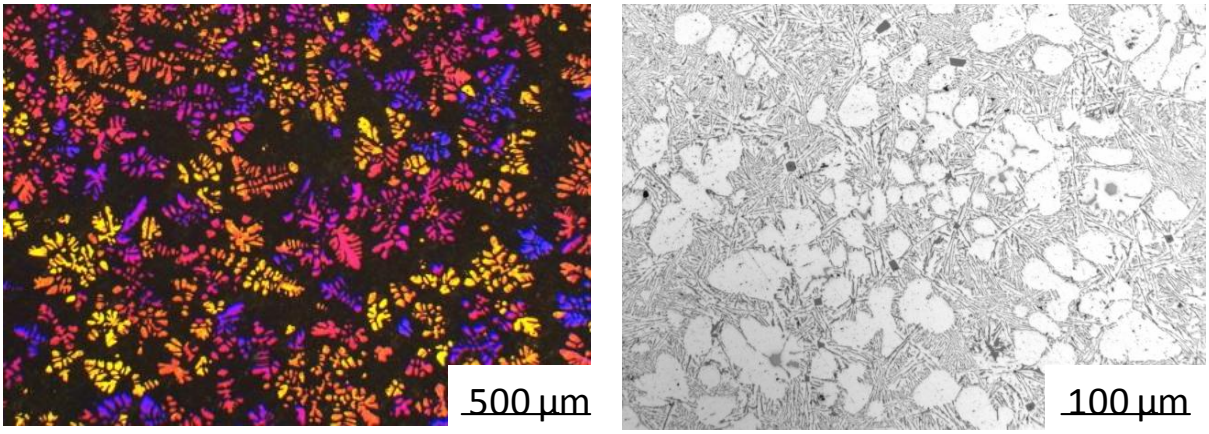

Figure 3.8 Typical micrographs of a colour etched sample and a polished sample (both LM6 with grain refiner addition)

3.3.3 Scanning Electron Microscopy (SEM)

The scanning electron microscope employs the beam electrons directed at the specimen. SEM examinations were performed on the Al-Nb-B novel master alloy sample using a Zeiss Supra 35VP FEG scanning electron microscope. For chemical composition analysis, the SEM equipped with an energy dispersive X-ray spectrometer (EDX), Oxford instruments Inca was used and the data were matrix corrected (ZAF). The advantage of SEM over optical microscopy is the large depth of field and higher resolution, thus producing high resolution images at high magnification (up to 50,000 times). A good explanation of the procedures and the use of SEM and EDX are given by Watt [Watt, 1997]. A sample SEM micrograph and chemical analysis are shown in Figure 3.9.

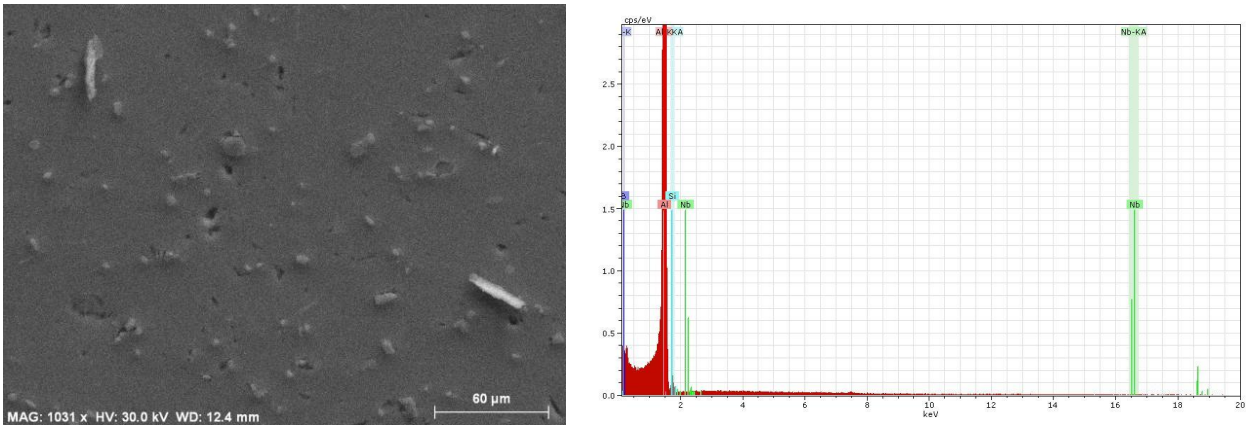

Figure 3.9 Example of SEM micrographs and EDX analysis of the specimen.

3.3.4 Transmission Electron Microscope (TEM)

The transmission electron microscope (TEM) operates on the same basic principles as the light microscope but uses electrons instead of light. What we can see with a light microscope is limited by the wavelength of light. In the TEM technique whereby a beam of electrons is transmitted through an ultra thin specimen, interacting with the specimen as it passes through it. An image is formed from the interaction of the electrons transmitted through the specimen. In this study the TEM was used to investigate the inclusions in the master alloy. A JEOL 2200F field emission gun TEM operating at 200 kV was used in this study. The key step in TEM is to prepare a thin sample suitable to transmit electrons. Discs of 3 mm diameter were punched from the rolled material (~150 μm thick) using a Gatan hole punch. Thin foils suitable for TEM were prepared by electropolishing using a solution of 33 vol.% HNO_3 (nitric acid) and 67 vol.% CH_3OH (methanol) at approximately −30°C and ~25-35 V (~0.1A) on a Struers TenuPol-5 twin-jet electropolishing unit. Upon perforation of the disc, as detected by the photo-sensors, the foil was carefully removed, washed thoroughly in methanol and dried in air. Specimens were observed by TEM within 24 hours of electropolishing. We studied smaller particles down to near atomic levels. The possibility for high magnifications has made the TEM a valuable tool in this research. A typical TEM image is shown in Figure 3.10.

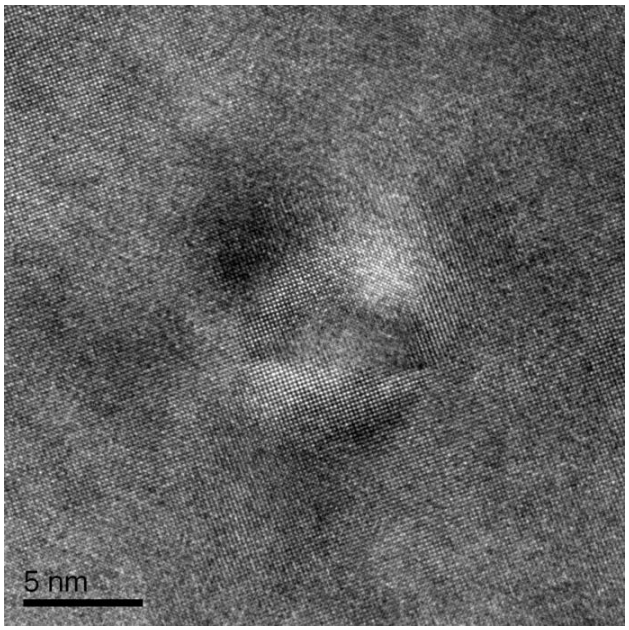

Figure 3.10 TEM image of Al-Nb-B master alloy.

3.3.5 Quantitative Metallographiy

Quantitative metallographic analysis was carried out on OM images using image processing software Axioskop 2 MAT0. The measurements of equiaxed grains and large dendrite grains were carried out on colour etched samples using the mean line intercept method as shown in figure 3.11. The mean intercept length $\bar{l}$, which is used as the grain size,is calculated from the equation:

$$\bar{l} = \frac{L_T}{N_i} \quad \textbf{(3.1)}$$

Where L_T is the total length of the test lines and N_i the total number of grain boundary intersections on each test line. The standard deviation calculations from the average grain size were used as the error in measured grain size.

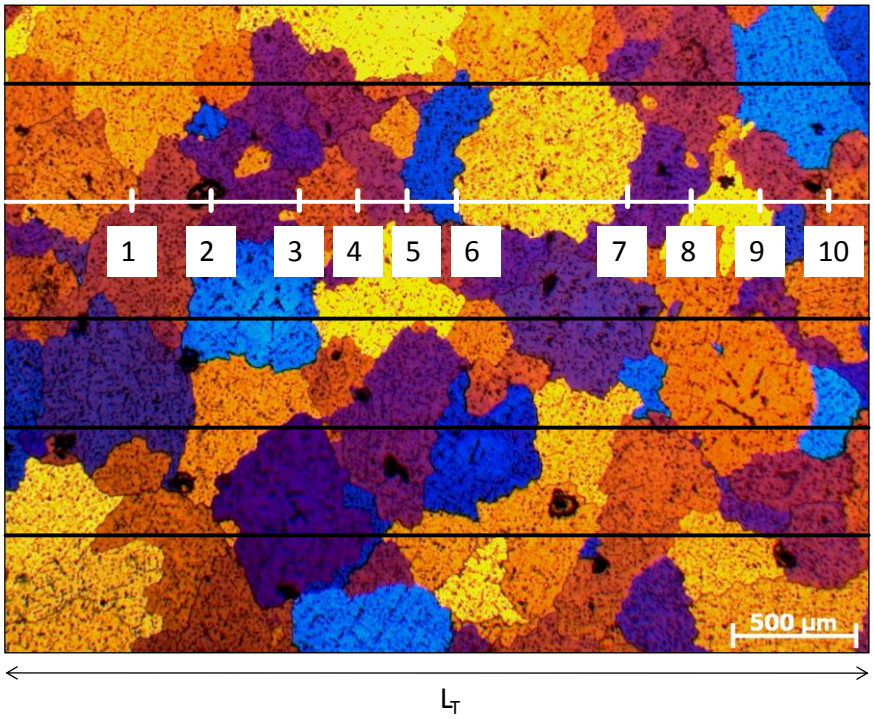

Figure 3.11 Schematic representation of the mean line intercept method performed on the microstructure of an aluminium alloy

3.4 Mechanical Properties Testing

3.4.1 Tensile Testing

The tensile property testing was carried out using a universal materials testing machine (Instron ® 5569) at a cross head speed of 2 mm / minute (strain rate: 1.33×10^{-3} s^{-1}). The tensile

testing system was connected to a PC for automated testing and calculation of tensile test results such as yield stress, ultimate tensile strength and Young's modulus. During the test, a sample is extended at a constant rate, and the load needed to maintain this rate is measured. An external extensometer of 25 mm gauge length was attached to each test sample during testing to get accurate elongation results. The stress σ calculated from the load and cross-sectional area and the strain ε calculated from the extension is plotted as a stress-strain curve, Figure 3.12. The yield strength was measured as 0.2% proof strength on the stress-strain curve. All samples were tested at room temperature.

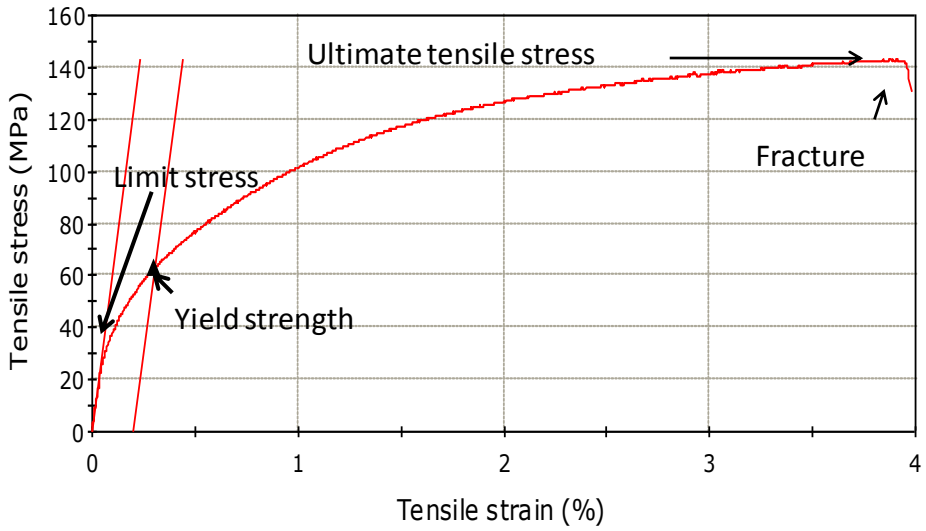

Figure 3.12 The typical stress versus strain curve

3.4.2 Hardness Testing

The Vickers diamond pyramid indentation technique was used to determine the micro hardness of the alloys. Each polished sample was placed on the platform of the test machine and a load was applied on the sample surface with the diamond pyramid to make an indentation point on the sample. The Vickers hardness (HV) is given by the following equation:

$$HV = \frac{F}{A} = \frac{0.1891F}{d^2} \quad \textbf{(3.2)}$$

Where *F* is the force applied to the diamond in kilograms-force and A is the surface area of the resulting indentation in square millimetres. *A* can be determined by the formula:

$$A = \frac{d^2}{2\sin\frac{136^0}{2}} \quad \textbf{(3.3)}$$

The indentation diagonals, d_1 and d_2 are measured and the Vickers hardness is calculated using the average diagonal length *($d = (d_1 + d_2)/2$),* as seen in Figure 3.13, and reference tables are used to convert the measured length to a hardness value. On average, 10 indentations were measured for each sample. A Vickers pyramid hardness testing machine, *Vickers – Armstrongs Ltd., London & Crayford, UK*, was used.

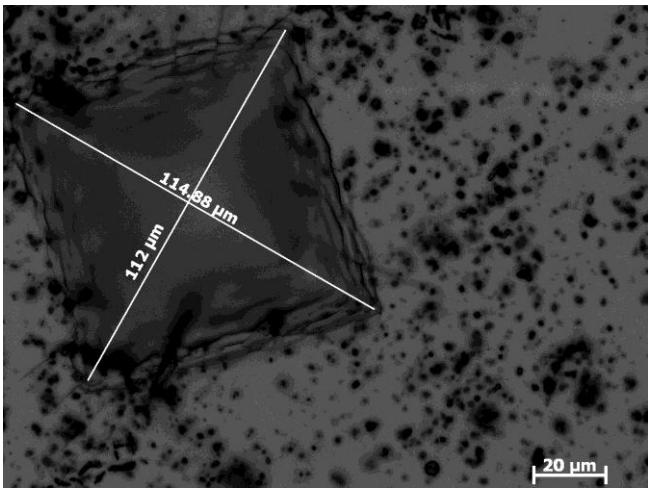

Figure 3.13 Typical indentation in the surface of Al alloy.

3.5 Thermal Analysis

The cooling curves were measured with the use of VI Logger software. The measurements were set up for a time of 1 s. The data provided by VI Logger to produce the cooling curve was the temperature of the melt, logged every 1 s. The data was then plotted into the cooling curve and thermal analysis was carried out. The samples were melted in the furnace and then poured to the crucibles. The measurements of cooling rate began when the thermocouple connected to VI Logger software was inserted into the melt. Thermal analysis was interpreted to see if the heterogeneous nucleation was taking place without and with addition of grain refiners, based on terminologies developed by Bäckerud et al. (Bäckerud L. 1990). The points for thermal analysis shown on Figure 3.14 are:

- T_{nucl}: Start of primary α-Al dendrites nucleation temperature
- T_{minAl}: Unsteady state growth temperature, the temperature beyond which the newly nucleated crystal grows to such extent that the latent heat liberated surpasses the heat extracted from the sample
- T_{gAl}: Recalescence of steady growth due to release of latent heat of primary α-Al dendrites
- ΔT: the undercooling. Temperature difference between unsteady (T_{minAl}) and steady (T_{gAl}) state growth temperatures of primary α-Al particles

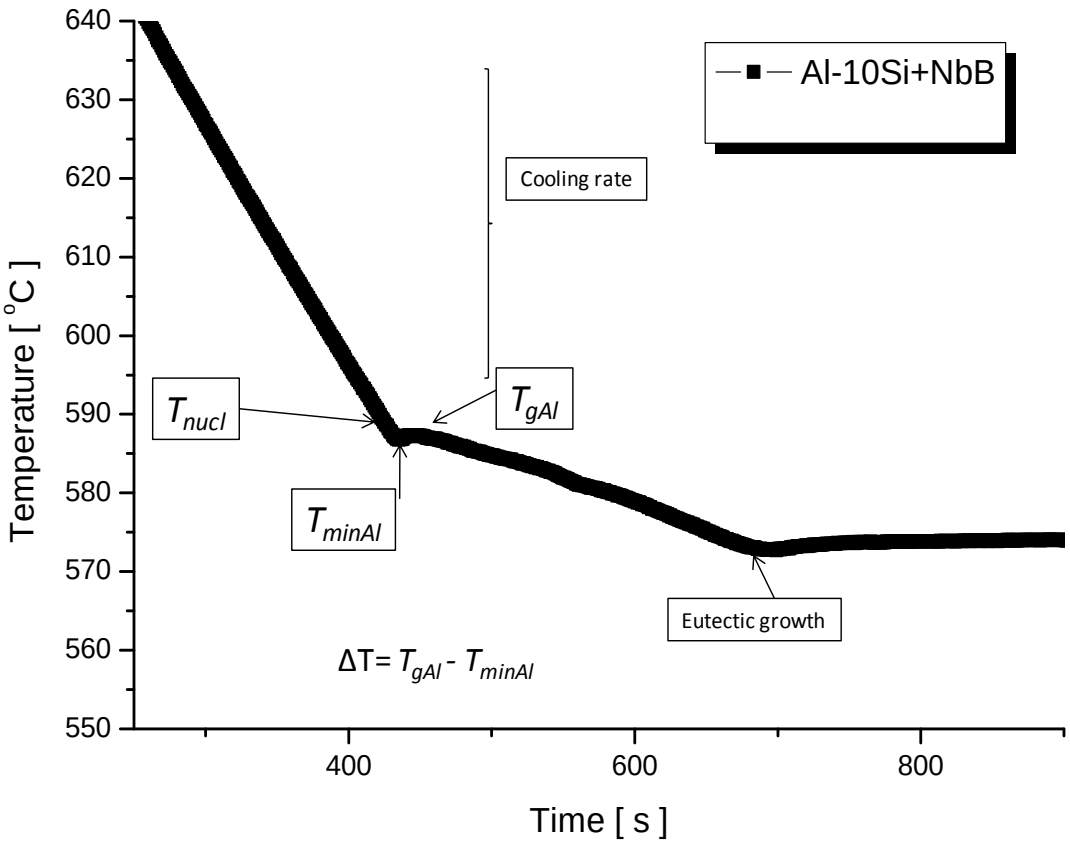

Figure 3.14 Example of a cooling curve of an Al-10Si alloy, with various aspects indicated.

3.6 Summary of Experiments and Alloys Studied.

The experiments were carried out for different alloys using several casting methods and moulds described in this chapter like TP-1, cylindrical moulds (30 mm and 40 mm), V-shape mould, insulated crucible (slow cooling 0.03 °C/s), cone shaped and HPDC , Table 3.6 shows the list of alloys and relevant experiments carried out in this thesis. Also different preparation methods and measurements were used for different alloys. The master alloy was produced with different Nb to B molar ratios. Then the master alloys were added to Al alloys and Table 3.7 shows all the experimental data and analysis performed for these alloys.

	MOULD								Preparation					Measurments			
Alloy	TP-1	30mm	40mm	V-shape	Insulated crucible	HPDC	cone shaped	bars	grinding	dimond polishing	silca suspantion	electro-polishing	Macro-etched	cooling curves	grain size	hardness	tensile test
Al	x							x	x	x		x	x	x	x	x	x
Al-1Si	x								x		x				x		
Al-2Si	x								x		x				x		
Al-4Si	x								x		x				x		
Al-5Si	x				x				x		x			x	x		
Al-6Si	x								x		x				x		
Al-7Si	x								x		x				x		
Al-8Si	x								x		x				x		
Al-10Si	x								x		x		x		x		
Al-12.6Si	x								x		x				x		
Al-14Si	x								x		x				x		
Al16Si			x						x		x				x		
Al18Si			x						x		x				x		
Al27Si			x						x		x				x		
LM6	x	x	x	x	x	x	x	x	x		x		x	x	x	x	x
LM13				x					x		x				x		
LM24	x					x			x		x		x		x		x
LM25	x							x	x		x		x	x	x		x
LM28			x						x		x				x		
LM30			x						x		x				x		

Table 3.6 The aluminium alloys, their experimental preparation and testing

Master Alloy	TP-1	cone shape	bars	30 mm	grinding	silca suspantion	dimond suspention	electro-polishing	Macro-etched	grain size	SEM	TEM
Al-1Nb-1B (MA1)			x	x	x		x	x		x		
Al-2Nb-1B (MA2)			x	x	x		x					
Al-3Nb-1B (MA3)			x	x	x		x					
Al+5NbB$_2$ (MA4)			x	x	x		x	x			x	x
Alloys+MA												
Al+MA1	x				x		x	x		x		
LM6+ MA1	x	x			x	x			x	x		
LM6+MA2		x			x	x			x	x		
LM6+MA3		x			x	x			x	x		
Al-10Si + MA1		x			x	x			x	x		
Al-10Si + MA2		x			x	x			x	x		
Al-10Si + MA3		x			x	x			x	x		
LM25+MA4	x				x	x				x		
LM6+xNbB$_2$	x				x	x				x		
x=0.01-1wt% NbB2												

Table 3.7 The master alloys and their preparation. Aluminium alloys with addition of master alloys and experimental analysis.

Chapter 4. Development of New Grain Refiner

4.1 Introduction

Grain refinement development has scientific and practical significance in alloy casting as a fine and equiaxed grain structure is usually desirable. In this chapter the development of a new grain refiner is described. The grain refinement by inoculation brings many benefits in the casting process and has influence on mechanical properties (McCartney D.G. 1989). It is proven that the fine equiaxed grain structure imparts high yield strength $\sigma_y = \sigma_0 + kd^{-1/2}$ (where σ_0 is the intrinsic yield stress, and k is a constant for a given material), high toughness, good extrudability, and uniform distribution of second phase (Granger D.A. 1998) and microporosity on a fine scale resulting in improved machinability, good surface finish, resistance to hot tearing, and various other desirable properties (Hunt J.D. 1984).Grain refinement is advantageous to the casting process; however, the inoculant particles introduced are sometimes present as unwanted inclusions in downstream processing of ingots (Rooy E.R. 1989). For this reason, and also cost, the amount of master alloy and the volume fraction of inoculants should be minimised, while still obtaining a fine, equiaxed microstructure. This can be achieved through an understanding of the mechanism of grain refinement. In aluminium alloys the most used grain refiners are Al-Ti-B master alloys. Good heterogeneous nucleation site should have a higher melting temperature than aluminium. Attempts have been made in the past to achieve fine equiaxed grain structure in as-cast aluminium alloys by small additions of number of elements, such as Titanium (Ti), Boron (B), Zirconium (Zr), Niobium (Nb), Vanadium (V), Tungsten (W), Tantalum (Ta), Cerium (Ce), (commonly referred to as hardeners), molten metal before casting (Cibula A. 1949-1950). Even though these elements can impart a certain level of grain refinement in aluminium, these have been largely ignored and the research work was highly concentrated on titanium addition to Al. In this research the usage of Mo, Nb, Ta and W as grain refinement in Al alloys was investigated. Based on this research work, we identified that Nb has effective grain refining characteristics and then developed a new grain refiner that consists of niobium and boron. This chapter is focused on the solidification of commercial pure aluminium.

4.2 Phase Diagrams Analysis

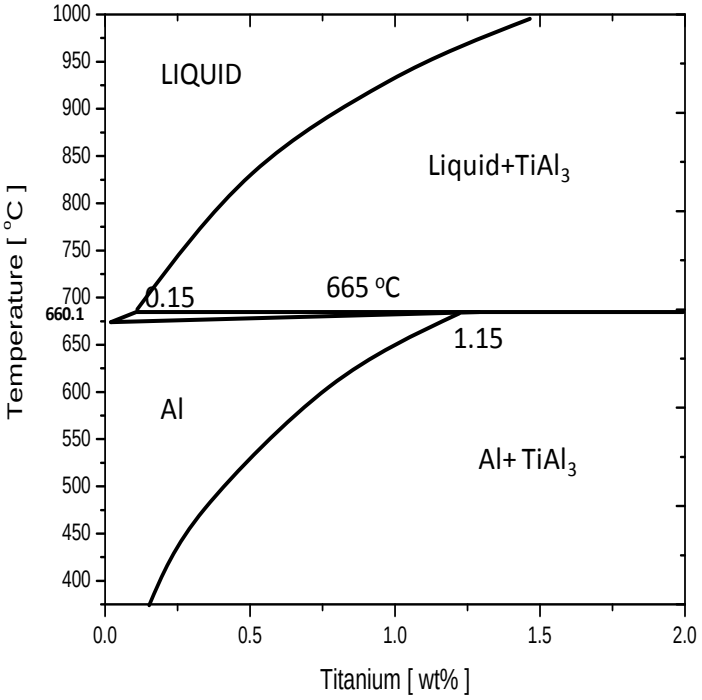

Figure 4.1 Phase diagram of Al-Ti. The peritectic point is 0.12 % Ti and the peritectic reaction occurs at 938 K (664 °C). Al_3Ti formation is a potential nucleation site for heterogeneous nucleation.

Titanium is a well known grain refiner for aluminium. By comparing Al-Ti and Al-Nb, Al-W, Al-Ta, Al-Mo equilibrium phase diagrams, it can be noted that all systems present a peritectic reaction between liquid aluminium and XAl_3 solid particles, where X = Ti, Nb, W, Ta and Mo. In the heterogeneous nucleation process, the lattice match between Al and intermetallic phases is very important (see Chapter 2). For this reason the cell parameters of Nb, W, Ta and Mo phases with Al were analysed to compare them with the well known $TiAl_3$.

At the aluminium end of the Al-Ti diagram there is a peritectic reaction (Figure 4.1):

Liquid + $TiAl_3$ → Al_{ss} (Al_{ss} is Al-Ti solid solution)

This reaction occurs at 938 K (664 °C), in which the liquid contains 0.12 - 0.15 % Ti and the Al_{ss} 1.2 - 1.4 % Ti (Mondolfo F. 1976). The $TiAl_3$ is tetragonal phase with 8 atoms in the unit cell. The lattice parameters are a = 3.851 Å and c = 8.608 Å.

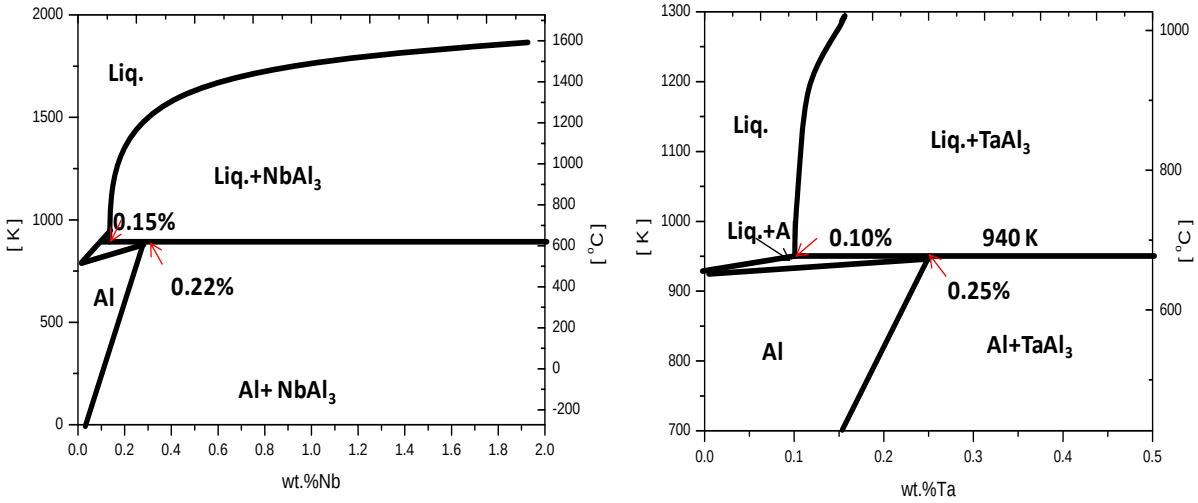

Figure 4.2 The Al-Nb and Al-Ta phase diagram. They are both peritectic with similarities to the Al-Ti diagram. The peritectic point for Al-Nb is 0.15 % Nb and for Al-Ta it is 0.10 % Ta. The formation of intermetalic phases $NbAl_3$ and Al_3Ta occurs in both systems.

Similar to in the Al-Ti system, the potential grain refiners of Nb and Ta also exhibit a peritectic point. The phase diagram of Al-Nb is shown in Figure 4.2 showing the peritectic reaction: Liquid + $NbAl_3$ → $Al_{ss,}$ at the temperature of 934 K (661.4 °C) in which the liquid contains 0.15-0.22 % Nb. Similar to Al_3Ti, $NbAl_3$ is also a tetragonal structure with 8 atoms per unit cell with parameters of a = 3.84 Å, c = 8.58 Å. The Al-Ta phase diagram shown in Figure 4.2 is almost similar to Al-Ti with a peritectic reaction of: Liquid + $TaAl_3$ → Al_{ss}, at 0.25 % of Ta at the temperature of 935-941 K (662-668 °C). The $TaAl_3$ is also tetragonal with 8 atoms to the unit cell with parameters of a = 3.84 Å and c = 8.537 Å. The next two analyses were made for Al-Mo and Al-W. Mo and W have been added to aluminium alloys as grain refiner however with limited success. The phase diagrams (Figure 4.3) shows phase relations.

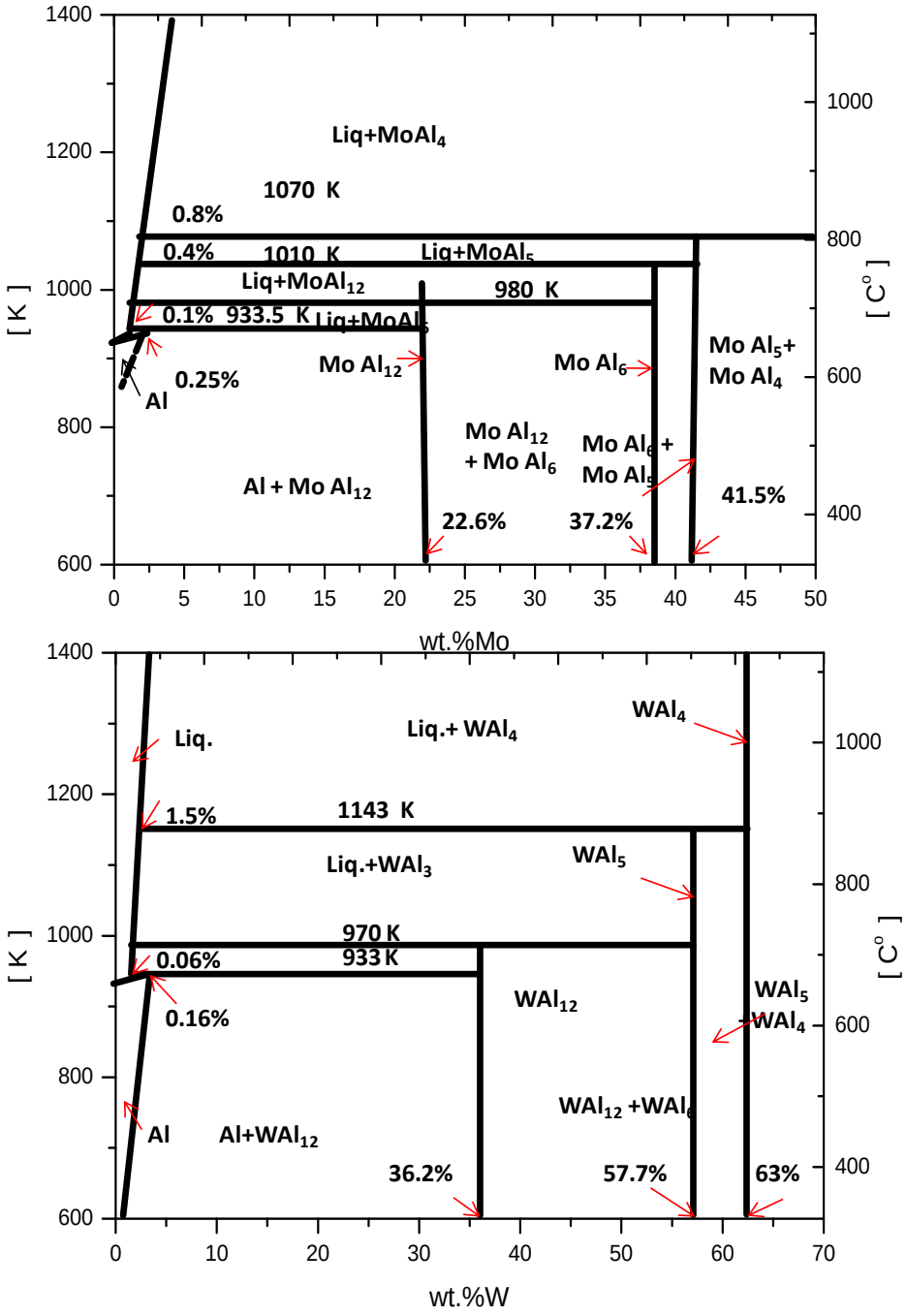

Figure 4.3 Al-Mo and Al-W phase diagram. They are both peritectic with similarities to the Al-Ti diagram. The peritectic point for Al-Mo is 0.10%Mo and for Al-W it is 0.06%Ta. The formation of intermetallic phases $MoAl_{12}$ and $WA1_{12}$ occurs.

The diagrams are more complicated although they exhibit a peritectic point. At the aluminium end there is a peritectic reaction of:

Liquid + $MoAl_{12} \rightarrow Al_{ss}$,

at the temperature of 933.3 K (660 °C) and 0.25 % Mo. The $MoAl_{12}$ forms by peritectic reaction from $MoAl_6$ at 980 K (707 °C). The $MoAl_{12}$ is body centred cubic with 26 atoms in the unit cells and lattice parameters of a = 7.573 Å.

There is also a peritectic reaction for Al-W system as well,

Liquid + $WAl_{12} \rightarrow Al_{ss}$,

at 933.2 with the 0.06 % W and the maximum solid solubility is between 0.16 and 0.20 % W. The WAl_{12} is body centred cubic with 26 atoms in the unit cells and the lattice parameters a = 7.58 Å.

The lattice parameters of Mo, Nb, Ta and W show in Table 2.1 (Chapter 2) have a small mismatch with aluminium. The calculations were made using the equation (Burke J.E. and Turnbull D., 1952, Frank F.C. and Van der Merwe J.H., 1949):

$$f = \frac{lattice\ constant\ of\ solid - lattice\ constant\ of\ substrate}{lattice\ constant\ of\ substrate}$$

where *f* is lattice parameter mismatch.

Lower mismatch chemicals should work as potential grain refiners. A system with good mismatch has a small wetting angle, it is clear that the barrier to nucleation is also small, and this can satisfactorily account for the low undercoolings. Turnbull and Vonnegut (Vonnegut B. and Turnbull D., 1952) related undercooling necessary for heterogeneous nucleation to the mistmatch between the lattices of the crystal nucleus and substrate at the interface.

4.3 Results and Discussion

The purpose of the present study was to examine the influence of Mo, Nb, Ta and W on gthe rain refinement of aluminium in order to find a new potential element which could replace Ti. The literature suggested that refractory metals will diffuse in Al even in lower temperatures. The dissolution of solid metal in liquid metal is described by the equation:

$$c = c_s \left[1 - exp\left(-\frac{kst}{v}\right)\right] \quad \textbf{(4.1)}$$

Where c is the concentration of the dissolved metal in the bulk of the melt measured at the time, t, c_s is the saturation concentration, k is the dissolution rate constant, s is the specimen surface area and v is the melt volume (Yeremenko V.N. 1981). Table 4.2 shows the solubility levels for Nb, Ta, Mo and W at different temperatures. From those solubility levels the experiments were planned. The melting temperature used for most of the samples was 720 °C and the additions were between 0.1-2 wt%.

T(°C)	700	750	800	850
Nb	0.0197	0.0337	0.057	0.101
Ta	0.105	0.17	0.25	0.37
Mo	0.215	0.44	0.71	1.14
W	0.230	0.40	0.84	1.16

Table 4.1 The solubility of the refractory metals in liquid aluminium in weight % (Yeremenko V.N. 1981)

Table 4.3 presents the physical properties of the refractory elements, niobium, molybdenum, tantalum and tungsten. The melting temperature is higher than Al which is good for refinement.

	Nb	$NbAl_3$	Mo	$MoAl_{12}$	Ta	Al_3Ta	W	$WA1_{12}$
Melting point °C	2468	1680	2610	-	2996	1551	3410	-
Density g/cm^3	8.4	4.54	10.2	-	16.6		19.3	-

Table 4.2 The physical properties of the refractory elements, niobium, molybdenum, tantalum and tungsten.

4.3.1 The Mo, W, Nb and Ta addition to Al

The influence of Mo, W, Nb and Ta on the grain size of Al was investigated by way of simple experiments. Since molybdenum has good lattice match, it was added with different concentrations to molten Al. The melt was held in the furnace for about 1 h to dissolve the Mo in Al. The melt was mixed several times to spread the particles in all Al and cast in the crucible with the slow cooling rate about 0.4 °C/s. The etched microstructures shown in Figure 4.4 reveal that the different addition of Mo has an effect on the grain sizes; however this is not very significant. From the pictures we can clearly see that equiaxed grains form in the sample with 1 % Mo the

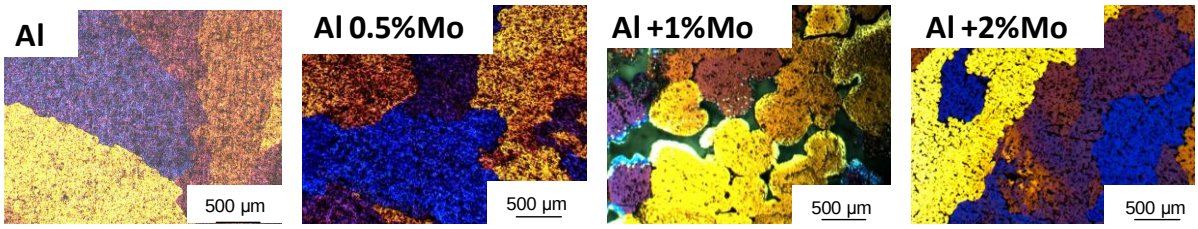

Figure 4.4 The colour etched microstructure of Al with addition of Mo with 0.5, 1 and 2 weight %. Melted at 720 °C and solidified in the small crucible (Chapter 3) with a cooling rate of approximately 0.4 °C/s.

The research trials were continued with tungsten. Tungsten has very high density 19.25 gcm^{-3}, and it is the second heaviest metal in the earth. The high melting point of 3410 °C makes it a potential grain refiner for aluminium. The pure aluminium was melted at 720 °C and different additions, 0.1-2 wt %, of tungsten were added to the melt. The cooling rate of this casting was 0.4 °C/s. Figure 4.5 shows the colour etched samples of Al with W. The influence of tungsten on grain refinement of aluminium is negligible. Unfortunately, we could not observe the grain refiner effect of W on aluminium. This could be due to too long a holding time of about 1h and to its very high density. Considering the low cooling rate in the experiment, all the particles could have settled in the crucible, thus minimising the number of heterogeneous nucleation sites.

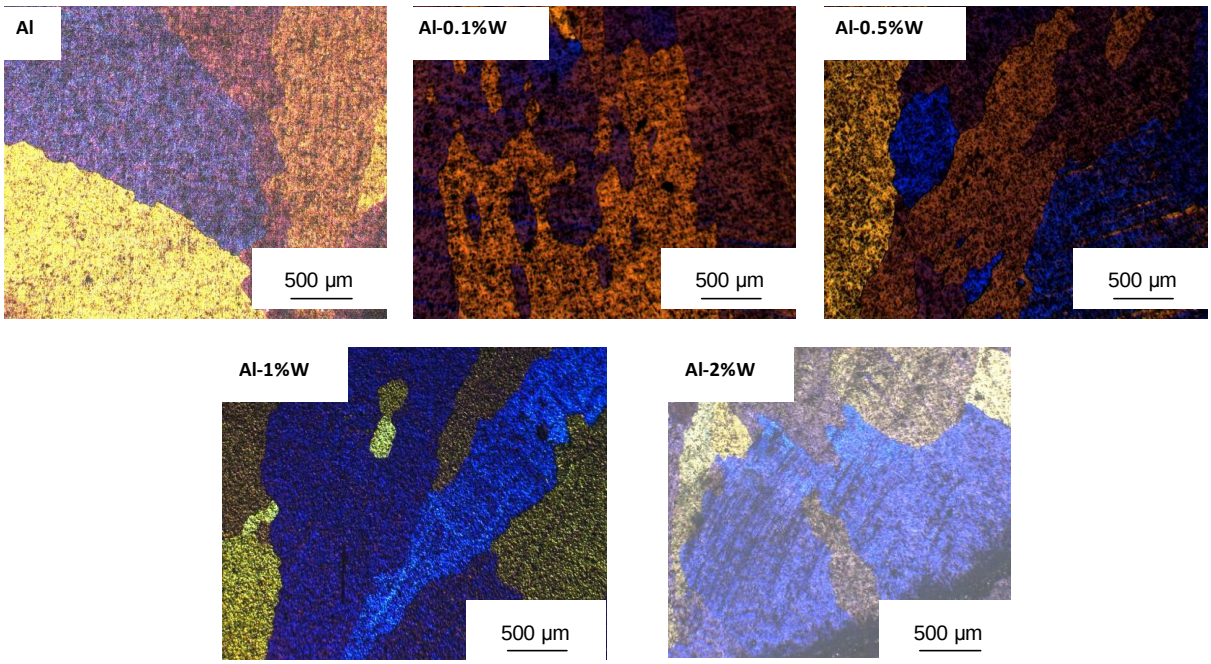

Figure 4.5 The colour etched samples reveal the grain sizes of commercial aluminium and Al with different additions of W (0.1-2 wt. %) melt at 720 °C and solidified in the crucible. Overall the grain sizes of Al with addition of W are finer although not significantly. The cooling rate was very slow, approximately 0.4 °C/s.

For the experiments with tantalum we used a plate to see if it diffused into the aluminium at low temperatures and if it has any influence on grain size. Figure 4.6 shows the effect of the tantalum plate on Al and the effect of the small plate particles mixing. The tantalum lattice parameters are very similar to titanium; respectively a = 3.84 Å and c = 8.537 Å and a = 3.851 Å and c = 8.608 Å. Alloys based on the Al-Ta systems are promising candidate materials for various structural applications. Those alloys have excellent potential to become important next generation aerospace materials because of their low density, high melting temperature, good elevated-temperature strength, high resistance to oxidation and hydrogen absorption, and excellent creep properties.

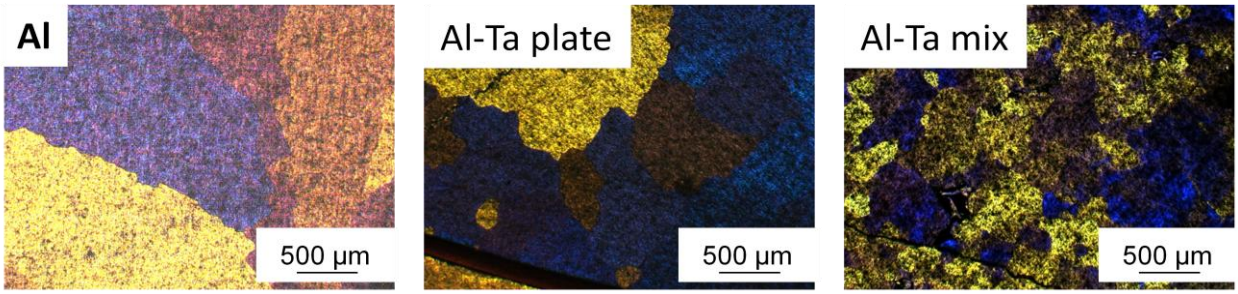

Figure 4.6 The colour etched samples revealing the grain sizes for commercial pure aluminium and Al with the addition of Ta in plate form and with little pieces (~2 mm x 2 mm) mixed together. The samples were melted at 720 °C and solidified in the crucible with addition of 1wt% of Ta. Overall the grain sizes of Al with addition of Ta are finer. The cooling rate was very slow, approximately 0.4 °C/s.

The micro-etched samples revealed that the tantalum acts like a grain refiner in aluminium. The grain morphology is equiaxed and the size is ~400 µm. The next step was to investigate the niobium diffusion on Al.

In the literature there are relatively low reports regarding niobium's influence on aluminium. However, it is generally known that niobium base alloys are prime candidates for many high-temperature aerospace applications, due to their high melting temperature, excellent high-temperature creep and oxidation resistance of several aluminide and silicide phases (Munitz, Gokhale and Abbaschian 2000). In this respect, many studies have focused on evaluating the potential of Nb aluminides, monoliths, and composites. Niobium aluminides are of interest as candidates for high-temperature structural materials due to their high melting point, high elastic modulus, excellent oxidation resistance and low densities. In addition, Nb_3Al has also been considered for high-magnetic field applications, due to the superconductivity in this phase (Lo K. 1977, Takeuchi T. 2005).

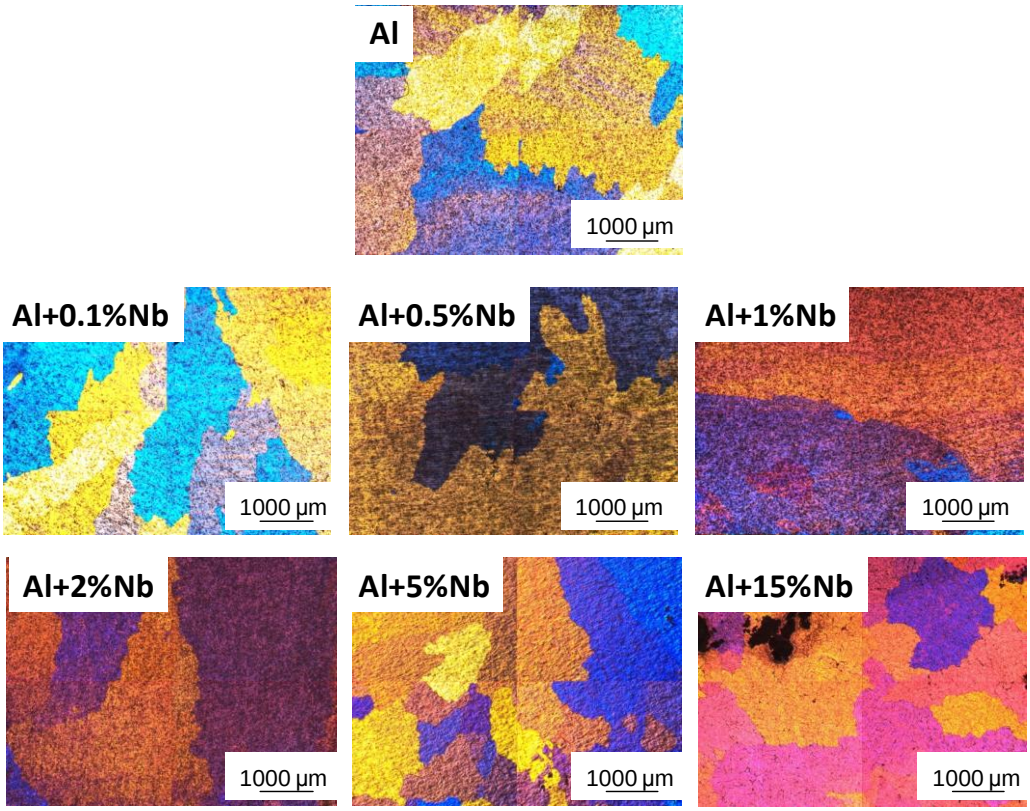

Figure 4.7 Etched samples revealing the grain sizes of commercial aluminium and Al with different addition levels of Nb (0.1-15 wt. %) melt at 720 °C and solidified in the crucible. Overall the grain sizes of Al with addition of Nb are finer however not significantly. The cooling rate was very slow, approximately 0.4 °C/s.

The pure Al and Al with different addition of Nb (0.1-15 %) content were melted at 720 °C and solidified in the crucible with a cooling rate of about 0.4 °C/s. The results were not as expected by Pontes (Pontes P.S. 1979). Overall the grains were large as shown in Figure 4.7, although in bottom parts of the crucible we could notice smaller grains. This was due to the Nb which did not diffuse properly and all the particles settle down at the bottom of the crucible. All microstructures were taken from the middle of sample.

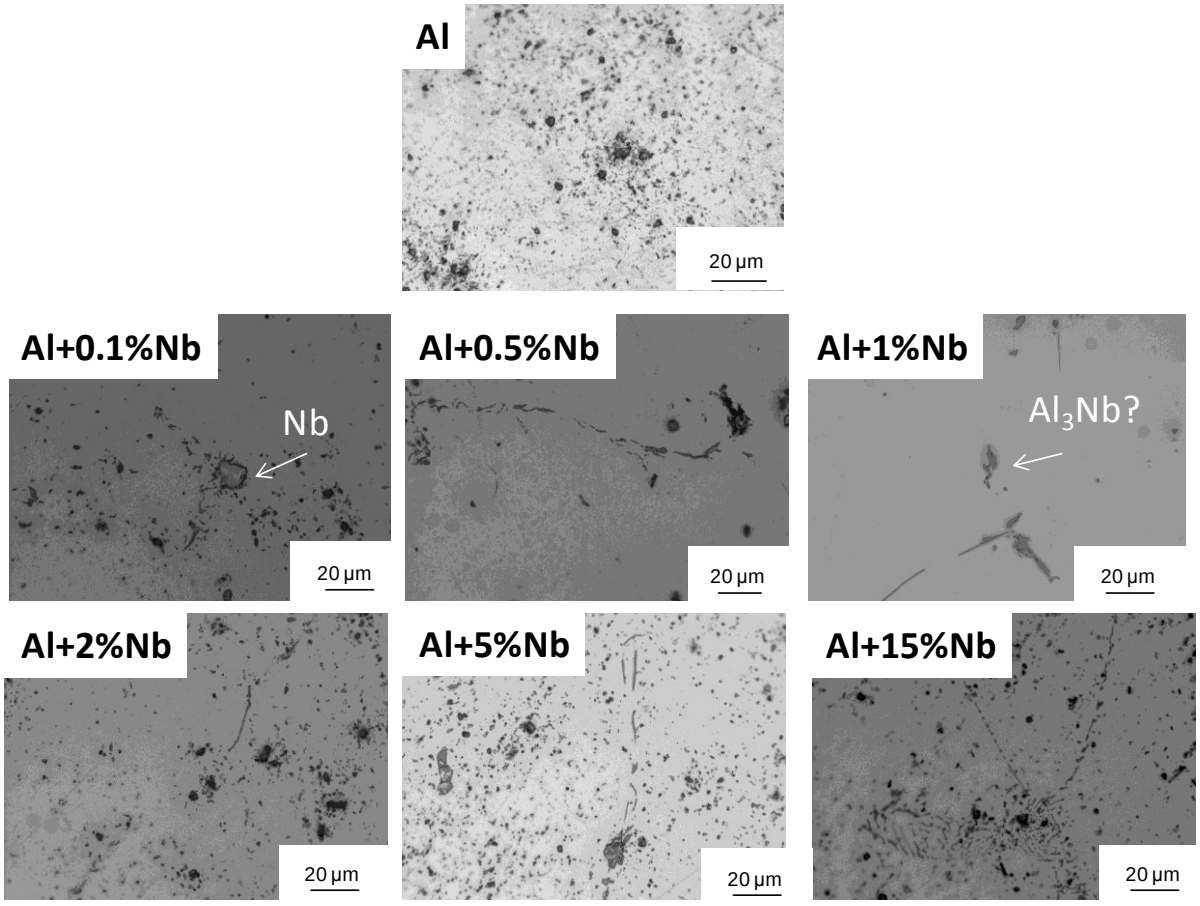

Figure 4.8 The microstructure of commercial Al and Al with different additions of Nb. The intermetallics of Al_3Nb and unmelted Nb are apparent in the pictures

The intermetallic compounds of Nb and $NbAl_3$ were observed in the microstructure of Al with different additions of Nb as shown in Figure 4.8. Niobium has a higher density (8.57 $g \cdot cm^{-3}$) than aluminium (2.70 $g \cdot cm^{-3}$) and without mixing the niobium will settle at the bottom of the crucible (Figure 4.9.) The literature suggests that some of the particles form Al_3Nb (Clyne T.W. 1980) and according to x-ray analyses made by Brauer (Brauer G. 1939), this phase forms at 700°- 850 °C in the Al-Nb system.

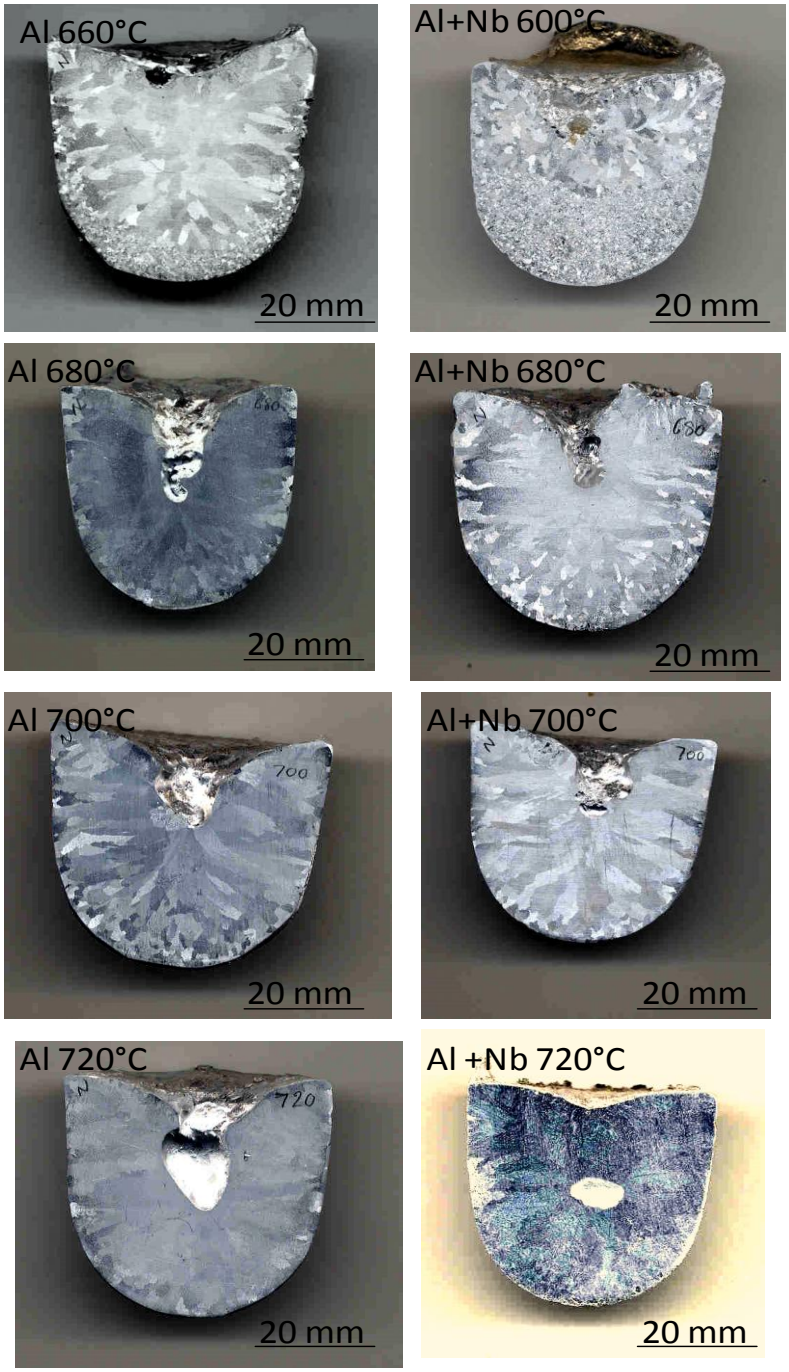

Figure 4.9 Influence of different melting temperatures on grain structure. a) The samples of commercial aluminium melted at 750 °C with 1wt% of Nb and cast in the crucible. The melt was mixed until it reached the desired temperature and then was left to solidify. b) The Al with addition of Nb melted at 750 °C and then mixed until it reached the desired temperature and left until it was cast. The Al-Nb samples have smaller grain sizes in the bottom of the crucibles

The experiments were done for Al and Al with addition of Nb. Aluminium was melted in 750 °C, the Nb was added and held for 1 h in the furnace. The melt was mixed to achieve appropriate temperature and left to solidify in the crucible. Small grain sizes are noticeable only at the bottom of the crucible as shown in Figure 4.9. Figure 4.10 shows the schematic illustration of the particles at the bottom of the crucible and microstructures.

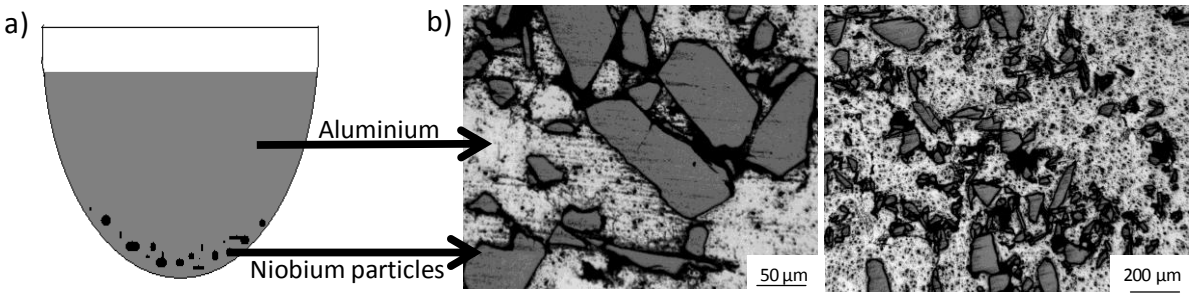

Figure 4.10 a) Schematic illustration of the cross section of the Al containing Nb cast in the crucible. Nb particles settlement is depicted in the picture. b) Microstructures revealing unreacted Nb particles that are not dissolved in Al.

One of the reasons that we could not obtain appropriate fine grain sizes is because the solidification was carried in a small crucible with a slow cooling rate, which will affect the grain size (Easton M.A. 2008).

Figure 4.11 shows the transformation of unmelted Nb particles with 4 interfaces. Different Nb contents to the pure Al produce different microstructures: Nb_{ss}, Nb_3Al, Nb_2Al and $NbAl_3$. The phase diagram shows the composition of the intermetallic phases of Nb with aluminium. The literature suggests that $NbAl_3$ phase always forms even in low temperatures like 700°C (Slama G. and Vignes A. 1971). The operational conditions of Al_3Nb substrate formation and Al_3Nb particle coalescence is extremely important in a grain refinement process based on established chemical principles (Pontes P.S. 1979).

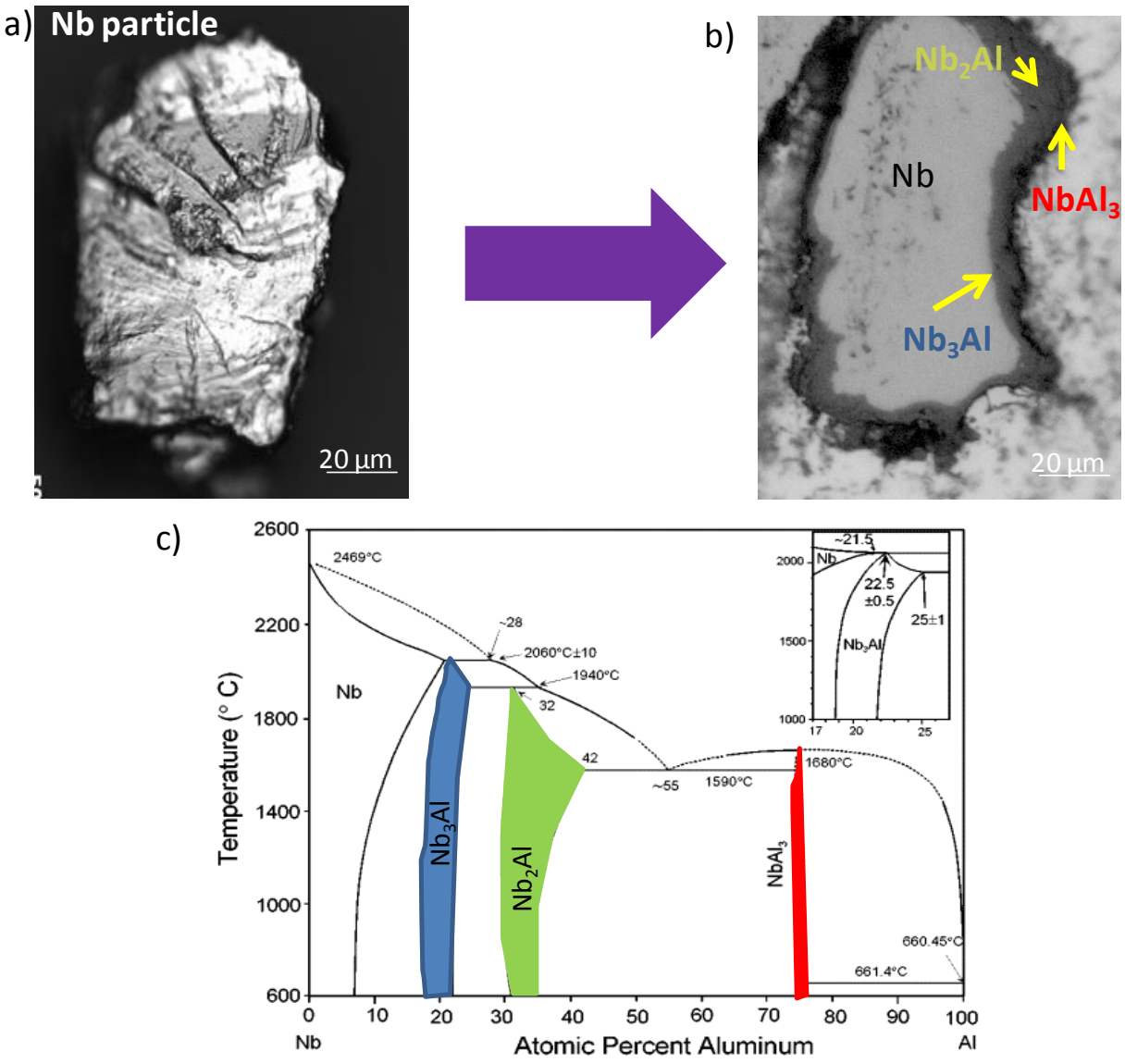

Figure 4.11 The phases formed between Nb and Al. a) Microstructure of Nb powder, b) The Nb particle melted in Al consisting of 3 new phases Nb_3Al, Nb_2Al and $NbAl_3$. c) The phase diagram of Nb-Al system showing Nb_3Al, Nb_2Al and $NbAl_3$ intermetallic phases

Since Nb is a superconducting material with transition temperature of 9 K, the presence of any unreacted Nb can be detected by measuring the magnetic moment. The commercial aluminium was melted at 750 °C and the 5wt% of niobium was added to the melt to prepare a sample for the magnetic moment measurements. The sample was placed in a SQUID magnetometer which measured the magnetic moment as a function of temperature under a 100 Oe magnetic field. The diamagnetic moment was found and the superconducting transition temperature was

measured to be 9.2 K, suggesting that all Nb did not transform to Al_3Nb phase under these melt condition.

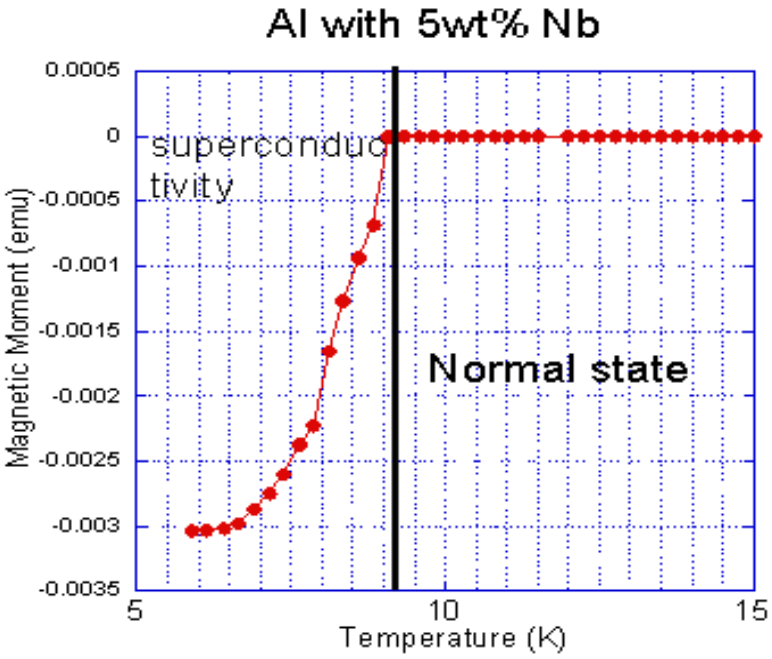

Figure 4.12 The magnetic moment as a function of temperature under 100 Oe applied magnetic field for 5 wt% Nb containing Al. Average Nb particle size is 100 µm. Superconductivity is observed due to unmolten Nb metallic powder.

Further the temperature was increased to 800 °C and the holding time was 2h after addition, the mixing was also optimized and the TP-1 test was used for casting to obtain appropriate results. The equiaxed grain size varies strongly with the solidification condition (Quested T.E. and Greer A.L. 2005). For this experiment all samples were prepared under the same conditions and pouring temperatures.

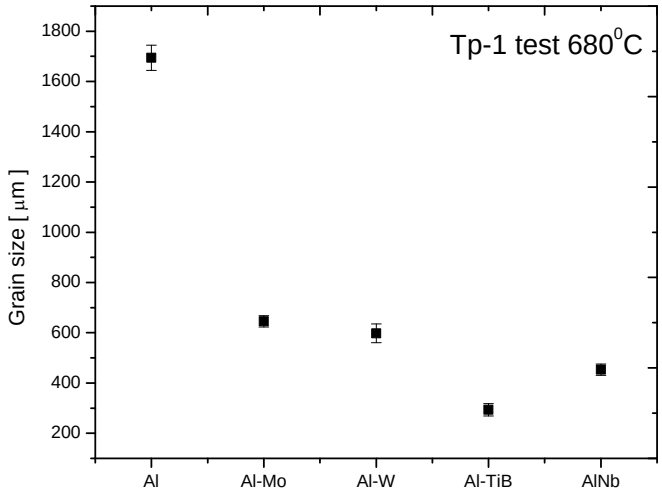

Figure 4.13 The TP-1 test was done to calculate the grain sizes of Al with addition of Mo, W, Al-5Ti-B and Nb. The TP-1 test is expected to provide constant cooling rates thus enabling the comparison of grain sizes with the addition of various chemicals. Aluminium with the addition of refractory metals has smaller grain sizes.

Figure 4.13 shows grain sizes for commercial aluminium without any addition and with the addition of 0.1 wt% of Mo, W, Nb and well known grain refiner, Al-5Ti-B. The results show that the elements can be grain refiners are not good enough to replace commercially known Al-5Ti-B grain refiner.

Further research investigates the influence of Mo, Nb, W and Ta on hardness of commercial aluminium. Generally the hardness improvement of Al is done by work and age hardening or heat treatment. The Nb, Mo, W and Ta are well known hardeners for superalloys solid solution like Nickel (Guo E. and Ma F. 1980) or steels. The tests were done to investigate Vickers hardness of Al with different addition of those elements. The hardness is increased by about 30%.

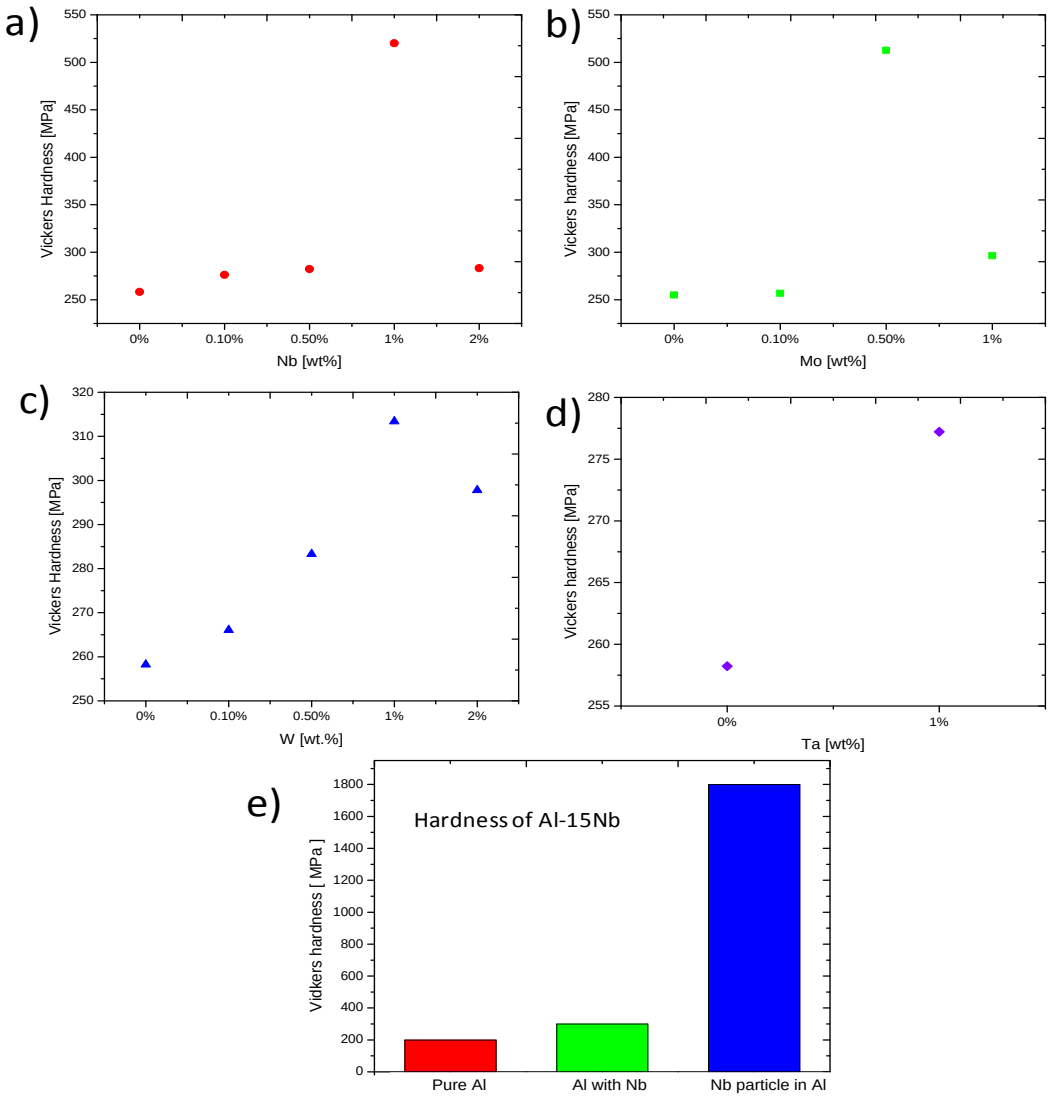

Figure 4.14 The Vickers hardness was analysed to check whether the refractory metals have any influence on improving the mechanical properties of aluminium or not. a) The diagram of Al with different additions of Nb shows that the hardness improved with 1%Nb. b) The diagram of Al with different addition of Mo shows that the hardness improved with 0.5% Mo. c) The diagram of Al with different additions of W shows that the hardness improved with 1%W. d) The diagram of Al with addition of Ta shows that the hardness improved with 1%Ta. e) The Vickers hardness for commercial aluminium; Al with Nb and unmelted Nb particles in Al-15Nb alloy. The results cannot be analysed properly as the samples weren't properly molten and some of the powders didn't diffuse to the melt.

4.3.2 The Nb-B Grain Refiner Discovery

Our research was based on proposed nucleation theories for Al-Ti-B grain refiner. The nucleant-particle theories and the phase diagram theories are related to two types of particles present in the Al-Ti-B master alloy. The first theory suggests that the nucleation occurs on the borides in master alloy (TiB_2, AlB_2 and (Ti, Al)B_2), while the second theory explains the grain refinement by nucleation on Al_3Ti, the hypoperitectic phase. The nucleant-particle theories were proposed by Cibula (Cibula A. 1949-1950). He suggested that nucleation happened on the borides or carbides when they were present. Schumacher and Greer (Schumacher P. and Greer A.L. 1995) gave the most sensible evidence for boron addition. They proposed that a layer of Al_3Ti forms at the boride-melt interface which in turn nucleates α-Al. The joint addition of both titanium and boron is responsible for a grain refining effect larger than the addition of either element singly (Delamore G.W. and Smith R.W. 1971). Our research analysed the lattice parameters for NbB_2 and TaB_2. The parameters are respectively a = 3.102 Å, c = 3.285 Å and a = 3.074 Å, c = 3.209 Å (Shein R. 2008).The experiments were done to see the influence of borides and carbides on grain refining of Al.

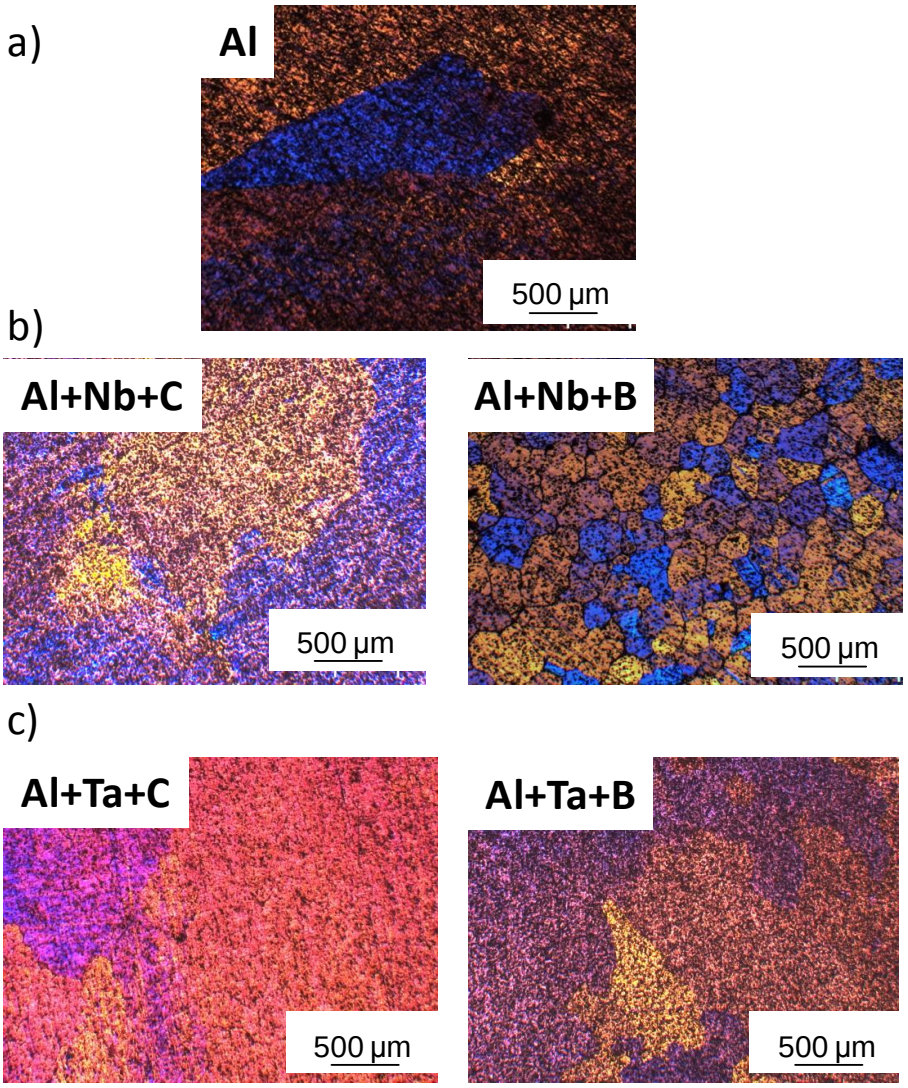

Figure 4.15 The colour etched samples of Al with addition of Nb and Ta revealing the grain sizes. Nb, Ta, B, C were added to the, Al melt at 750 °C and the melt was left to solidify in the crucible. a) Commercial aluminium, b) Al-1Nb with addition of 0.1 wt% carbon and 0.5 wt% boron, c) Al-1Ta with C and B. Among these experiments, the Al with Nb-B addition has shown the smallest grain size.

The pure Al was melted at 750 °C, the elements of Nb-C, Nb-B, Ta-C and Ta-B were added and held for 1h. Then the crucibles with the melt were removed from the furnace to solidify. Figure 4.15 presents the colour etched microstructures of the above additions. The results achieved by addition of Nb and B powders are remarkable. The grain sizes were about 350 µm. The existing literature makes no mention of the addition of Nb and B together to

aluminium for grain refinement. During the experiments we faced the problem of adding the Boron powder to Al properly. The boron density of 2.08 $g \cdot cm^{-3}$ is lower than aluminium of 2.40 $g \cdot cm^{-3}$, which means that it flows at the surface of liquid Al and also, due to non-wetting behaviour with liquid Al, it is difficult to introduce it into the melt. In industry, Potassium Fluoborate KBF_4 is a key ingredient in grain refining composition for aluminium and can be used separately or combined with Potassium Titanium Fluoride (K_2TiF_6) to form grain refining flux. Titanium and other elements like Nb can form TiB_2 and other borides that act as grain nucleation agents, providing a cast structure of fine grains. To enable boron to enter into liquid melt, in the later stages of research an addition of KBF_4 was introduced to the melt, instead of boron powder.

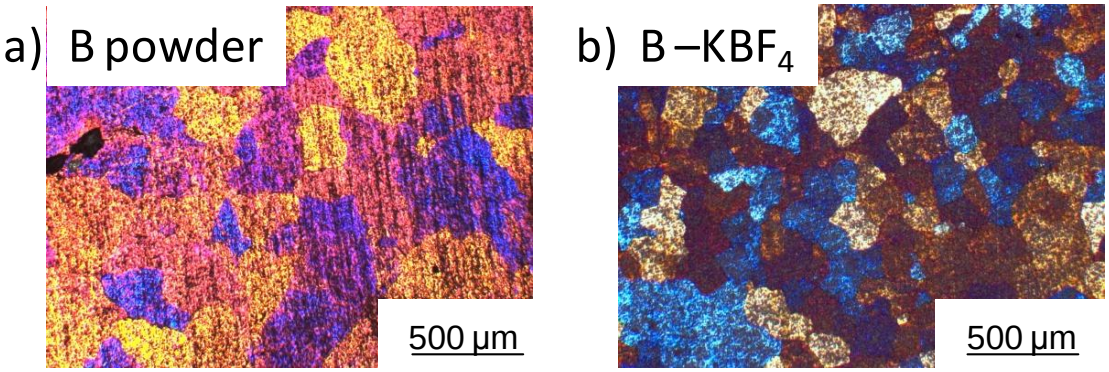

.

Figure 4.16 The colour etched samples of Al with 0.1 wt% Nb and 0.5 wt% B addition. Al was melted at 750 °C, Nb and B or KBF4 are added to the melt. The melt was mixed until the temperature reached 680 °C and then cast. a) The Boron is in the form of crystallized powder, b) Boron in the form of flux salt addition KBF_4 (Potassium Fluoborate)

The boron and titanium salts are known to dissolve and react with aluminium in the following chemical reaction:

$$17Al+2K_2TiF_6+2KBF_4 \rightarrow TiB_2+TiAl_3+6KF+14AlF$$

When Nb and KBF_4 are used the reaction will be similar to the above:

$$5Al+2Nb+2KBF_4 \rightarrow NbB_2+NbAl_3+2KAlF_4$$

The reaction between salt and Al is known to be exothermic and the local temperature of the melt is expected to reach >1500 $^{\circ}C$ for a short period. As a result, the addition of KBF_4 salt

was observed to be highly effective in dissolving Nb. After the microstructural analyses, no unmelted niobium was found. To confirm that the Nb was completely melted, the magnetic moment was measured using a SQUID magnetometer. The addition of flux salt resulted in the absence of diamagnetism suggesting that the Nb completely dissolved in Al as shown in Figure 4.17. The standard production of Al-B master alloys involves direct addition of KBF_4 salt into molten aluminium (Wang X. 2005).

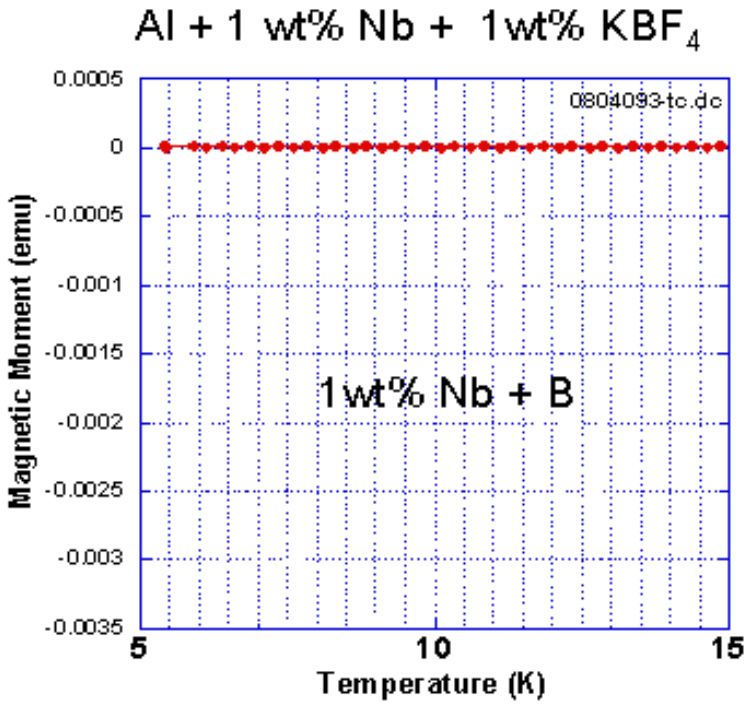

Figure 4.17 Magnetic moment of Al + Nb + KBF_4 sample. The addition of KBF_4 flux salt resulted in the absence of diamagnetism suggesting that the Nb completely dissolved in Al.

It is well known that the addition of Al-5Ti-B to Al decreases the undercooling. At atmospheric pressure pure aluminium has a unique melting point at 933 °K (660 °C), which is co-incident with its freezing point when solidifying from liquid to solid. Experimentally the freezing point may be determined by measurement of a cooling curve from liquid to solid, as shown schematically in Figure 4.18.

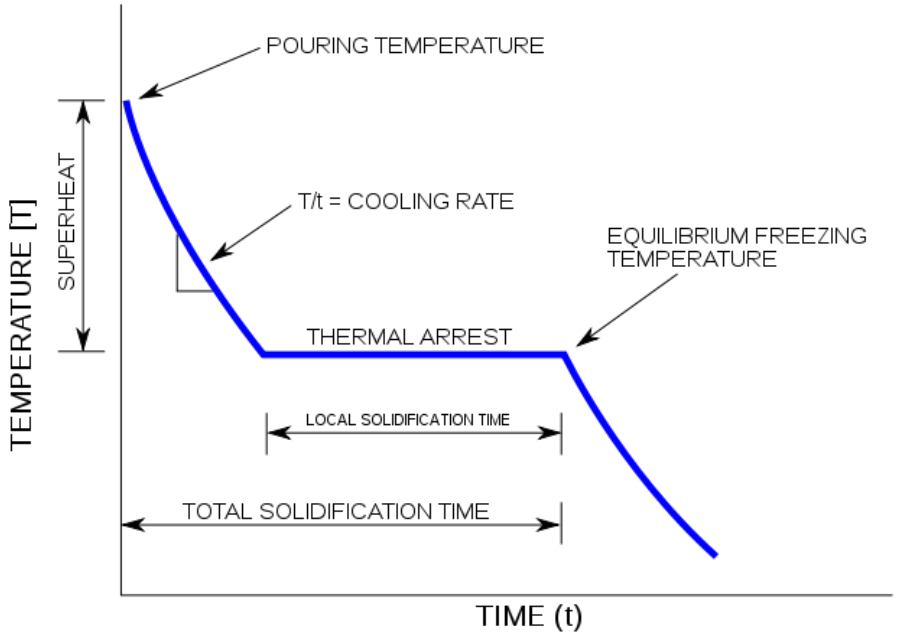

Figure 4.18 Example of a cooling curve of a pure metal or eutectic alloy, with various aspects pointed out. (Degarmo 2003)

The transformation from liquid to solid during solidification at the freezing point is accompanied by the evolution of latent heat. This causes a temporary arrest in the cooling curve at the freezing point. From our measurements, Figure 4.19, the time of arrest for Al is 60 s, whereas for Al-Nb-B it is just 10 s. Although the experimental cooling conditions are similar for both Al and Al-Nb-B, we have observed small differences in the cooling rate. The measured cooling rates for Al and Al-Nb-B during solidification processes are 0.034 °C/s and 0.032 °C/s, respectively. The transformation from liquid to solid was also shifted down for about 1°C for Al-Nb-B in comparison with pure Al. Crystallites of α-Al are initiated on the surface of particles at small undercoolings (Granger D.A. 1998, Schumacher P. 1998, Johnsson M., Backerud I., Sigworth G.K., 1993). The presence of solute elements allow the melt to become undercooled, thus allowing a greater proportion of the particles to initiate grains. Undercoolings observed by Maxwell and Hellawell (Maxwell I. and Hellawell A. 1975) of Al-Ti system lie in the range 0-2 °C. The undercooling of Al-Nb-B is 0.3 °C.

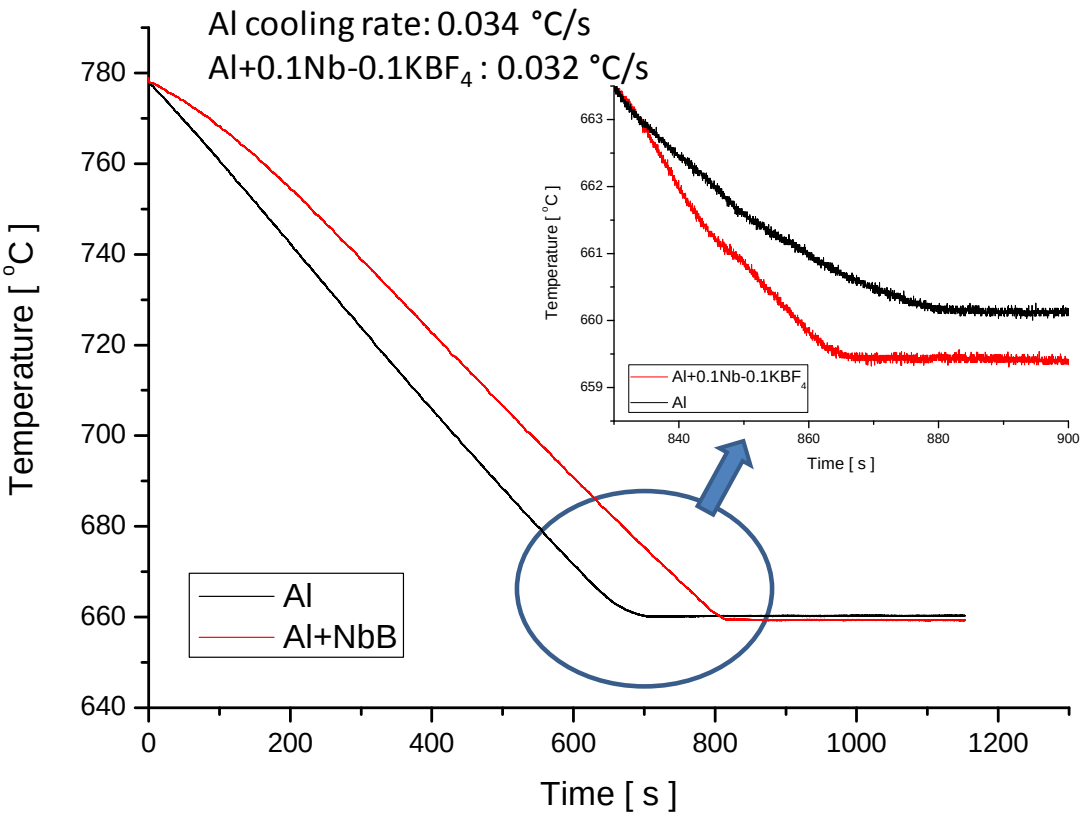

Figure 4.19 The cooling curve measurements for Al without and with Nb-B addition. The samples were melted at 800 °C. Crucibles are insulated with thermal insulation material during solidification to reduce the cooling rate. The cooling curves were measured with the use of VI Logger software (Chapter 3).

The reduced under-cooling confirms that Nb-B is a grain refiner for aluminium.

Further analyses were concentrated on optimization of the Nb-B addition. The Al was melted at 800 °C and different levels of elements were added to the melt. The TP-1 test was performed to achieve the same casting conditions. The optimization of Al with addition of Nb and B was done to achieve the best composition. The results on the Figure 4.20 show that the excess addition of boron 0.1-1 wt% is helping to form with the Nb an appropriate nucleation site and achieve smaller grain sizes. The addition of Nb is between 0.01 to 5 wt% and it works in each case with boron from 0.1 to 1 wt%. Grain refinement is complex because of competing effects. When the population of inoculant particles is increased (by adding more refiner), the

density of grains at given undercooling increases proportionally (Quested T.E. and Greer A.L. 2004).

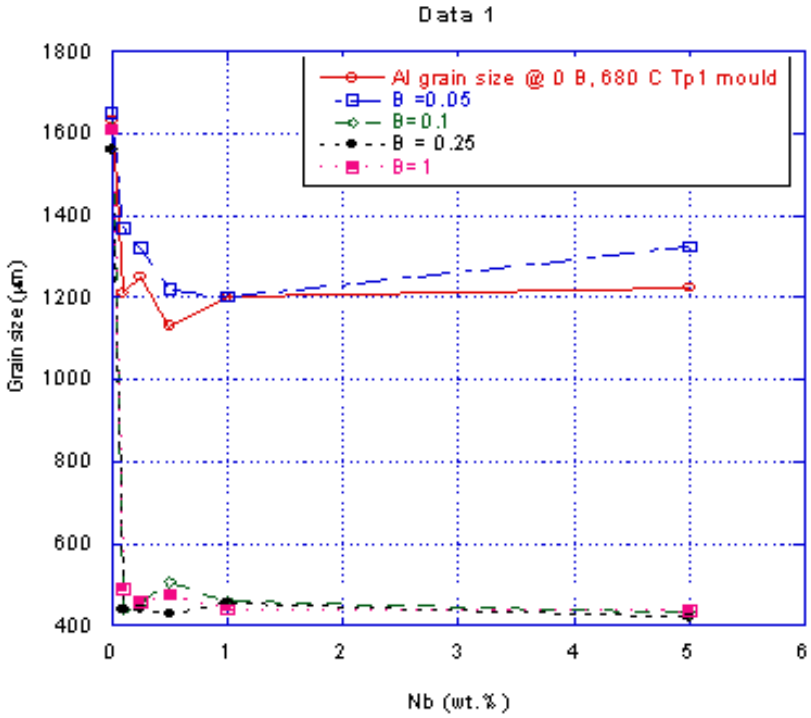

Figure 4.20 The optimization of Nb-B addition to aluminium. The Al was melted at 800 °C and the TP1 test was done with the casting temperature of 680 °C and cooling rate of 3.5 °C/s.

The TP-1 samples were produced to investigate 0.1 wt% Nb – 0.1 wt% B influence on Al with different pouring temperatures 660-720 °C. Figure 4.21 shows the colour etched microstructures of Al without and with commercially known grain refiner of Al-5Ti-B and with our new development of Nb-B.

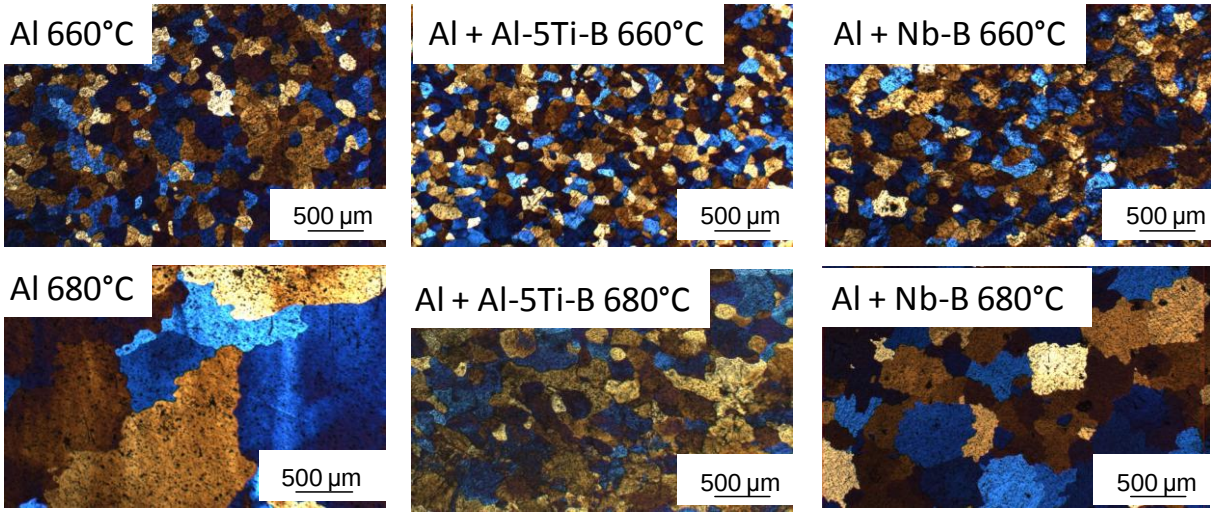

Figure 4.21 The colour etched samples revealing the grain sizes of Al, Al with addition of Al-5Ti-B and Nb-B. The Tp-1 test was done to have the same cooling rate of 3.5 °C/s for all samples with different casting temperatures 660 °C and 680 °C. The grain sizes of Al cast in 680 °C with novel grain refiner are smaller (~450 µm) than of commercial aluminium (~1600 µm) although not small enough when compared to commercial Al-5Ti-B grain refiner (~220 µm).

The TP-1 samples were macro-etched to reveal the difference in the grain sizes between Al and Al with Nb-B. Figure 4.22 shows the samples of the TP-1 test done at different temperatures 660 °C, 680 °C, 700 °C and 720 °C. We can see noticeable grain refinement with Nb-B addition. Figure 4.23 shows the value of measurement of the grain sizes. The grain sizes decrease by 50% even at higher casting temperatures. Figure 4.23 compares the measured grain size of Al with Nb - B addition as a function of pouring temperature.

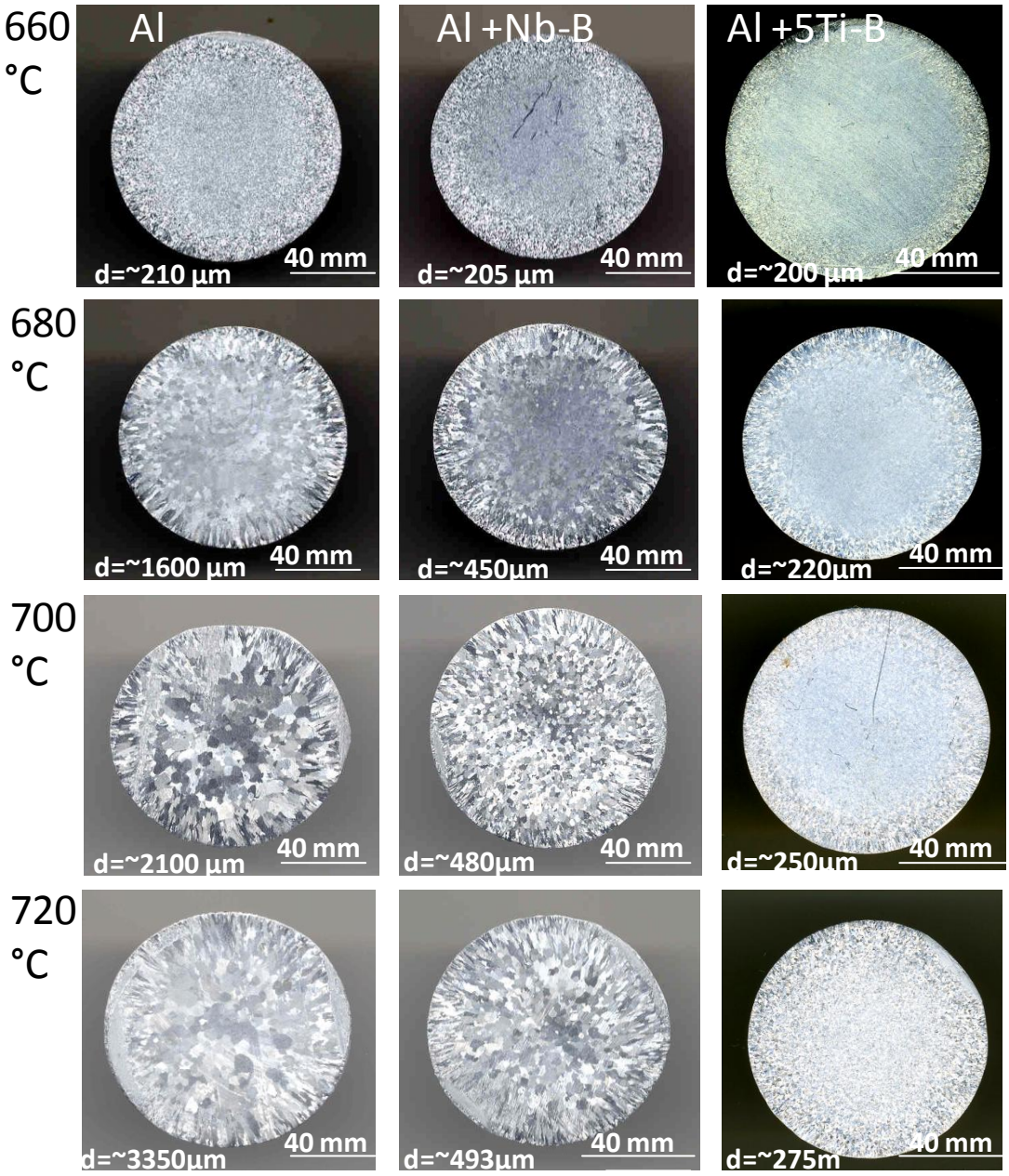

Figure 4.22 The cross-sections of macro-etched TP-1 samples of Al and Al with addition of 0.1Nb-0.1B as a function of casting temperature. The commercial TP-1 test was done to have the same cooling rate of 3.5 °C/s for all samples with different casting temperatures from 660 to 720 °C. The grain sizes of the novel grain refiner are smaller than those of commercial aluminium.

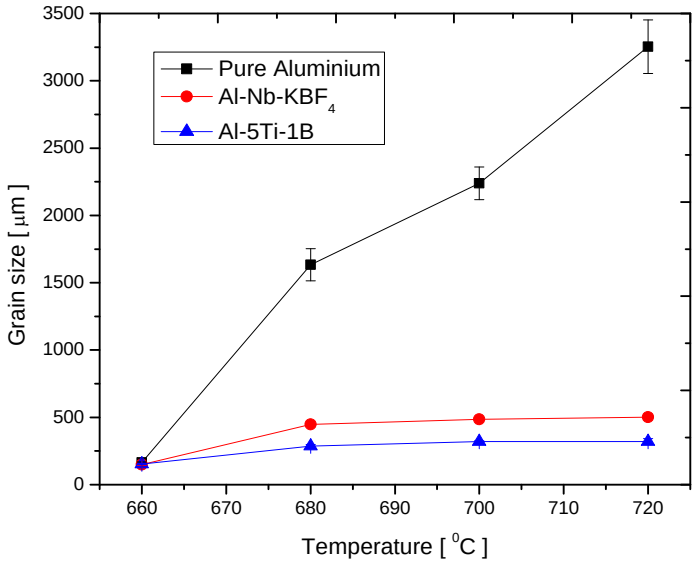

Figure 4.23 The diagram of Al with addition of Nb-B and commercial used grain refiner Al-5Ti-B. The commercial TP-1 test was done to have the same cooling rate of all samples (3.5 °C/s) with different casting temperatures from 660 to 720 °C. The grain sizes of the novel grain refiner are smaller than of commercial aluminium however not small enough to replace Al-5Ti-B.

From Figure 4.23 we can see the results of the optimization and development of Nb-B novel grain refiner. The results show that the low temperature (660 °C) casting gives the similar grain sizes for all samples. It means that with a fast cooling rate and low temperature of casting one can achieve fine grain structure, however, for industrial applications, for better feeding into mould, the casting temperatures will be at least >50°C above the liquid temperature and thereby suggesting the need for grain refiners. The Al in practice is cast at higher temperatures well above 780 °C. We can see on the diagram that Al grain sizes increase with increasing the pouring temperature for pure Al, whereas when Nb-B and Al-5Ti-B are added the grain sizes are finer even at higher temperatures. The decrease in grain size is about 88%. The addition of Nb-B to the pure aluminium has a significant effect on its grain sizes.

4.4 Conclusion

The Chapter 4 presents the experimental data and theoretical background of the grain refinement. The lattice parameters and phase diagrams were analysed for different potential

grain refiners. The research confirms that refractory elements like Mo, Nb, Ta and W have the potential to grain refine aluminium. The grain sizes of Al in TP-1 test are reduced from 1700 μm to less than 600 μm with addition of any of the heterogeneous particles Ti, W, Nb, Ta. The research was concentrated on development of grain refinement based on Nb-B addition as the data presented in this chapter has confirmed that Nb-B chemical composition can have good effect on reducing the grain sizes. Although the new grain refiner, Nb-B, with appropriate chemical concentration and conditions could be real competition for Al-5Ti-1B. The research could have significant impact on solidification science and the aluminium industry.

Chapter 5. Aluminium-Silicon Alloys Grain Refinement

5.1 Introduction

Grain refinement is one of the most important and popular melt treatment processes for aluminium alloys. Grain refinement improves the quality of castings by reducing the size of primary α-Al grains in the casting, which will generally solidify with a coarse columnar grain structure. It is well known that fine grain structure during solidification results in uniform distribution of second phases and microporosity, improved feeding ability (McCartney D.G. 1989) and high yield strength (Spittle J.A. 1997). There are several methods of grain refinement depending on the alloy composition, casting condition and the types of the nucleation substrates present in the melt (Hunt J.D. 1984). Aluminium-Silicon alloys are widely used for shape castings due to their high fluidity, ease of casting, low density and controllable mechanical properties. They comprise aluminium with silicon additions of up to 11% (a) hypoeutectic 11 to 13% (b) eutectic or over 13% (c) hypereutectic (Figure 5.1). Depending on the silicon concentration in the alloy and the cooling conditions, the structure of the casting will essentially comprise mixtures of aluminium grains, silicon crystals and aluminium-silicon eutectic as well as various intermetallic phases formed from alloying elements.

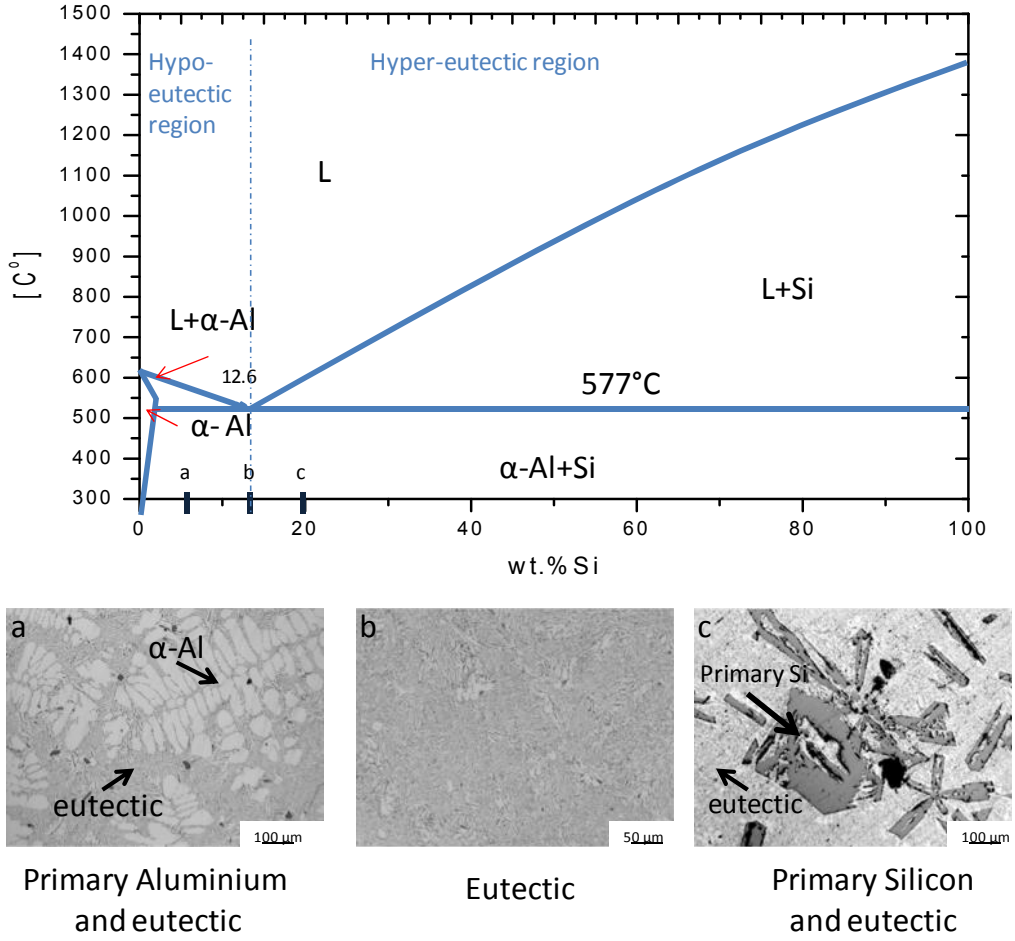

Figure 5.1 Phase diagram of Al-Si alloys and microstructures of alloys with various concentration levels a) predominantly contain primary aluminium (also called α-Al) and Al-Si eutectic phase, b) the Al-Si eutectic phase and c) the eutectic and primary silicon phases.

To achieve the optimum casting or mechanical properties, various other elements such as Fe, Cu, Mg, Ni, Zn are added to Al-Si alloys. The casting alloys can be refined by using the heterogeneous nucleation process. The addition of phosphorus to hyper-eutectic alloys known to refine primary Si and strontium addition is known to modify the eutectic Si. However, it is very difficult to refine the primary α-Al in hyper-eutectic silicon alloys. Johnsson (Johnsson M. 1994) showed that the Al-5Ti-1B master alloy is poisoning the Al-Si alloys when Si concentration is above 3 wt% as shown in Figure 5.2.

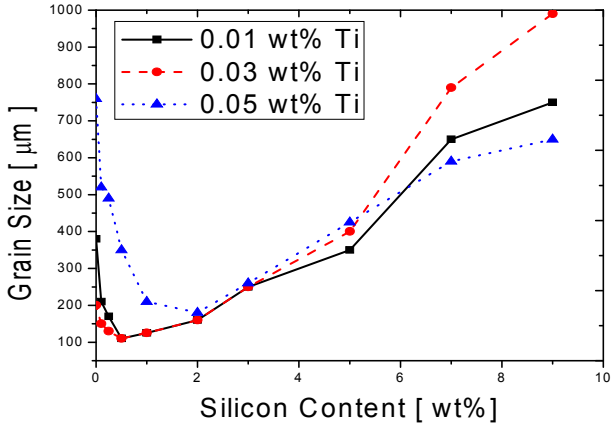

Figure 5.2 The grain size of Al-Si alloy as a function of Silicon content for different amounts of Ti addition in the form of Al-5Ti-B. The grain sizes are increasing with silicon content as a result of the formation of Ti silicides (process known as poisoning).

It is generally believed that the poisoning elements interact with the grain refining constituents of the Al-Ti-B master alloys (Al_3Ti and TiB_2) and make them ineffective or less effective (Jones G.P. and Pearson J. 1976, Arjuna Rao A. 1996, Young D.K. 1991) The reason for poisoning is that the titanium is consumed by the silicon and forms the $TiSi_2$ phase as shown in Figure 5.3. There is a large interaction between titanium and silicon in both the liquid and α-Al. The strong interaction favours the formation of silicon and titanium containing phases TiSi and $TiSi_2$. Sigworth and Guzowski (Sigworth G.K. and Guzowski M.M. 1985) suggested that titanium silicide coats the surface of $TiAl_3$ and poisons the effectiveness of the nuclei present in the Al-Ti master alloy. On the other hand, when the Al-B master alloy is used as the grain refiner, it is proposed that AlB_2 phase acts as the nucleant, and the presence of Si enhances its nucleation potential. The researchers (Young D.K. 1991, Mayes C.D. 1993) proved that Al-B and Al-3Ti-3B master alloys containing AlB_2 and $(Al,Ti)B_2$ perform more effectively in Al-Si alloys than Al-5Ti-1B master alloys containing TiB_2 and $TiAl_3$. Spittle et al. (Spittle J.A. 1997) and Sritharan with Li (Sritharan T. and Li H. 1997) have shown that the Al-Ti-B master alloy with the Ti-B ratio 1:2.2 are more effective in Al-Si alloys as they contain excess boron and easily

form AlB_2 than commercially known Al-5Ti-1B. Mohanty and Gruzelski (Mohanty P.S. 1995) have proposed a mechanism of nucleation of Al in hypoeutectic Al-Si alloys.

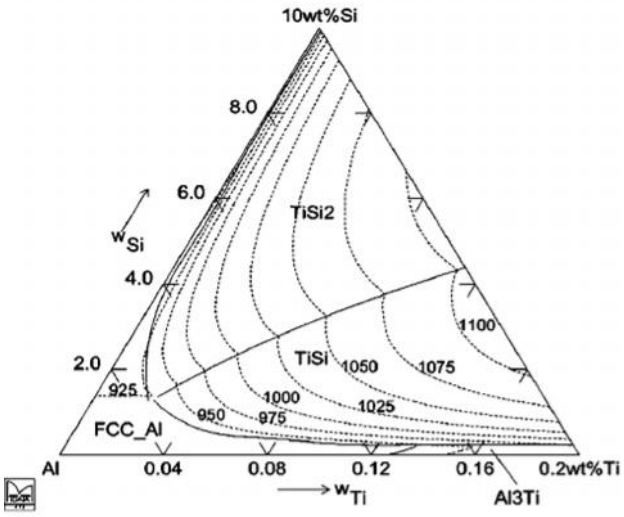

Figure 5.3 Primary phase map of Aluminium rich corner of Al-Si-Ti system: solid lines separate different primary phases. The contours of liquidus temperature are superimposed as broken lines. The temperature is in Kelvin. (Quested T.E., Thermodynamic evidence for poisoning mechanism in the Al-Si -Ti system 2006)

Figure 5.3 describes the compositional range over which each of the silicide phases is the first to solidify from the melt, if equilibrium is maintained. As the silicon content of the alloy is increased, the titanium content required to form $TiSi_2$ like a primary phase decreases: for Al-3Si alloy, ~0.01Ti is required and at 7%Si, <0.005%Ti will be sufficient.

The constitutive binary phase diagrams of Nb-Ti-Si system i.e. Nb-Si (Zhao J.C. 2001, Shlesinger M.E. 1993, Bewlay B.P. 1995), Ti-Si (Murray J.L. 1990, Seifert H.J 1996) and Nb-Ti (Murray J.L. 1990) are already available in the literature. The Nb-Si phase diagram was assessed by Schlesinger et al. (Shlesinger M.E. 1993) and modified (Figure 5.4 a) by Zhao (Zhao J.C., Jackson M.R., Peluso L.A., 2004) with the eutectoid temperature being adjusted to ~ 1700 °C based on the results reported by Mendiratta and Dimiduk (Mendiratta M.G., Dimiduk D.M 1991). The L → bcc (Nb) + Nb_3Si eutectic reaction is adjusted to 1880°C and 18.2 at% to reflect the temperature and composition obtained by

Bewlay et al (Bewlay B.P. 1995). The Nb_5Si_3 phase forms after the decomposition of the Nb_3Si phase via an eutectoid reaction $Nb_3Si \rightarrow$ bcc (Nb) + Nb_5Si_3 at ~ 1700 °C or as the primary solidification product in hypereutectic alloys. The two different Nb_5Si_3 phases have the same crystal structure *(tI32*) with different lattice parameters. The high temperature phase β-Nb_5Si_3 *(a=1.004nm, c=0.5081nm*) and low temperature phase α-Nb_5Si_3 (*a=0.6571nm, c=1.1889nm*). The Ti-Si system is very similar to Nb-Si except that the Ti_3Si is stable at lower temperatures <1170 °C as compared to Nb_3Si, which is stable between ~1700 °C and 1980 °C. There are five intermetallic compounds Ti_3Si, Ti_5Si_3, Ti_5Si_4, TiSi and $TiSi_2$ in the Ti-Si binary phase diagram, whereas in the Nb-Si system there are Nb_3Si and Nb_5Si_3. The phase diagram of Nb-Si (Figure 5.4) shows all the silicides that could form when Nb is added to Al-Si alloys.

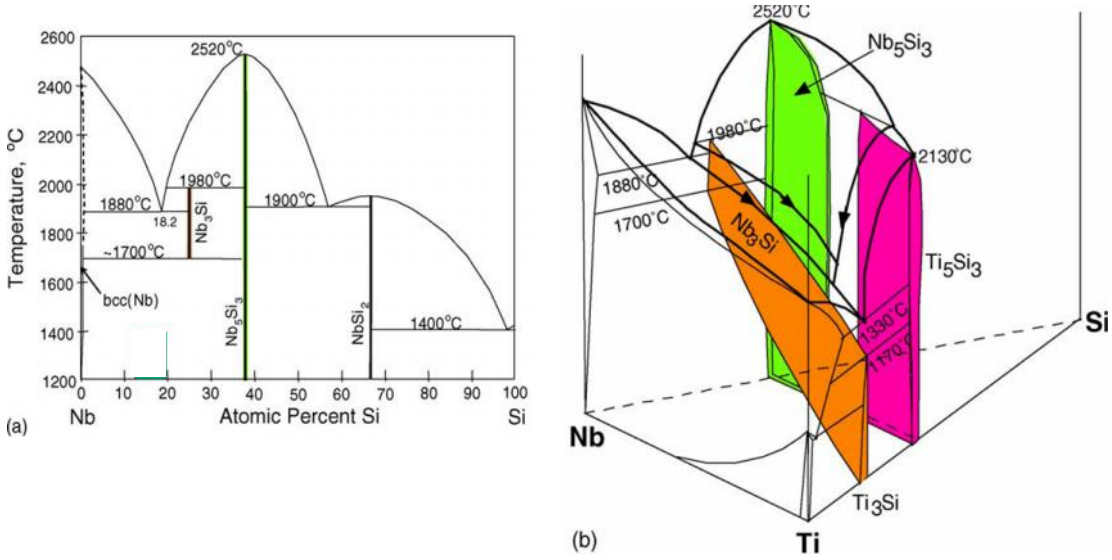

Figure 5.4 a) Phase diagram of Nb-Si, b) The Nb-Ti-Si ternary system (Zhao J.C., Jackson M.R., Peluso L.A., 2004).

This research concentrated on the influence of the novel grain refiner on aluminium-silicon alloys. Through analysis of the phase diagrams we anticipate that that the Nb element in the Nb-B based grain refiner should not be consumed by the silicon and as a result, unlike Ti-B, one can expect that the Nb-B can be a potential grain refiner for Al-Si alloys

5.2 Results and Discussion

The experiments were done for hypoeutectic and hypereutectic aluminium-silicon alloys. In this part of the discussion the influence of Nb-B grain refiner will be analysed and compared with well known Al-5Ti-B grain refiner additions.

5.2.1 Hypoeutectic Aluminium Silicon Alloys

The binary alloys (100-xAl + XSi) were prepared and cast into a 1 kg billet with Si levels of 1, 2, 4, 6, 7, 8, 9 and 10. The binary alloys were prepared from pure Al (about 1.2 kg each) and Al-50Si to achieve the desirable Si concentration. Furthermore the samples were melted at 800 °C in the same conditions and solidified in the TP-1 mould to achieve the same cooling rate of 3.5 °C/s. The grain sizes were calculated using the line intercept method described in Chapter 3. The results are plotted in the Figure 5.5. The black line (square data points) represents commercial aluminium grain sizes as a function of the different silicon addition. Our results confirm that as silicon concentration is increased the grain size decreases (by up to 3%). However when it reaches more than 3%, the grain size starts increasing. The red line (circle data points) represents the aluminium grain size with the addition of 0.1 wt% of Al-5Ti-B as a function of silicon addition. The grain size increases above a silicon content of 3% of which suggest that there is a poisoning effect (Johnsson M. 1994). However the addition of Nb-B to the aluminium with different silicon concentrations is noticeably very effective as the grain sizes remain small and stable as a function of Si content. In Chapter 4 it is shown that Nb-B is not as effective a grain refiner as Al-5Ti-B in pure aluminium. On the Figure 5.5, shows that for lower silicon concentrations, Al-5Ti-B addition refines better than Nb-B, however for higher silicon concentrations it is the opposite. Nb-B addition is highly effective for Al-Si alloys with Si above 4wt%. Si levels in commercial alloys used in industry contain more than 4%, the effect of Nb-B addition to LM24, LM25, LM6 and LM13 is described in the coming sections. This is an extraordinary result and is the first time Nb-B chemical composition was used to achieve small grain sizes in hypoeutectic alloys containing higher silicon addition. To secure IPR for this technical development a patent application was filed at the UK Patent Office on 23rd February 2011.

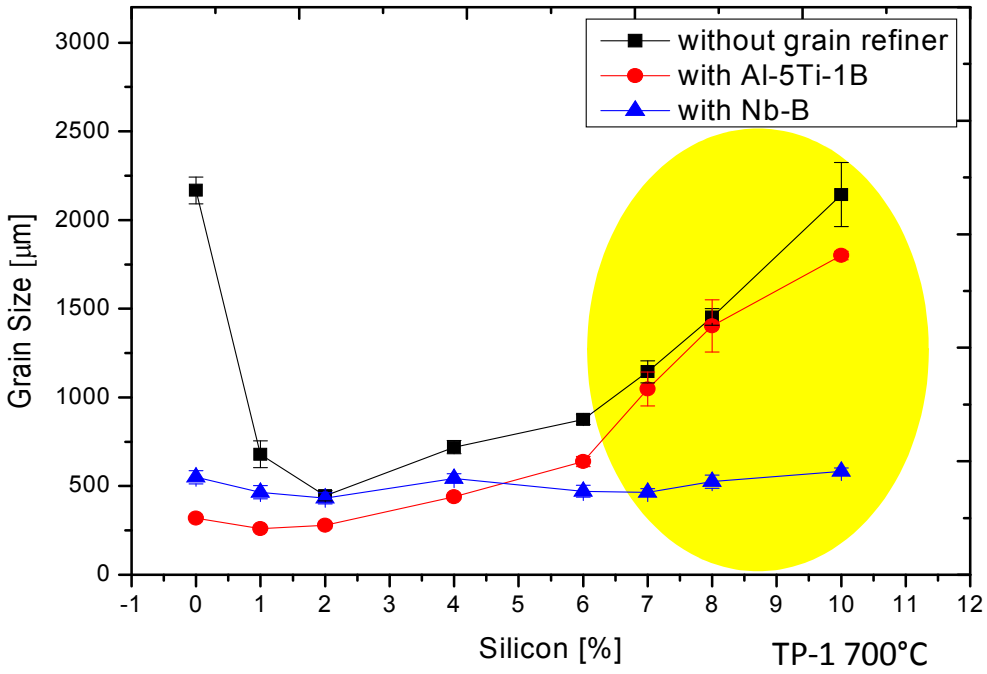

Figure 5.5 Grain size as a function of silicon addition content for Al-Si binary alloys without and with additions of 0.1 wt%Al-5Ti-B and 0.1 wt% Nb-0.1 wt% B. The TP-1 mould was used and the pouring temperature was at 700 °C, the cooling rate was 3.5 °C/s.

Figure 5.6 shows the microstructural difference between Al-Si alloys without any addition, with commercially known Al-5Ti-B (supplied by London Scandinavian Metallurgy – LSM) and with Nb-B novel grain refiner. The first column presents the microstructures of commercial aluminium as a function of different silicon additions. We can clearly see that the grain size is increasing with the silicon addition. The second column is the Al-Si with Al-5Ti-B grain refiner addition. The grain size is very small (~200 - ~400 µm) up to Si of 4 wt% and then it is increasing with the silicon addition (~520 - ~1850 µm). The morphology of grains is also changing to dendritic morphology as the Si concentration increases. The last column is Al-Si with our novel grain refiner, Nb-B; the fine grain structure is evident even when Si content reaches 10%.

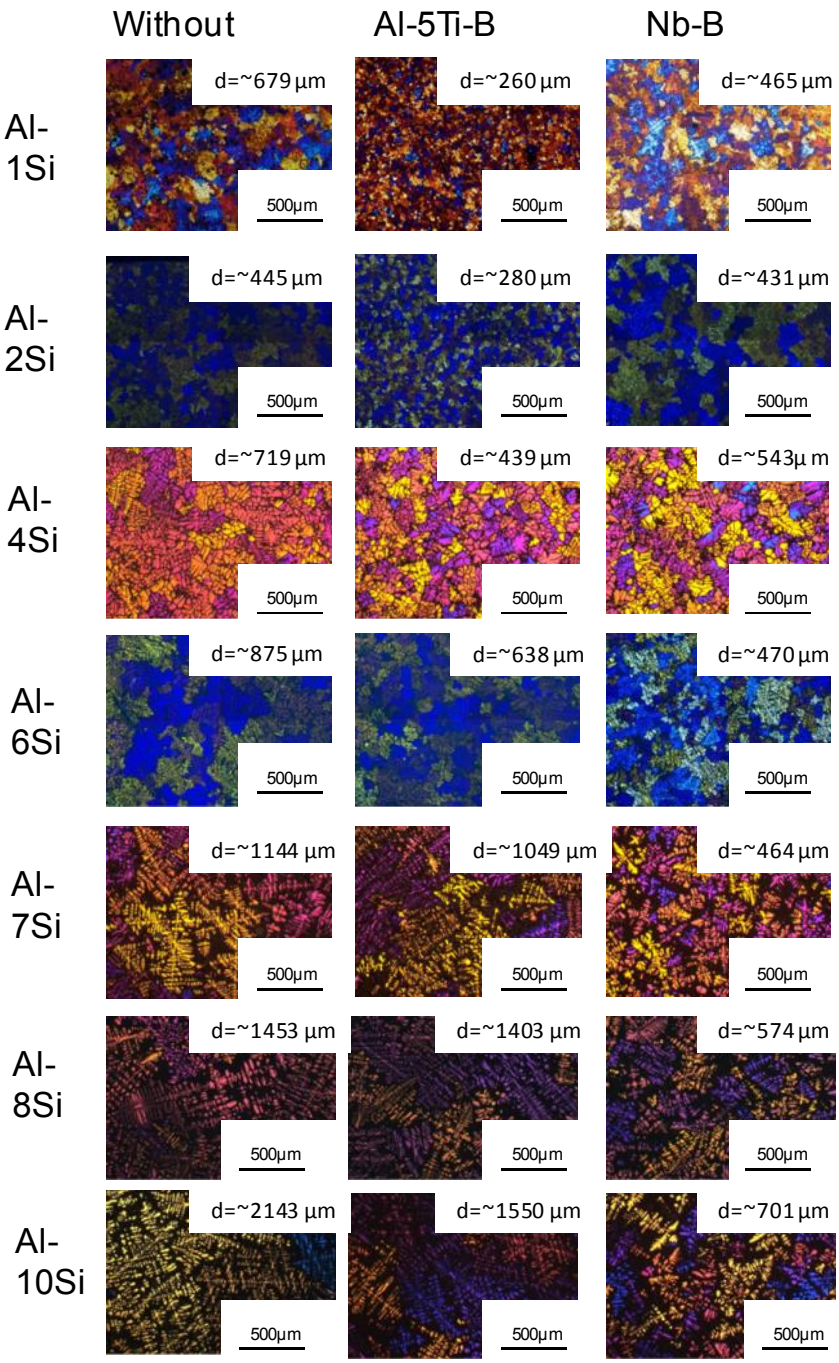

Figure 5.6 The colour etched samples of Al-Si without addition and with 0.1 wt% Al-5Ti-B and 0.1 wt% Nb- 0.1 wt% B. All TP-1 samples are cast at 700 °C and with a cooling rate of 3.5 °C/s.

The grain refinement efficiency means that there are sufficient active nucleis to promote the formation of smaller grains. If the distance between the nucleates is small at the beginning of the solidification, the resulting grains should not grow much due to a limited diffusion and transport field. The change in grain morphology was observed in our samples. Below 2-3 wt% of Si, grains are observed to be globular (or equiaxed cellular) in shape whereas above these values, high branched 'orthogonal' dendrites are observed for Al-Si without addition and with A-5Ti-B. It has been argued that this change in grain morphology was responsible for the increased grain size (Johnsson M. 1994, Jhonsson M. and Backerud L. 1996, Quested T.E. 2005). The highly branched dendrites have a smaller dendrite tip radius and are therefore able to disperse solute sideways as opposed to globular dendrite tips, which push solute ahead of the solid/liquid interface. It was suggested that sharp dendrites would be able to grow more rapidly than blunter dendrites at a given undercooling, leading to a coarse grain size.

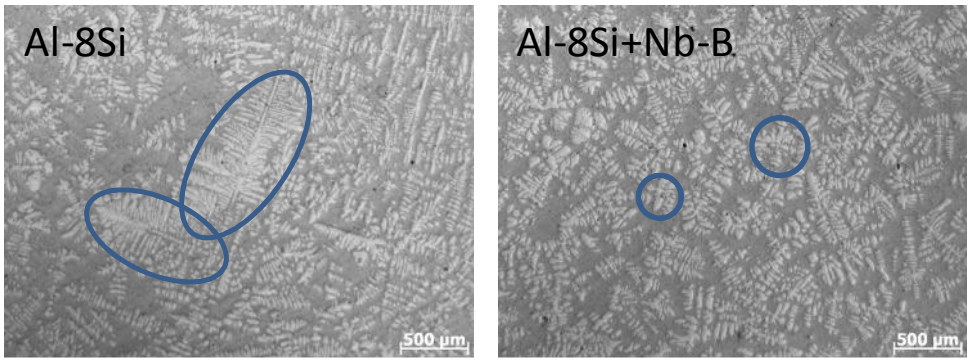

Figure 5.7 The difference in grain size morphology of Al-8Si without addition and with 0.1Nb-0.1B.

Figure 5.7 shows the difference of grain morphology of Al-8Si without addition and with the novel grain refiner. The grains are equiaxed for high concentration of Al-Si alloys (Si ≥ 5 wt. %) when Nb-B is added.

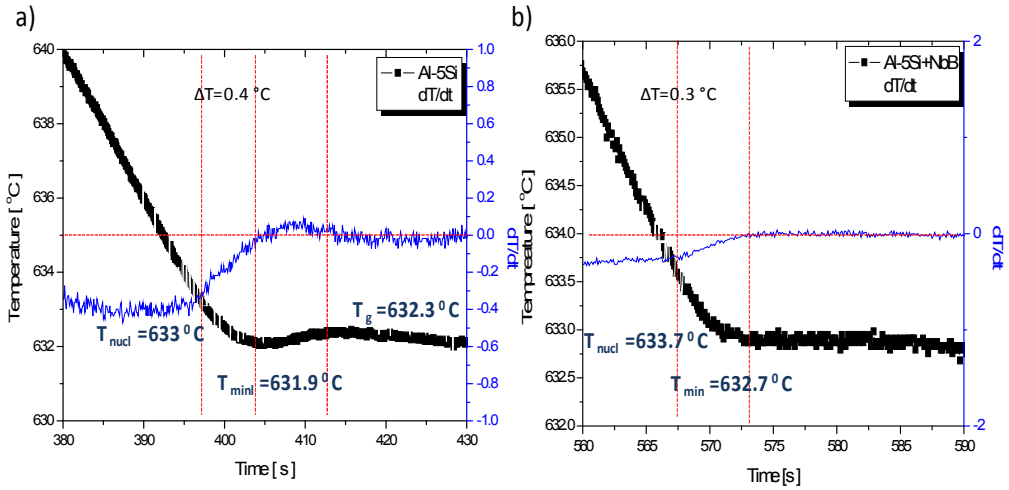

Figure 5.8 The thermal analysis of Al- 5Si was done to investigate the undercooling and nucleation temperature. The cooling curves of a) Al-5Si with undercooling of 0.4 °C, nucleation temperature of 633 °C and cooling rate of 0.04 °C/s b) Al-5Si with Nb-B addition with undercooling of ~0.1 °C, nucleation temperature of 633.7 °C and a cooling rate of 0.03 °C/s.

Thermal analyses were interpreted to see if the heterogeneous nucleation was taking place without and with addition of Nb-B, based on terminologies developed by Backerud et al. (Backerud L. 1990). Furthermore, the morphologies of the grains of solidified ingots were analysed after recording the temperature as a function of time during solidification. Chapter 3 describes this in detail.

By analysing the cooling curves shown in Figure 5.8 we determine the nucleation temperature and undercoooling. Lowering the undercooling has a great influence on growth of primary α-Al particles. In untreated alloys, the existence of undercooling means that heat generated with the commencement of solidification could not be transferred out of the mould completely and therefore the heat balance leads to the appearance of undercooling. However this is not a case for the grain refined alloy. In the refined alloy, shown in Figure 5.8 b, the nucleation temperature is increasing. The macro-etched surfaces of ingots that are produced as a result of cooling curve measurements are shown in Figure

5.9. A big difference in grain size is achieved with the usage of Nb-B addition for very slow cooling rates of 0.04°C/s, similar to the sand casting process that is commonly used by industries to produce large cast structures for automotive applications.

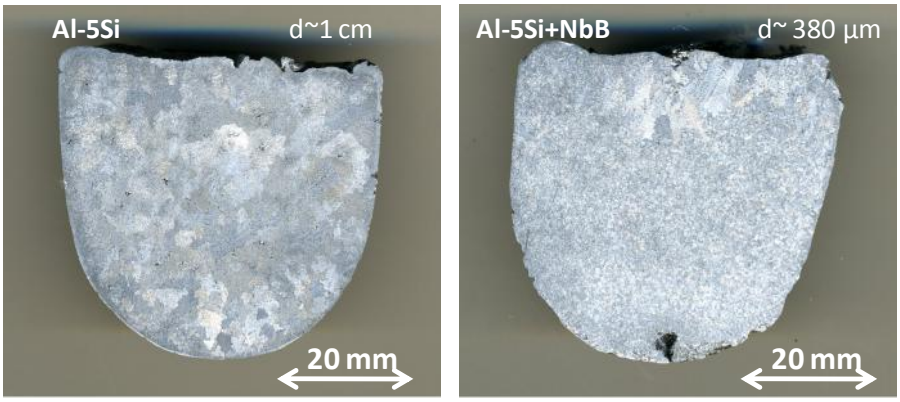

Figure 5.9 The samples of Al-5Si without addition and with Nb-B. A slow cooling rate of 0.04 °C/s was imposed during solidification. The grain size of Al-5Si is about 1 cm and when Nb-B is added decreases to 380µm.

The addition of Nb-B is highly effective for fast and slow cooling rates, which means that more complicated sample shapes can now be cast with the same grain morphology.

The research was continued to investigate the influence of Nb-B addition on eutectic grain structure. A previous study on the eutectic solidification mechanism in hypoeutectic Al-Si alloys has identified large difference in the nucleation and growth modes of unmodified and impure alloys (McDonald S.D. 2002, Dahle A.K. 2001). Eutectic nucleation in unmodified alloys occurs by the nucleation of a large number of α-Al eutectic phases, at or near the primary aluminium dendrite-liquid interface. Relatively, in modified alloys with strontium addition, α-Al eutectic phase nucleate is independent of the surrounding dendrites. Analyses of the eutectic structure with the addition of Nb-B were investigated. The results shown in Figure 5.10 suggest that the eutectic Si size is refined. To achieve the fibrous like eutectic structure, the addition of Strontium is used in industry. However with the addition of Nb-B the structure is still plate like, the density of α-Al eutectic phase is significantly increased; the addition of Nb-B to Al-Si alloys enhances a large amount of nucleation sites for primary α-Al phase, remarkably refining the dendrite grains. The lattice

constants of the eutectic α-Al phase are very close to those of the primary α-Al phase, so it is rational to think that addition of Nb-B also enhances a grain refining of α-Al phase in eutectic.

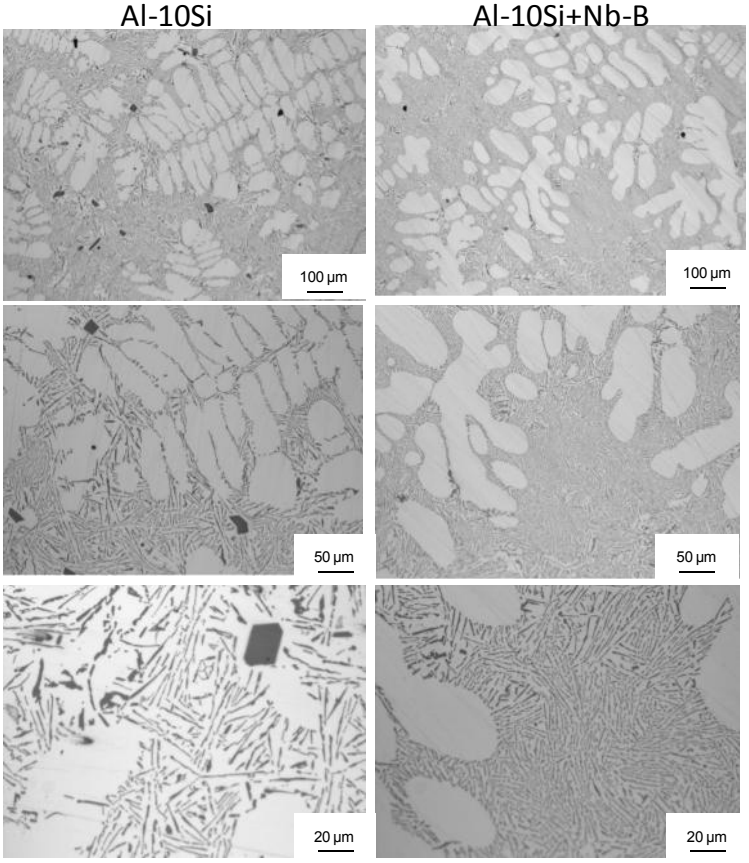

Figure 5.10 The microstructure of Al-10 Si without and with Nb-B addition. The samples were cast at 700 °C into the TP-1 mould that provides the cooling rate of 3.5 °C/s. The Nb-B addition refines the α-Al and the eutectic phases.

Cooling below the eutectic temperature is required to initiate nucleation growth of the eutectic, this is called eutectic undercooling. As the eutectic liquid solidifies, heat is liberated and the temperature will rise to the eutectic plateau until solidification of the aluminium-silicon is complete. The Al-Si alloys are irregular eutectics which exhibit larger undercoolings and interflake spacing. The directional solidification studies by Day and Hellawell et.al (Day M.G. 1967, Hellawell A. 1968), have led to a much better

understanding of the formation of irregular eutectic structure. During solidification of two eutectic phases grow independently and faceted Si flakes occur in Al-matrix which solidifies with nonplanar interface during solidification. Modified/refined alloys have larger undercooling and lower eutectic temperatures than non-modified or unrefined alloys as the action of the modifier or refiner is to infer with the growth of silicon, thus requiring a greater driving force for growth.

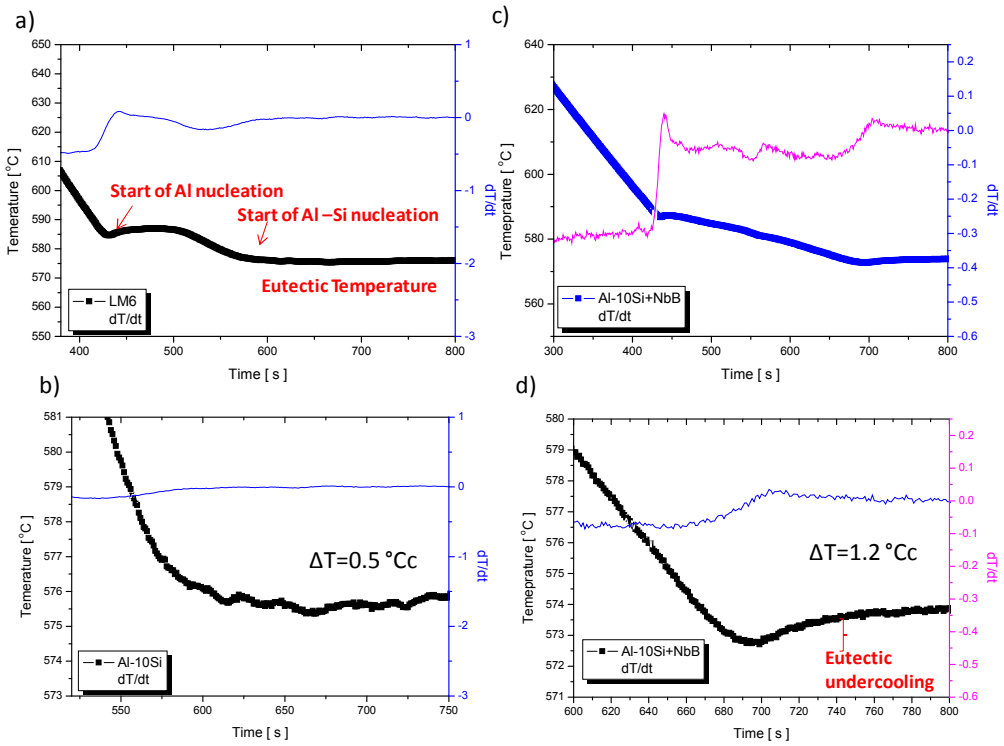

Figure 5.11 The cooling curve for Al-10Si. a) Al-10Si without any addition b) the eutectic undercooling of Al-10 Si is negligible. c) Cooling curve for Al-10 Si with Nb-B addition and d) the undercooling for Al-10Si with Nb-B addition. The undercooling is larger for Nb-B added alloys, which means that there is an enhanced heterogeneous nucleation of eutectic phases.

The Figure 5.11 presents the cooling curves of Al-10 Si without addition of grain refiners /modifiers and Al-10-Si with addition of novel grain refiner Nb-B. The cooling curves analysis confirmed that with addition of Nb-B the eutectic undercooling is greater ~1.02 °C

when compared to no addition, 0.5 °C. The main difference is in the eutectic temperature, where Al-10Si with Nb-B lowers the temperature by 2 °C from 576 °C to 574 °C. It is well known that the modification with strontium is very difficult for slow cooling rates. Although, the imposed cooling rate for this experiment is 0.04°C/s, which is very low for both Al-10Si with and without Nb-B addition and we still can observe the influence of grain refining not only or α-Al but also on the eutectic phases.

5.2.2 Hypo-eutectic Commercial Alloys: LM6, LM24 and LM25

For practical applications, any effective grain refiner needs to be chemically stable with commercially used alloying elements such as Mg, Fe or Cu. The following experiments were carried out to investigate the behaviour of Nb-B addition on LM6 (Al-12Si-0.6Fe), LM24 (Al-8Si-3Cu-2Mg) and LM25 (Al-7Si-0.5Fe). The alloys characteristics are described in Chapter 2. The alloys were melted at 800°C in two different crucibles and then Nb-B and Al-5Ti-B grain refiners were added prior to solidification.

Analyses were carried out on the measured cooling curves. From Figure 5.12 we obtained the nucleation temperature and undercooling. Thermal analyses were interpreted based on terminologies developed by Backerud *et al* (Backerud L. 1990) to investigate if there exists enhanced heterogeneous nuclei in the melt.

Lowering the undercooling has a great influence on the growth of primary α-Al particles. In untreated alloys (without addition of Nb-B), the existence of undercooling means that heat generated with the commencement of solidification could not be transferred out of the mould completely and therefore the heat balance leads to the appearance of undercooling. However this is not a case for the grain refined alloy. In the refined alloy, Figure 5.12 b, the nucleation temperature is increased by 0.8 °C. The reduced undercooling for LM6 with the addition of Nb-B confirms that enhanced heterogeneous nucleation is taking place.

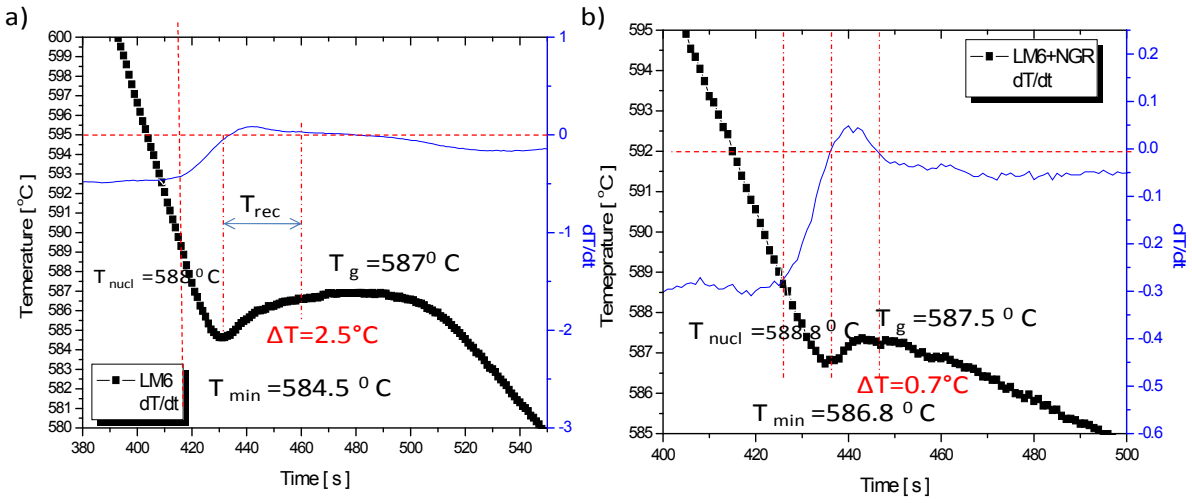

Figure 5.12 (a) The cooling curve for LM6. The measured cooling rate is 0.04 °C/s, the large undercooling of ~2.5 °C is observed and the nucleation temperature is 588 °C. (b) The measurement of the cooling curve for LM6 with Nb-B addition. A lower undercooling of ~0.7 °C is measured and nucleation temperature of 588.8 °C with cooling rate of 0.03 °C/s is observed when the melt was solidified in identical condition.

The analyses confirmed that Nb-B is an effective grain refiner for commercial Al-Si alloys. The experiments were carried out with the use of the TP-1 mould to compare the grain size for alloys with addition of Nb-B, with well known Al-5Ti-B and without any addition. Figure 5.13 shows the colour-etched micrographs revealing grain sizes for the LM6 alloy cast at various casting temperatures and the measured grain size is plotted as a function of cast temperature.

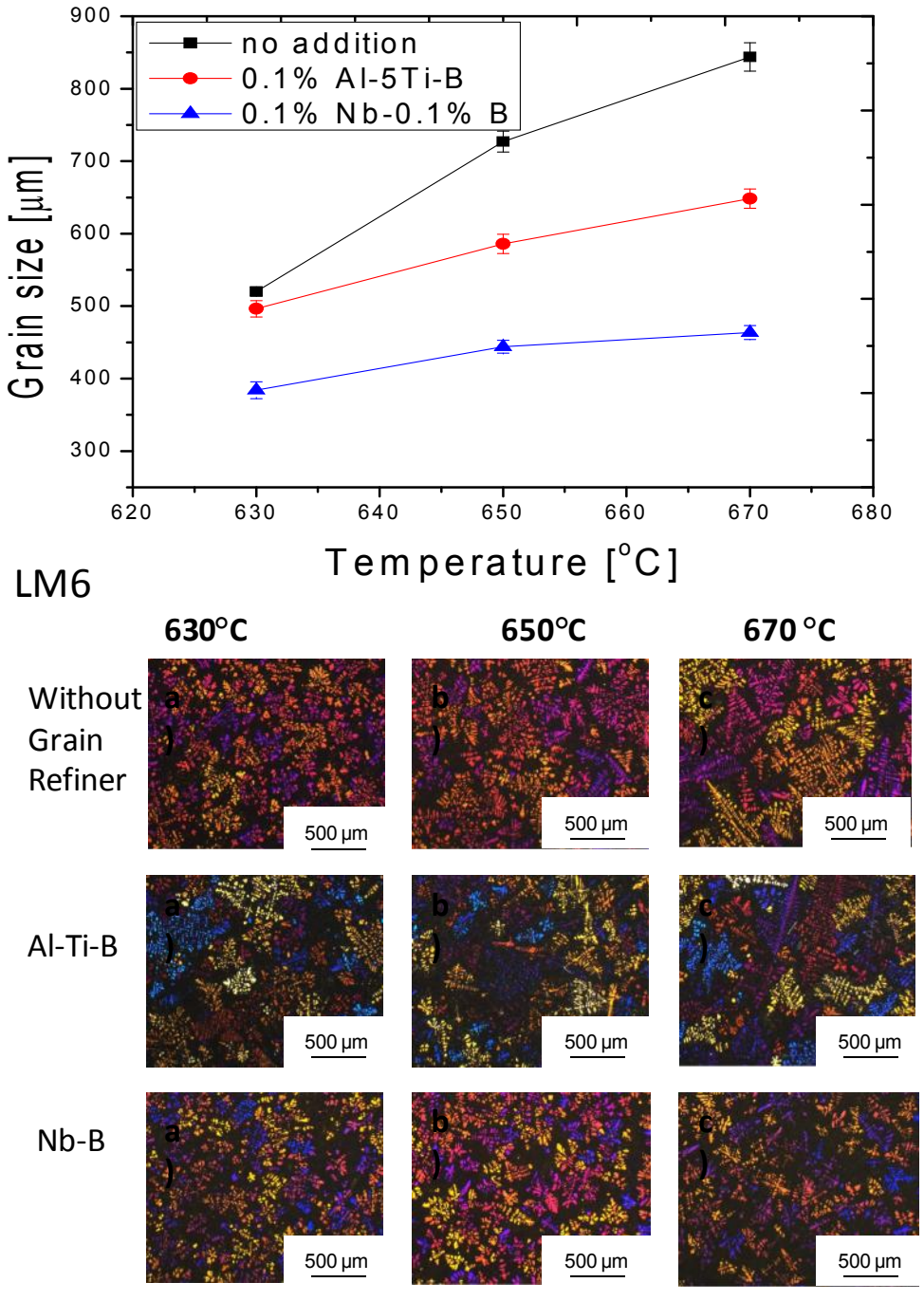

Figure 5.13 The grain size versus casting temperature in TP-1 test, cooling rate 3.5 °C/s. a) LM6 without any addition (black line; ■) , with well known grain refiner Al-5Ti-B (red line ;●) and with Nb-B (blue line; ▲) b) Microstructures of LM6 without any addition, with 0.1wt% of Al-5Ti-B and with 0.1 wt% Nb-0.1 wt% B

The morphology of the grains changes to more cellular with addition of Nb-B also from Figure 5.14, the grain refinement for the eutectic phase is noticeable.

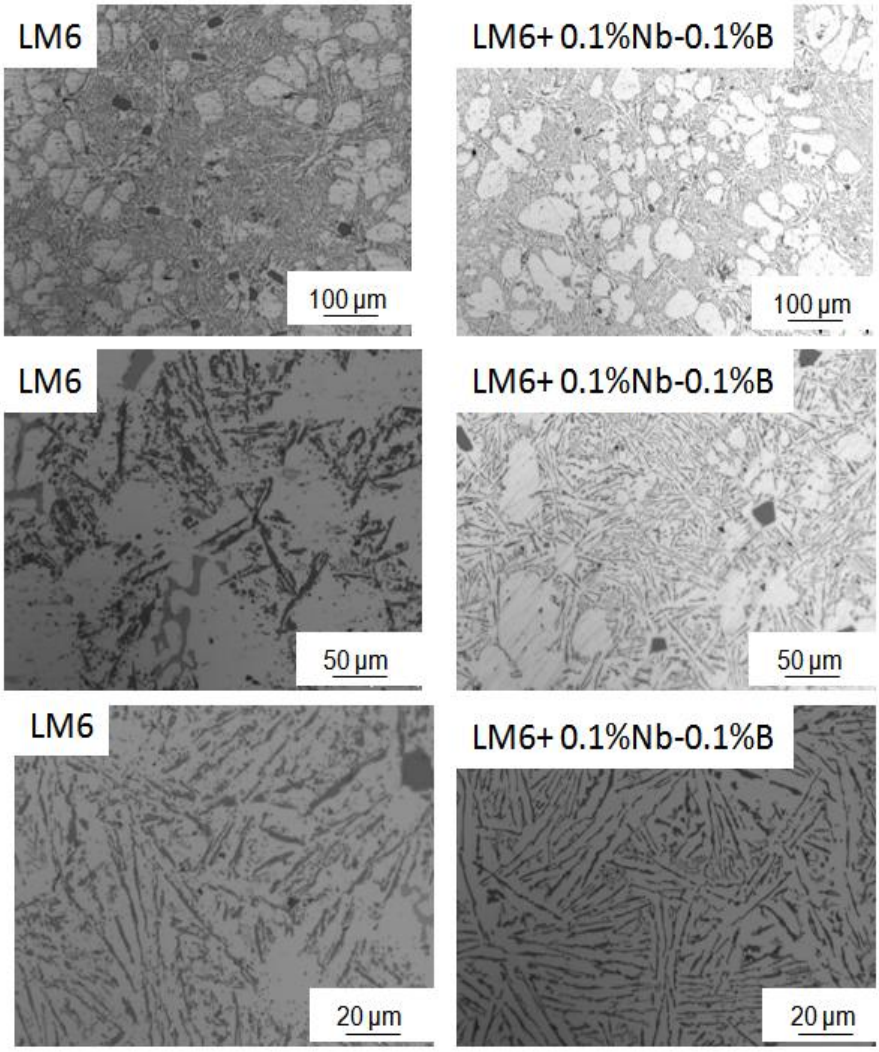

Figure 5.14 The LM6 without any addition and with addition of 0.1%Nb-0.1%B. The refinement of eutectic in LM6 with Nb-B is significant; the eutectic grains are thinner.

Wang et al (Wang L. 2000) suggests that the Al-B master alloy addition to Al-Si alloys can refine the primary α-Al as well as the eutectic composition. From Figure 5.15, our experiments suggest that for LM6 alloy, the addition of B alone is not as effective as the addition of the Nb-B combination.

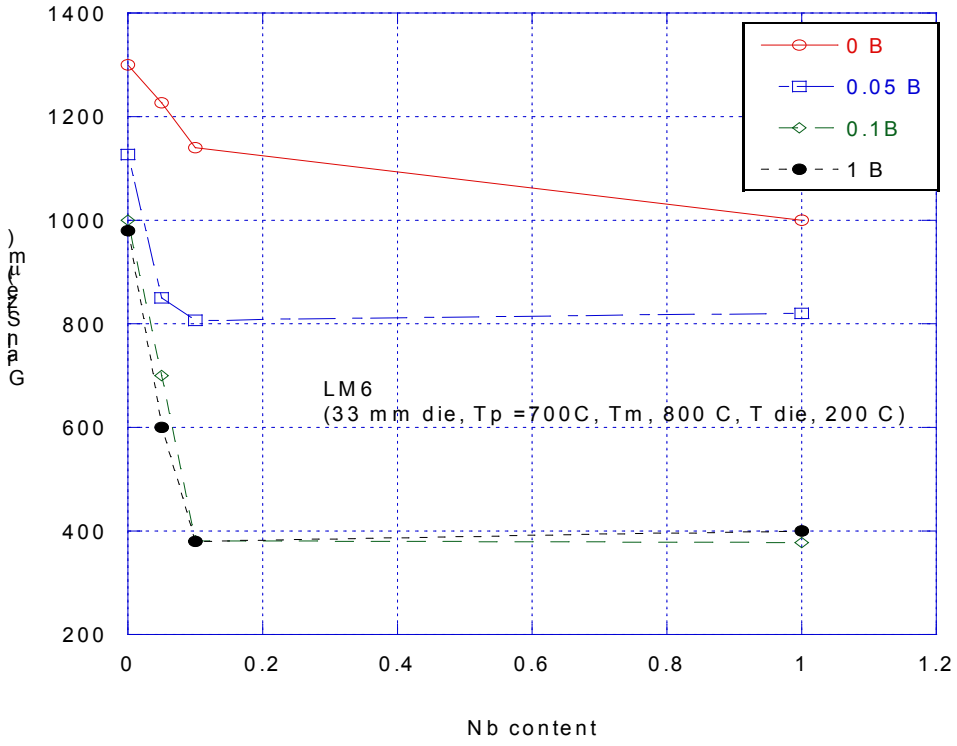

Figure 5.15 The influence of different levels of Nb and B addition to LM6 alloy.

The diagram shows that the addition of B is less effective than addition of Nb and B into the melt. Also a TP-1 test experiment was carried out for LM6 with addition of Nb, B, Al-5Ti-B and Nb-B. From the Figure 5.16, it is noticeable that the grain sizes of LM6 with Nb-B are relatively smaller than LM6 with all of the other additions.

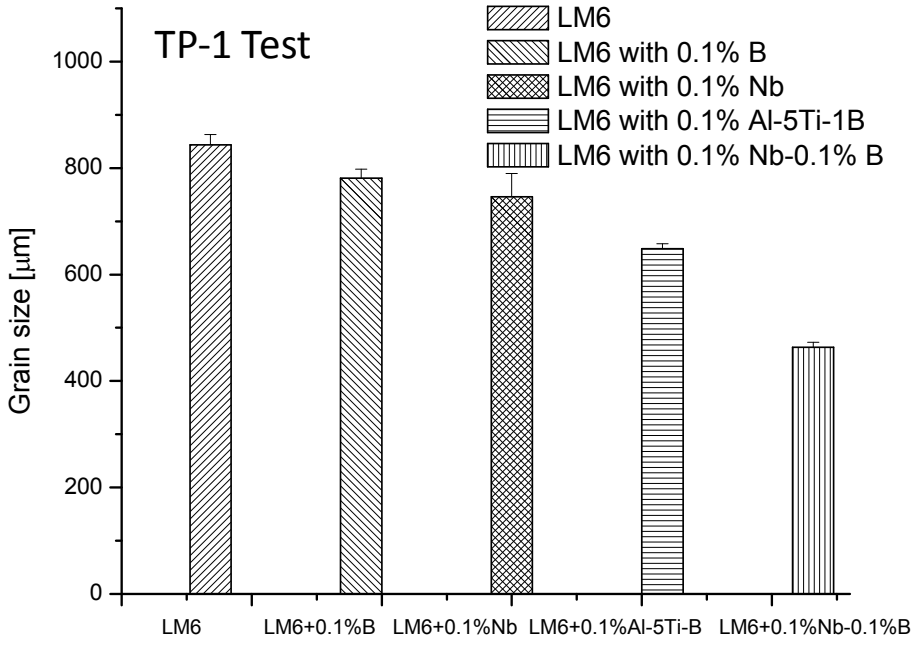

Figure 5.16 The grain sizes of LM6 cast in the TP-1 mould at 670 °C with different additions (Nb, B, Al-5Ti-B and Nb-B). The grain sizes of LM6 with Nb-B are the smallest (~450 µm).

Similar to the above study, the LM25 alloy was also investigated and in Figure 5.17 the diagram of grain size versus temperature is presented together with the microstructures.

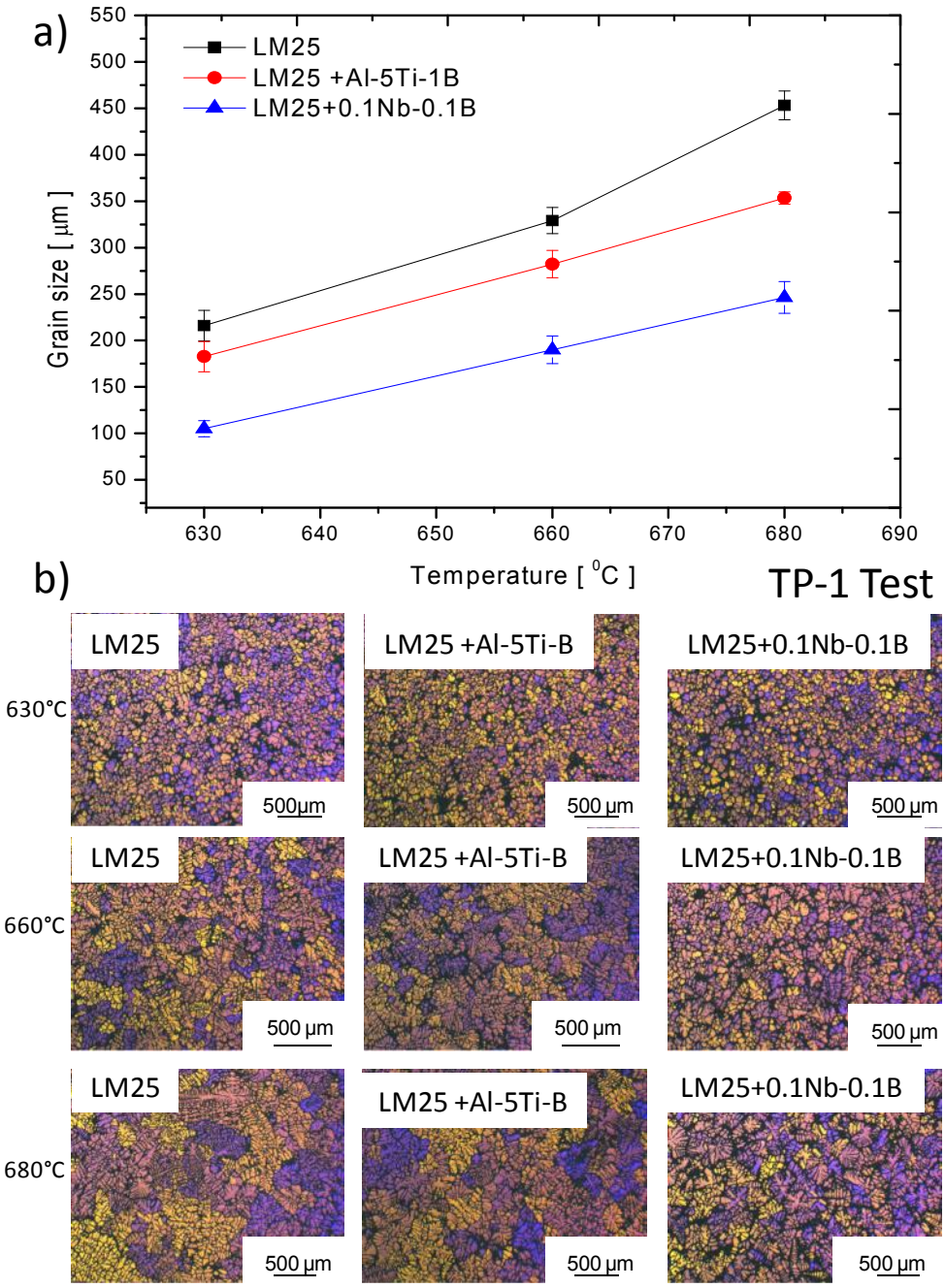

Figure 5.17 The grain size versus casting temperature in the TP-1 test, with a cooling rate of 3.5 °C/s. a) LM25 without any addition (black line ;■) , with well known grain refiner Al-5Ti-B (red line; ●) and with Nb-B (blue line ;▲) b) Microstructures of LM25 without any addition with 0.1wt% of Al-5Ti-B and with 0.1wt%Nb-0.1wt%B

The LM25 alloy is used in industry to produce engine blocks. The ability of refining this alloy can allow casting of thinner walls of engines as the grain sizes can be refined in all sections. The mechanical properties analyses are presented in Chapter 6. Figure 5.18 presents the cross section of the LM25 TP-1 test. The grain size decreases from ~455 μm to ~250 μm with the addition of 0.1wt%Nb-0.1wt%B.

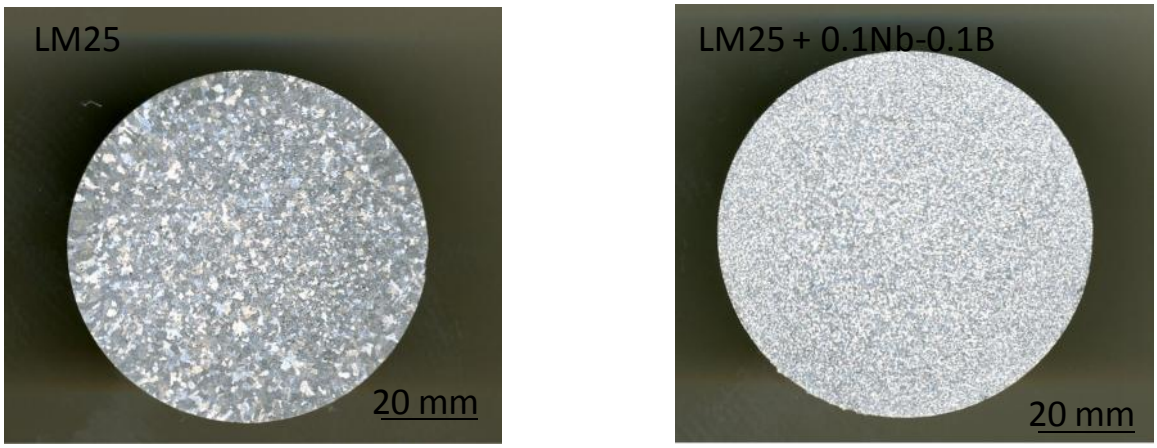

Figure 5.18 Cross section of macro-etched TP-1 samples of LM25 without any addition and with 0.1%Nb-0.1%B, cast at 700 °C with a 3.5 °C/s cooling rate.

The re-melted LM24 was cast with the addition of 0.1% Nb-0.1% B, without any addition and with Al-5Ti-B. The silicon content in this alloy is only 5wt%. The Nb-B addition still refined the grain, however, as shown in the previous analyses for binary alloys, although there is not a big difference in grain sizes of high cooling rates compared to those of low cooling rates. Figure 5.19 shows the grain sizes versus the casting temperatures and microstructures of the alloy containing, 0.1wt% Al-5Ti-B and 0.1% Nb-0.1% B addition.

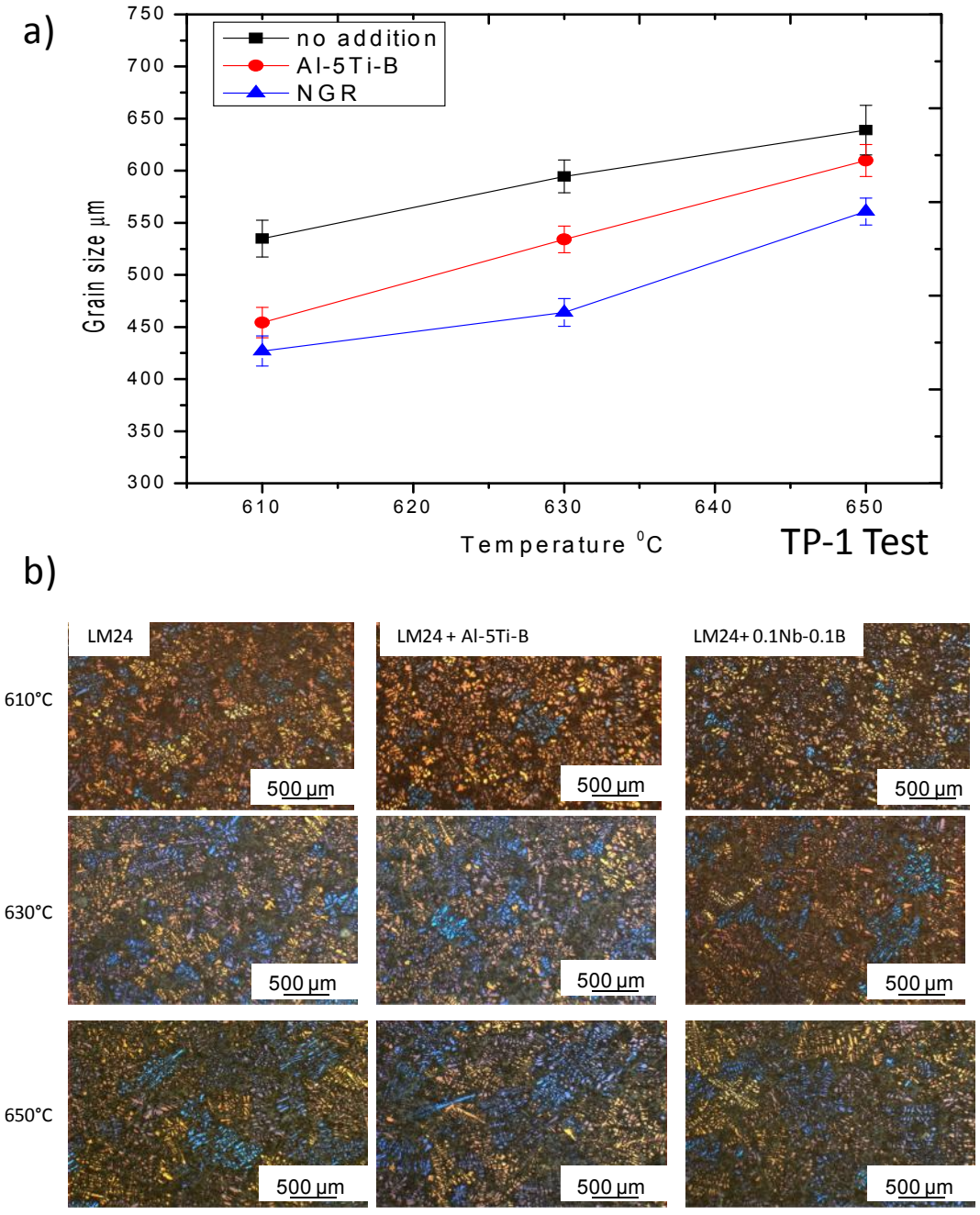

Figure 5.19 The grain size versus casting temperature in the TP-1 test, with a cooling rate of 3.5 °C/s. a) LM25 without any addition (black line ■) , with well known grain refiner Al-5Ti-B (red line ●) and with Nb-B (blue line ▲) b) Microstructures of LM25 without any addition with 0.1wt% of Al-5Ti-B and with 0.1wt%Nb-0.1wt%B

5.2.3 Hyper-eutectic Al-Si Alloys

The research work has been extended to hypereutectic binary alloys with 14-25 wt% of Si to investigate the influence of Nb-B on eutectic and primary silicon. All samples were melted at 800°C and cast into preheated moulds at 200 °C. Binary Al-Si alloys close to eutectic composition (12.6 wt% Si) exhibit, in the unmodified state, an acicular or lamellar eutectic silicon which is in the form of large plates with sharp sides and edges. Al-Si alloys containing more than 12.6 wt% Si exhibit a hypereutectic microstructure normally consisting of primary silicon phase in a eutectic matrix (Gruzelski J.E. and Closset B.M. 1990). Cast eutectic alloys with coarse acicular silicon display low strength and ductility because of the coarse plate-like nature of the Si phase that leads to premature crack initiation and fracture tension. The primary silicon in hypereutectic alloys is usually very coarse and imparts poor properties to these alloys. Therefore, alloys with large eutectic needles structure must be modified to ensure adequate mechanical strength and ductility. It is widely recognised those elements: Na, Mg, Ca and Sr are effective modifiers of Al-Si eutectic, however only sodium and strontium are used in commercial production of these alloys (Gruzelski J.E. and Closset B.M. 1990). Refinement of primary silicon is usually achieved by the addition of phosphor to the melt. The literature (Ye B.J. 1985, Ravi M. 1996) reports that rare earth (RE) metals are also capable of modifying the eutectic structure of cast aluminium silicon alloys. Our research concentrated on Nb-B addition to high silicon alloys.

The first experiments were done for Al-14 Si near the eutectic points. The samples were melted at 800°C and cast into the TP-1 mould with a 3.5 °C/s cooling rate. The results are shown in Figure 5.20.

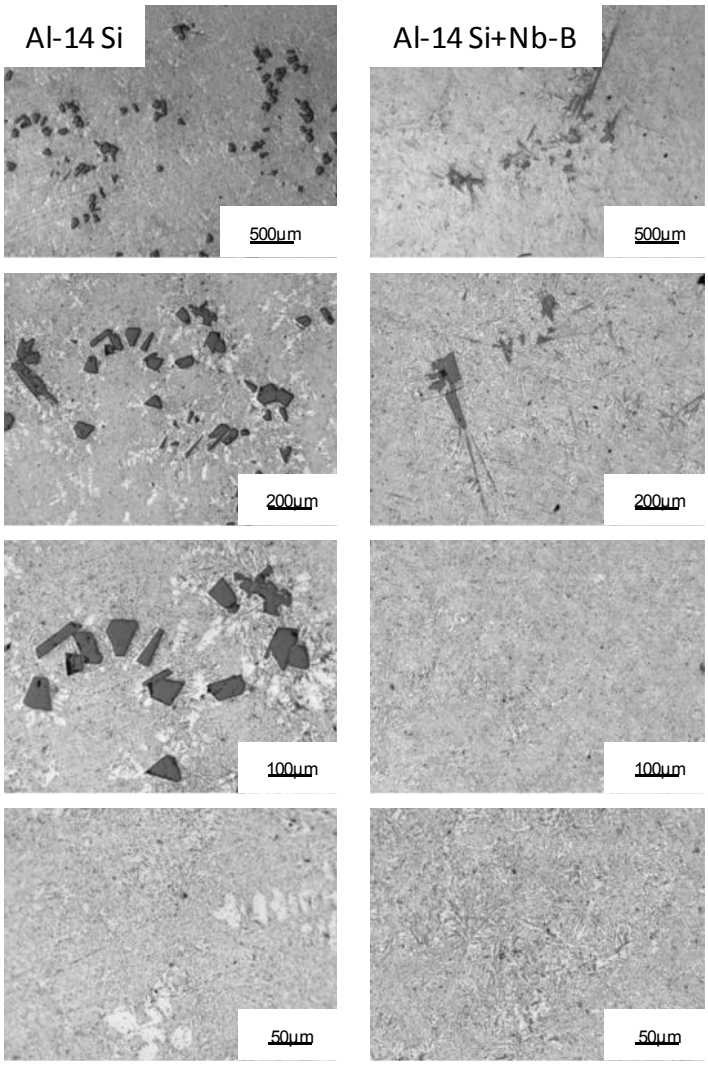

Figure 5.20 The binary alloy Al-14Si melted at 800 °C and cast into the TP-1 mould without and with Nb-B addition (cooling rate 3.5 °C/s). The α-Al grains are negligible and also the distribution of primary silicon is smaller in Al-14Si with 0.1wt%Nb-0.1wt%B.

From Figure 5.20 it is noticeable that Al-14Si alloy with addition of Nb-B has less primary silicon particles and there are different shapes: hopers (square shape) and fish-bone (long looking like a fish bone). Fish-bone shape primary silicon particles are at the edges of the sample (near the mould wall) whereas the hoper shapes are at the middle of the sample. Gayler (Gayler M.L.V. 1927) has stated that a eutectic structure could be formed below the

eutectic temperature, and the eutectic point apparently shifted to higher silicon content by 1-2 wt%. Later researchers found that the eutectic point could be changed by the minor addition of a foreign chemical element. Kobayashi (Kobayashi K. 1976) and Hanna (Hanna M.D. 1984) treated hypereutectic Al-Si alloys with sodium and rapid cooling rates and concluded that shifting of the eutectic point increases towards a higher silicon concentration. The microstructure of Al-14Si with Nb-B addition suggests that the eutectic point shifted from 12.6 to 14 wt% of silicon.

Figure 5.21 shows Al-14Si with and without Nb-B addition and well known grain refiner Al-5Ti-B. The difference in the microstructure is significant. The Nb-B addition to Al-14 Si made the primary silicon particles noticeably finer.

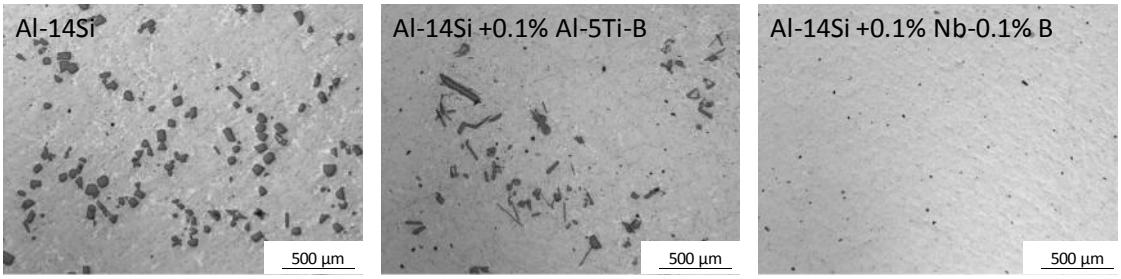

Figure 5.21 The microstructure of Al-14Si without addition, with 0.1wt% Al-5Ti-B and 0.1 wt% Nb-0.1 wt% B addition. Samples cast into the TP-1 mould with pouring temperature of 700 °C and a cooling rate of 3.5 °C/s.

As it can be seen in the Figure 5.21 the primary silicon particle size of Al-14Si with addition of Nb-B is definitely smaller. It decreases from 100 µm to 20 µm. Figure 5.22 presents the schematic cross-section of the TP-1 sample of Al-14 Si with Nb-B addition and the resulting microstructures.

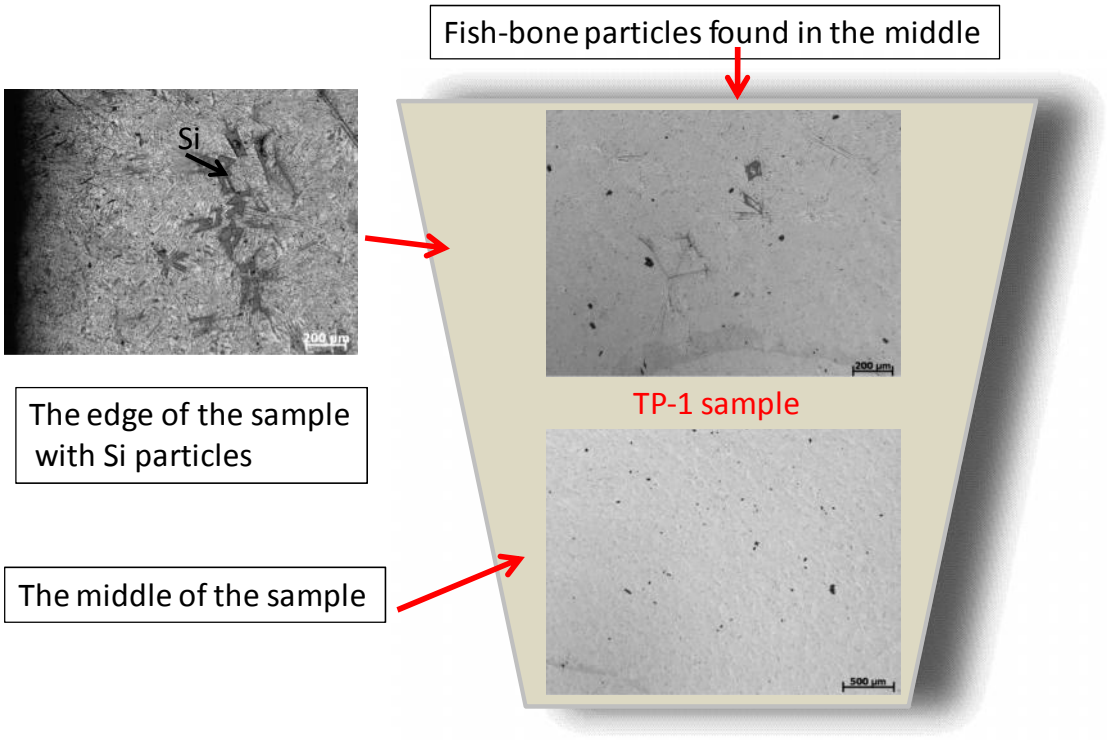

Figure 5.22 The schematic cross-section of the TP-1 sample of Al-14Si with addition of Nb-B and different microstructures. The bigger particles were found at the edge of the sample whereas in the middle are the finer ones.

The cross-section of the TP-1 sample of Al-14Si revealed that the Si particles are bigger at the edge of the sample. However the middle of the sample is filled with eutectic and a small amount of fish-bone, and star-like in appearance, Si particles. As mentioned above this microstructure suggests that the eutectic point may have been shifted towards Si rich.

Nevertheless the experiments were done using different moulds to achieve different cooling rates: 1 °C/s and 5 °C/s. Figure 5.23 shows the difference in primary silicon size with increasing the cooling rate. The same changes of eutectic point were noticeable in Al-14Si with Nb-B, with the slower cooling rate of about 1 °C/s. The hoper like crystals are dispersed only near the wall where the higher cooling rate is and they took about 10% of the whole sample area. However in the middle of the sample the primary silicon particles grew as fishbone morphology.

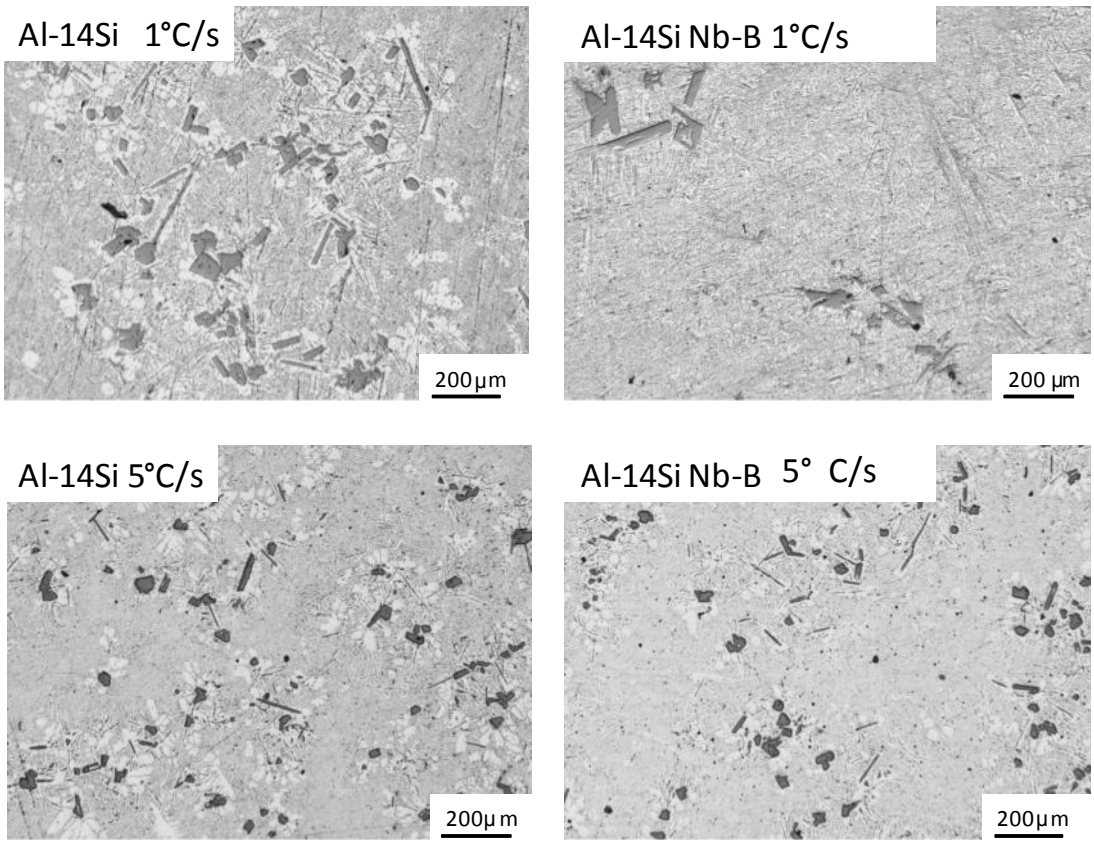

Figure 5.23 The Al-14Si without any addition and with Nb-B, melted in 800 °C and was cast into two moulds with different cooling rates 1 °C/s and 5 °C/s. Primary silicon particles size decreases with higher cooling rates.

It is well known that the solidification rate plays an important role in the refinement of metal structures and it significantly affects the mechanical properties. A high cooling rate and a short solidification time can lead to the formation of a more refined microstructure, an extended solute solubility and even metastable phases (Cantor B. 2001, Jones H. 1996). Figure 5.24 shows the particle size frequency count for both of the cooling rates

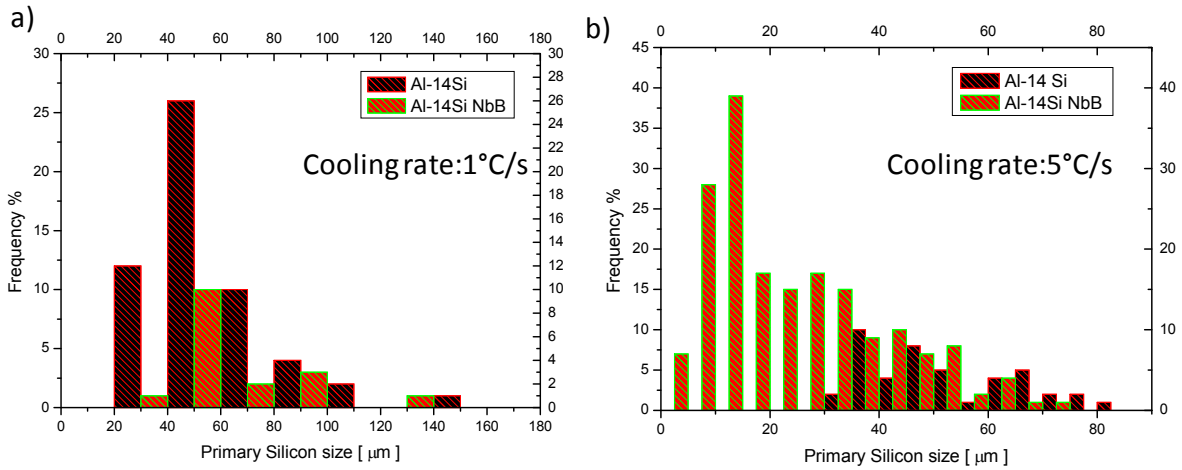

Figure 5.24 Histograms showing the particle size distribution of Al-14 Si without (red bars) and with Nb-B (green bars) melted in 800 °C and cast into two moulds with different cooling rates a) 1 °C/s and b) 5 °C/s. Primary silicon particles size decreases with higher cooling rates.

This experiment confirms that the cooling rate is significantly important in the solidification process for Al-Si alloys. The primary silicon particles size is decreasing with a higher cooling rate for Al-14 Si with Nb-B from 55 μm to 17 μm. In the case of Al-14Si without addition the change of the Si particles size is not significant from 50 μm to 35 μm. Also change in the size of α-Al was noticeable in alloys containing Nb-B the α-Al is much finer than in alloys without addition. The experiments were carried out for diverse aluminium silicon alloys with the same cooling rate of about 1 °C/s to have a good comparison of Al-Si with and without grain refiner.

Figure 5.25 shows that the addition of Nb-B to Al-16Si helps in decreasing the primary silicon. However Al-16Si with Nb-B contains large particles and has very small ones compared with Al-16Si without any addition. It is possible that the Nb-B addition helps to refine the primary Silicon.

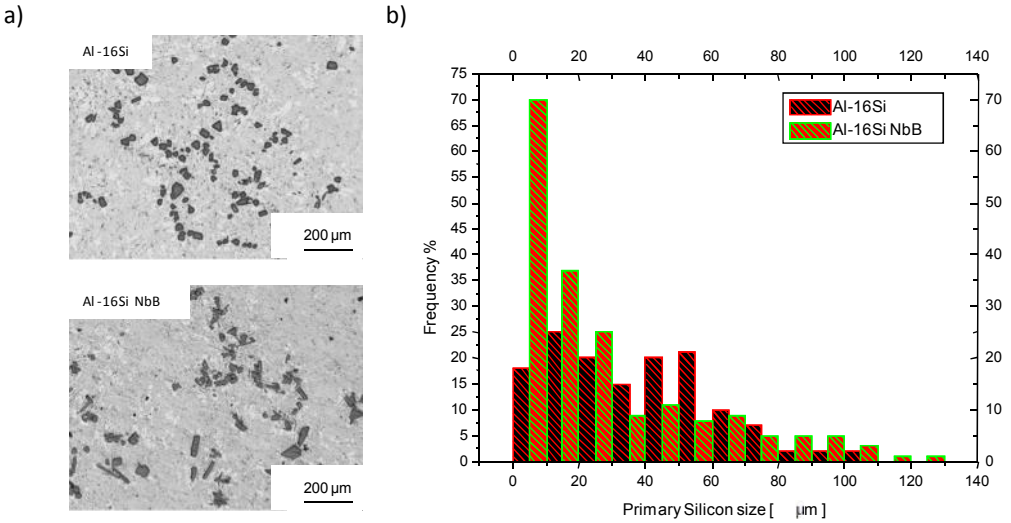

Figure 5.25 The Al-16Si alloy was melted in 800 °C and cast to the mould with cooling rate of about 5°C/s without any addition and with Nb-B a) microstructures of primary silicon particles, b) histogram showing the particle distribution in Al-16Si without and with Nb-B.

The quantitative analysis was performed for the eutectic needle length using microscope Axio Vison automatic calculations with manual selection of eutectic needles. From Figure 5.26, it is clearly seen that the eutectic is much finer with addition of Nb-B. It can be assumed that the Nb-B is refining α-Al and primary silicon. However detailed experiments are needed to confirm this.

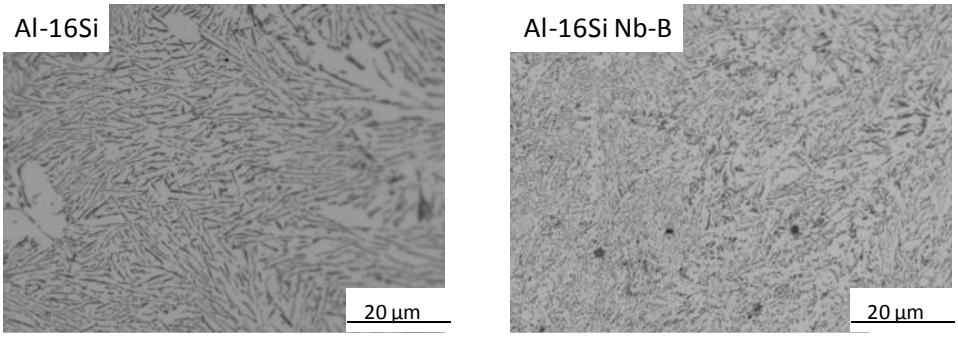

Figure 5.26 The microstructure of eutectic in Al-16Si without and with addition of Nb-B. The eutectic is finer with the addition of grain refiner.

Analyses were done for the eutectic Si size for higher silicon content like Al-18Si alloy and it is shown that the eutectic is still refined. The eutectic of α-Al and silicon is more fibrous and is not a coarse-like structure, as is commonly seen in Al-18Si without any addition.

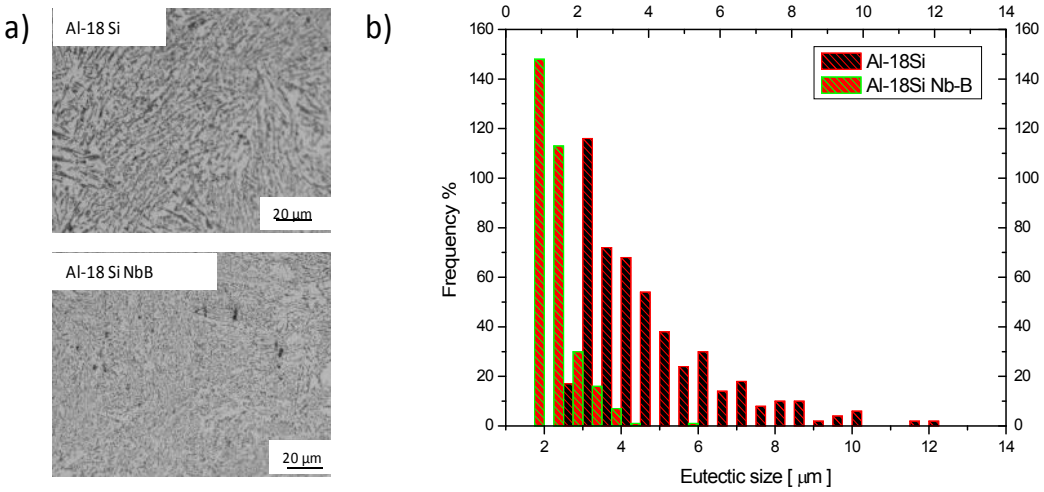

Figure 5.27 The Al-18Si alloy was melted at 800°C and cast into the mould with a cooling rate of about 5°C/s without any addition and with Nb-B a) microstructures of eutectic, b) histogram showing the eutectic size distribution in Al-18Si without and with Nb-B.

5.2.4 Commercial Hyper-eutectic Alloy LM13 (Al-13Si-0.8Cu)

The alloy LM13 is used in production of pistons for automotive applications. The influence of Nb-B as well as Sr and P addition to LM13 are investigated. Eutectic Si size and morphology modification is common practice for LM13 alloys to improve mechanical properties through promoting a structural refinement of the inherently brittle eutectic silicon phase. It is well known that additions of strontium to Al-Si alloys result in a transformation of the eutectic silicon morphology from coarse plate like structure to a well refined fibrous structure (Lu S. 1987) . The experiments were conducted to investigate the addition of Nb-B and Sr to the LM13 alloy. Figure 5.28 demonstrates the morphological difference in macrostructures.

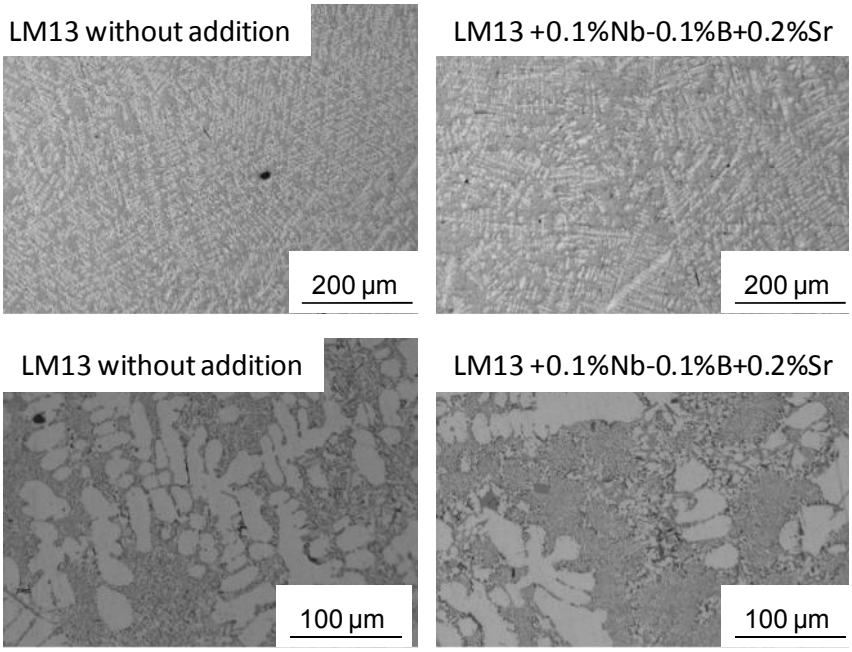

Figure 5.28 LM13 without any addition with 0.1%Nb-0.1%B and with 0.1%Nb-0.1%B-0.02%Sr, cast in 700°C into a cylindrical mould with a 0.1 °C/s cooling rate.

In LM6 with Nb-B + Sr addition the refining of α-Al is taking place as well as modification of the eutectic. It has been proposed that the addition of Al-B master alloy in Sr modified Al-11.6%Si alloy affords a large amount of nucleation sites for primary α-Al phase, remarkably refining the dendrites α-Al (Laio H. 2004). However as it was explained in the previous section, boron is not as effective as a combination of Nb-B. The lattice constants of eutectic α-Al phase are much closer to those of primary α-Al phase, so it is rational to think that the addition of Nb-B also enhances a large number of efficient sites in the melt for the nucleation of α-Al phase in eutectic, consequently favouring nucleation events of eutectic grains.

The hypoeutectic and hypereutectic Al-Si alloys are widely used for the tribological components of internal combustion engines in dry or lubricated contacts for a long time. The addition of higher concentrations of silicon to Al alloys, apart from reducing the coefficient of thermal expansion, results in alloys with good wear, corrosion, casting and machining characteristics. Okabayashi et al. (Okabayashi K. 1964) have studied the wear and friction characteristics of Al-Si alloys and concluded that the hypoeutectic Al-Si alloys

had higher wear resistance than hypereutectic alloys. They showed that the refinement of primary silicon scarcely improved the wear resistance of hypereutectic Al-Si alloys. Since the well known primary silicon refiner is phosphorus, a series of casting experiments were carried out to investigate the influence of Nb-B - P addition and the results are shown in Figure 5.29. The P refined the primary Si.

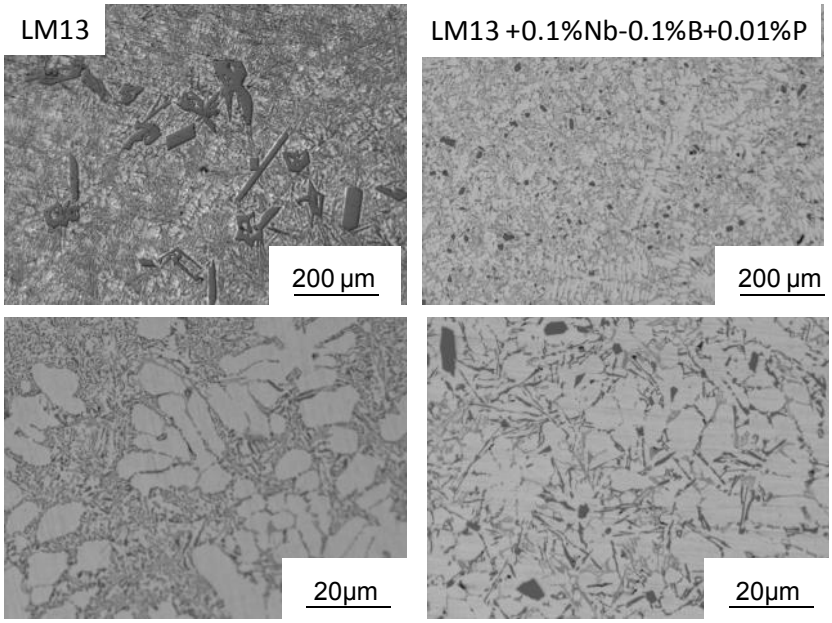

Figure 5.29 The LM13 without any addition, with Nb-B and with 1%Nb-1%B-0.01%P. The samples were cast into a cylindrical mould and preheated to 200°C.

5.3 Conclusion

The newly developed Nb-B grain refiner is identified to be very effective for Al-Si alloys. S it was previously mentioned the well know Ti is poisoning the Al-Si alloys and it is not effective grain refiner as it form silicides. After analysing the phase diagrams of Nb-Si and Ti-Si the conclusion can be made that Nb should not form poison the Al-Si alloys as the silicides are form in higher temperatures above 1700 °C. The experiments conform that primary α aluminium grain sizes are fine for hypo-eutectic alloys even for alloys with higher silicon concentration. In addition the experiments revealed that the addition of Nb-B refine the eutectic structure. In hyper-eutectic Al-Si alloys, the primary and eutectic Si size is also observed to be refined.

Chapter 6. Influence of Nb-B addition on Al-Si Alloys Properties

6.1 Introduction

The mechanical properties of cast aluminium alloys are very sensitive to composition, metallurgy, heat treatment, casting processes, formation of defects during mould filling and solidification. The coarseness of the microstructure and the type of phases that evolve during solidification are fundamental to the mechanical behaviour of the material. Current research on Nb-B addition to Al-Si alloys has identified it as effective in grain refinement as well as refinement of eutectic structure. Al-Si foundry alloys are popular because of their good castability, surface finish and resistance to corrosion. Typically, ~50-100% of the volume of Al-Si casting alloy is a eutectic mixture of aluminium and silicon. Solidification of the eutectic is one of the last reactions to occur during cooling and this is where most casting defects, such as porosity and hot tears, are formed. Those defects reduce the mechanical properties, compromise the ability of the casting to contain liquid or gas under pressure, interfere with coating and machining operations and can detract from the appearance of the product, in addition to causing a high reject rate. Mechanical properties of the aluminium alloys are strongly dependent on the effect of dendrite arm spacing (DAS). The DAS is a fundamental characteristic of the microstructure and has been used over the years as a means of fineness and therefore is a measure of the quality of cast products. It has also been established that DAS has a significant influence on extrudability. Since the cooling rate has a big influence on grain sizes and the alloys properties, in this chapter, we explored the use of Nb-B for the high cooling rate casting like High Pressure Die Casting (HPDC) and slow cooling casting like sand casting. The slow cooling rate used in sand casting is a source of many casting problems like cavities, porosity or huge grain sizes. To improve the properties of cast structures (e.g, engine blocks & brackets) produced with sand casting, a grain refiner which will work under slow cooling conditions is needed urgently. In this chapter the Nb-B addition to liquid metal and its influence on a wide range of cooling rates will be analysed. Improvement of mechanical properties and reduced porosity will be discussed.

6.2 Macrostructure Analysis

The microstructure formation during solidification depends on the alloy characteristics and is primarily a function of the temperature profiles at the solidification interface. When the metallic alloy is solidified, the most frequently observed solid morphology is the dendritic microstructure (Triverdi R. 1994). In the dendritic solidification of alloys, the solute redistributes due to the difference in solubility between the liquid and solid phases. The solute rejected from the solid-liquid interface develops a region in the liquid in which the actual temperature is lower than the liquidus temperature and leads to constitutional supercooling (Glicksman M.E. 1994). Dendritic microstructures are characterized by the microstructure parameters. Numerous solidification studies have been reported with a view to characterizing the microstructural parameters such as primary dendrite arm spacing, secondary dendrite arm spacing, dendrite tip radius and mushy zone depth as a function of temperature gradient and growth rate (Woodruff D.P. 1973, Bell J.A.E., and Winegard W.C 1963). In this chapter the influence of Nb-B addition on secondary dendrite arm spacing will be discussed. Dendrites grow in the liquid phase as α-solute solution and between two main dendrites secondary dendrites occur with α-β eutectic. The macrostructure analyses of dendrites in Al-Si alloys was controlled to investigate the influence of Nb-B on secondary dendrite arm spacing. It is known (Mihaichuk W. 1981) that the mechanical properties of these alloys may be improved by controlling their microstructure. Decreasing the secondary dendrite arm spacing can result in an increase in tensile strength and elongation. Cooling rate has been proven to be one of the effective parameters to control the microstructure of as cast alloys. By increasing the cooling rate the secondary arm spacing of the alloys decreases, as seen in the Figure 6.1 b. In general the dendrite arm spacing can be related to cooling rate as:

$$\lambda = (R^{-n}) \quad \textbf{(6.1)}$$

Where λ is SDAS and *n* is in the range of 1/3 to 1/2 for secondary spacing (Flemings M.C. 1974)

However the slow cooling rates used in sand casting results in lower tensile strength of materials. By reducing the grain size and SDAS, one can improve the mechanical properties of alloys.

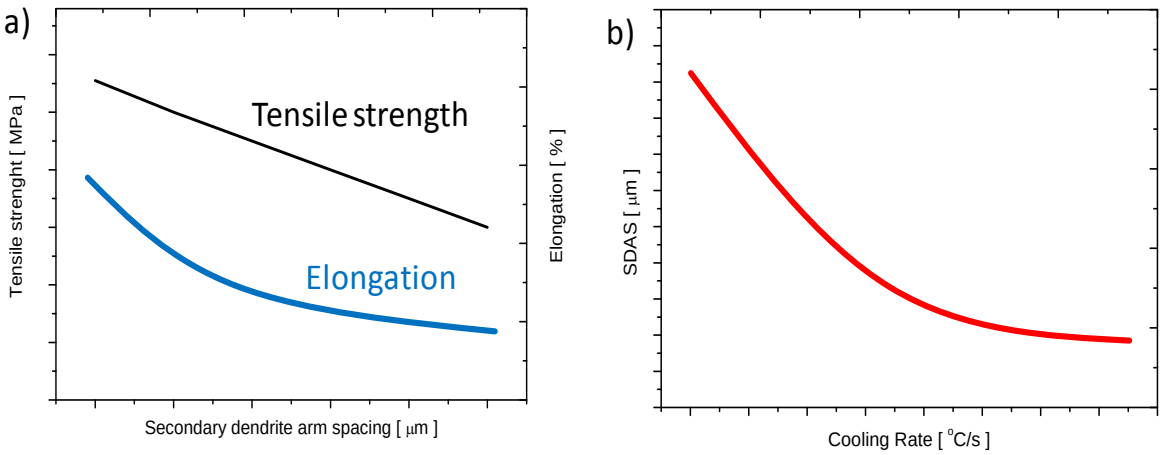

Figure 6.1 Schematic illustration. a) The effect of the secondary dendrite arm spacing on the properties of aluminium casting alloys. b) The SDAS as a function of cooling rate. (Mihaichuk W. 1981)

Measurement was done to calculate secondary dendrite arm spacing which is the distance between the middle of two consecutive secondary dendrites (Figure 6.2).

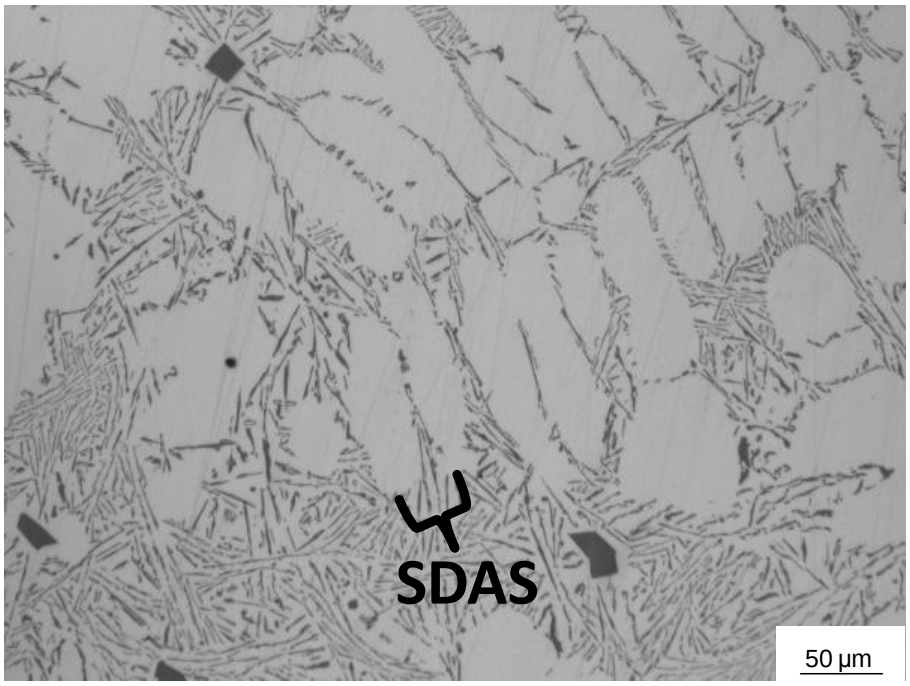

Figure 6.2 Description of measurement for the secondary dendrite arm spacing (SDAS).

The measurements were performed on several grains in the samples to obtain the SDAS which were averaged. Easton et al (Easton M., Davidson C., StJhon D., 2010) suggest that grain refiner has little effect on SDAS, rather composition of liquid at the temperature at which SDAS is determined is the most influential factor. Upon analysing the microstructures, it was found that the Nb-B grain refiner has an effect on SDAS formation as shown in Figure 6.3. However the assumption can be made that the Nb-B addition is changing the liquid composition during the SDAS formation especially in high content of silicon. The work of Bamberger et al (Bamberger M. 1987) has demonstrated that increasing the silicon content in aluminium reduces the cooling rate and hence influences the SDAS. The analyses were conducted for Al-Si alloys (5-9 wt% Si), with and without grain refiner addition, cast with TP-1 mould (3.5 °C/s).

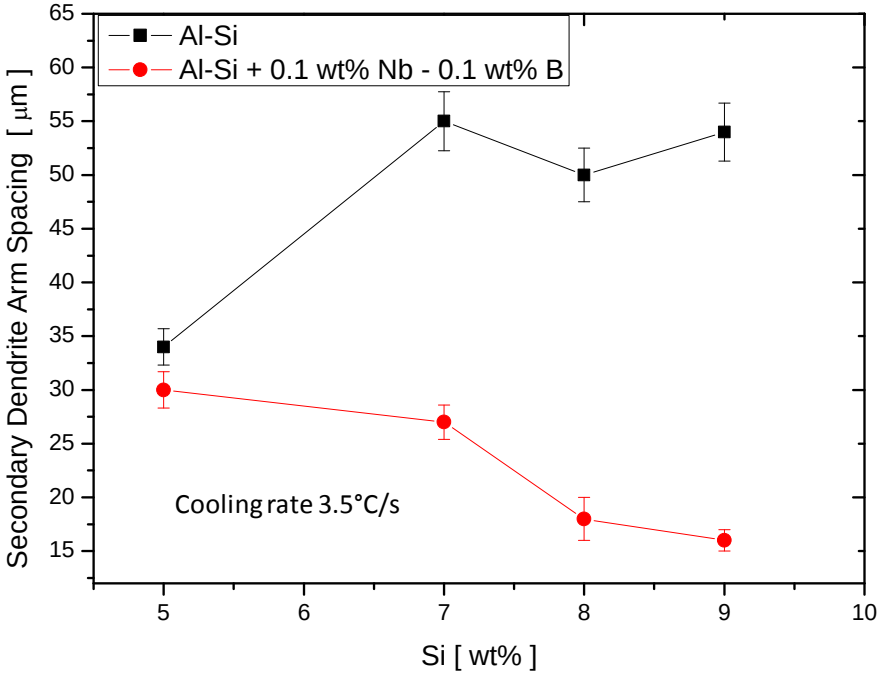

Figure 6.3 The influence of Nb-B on the size of secondary dendrite arm spacing. Cooling rate during solidification is 3.5 °C/s and the pouring temperature in the mould is 700°C.

Figure 6.3 presents the influence of Nb-B on the size of secondary dendrite arm spacing, at a fixed cooling rate of 3.5 °C/s. The secondary dendrite arms spacing is observed to decrease

with higher silicon additions in the grain refined samples. It is expected that the mechanical properties of those castings will be increased as illustrated in Figure 6.1. Figure 6.4 shows the difference in the grain size and the secondary dendrite arm spacing.

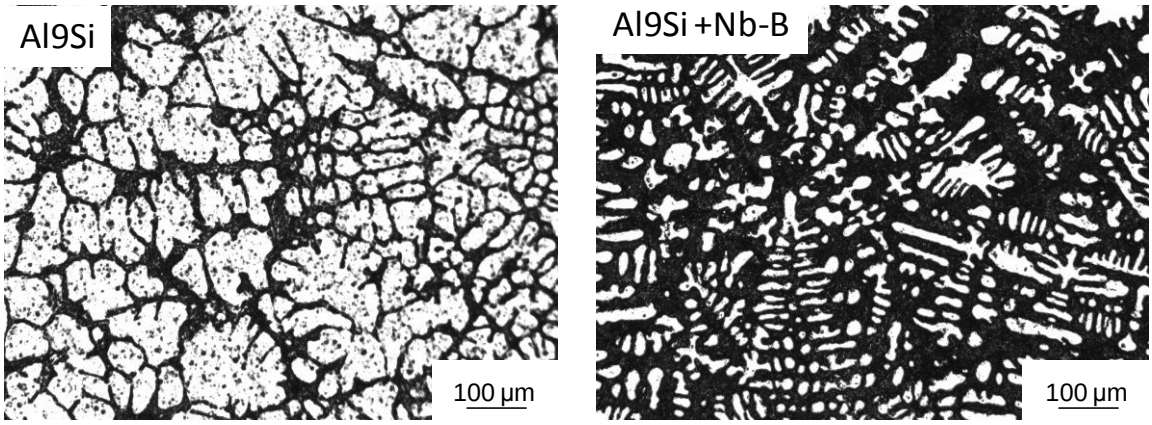

Figure 6.4 The macrostructures of Al-9Si without and with Nb-B addition. When the grain refiner is added, the length of secondary arm spacing is smaller.

It can be noticed that the grain sizes are significantly smaller in the sample with Nb-B and there is a notable change in the morphology of the grains. In the sample with Nb-B addition the α-Al secondary dendrites are finer and the sample consists more of the eutectic phase. The analysis as made to compare the SDAS with cooling rate. It is well known that by increasing the cooling rate the SDAS will be smaller. Figure 6.5 presents dependency between the cooling rate, the secondary arms spacing and grain size.

The secondary arms spacing measurements in Al-6Si without and with Nb-B addition show that it is sensitive to the cooling rate. With low cooling rates the SDAS is higher in comparison to higher cooling rates.

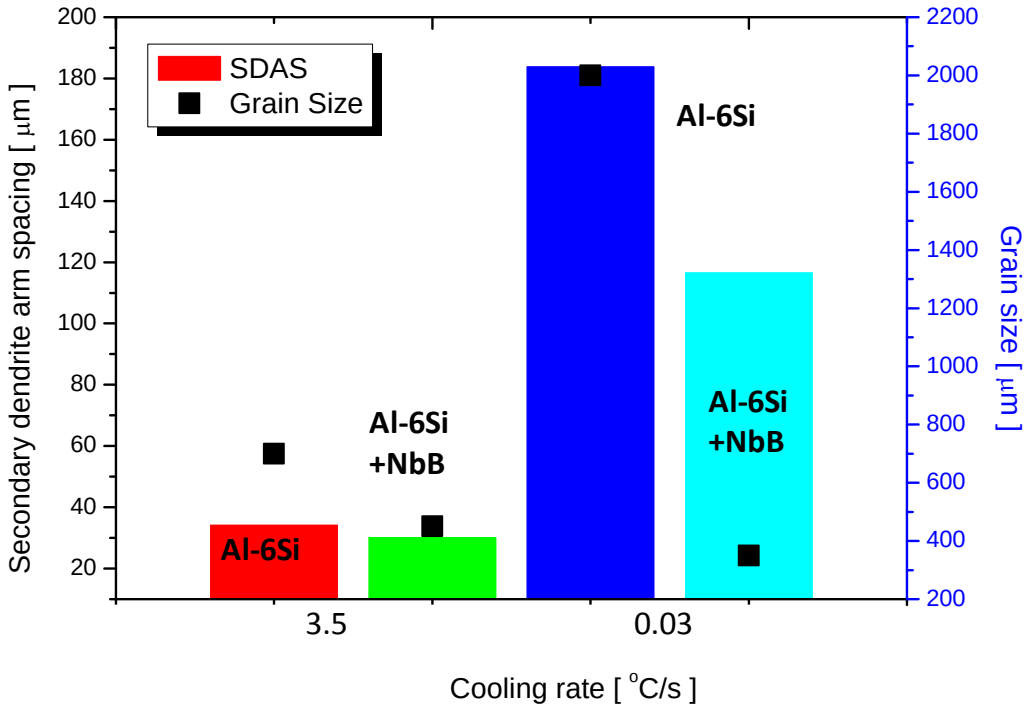

Figure 6.5 The secondary arms spacing and grain size as a function of cooling rate for Al-6Si without any addition and with Nb-B. The secondary arm spacing decreases as the cooling rate increases. The grain sizes have some influence on the SDAS.

6.3 Formation of the Intermetallics during Solidification

Commercially used Al-Si alloys have specific properties which are achieved by alloying elements such as Fe, Si, Cu, Mn etc. Commercial Al-alloys usually contain Fe, often as an undesirable impurity and occasionally as an useful minor alloying element. In industrial practice, the impurity Fe pickup results mainly from the use of steel tools during melting and casting, and the use of scrap materials. For the vast majority of Al-alloys such as Al-Si based cast alloys, the presence of Fe is detrimental to mechanical properties (Mondolfo F. 1976, Wang L., Makhlouf M., Apelian D., 1995) and Fe pickup is thus a major problem for industrial use and recycling of Al-alloys. Extensive efforts have to be made to keep the Fe levels as low as economically possible.

Although iron is highly soluble in liquid aluminium and its alloys, it has very little solubility in the solid and so it tends to combine with other elements to form intermetallic phase particles of various types. In the absence of Si, the dominant phases that form are Al_3Fe and Al_6Fe, but when Si is present, the dominant phases are Al_8Fe_2Si (known as alpha- or α-phase) and Al_5FeSi (known as beta- or β-phase). If Mg is also present with Si, an alternative called pi- or π-phase can form, $Al_8FeMg_3Si_6$. Another common phase that forms when Mn is present with Si is $Al_{15}(Fe, Mn)_3Si_2$, also confusingly known as an α-phase. This phase tends to form in preference to the other α-phase whenever Mn is present.

The iron-containing intermetallic phases listed above are quite obvious within the microstructures of Al-Si alloys and can usually be distinguished under the microscope by their dominant morphology and colour. Both of the so-called α-phases form in a script-like morphology (see Figure 6.6 b) but the $Al_{15}(Fe, Mn)_3Si_2$ version of α can also be found as a more compact, blocky form, and sometimes even as polyhedral crystals. The π-phase also forms with the a script-like morphology (Figure 6.6 d) and is often, but not always, closely connected to the β-phase (Figure 6.6 c) which, in turn forms, with a distinctive platelet morphology (Figure 6.6 a,c).

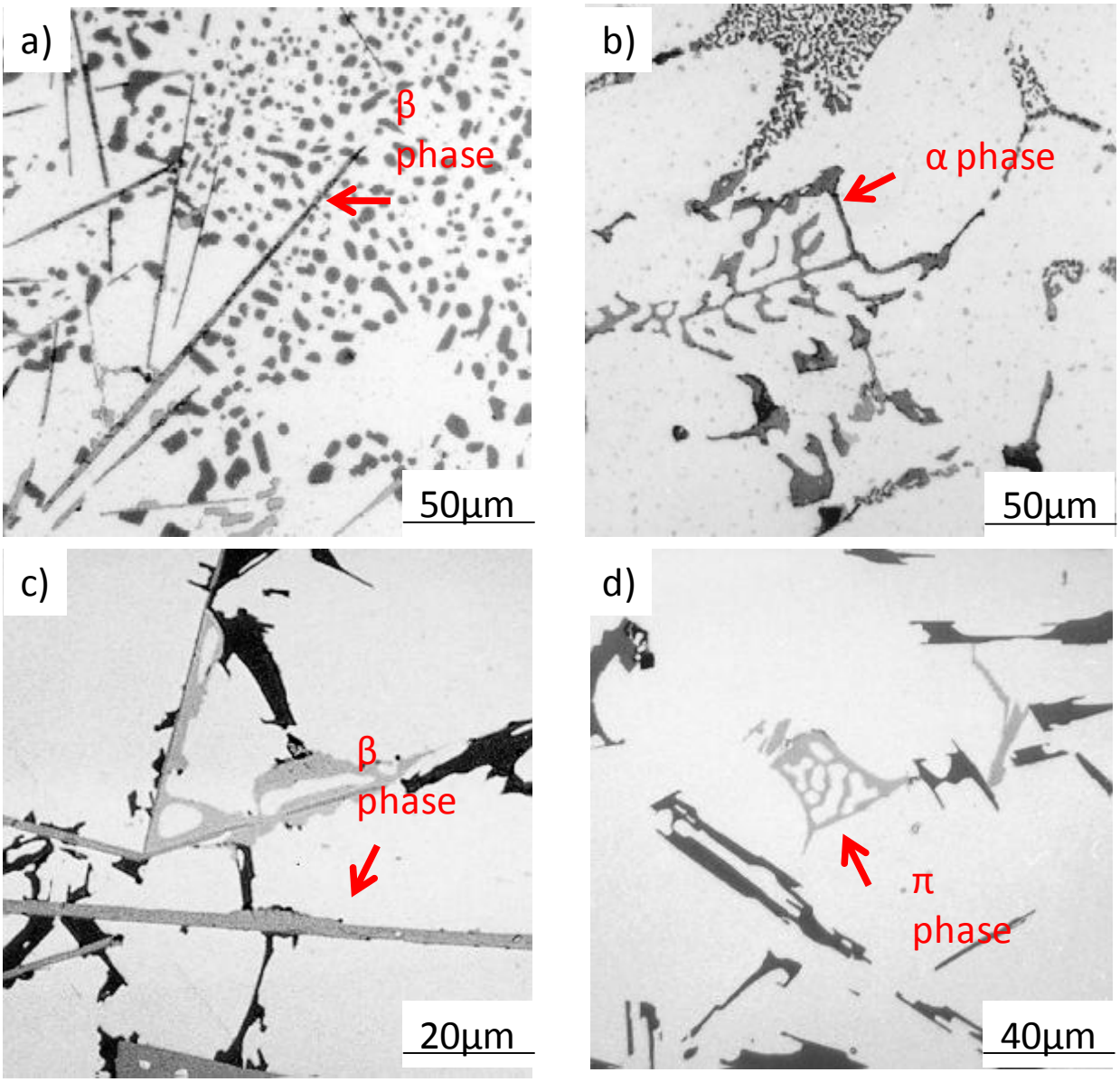

Figure 6.6 Microstructures of various common iron containing intermetallics showing their typical morphologies in Al-5%Si-1%Cu-0.5%Mg (Fe) alloys: a) β-Al_5FeSi plates; b) script like α-Al_8Fe_2Si; c) π-phase growing from β; d) script like π-phase. (Taylor 2004)

The analyses were carried out for LM6 and LM24 alloys and the effect of Nb-B addition on their intermetallics is investigated. The iron phases in LM6 without and with Nb-B have mostly the Chinese script morphology, however, the size and dispersion of the particles is different in LM6 with Nb-B. The iron phases are smaller and they disperse everywhere in the

sample in comparison to LM6 where the Fe phases are larger and are present in just a few locations.

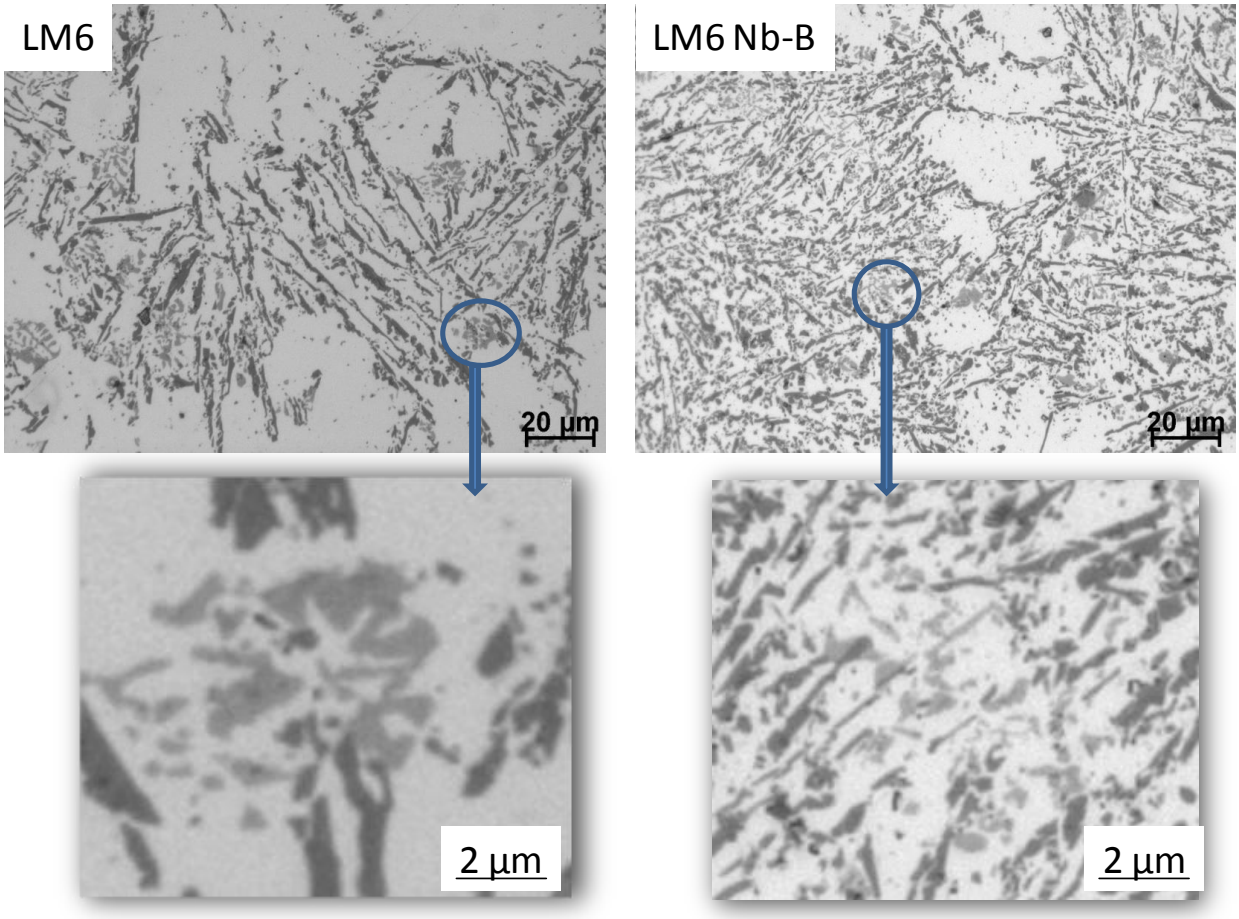

Figure 6.7 Microstructures of Fe phases in LM6 without and with Nb-B addition. The intermetallics have script-like morphology.

The cubic morphological intermetallics were found in the LM24 and LM6 samples cast with the high pressure die casting method (Figure 6.8). The iron particles are smaller by 40 % in LM24 with Nb-B due to smaller grain size and eutectic phases.

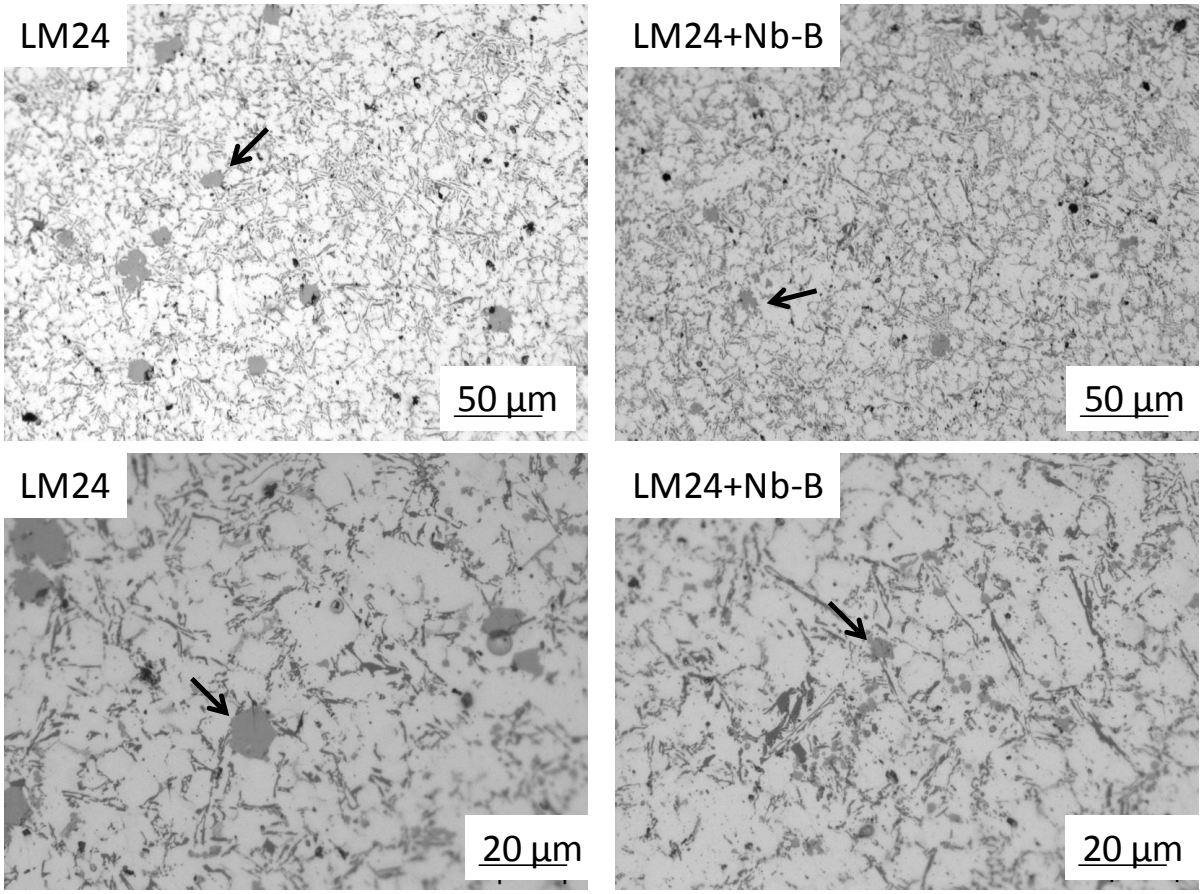

Figure 6.8 The microstructures of high pressure die cast LM24 without any addition and with 0.1 wt% Nb-0.1 wt% B. The Fe intermetallics (depicted by the arrows) are reduced from ~10 µm to ~5 µm

The effect of smaller grain sizes and intermetallics are expected to contribute to improved mechanical properties. The tensile tests were performed on ASTM standard tensile bars produced with the high pressure die casting process. Figure 6.9 shows the tensile test results for LM6 and LM24 without and with Nb-B addition. The diagram presents the average ultimate tensile strength of six samples versus elongation.

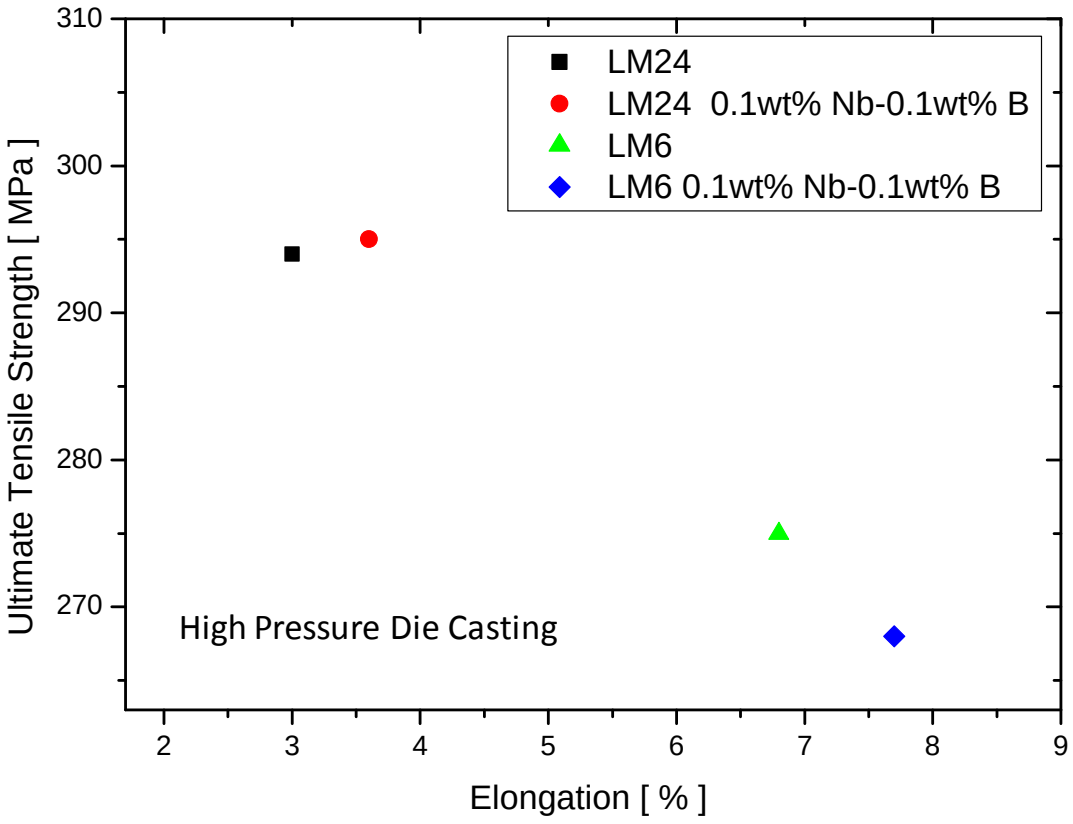

Figure 6.9 The ultimate tensile strength versus elongation for LM6 and LM24 without any addition and with Nb-B. The samples were melted at 800 °C and cast using the High Pressure Die Casting machine. The shapes of the cast samples are illustrated in Chapter 3.

The results presented show that the addition of Nb-B to commercial LM6 aluminium-silicon alloy has a positive effect on the mechanical properties especially on elongation. If two materials have the same strength and hardness, the one which has higher ductility is more desirable for practical applications.

6.4 Influence of Cooling Rate and Nb-B Addition on Grain Structure and Mechanical Properties of Al-Si Alloys

The Al-Si alloy automotive parts like engine blocks and brackets are usually formed by shape casting. A good casting is supposed to fill the mould cavity without defects. Thus, the gating system design, cooling rate and casting pressure can all affect the cast structure. The refinements of structure can often be achieved by controlling casting process parameters. Cooling rate is important in the formation of microporosity. A higher cooling rate reduces solidification time and grain size of casting. With a higher cooling rate, the grain density increases but dendrite arm spacing and the average pore size decrease. With a lower cooling rate, more gas can precipitate from the melt and thus produce higher porosity (Ceylan M. 1997). Low cooling rates with usage of sufficient grain refinement can be a good practice for the industry to produce more complicated shaped parts with thinner walls.

The following experiments were carried out to investigate the influence of Nb-B under different cooling rates. The alloy was melted at 800 °C, without and with Nb-B addition and cast into different moulds to achieve diverse cooling rates. Figure 6.10 shows the grain sizes as a function of cooling rate. It can be seen that the grain refiner is less sensitive to different cooling rates. Even with a cooling rate as low as 0.03 °C/s the grain sizes are still smaller.

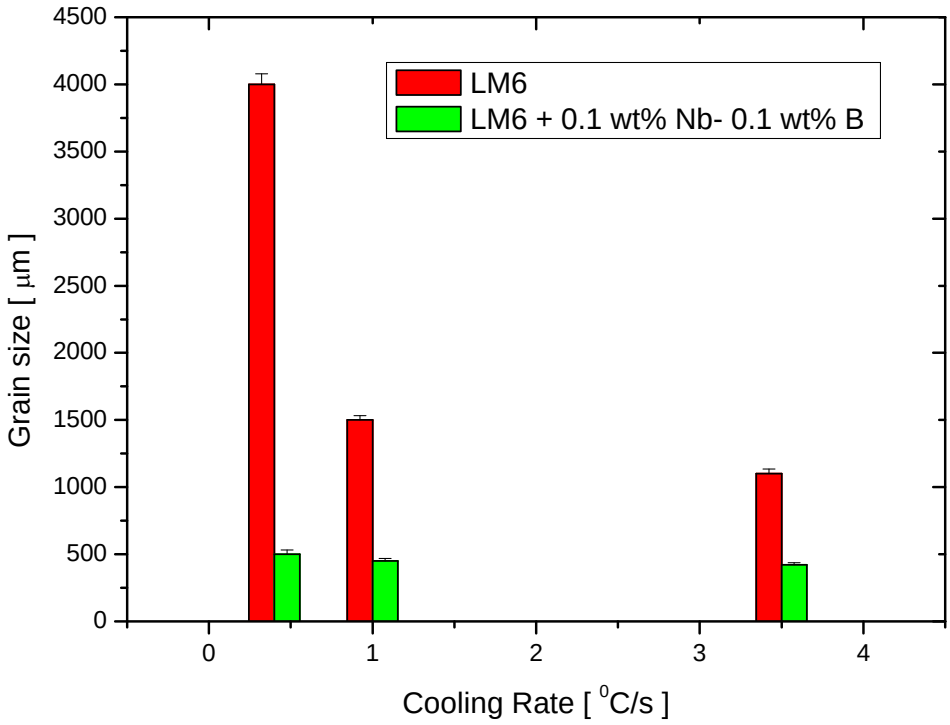

Figure 6.10 The grain sizes as a function of cooling rate for LM6 and LM6 with Nb-B. The samples were all melted at 800 °C and cast into the moulds that provides the cooling rates of 0.03 °C/s, 1 °C/s and 3.5 °C/s. The Nb-B added samples are less sensitive to cooling rate.

The literature suggests that with a lower cooling rate the porosity is higher (Ceylan M. 1997), although this may not be case for the aluminium-silicon alloys with grain refiner. However as Figure 6.11 shows, the Nb-B addition has a huge influence on the grain sizes and the porosity of the LM6. The grain sizes decreased from 4-6 mm to 450 μm and the porosity is noticeably reduced by 60%.

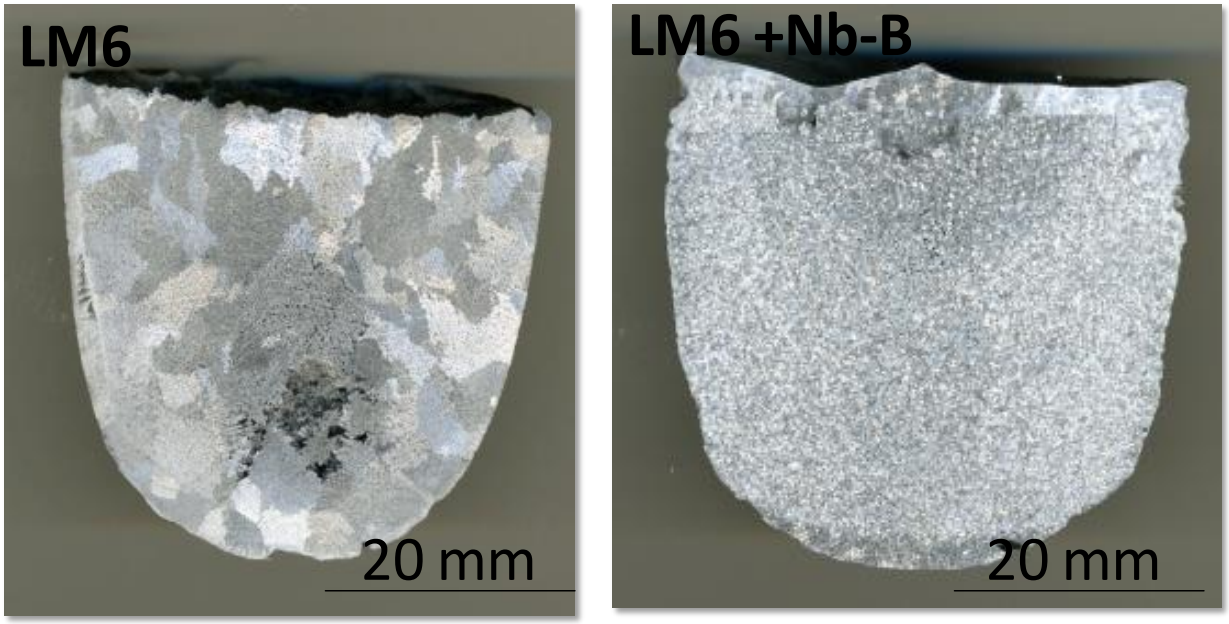

Figure 6.11 The LM6 macro-etched samples without any addition and with Nb-B. The cooling rate is 0.03 °C/s. The grain sizes decreased from 4-6 mm to 450 µm and the porosity is significantly reduced.

Experiments were also carried out for LM25 and the results presented in Figure 6.12 confirm that Nb-B is less sensitive to cooling rate and it can refine the alloys even in low cooling rates. The very low cooling rate of about 0.003 °C/s was used in this example.

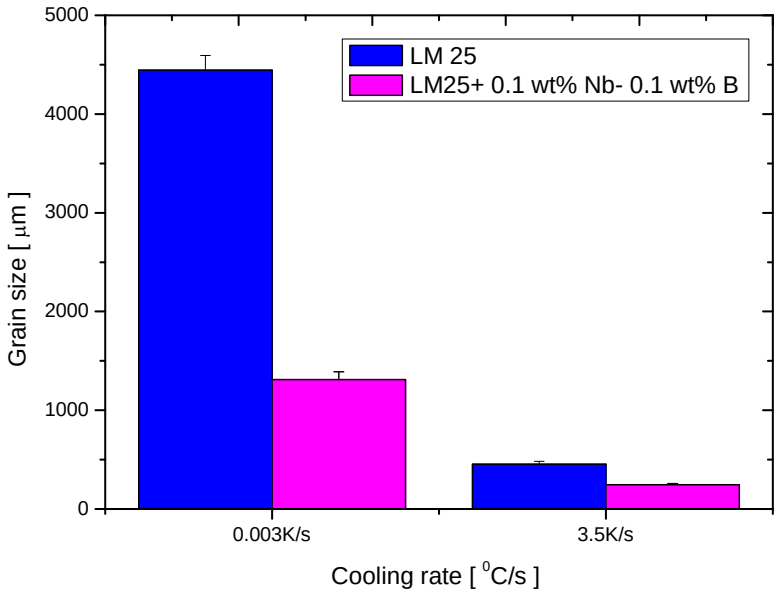

Figure 6.12 The grain sizes as a function of cooling rate for LM25 without any addition and with Nb-B. The cooling rates used are 0.003 °C/s and 3.5 °C/s. Nb-B addition has significantly reduced grain sizes at very low cooling rate.

To investigate the influence of Nb-B as a function of continuous change in cooling rate, the wedge-shape copper mould was used (Norman F. 1998). The liquid alloys were cast into a wedge copper mould which was designed to give a range of cooling rates. Accordingly, at the top surface of the mould, the cooling rate is estimated to be ~ 20 °C/s. At the distance of 30 mm from the wedge tip, the cooling rate is ~50 °C/s. At the wedge tip, an applied cooling rate of ~150 °C/s was estimated (Suarez M.A. 2010). Sections were taken from different positions along the central line. Figure 6.13 shows the LM6 casting without any addition, with 0.1wt% Al-5Ti-1B (a commercially known grain refiner) and with a 0.1wt% Nb - 0.1wt% B. The LM6 with Nb-B shows reduced gas and shrinkage porosity. Also uniform grain sizes among the sample are noticeable. The microstructure of wedge structure with Al-5Ti-1B and without any addition is similar.

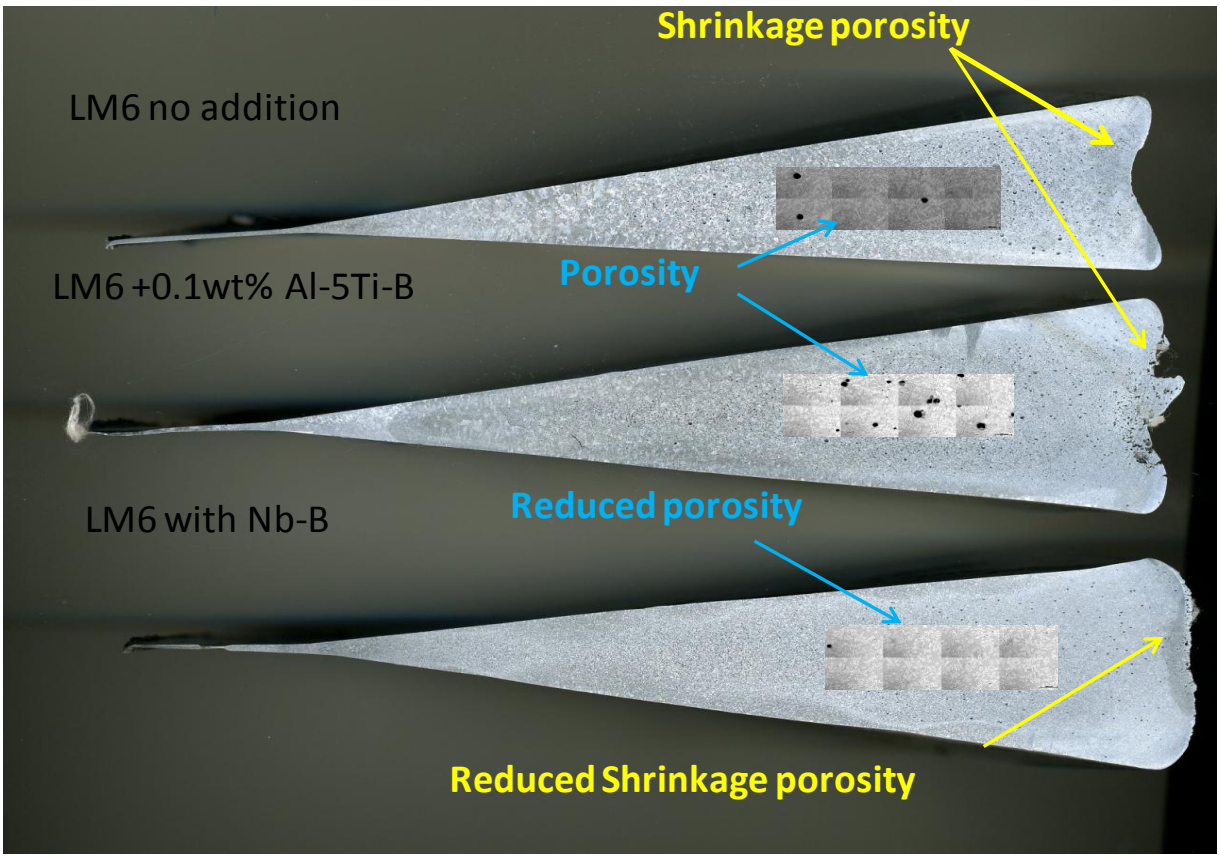

Figure 6.13 The copper wedge mould cast samples of LM6 without any addition with 0.1wt% Al-5Ti-B and 0.1wt%Nb-0.1wt%B; with the cooling rates from 20 °C/s to 150 °C/s. The reduced gas and shrinkage porosity is obtained with the use of Nb-B addition. The grain sizes are similar among whole LM6 with Nb-B sample.

From the above analyses the conclusion can be made that the addition of Nb-B results in fine grain sizes at different cooling rates. Nowadays foundry plants are forced to reduce the wall thickness of cast pieces and to minimize the surface roughness (suction canal).

It is possible that with Nb-B addition more complicated shapes could be cast with reduced porosity. Reduction of the wall thickness could be possible even in sand casting. For example engine blocks could be produced from aluminium-silicon alloys with reduced wall thickness, so that overall weight can be reduced. The measurements of the grain sizes were taken and the diagram below shows the LM6 without and with 0.1wt% of Nb and 0.1wt% of B addition.

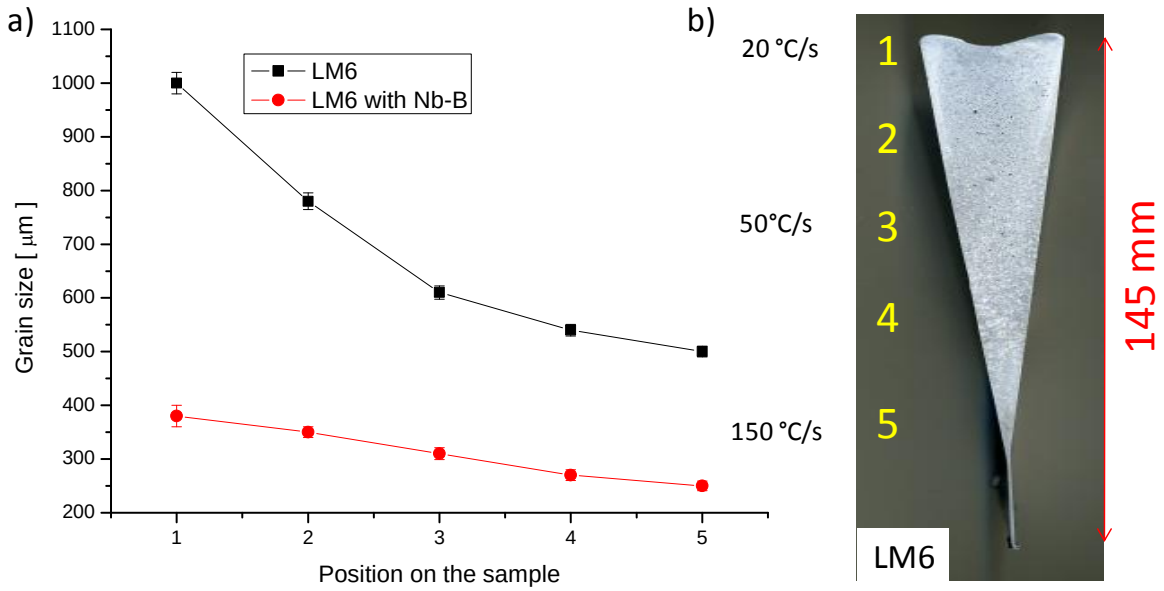

Figure 6.14 a) The grain sizes as a function of the position in the wedge cast sample of LM6 with 0.1 wt% Nb + 0.1 wt% B addition and LM6. b) The macrostructure of the wedge copper mould sample LM6. The samples were melted at 800°C and cast at 740°C into the copper wedge mould. The grain sizes of LM6 with Nb-B addition are less variable in all cross-sections than without addition.

The grain size is less variable in all the cross-section which suggests that the grain refiner is less sensitive to the cooling rate.

Microstructural analysis was made to investigate the cooling rate influence on eutectic structure. In Figure 6.15, eutectic Si size is shown for LM6 without addition and with Nb-B under different cooling rates.

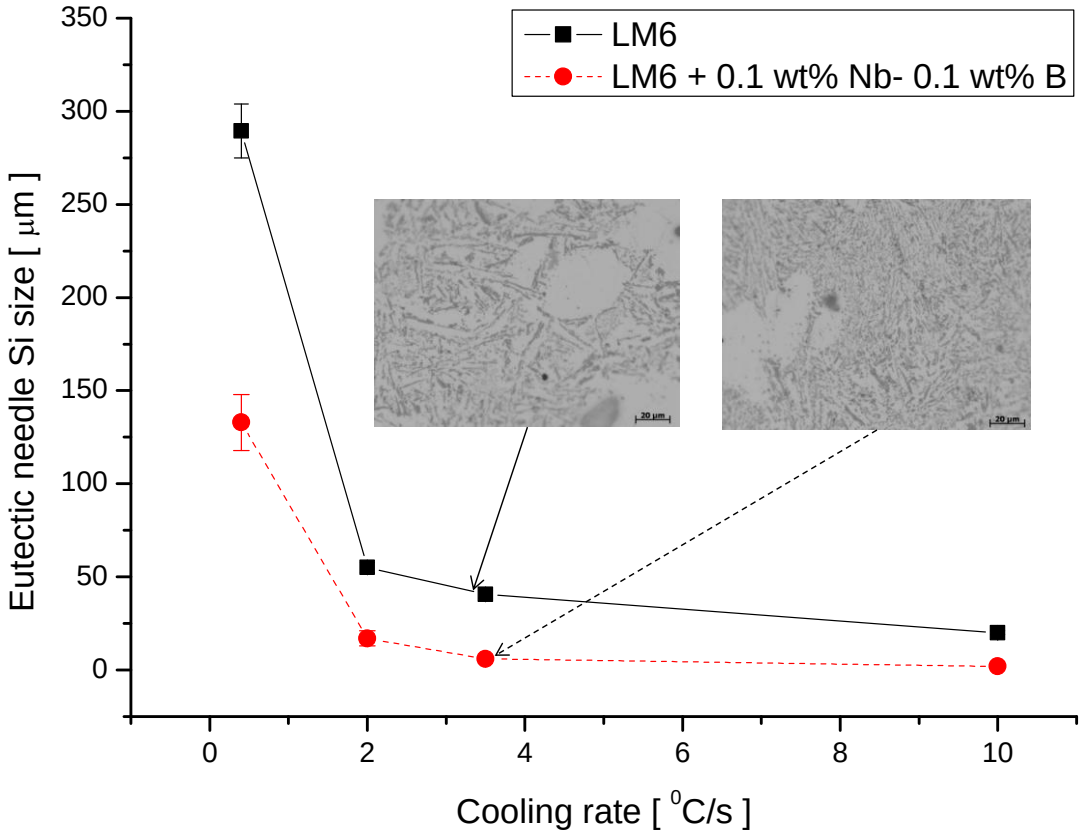

Figure 6.15 The eutectic size as a function of cooling rate for LM6 without addition and with 0.1wt% Nb - 0.1wt% B addition. The eutectic size is observed to reduce with usage of Nb-B grain refiner.

It is well known that eutectic modification with strontium addition is very difficult under slow cooling conditions. The LM6 with Nb-B addition and without any addition had a cooling rate of 0.03°C/s. Under such low cooling rate, with Nb-B addition, we still can observe the grain refinement not only for α-Al but also eutectic. It can be assumed that as Nb-B is refining the α-Al it can also have positive influence on the α-Al in eutectic system. The eutectic needle Si size decreases from 280 µm to 130 µm in the sample produce with cooling rate of 0.03 °C/s.

The porosity fraction was measured for LM6 at the middle of the samples of TP-1 test. The measured cross-section area is 2 cm x 1 cm and in Figure 6.16 it is shown that the Nb-B addition decreases porosity.

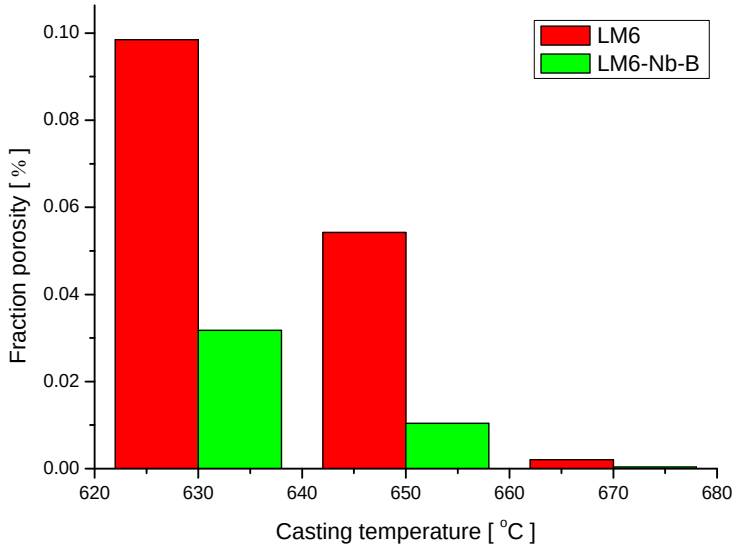

Figure 6.16 The porosity differs in LM6 without addition and with Nb-B. The melt was poured into the TP-1 mould at different pouring temperatures. The Nb-B addition has a positive influence on porosity.

The porosity is decreasing with the addition of Nb-B, also some of the conditions in the laboratory can have an effect on porosity. It does not mean that with a higher pouring temperature the lower porosity fraction is achieved.

Most aluminium castings are used in the 'as cast' condition, but there are certain applications that require higher mechanical properties, or different properties from the as cast material. The heat treatment of aluminium castings is carried out to change the properties of the as-cast alloys by subjecting the casting to a thermal cycle or series of thermal cycles. For sand castings and gravity die castings all heat treatments are possible, though not all are standardised. Pressure die castings however, cannot generally be heat treated.

Experiments were carried out to compare the tensile properties of LM25 without any addition and with Nb-B. Also the heat treatment was performed on the tensile bars to analyse the heat treatment influence on the metal. The samples were melted at 800 °C and poured into the preheated cylindrical mould for tensile bars preparation (Chapter 3). The LM25 was solution treated and stabilized for 5h at 532 °C and then quenched in hot water followed by stabilizing treatment at 250 °C for 3h (TB7). The diagram shown in Figure 6.17 presents the maximum

value of measured elongation as a function of the corresponding tensile stress for LM25 without addition and with Nb-B, heat treated and not heat treated.

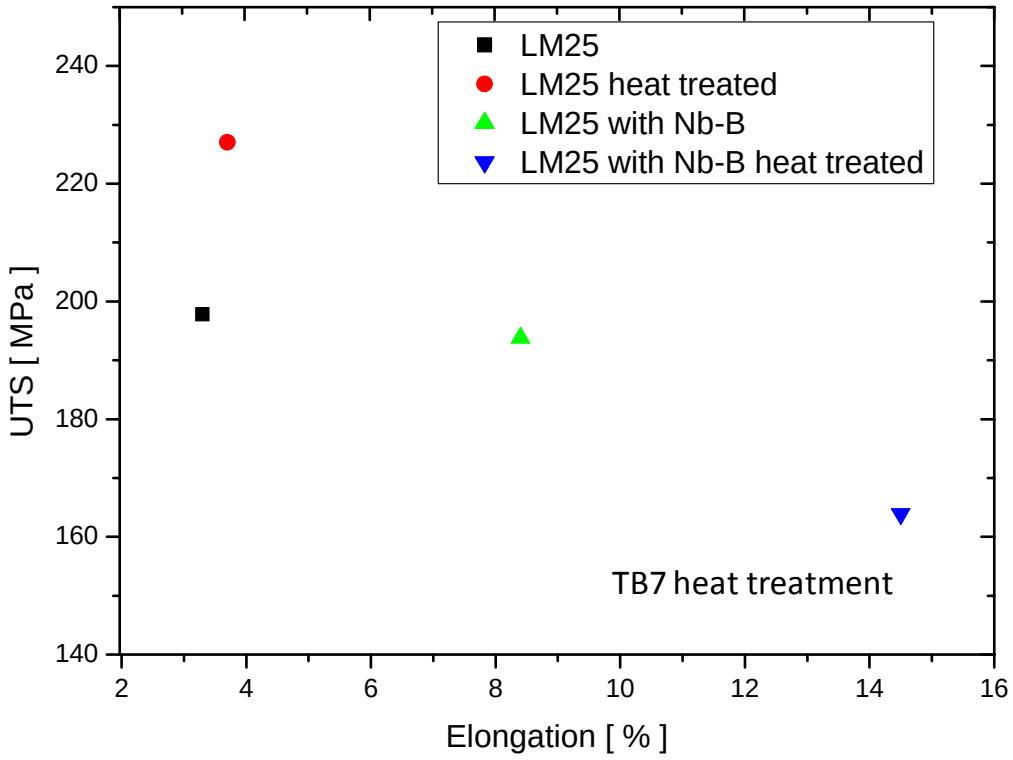

Figure 6.17 The tensile strength as a function of elongation for LM25 without and with Nb-B addition, with heat treatment and without.

As it is seen from diagram Figure 6.17, the heat treatment of LM25 has improved its tensile strength. The LM25 was supplied by *Norton Aluminium*, by analysing the mechanical properties data (BS 1940) and measurements made in BCAST we can conclude that the elongation and the tensile stress are similar (Table 6.1).

	LM25	LM25 TB7	**LM25 BCAST**	LM25 TB7 BCAST	LM25 TB7 BCAST (Nb-B)
UTS [MPA]	**160-200**	230	**197.8**	227	167
Elongation [%]	**~3**	~5	**~3.3**	~3.7	~14.7

Table 6.1 The Ultimate tensile strength and elongation measurements at Norton Aluminium and BCAST laboratory.

The addition of Nb-B improves the elongation and tensile strength of LM25. The heat treatment of LM25 with Nb-B improved significantly the elongation from 3.3-3.7 % for LM25 without any addition to 14.7%.

Experiments were done to investigate the cooling rate influence on mechanical properties such as tensile strength and elongation for commercial alloy LM6. Figure 6.18 presents the LM6 with and without addition of 0.1wt% of Nb and 0.1wt% of B. The cooling rate used was 1 °C/s. The mechanical properties LM6 data (BS 1490) suggest that UTS should be 280 MPa and elongation 2-3 %. Although UTS is lower in our case we are comparing LM6 cast in the same condition with and without Nb-B addition. The results show the improvement in UTS and in elongation from ~2.5-4.5% to 4.5-8%.

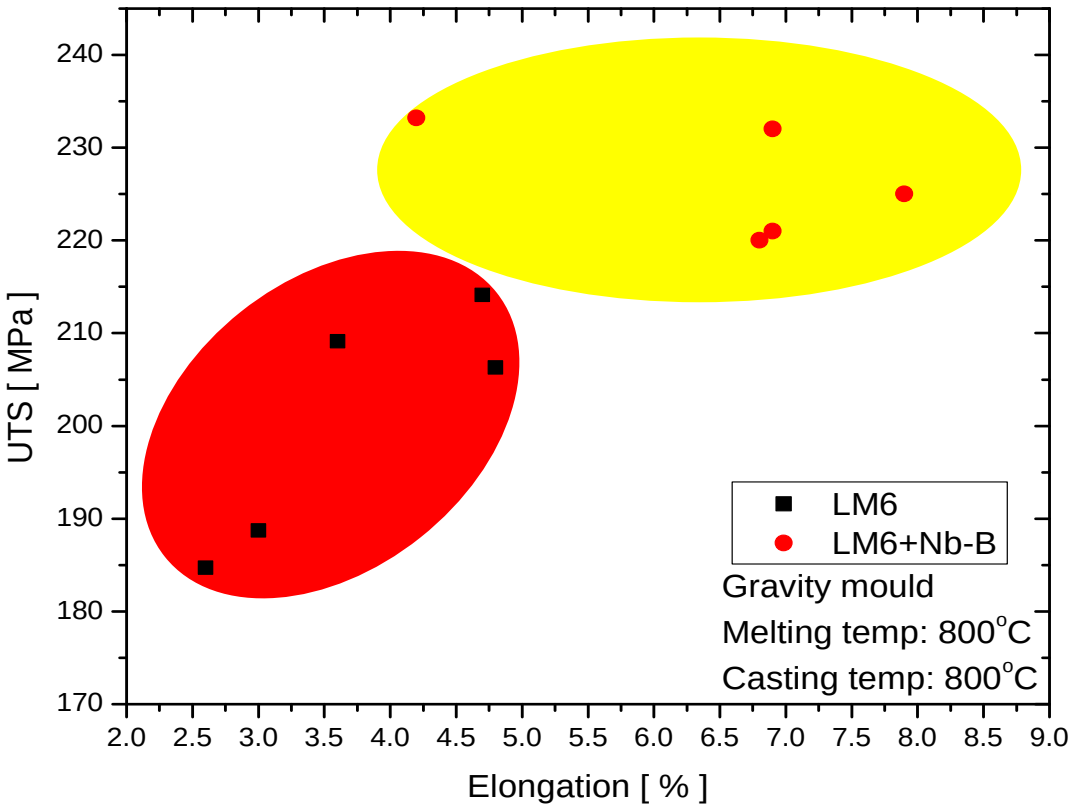

Figure 6.18 The Ultimate tensile strength as a function of elongation for LM6 with and without 0.1wt% Nb - 0.1wt% B. The LM6 with grain refiner has better strength and elongation than without any addition.

The experiments were carried on for sand casting alloys with usage of slow cooling rate. The samples of LM6 were melted at 800 °C and cast into the preheated mould (200 °C). The measured cooling rate is 0.1 °C/s. The samples were machined into the tensile bars. The results are shown in Figure 6.19. The mechanical properties LM6 data suggest that for slow cooling LM6 UTS is ~160 MPa and elongation is ~5%.

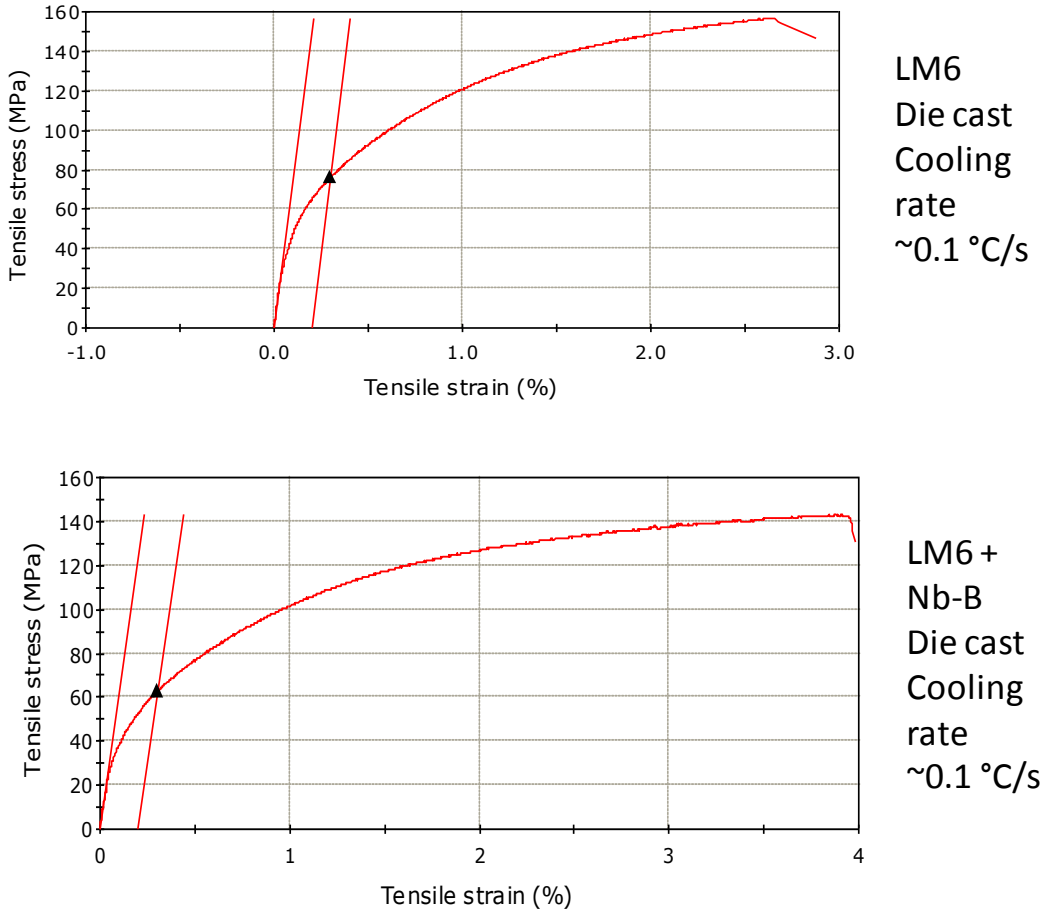

Figure 6.19 Tensile test diagram of LM6 and LM6 with Nb-b addition. The elongation of LM6 with Nb-B (bottom diagram) is slightly improved from 2.8 to 4%.

The most important is that the mechanical properties didn't decrease with addition of Nb-B.

The hardness of the material plays a significant role in the assessment of materials for applications. Vickers hardness measurements were performed on LM6 with different cooling

rates from 0.03 °C/s for the slow cooling rate to 1000 °C/s for the HPDC samples. Figure 6.20 shows the measurement of average hardness for 5 different positions in each sample.

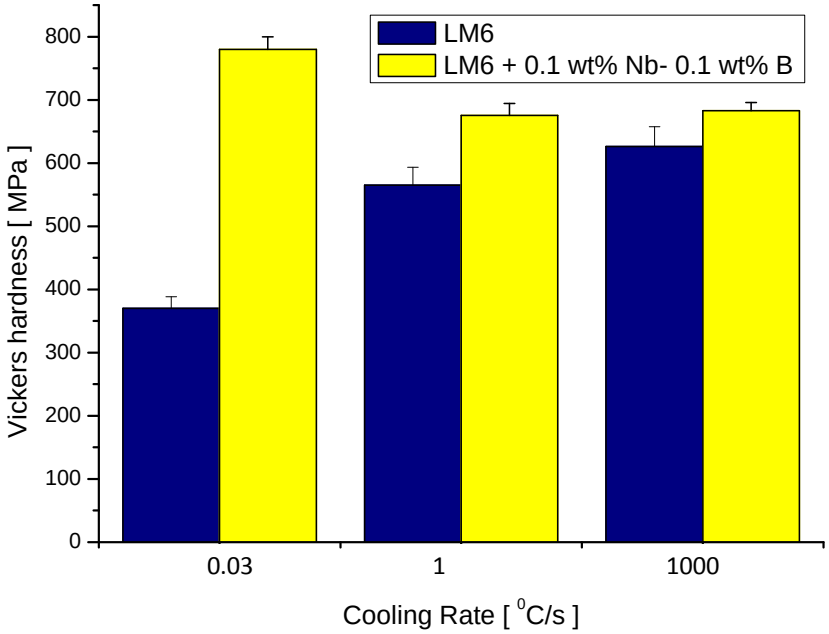

Figure 6.20 The Vickers hardness as a function of cooling rate for LM6 without and with Nb-B addition.

The Vickers hardness test shows that the addition of Nb-B has a positive influence on hardness especially in slow cooling samples. The Figure 6.11 shows the significant difference in grain sizes and it is known that it influences the mechanical properties. The data in Figure 6.20 suggests that small grain sizes improve micro-hardness of the material. Even though we do not have experimental evidence, the improved hardness could be attributed to the presence of $Al_{1-x}Nb_x$ solid solution formation, fine α-Al grain size and fine scale Al_3Nb and NbB_2 inclusions.

6.5 Influence of Casting Temperature on Grain Size

The casting temperatures have an effect on pure aluminium microstructure, with higher casting temperatures, larger grain sizes are expected, as was presented in Chapter 4. However with binary alloys the liquidus temperature is changing. With a higher concentration of silicon in hypoeutectic alloys the liquidus temperature decreases as shown in Figure 6.21.

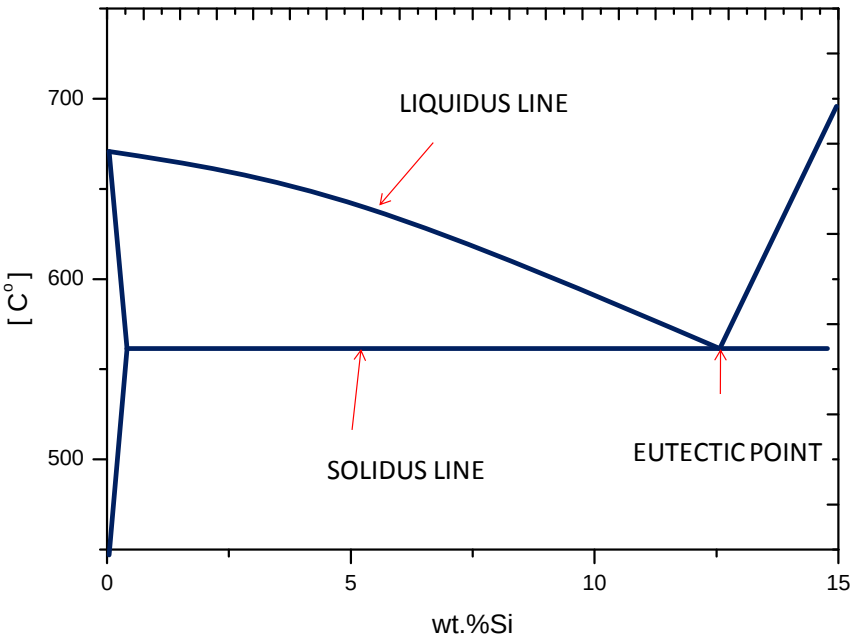

Figure 6.21 Phase diagram of Al-Si alloy. The change in the liquidus line in hypo-eutectic Al-Si alloys with silicon content.

The experiments were done for Al-Si binary alloys to investigate the influence of casting temperature on grain sizes. The alloys were melted at 800 °C in an electric resistance furnace and cast with constant superheat:

$$\Delta T_s = T_p - T_l \qquad (6.2)$$

Where T_p is pouring temperature and T_l is liquidus temperature. The ΔT_s was set up to 40 °C temperature above the liquidus line. The results are shown in Figure 6.22.

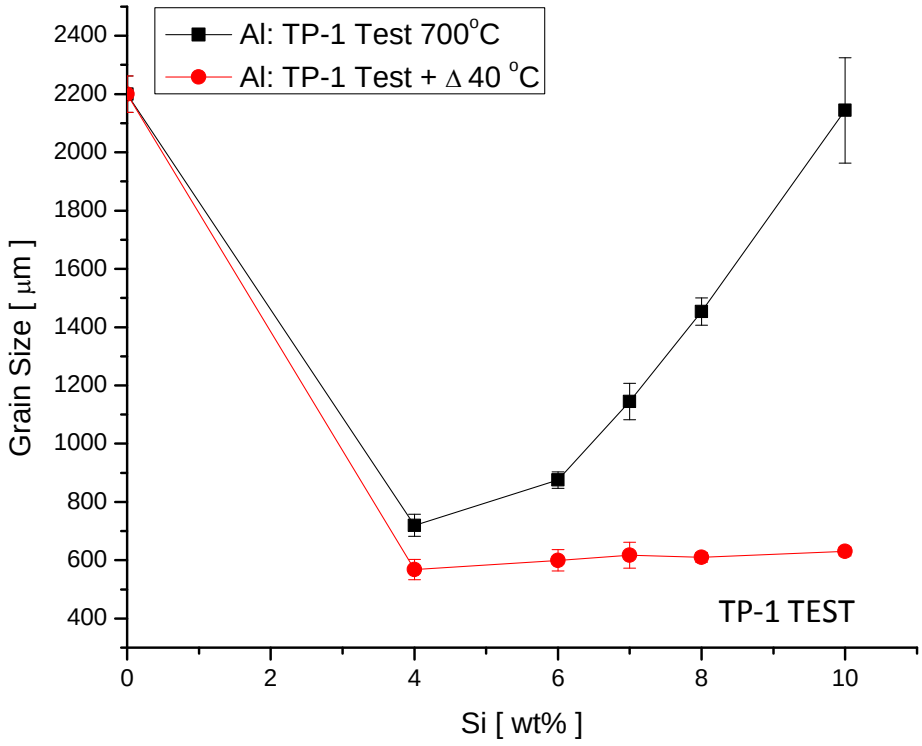

Figure 6.22 The Al-Si binary alloys cast at a constant pouring temperature of 700 °C and with ΔT_s = 40 °C above liquidus temperature into TP-1 test with cooling rate 3.5 °C/s.

The grain size of Al-Si alloys decreased with reduction of the pouring temperature. The initial pouring temperature for Al-10Si was 700 °C to obtain ΔT_s=40°C, the pouring temperature is lowered to 617 °C (83 °C lower), as Liquidus temperature 577 °C plus ΔT_s. As a result the grain sizes are reduced from 2200 µm to 600 µm. The experiment confirmed that pouring temperature definitely has a significant influence on grain size.

The same experiments were carried out for Al-Si alloys with Nb-B addition. Figure 6.23 shows how clearly the casting temperature changes the grain sizes.

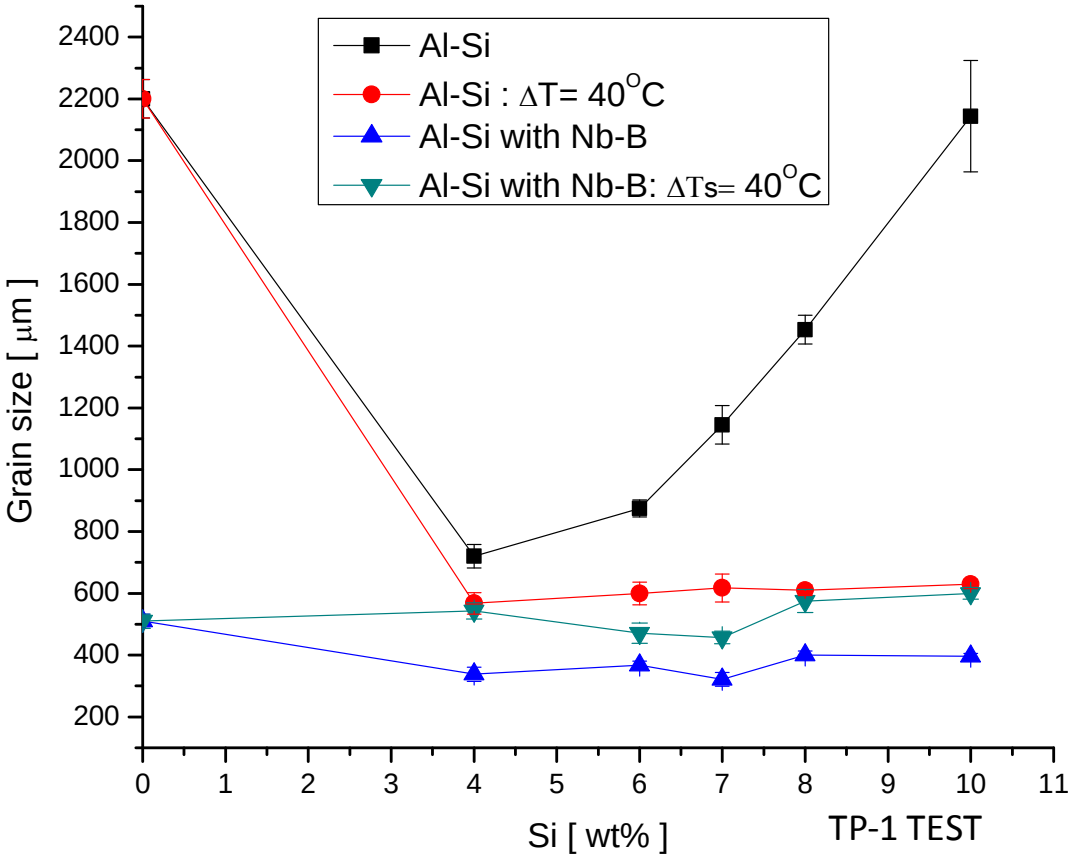

Figure 6.23 The Al-Si binary alloys without addition and with Nb-B cast with constant pouring temperature 700 °C and with ΔT_s = 40 °C above liquidus temperature into TP-1 test with cooling rate 3.5 °C/s.

The diagrams show the Al-Si binary alloys cast with constant temperature 700 °C and with ΔT_s = 40 °C above liquidus temperature into TP-1 test with cooling rate ~3.5 °C/s. The grain size for Al-Si with Nb-B cast at 700 °C and Al-Si cast with ΔT_s = 40 °C are similar. However casting temperature is one of the most important parameters influencing fluidity, as recently shown by Di Sabatino *et al.*(Di Sabatino M. 2005) who found that increasing the casting temperature has the most pronounced beneficial effect upon fluidity. Lowering the pouring temperature to achieve small grain sizes will influence the fluidity and casting of the materials. In the industry, LM6 which has about 10 wt% of Si addition is cast into the moulds between 740 and 760 °C. At such high pouring temperatures, obtaining fine grain size without a grain

refiner addition is not practically possible and hence the use of Nb-B grain refiner is of significant value for the industries.

Figure 6.24 shows the colour etched microstructure of Al-10Si without grain refiner and with Nb-B cast with constant temperature 700 °C and with ΔT = 40 °C above liquidus temperature into TP-1 test.

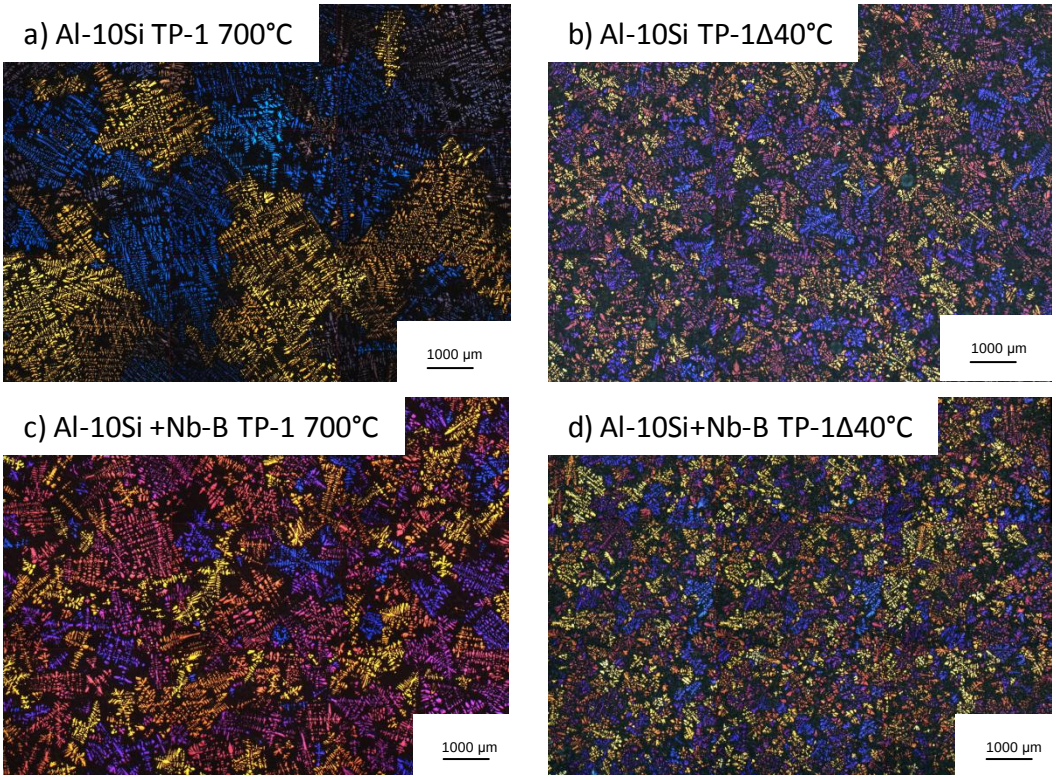

Figure 6.24 The colour etched microstructure of samples cast into TP-1 mould a) Al-10 Si poured at 700 °C, b) Al-10 Si poured at 617 °C, c) Al-10 Si with addition of 0.1 wt% Nb - 0.1 wt% B, poured at 700 °C and d) Al-10 Si with addition of 0.1 wt% Nb- 0.1 wt% B poured at 617 °C

6.6 Conclusions

As a result of addition of Nb-B the mechanical properties increased. The DAS prediction, that with smaller secondary dendrite spacing, the tensile strength and elongation will improve were confirmed by tensile tests. The improvement in elongation is significant especially for heat treated LM25 it increases from 3% to 14%. We could observe the reduction of Fe intermetallics in LM6 and LM25. The gas porosity in sand casting and wedge casting decrease

by 50%. There is significant decrease in grain size for LM6 with 0.1wt%Nb-0.1wt%B cast with cooling rate of 0.03 °C/s from 6 mm to 350 μm, which can have positive effect for sand casting industry.

The lowering pouring temperature will have significant effect on grain sizes for Al-Si alloys without any addition although it will not have a good influence on their fluidity and casting of materials.

Chapter 7. Master alloy of Aluminium-Niobium-Boron

7.1 Introduction

The formation of a primary as-cast microstructure composed of small, equiaxed grains of α-Al can be achieved by *inoculation*, the addition of inoculant particles to the melt prior to casting. These particles act as nucleation points for the α-aluminium grains at small undercoolings. The casting industry requires fast and easy grain refiner process which should be simple to introduce to the melt. The most common method for inoculation process at industry is the addition of a *master alloy* containing potent particles; master alloys based on the Al-Ti-B system are the most widely used. The master alloys are the best solution for foundries which can be obtained in the form of rod, nuggets, piglet, waffle plate or ingot. This Chapter concentrates on production of Al-Nb-B master alloy based on analysis and understanding the manufacturing process for commercially known Al-5Ti-B and other master alloys. The salt flux treatment for grain refining and production of Al-Ti and Al-Ti-B master alloys are both based on the interaction between double fluoride salts and aluminium melt in accordance with the following equation:

$$3K_2TiF_6 + 4Al \rightarrow 3Ti + 4AlF_3 + 6KF \quad \textbf{(7.1)}$$

$$2KBF_4 + 3Al \rightarrow AlB_2 + 2AlF_3 + 2KF \quad \textbf{(7.2)}$$

$$3K_2TiF_6 + 6KBF_4 + 10Al \rightarrow 3TiB_2 + 10AlF_3 + 12KF \quad \textbf{(7.3)}$$

Flux treatment leads to in-situ generation of the nucleants such as AlB_2 and TiB_2; the production of master alloys based on the above chemical equations results in a fine dispersion of the borides in aluminium which can subsequently be added to aluminium alloys.

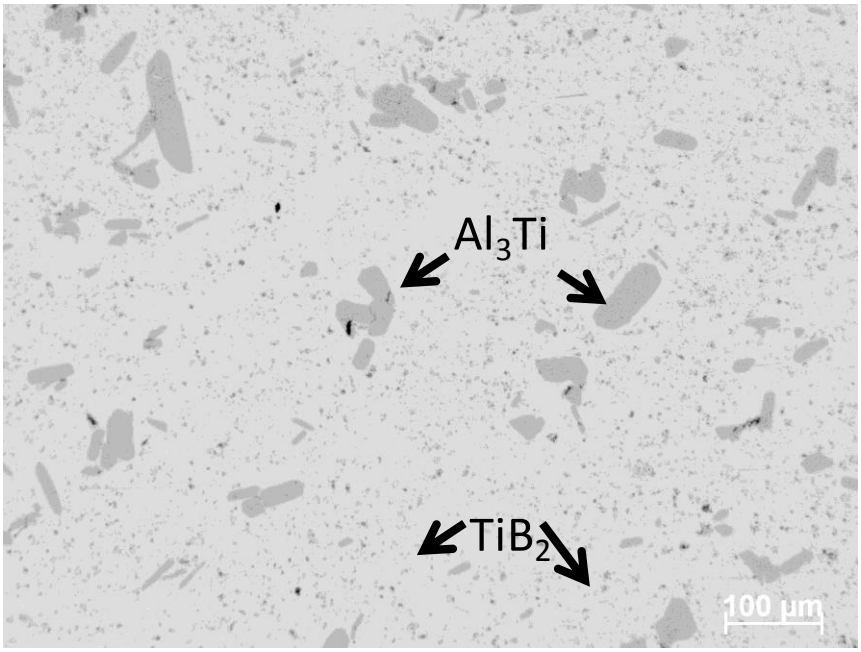

Figure 7.1 The microstructure of master alloy Al-5Ti-B supplied by LSM (London Scandinavian Metallurgy) with the potential nucleation cites of Al_3Ti and TiB_2 particles.

The Nb-B master alloy was developed from Nb powder and KBF_4, boron salt flux (Chapter 3). The analyses were done for different ratios of Nb:B; 1:2 (molar ratio), 1:1(weight ratio) and 2:1 (weight ratio). Also the addition of these master alloys to Al-Si alloys was investigated. Scanning Electron Microscope (SEM) was used to detect the Nb-B particles responsible for nucleation. Transmission Electron Microscope (TEM) was used to investigate the coherency between the particles and aluminium. In addition the fading studies were analysed and recycling abilities of LM6 with Nb-B addition were investigated.

7.2 Master Alloy Production

The master alloys were produced with different Nb-B molar ratios. An initial attempt was to produce the master alloy containing NbB_2. Commercial pure Al ingot was melted in an electric furnace at the temperature 850 ^oC and held for 2 hours. Niobium (Nb) and boron flux salt (KBF_4) are added to the melt with molar ratio of Nb:B is 1:2 with an aim to form 5 wt% of NbB_2 phase inclusions. The reaction between KBF_4 and Al is exothermic and the local temperatures can be in excess of 1500 °C for a short period of time and is believed that the high temperatures promote Nb dissolution into Al. The melt was stirred with non-reactive

ceramic rod for about 2 minutes at every 15 minute intervals. Slag on the surface of the melt was scooped and the liquid metal was poured into a cylindrical mould. The cast metal is referred as Al-Nb-B grain refiner master alloy. Addition of grain refiner master alloy is a common practice in the industry. It avoids use of corrosive KBF_4 salt in each casting. Instead of salt addition, one can add a small piece of Al-Nb-B master alloy for the Al-Si based liquid alloys to obtain a fine grain size.

The microscopic analyses were made to investigate the particles responsible for nucleation as shown on Figure 7.2.

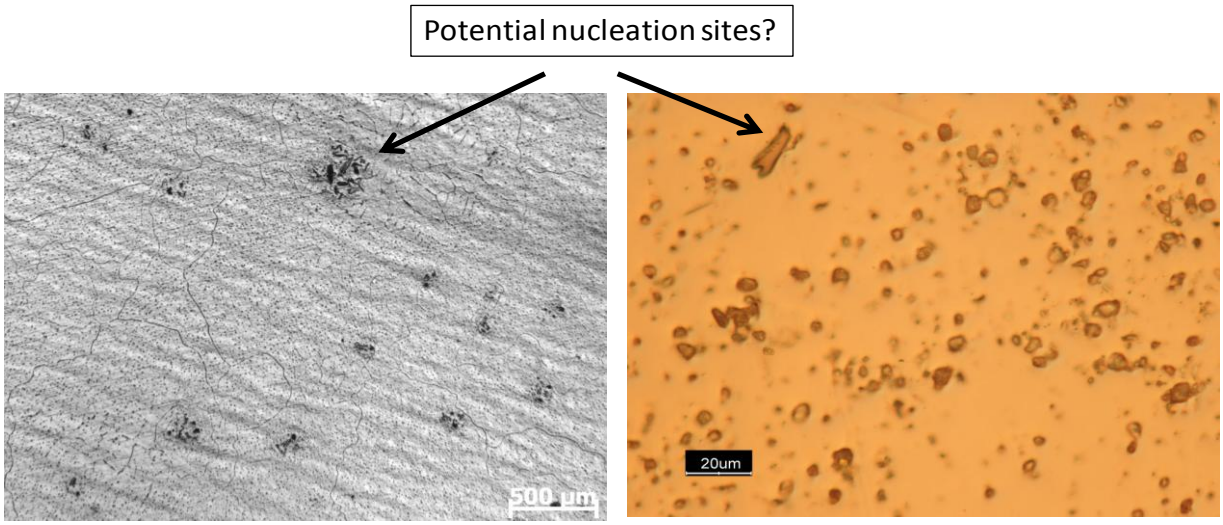

Figure 7.2 The microstructure of Al-Nb-B master alloy with initial composition of 95wt%Al - 5wt%NbB_2 (377 g Al + 15.268 g Nb + 39.54 g KBF_4) showing potential nucleation sites.

Figure 7.2 presents the potential nucleation sites of $NbAl_3$ or NbB_2. Further SEM analyses were made and will be presented in next part of this chapter. The master alloy was added to commercial aluminium to see if it works the same as with the Nb powder and KBF_4 salt addition. Figure 7.3 shows the colour-etched microstructures revealing the grain sizes.

The grain sizes significantly decreases from 2300 to 280 µm.

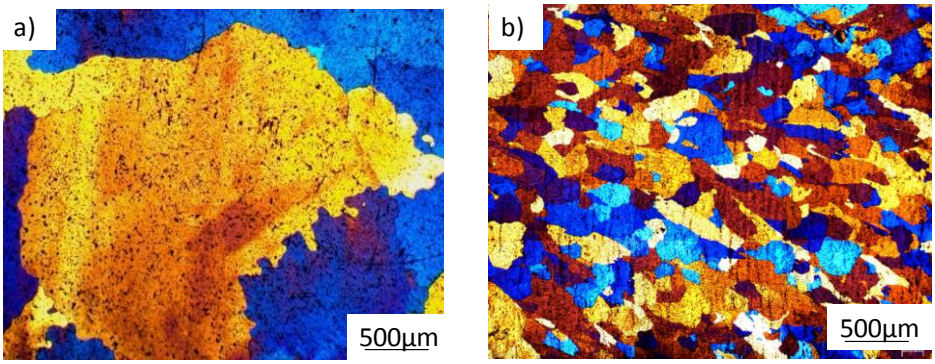

Figure 7.3 The colour etched microstructures of a) commercial Aluminium and b) Aluminium with Nb-B master alloy cast at 700 °C into the TP-1 mould (3.5 °C/s cooling rate). The grain sizes are reduced with addition of grain refiner.

The master alloy of Al-5NbB_2 is effective in pure aluminium. The investigation of this master alloy addition into the Al-Si alloys was made and the results are shown in Figure 7.4 for a commercial alloy (LM25). The LM25 was melt at 750 °C, cast into the TP-1 mould at 680 °C. The grain refiner was added and held for 30 min. The grain sizes are confirmed to be smaller and they decrease from 1 mm to 350 µm. The addition of Nb powder and the boron flux salt together decrease grains with the same effect than addition of master alloy as seen in Figure 7.4c.

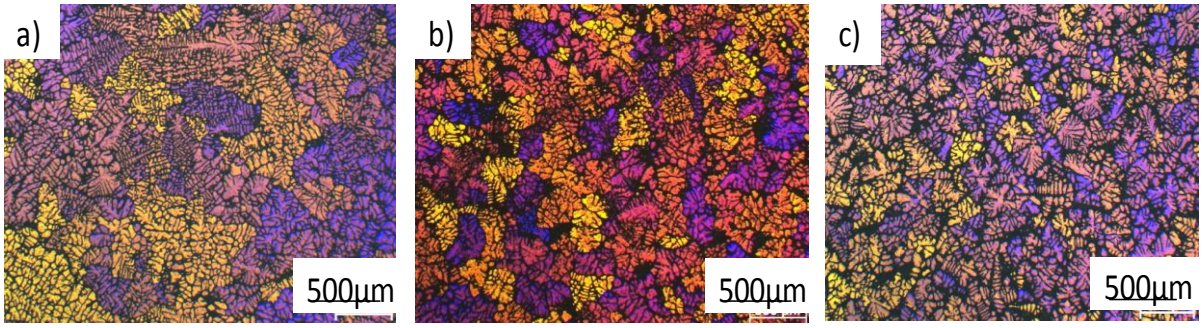

Figure 7.4 Colour-etched microstructures of a) LM25, b) LM25 with Nb-B master alloy, c) 0.1 wt%Nb-0.1 wt% B, cast at 680 °C into TP-1 mould (3.5 °C/s cooling rate). The grain sizes are reduced with addition of grain refiner.

Experiments were done also for LM6 using steel cylindrical mould, which provides a cooling rate of 2 °C/s. The alloy was melted in electric resistant furnace at 800 °C and cast at temperature of 680 °C with and without Al-Nb-B (Al-5wt%NbB_2) master alloy addition. High

meting temperature was used to help with nucleation sites dissolution. Figure 7.5 shows the grain sizes as a function of NbB_2 addition. From this figure, it can be seen that the small addition of Al-Nb-B master alloy is observed to decrease the grain size of LM6, significantly. Since NbB_2 or Al_3Nb based particles are not uniformly distributed in the whole Al-Nb-B master alloy, this can cause in reduction of grain refinement for LM6 when small quantity (0.025 wt% NbB_2) was added. Fine grain structure is obtained when the addition level of 0.1 wt% of NbB_2 is added.

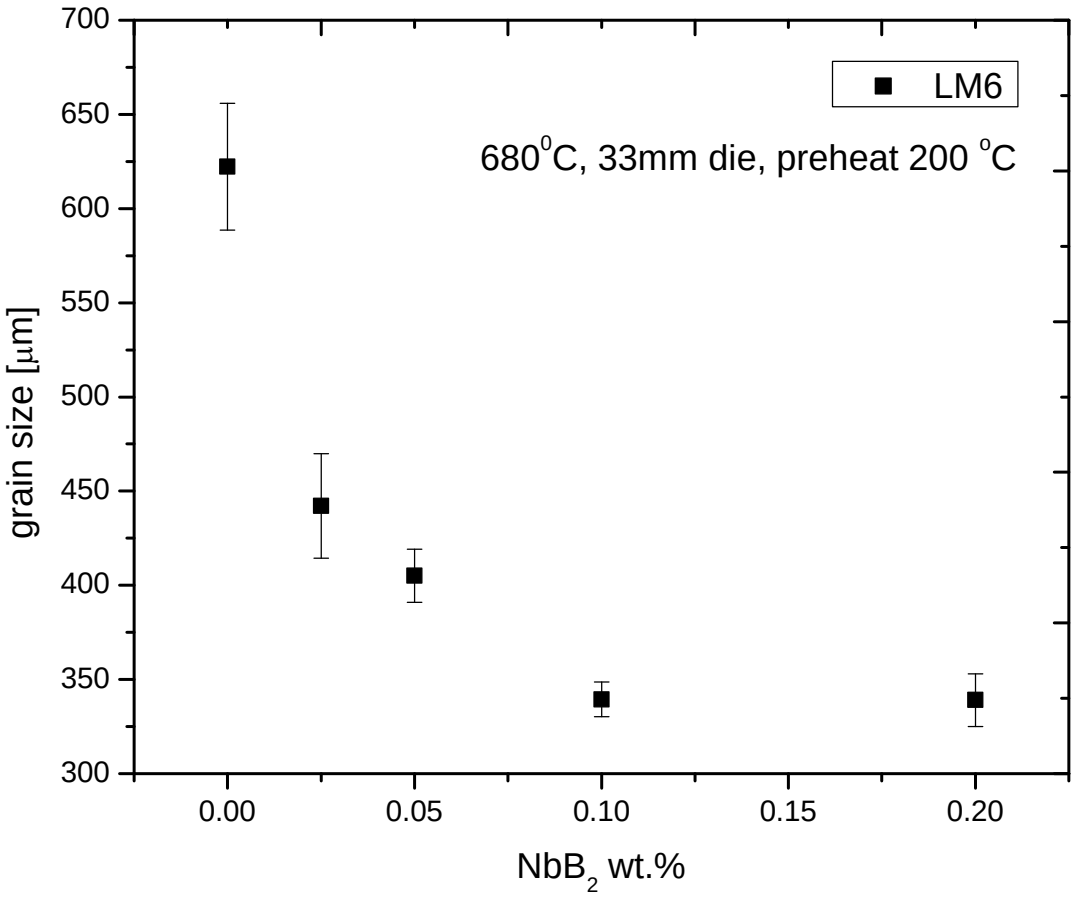

Figure 7.5 LM6 grain sizes as a function of different wt% addition levels of NbB_2. Samples are cast into a steel cylindrical mould, preheated to 200 °C. The pouring temperature is 680 °C.

The next attempt to a produce master alloy was to achieve the Nb-B weight ratio of 1:1. As the previous experiments described in Chapter 5 & 6 always had 1:1 ratio of Nb-B and the logic was to see if the excess of boron is necessary or not. To produce Al-Nb-B master alloys, the commercial aluminium was melted at 850°C and the Nb powders mixed with the KBF_4 flux salt were added to the melt. After one hour with occasional mixing of the melt the sample was cast into the bars. The microstructure of the Al-Nb-B master alloy is shown on the Figure 7.6.

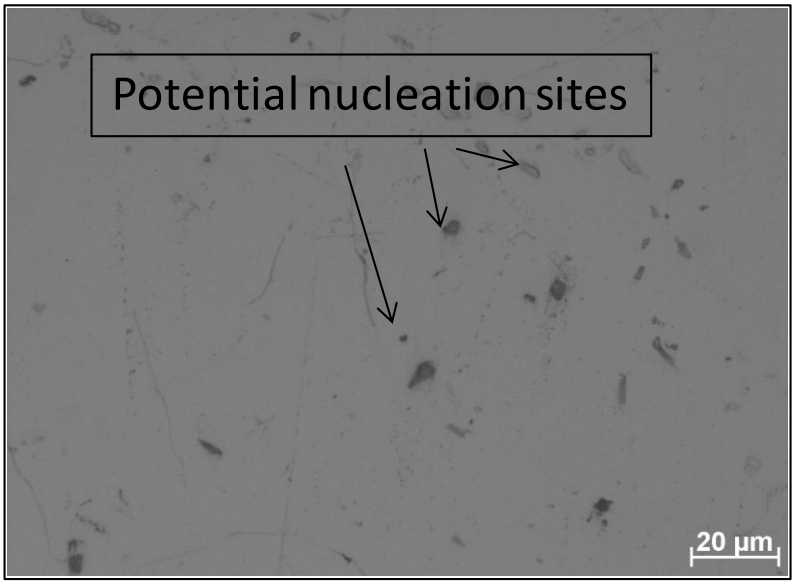

Figure 7.6 The microstructure of Al-Nb-B master alloy (weight ration of Nb:B is 1:1) with potential nucleation sites.

The master alloy was added to LM6 to check whether it had any influence on the grain size. For this, the LM6 was melted at 800 °C and the master alloy was added to the melt and held for 15 min. The different weight percentages of Nb and B ranging from 0.025 to 0.1 were added to investigate the grain refining abilities. The samples were cast at the same pouring temperature of 740 °C into the steel mould which was preheated to 200 °C.

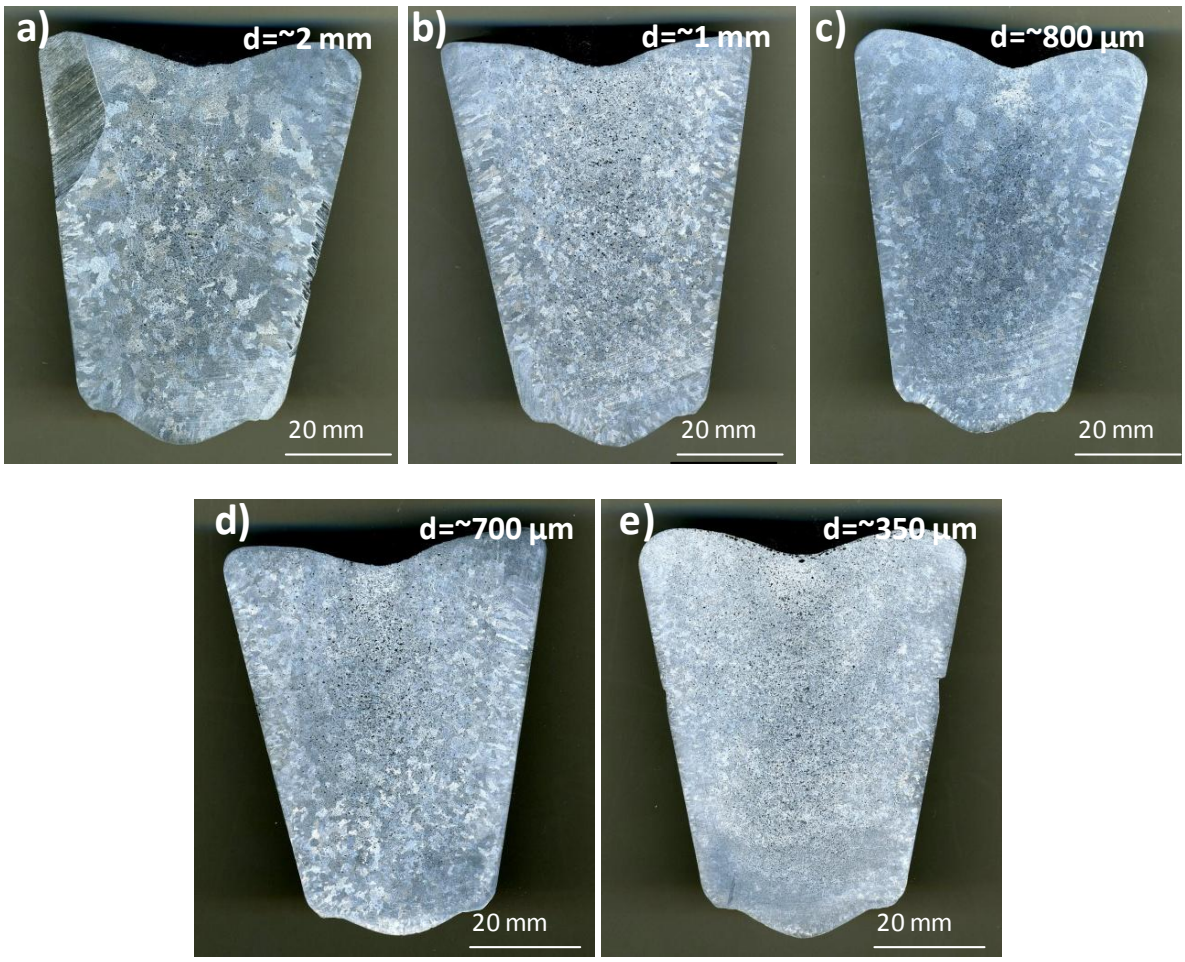

Figure 7.7 The LM6 alloy cast at 740 °C into the steel mould preheated to 200 °C with the addition of master alloy Al-1Nb-1B with different weight percentage of Nb and B a) without any addition; b) 0.01 wt% Nb + 0.01 wt% B; c) 0.025 wt% Nb + 0.025 wt% B; d) 0.05 wt% Nb + 0.05 wt% B; e) 0.1 wt% Nb + 0.1 wt % B.

It can be seen from Figure 7.8, that the grain sizes are decreasing progressively with the higher addition of master alloy. As it has been explained before that the concentration of the nucleation particles in master alloy is unknown. The assumption can be made that with higher addition of master alloy we can get enough active particles to act as a nucleation site.

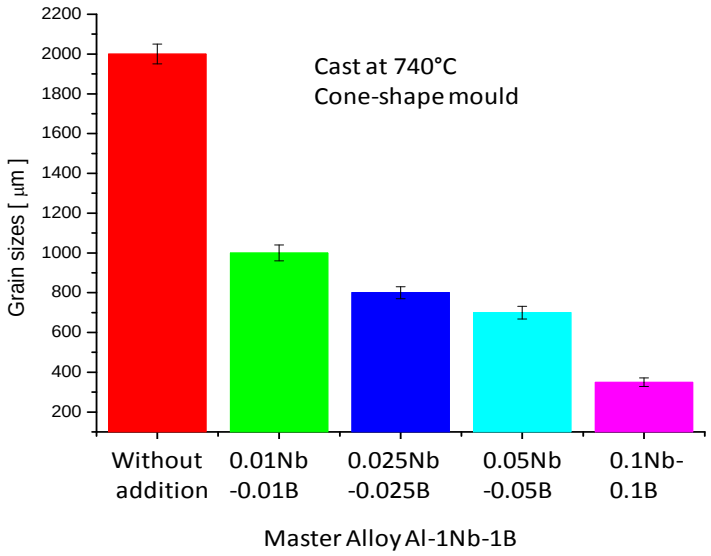

Figure 7.8 The grain sizes as a function of Nb/B concentration levels

Further, the master alloy with 2:1 weight ratio of Nb:B was produced. For this, commercial aluminium was melted at 850°C and the Nb powders mixed with the KBF_4 flux salt were added to the melt. After one hour with occasional mixing of the melt the sample was cast into bars. The microstructure of the Al-Nb-B master alloy is shown on the Figure 7.9.

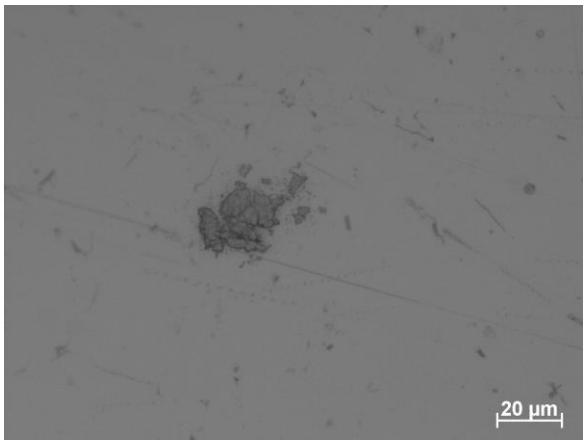

Figure 7.9 The microstructure of master alloy of Al-2Nb-1B showing potential nucleation sites.

Al-10Si alloy was used for testing of master alloy produced at Brunel University. The Al-10Si was melted in the furnace at 800 °C and the master alloy with initial composition of Al-2Nb-

1B was added in two different combinations. The first one was Al-0.025wt %Nb-0.0125 wt% B and the second combination was 0.1 wt% Nb- 0.05 %B. The Al-10Si with addition of powder 0.1 wt% Nb and 0.1 wt% B (in the form of KBF_4) was also produced for comparison purposes.

Figure 7.10 shows the different additions of master alloy and powder addition. The grain sizes decreased significantly from 1 mm to 350 µm.

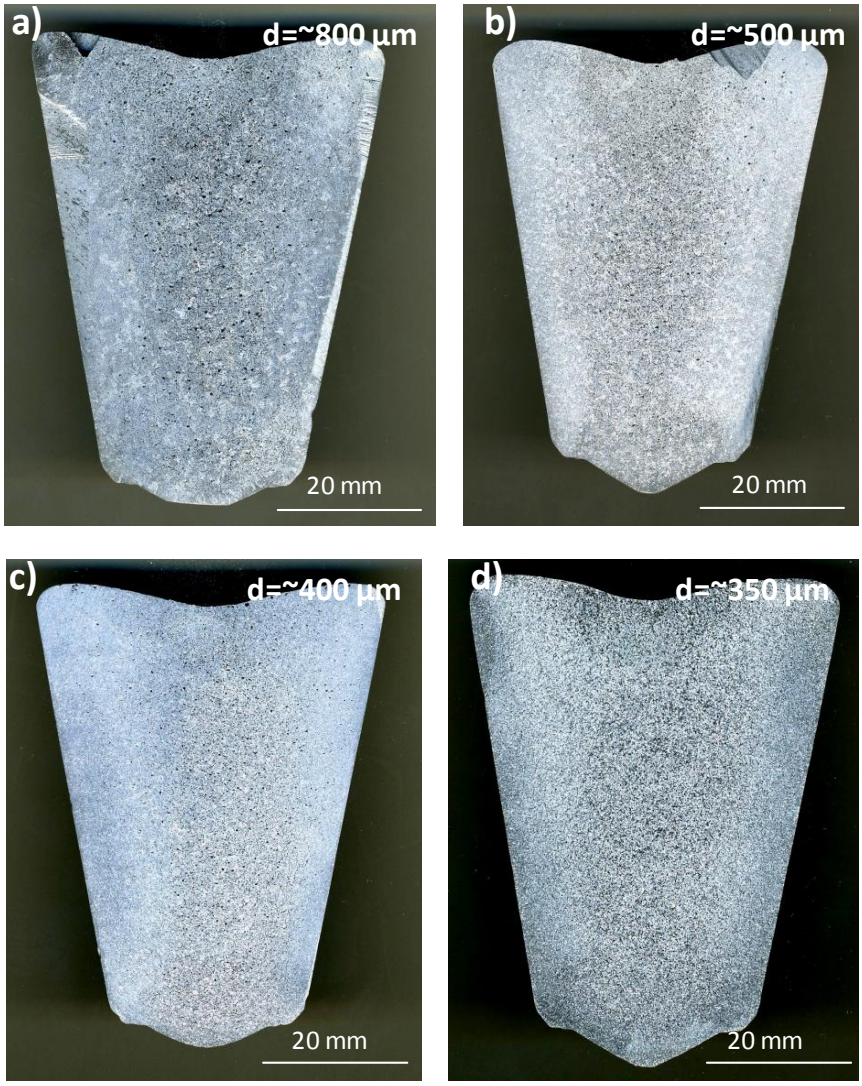

Figure 7.10 The Al-10Si cast at 740 °C into the steel mould preheated to 200 °C with the addition of Al-2Nb-1B master alloy with different weight percentage of Nb and B a) without any addition; b) 0.025 wt% Nb + 0.0125 wt% B; c) 0.1 wt% Nb + 0.05 wt % B; d) 0.1 wt% Nb powder and 0.1 wt% B (KBF_4)

The experiment to compare the addition of 1:1 ratio with 2:1 ratio of Nb-B was done for LM6. The LM6 was prepared the same way (see above) the master alloy was added and after 15 min holding time the metal was cast from 740 °C into the steel mould which was preheated to 200 °C. Figure 7.11 shows the commercial LM6 without any addition with addition of 1:1 ratio and 2:1 ratio of Nb:B. The composition of Nb and B was chosen to be 0.1 wt% Nb and 0.1 wt% B for the first sample and 0.1 wt% Nb – 0.05 wt% B for the second sample.

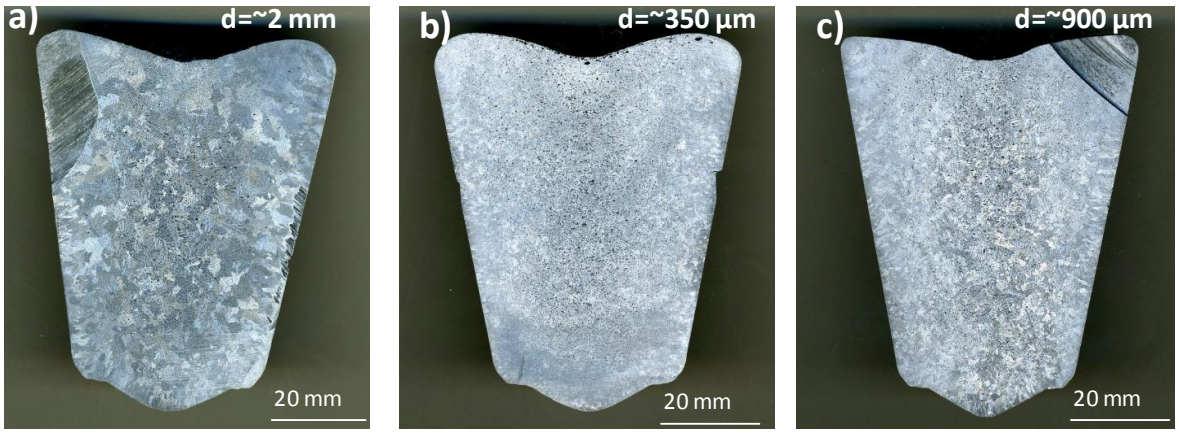

Figure 7.11 LM6 with the addition of master alloy at various concentration of Nb and B a) without any addition; b) with Al-Nb-B master alloy addition (0.1 wt% Nb- 0.1wt% B); c) Al-2Nb-B master alloy (0.1 wt% Nb-0.05 wt% B) cast at 740 °C into the steel mould, preheated to 200 °C

As it can be seen from Figure 7.11 the LM6 with 1:1 ratio master alloy has a smaller grain size than sample with 2:1 master alloy. Also the grains are smaller when compared to Al-10Si alloy. Chemical analyses were done to those alloys to find out why the LM6 alloy needs higher amount of Boron to be refined. The Table 7.1 shows the chemical analyses in weigh percent (wt %) of those two alloys.

	Si	Fe	Cu	Mn	Mg	Cr	Ni	Zn	Ti	B	Zr	Pb
Al-10Si	9.9	.09	.0017	.005	.005	.001	.004	.005	.027	.001	.0015	.001
LM6	11	0.5	0.02	0.4	0.07	0.02	0.01	0.014	0.038	0.0009	0.0256	0.014

Table 7.1 The composition of Al-10Si alloy and LM6.

The Al-10Si is mostly a binary type alloy and LM6 which has many other alloying elements like Iron (Fe) and Manganese (Mn). The research (Kaptay G. 1999) explains the preferable formation of borides in Al systems. It is well known that, when Boron is added to the alloy that contain several alloying elements, based on the free energy formation of compounds, the preferable borides are TiB_2, ZrB_2 and followed by NbB_2. In the case of LM6 which has more alloying elements higher boron concentration is required to form NbB_2 nucleation site. Table 7.2 shows lattice parameters for these particular borides. The presence of alloying elements restricts the growth rate of primary alpha phase and it governs how fast nucleated crystals will grow. This growth restriction has a very large impact on the final grain size (Quested T.E. 2005) and is essentially a function of the melt composition. In principle the higher the concentration of alloying elements, the greater the restriction in grain growth is noticeable. However, the growth restriction imposed by different alloying elements varies considerably.

	Al	NbB_2	MgB_2	MnB_2	TiB_2	AlB_2
a	4.05 Å	3.102 Å	3.08 Å	2.769 Å	3.02 Å	3.007 Å
c		3.285 Å	3.53 Å	6.949 Å	3.22 Å	3.267 Å

Table 7.2 The borides which could form in the Al-Si alloys during solidification and their lattice parameters.

In the case of Al-Ti-B, there is a marked difference between the grain-refining ability of super-stoichiometric master alloys (containing excess titanium) and sub-stoichiometric master alloys – the most extreme case being Al-B, which contains no titanium. Sub-stoichiometric master alloys fail to grain refine super-purity aluminium under typical casting conditions (Cornish A.J. 1975) whereas super-stoichiometric master alloys are able to refine super-purity aluminium. In general, super stoichiometric master alloys outperform sub-stoichiometric

master alloys when assessed as a function of boron content, which is indicative of the volume fraction of borides. The researchers (Sigworth G.K and Guzowski M.M., 1985), claim that the Al-B master alloys and sub-stoichiometric Al-Ti-B alloys are able to grain refine Al-Si foundry alloys. However, they are not as effective as the addition of Nb-B. In the case of relatively pure Al-10 Si alloy where lower concentration of Boron could refine the grain size significantly whereas in LM6, which has many alloying elements, the excess of Boron was needed for grain refinement. Therefore it is suggested that formation excess boron is needed to form $NbB_{2.}$ These experiments suggest that the presence of NbB_2 phase in the liquid metal is essential for enhancing the grain refinement and the potential nucleation site would be NbB_2 for the grain refinement of α-Al containing Si as a solid solution.

7.3 Scanning Electron Microscopy (SEM) Analyses of Master Alloys

Scanning electron microscopy was used to detect the nucleation sites responsible from grain refining. The analyses were made in three different centres at University of Sydney, Oxford University and Brunel University. Several of the analyses are presented below. The signal from specimen is capable of yielding information about composition. The secondary electron coefficient does not depend significantly on the composition of the sample, although it may be sensitive to the surface condition and electronic structure of the material. However, the backscattered coefficient η varies monotonically with atomic number Z. The image mode in the SEM was used with conjunction of energy dispersive X-ray detection. The areas of compositional interest were first identified by backscattering imaging and the phase compositions were then determined by spot analysis with the X-ray signal. Figure 7.12 presents the mapping signal obtained from the Al-5NbB_2 master alloy sample. The elements detected in the samples are Al, Nb, B and Si.

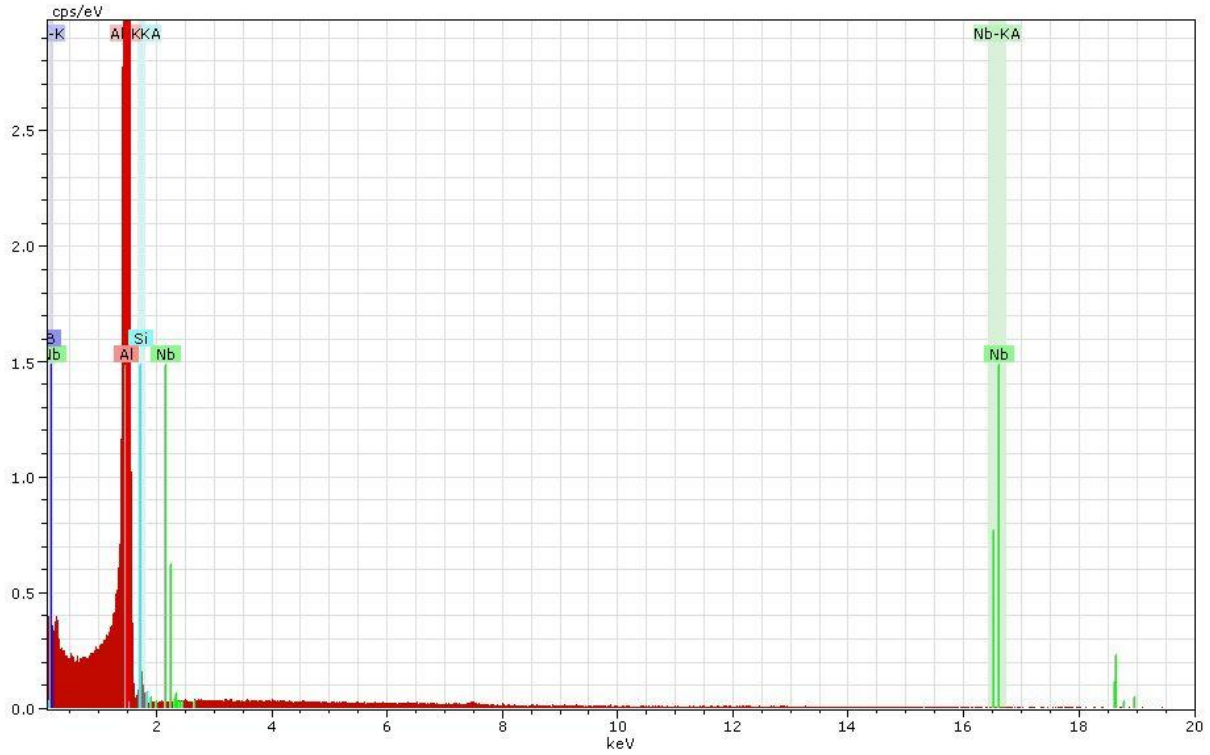

Figure 7.12 Backscattering signals from the master alloy of Al-5NbB_2. The Nb and B is present in the sample so it is possible that the formation of NbB_2 is taking place in solidification of this master alloy.

The SEM micrographs shown in Figure 7.13 represent the mapping of the particles present in the Al-5NbB_2 master alloy. Elements detected are Aluminium (the matrix), Niobium and Boron based particles. Silicon is also present in the sample however it could be that silicon particle could have been embedded in the soft Al matrix during grinding with Si paper.

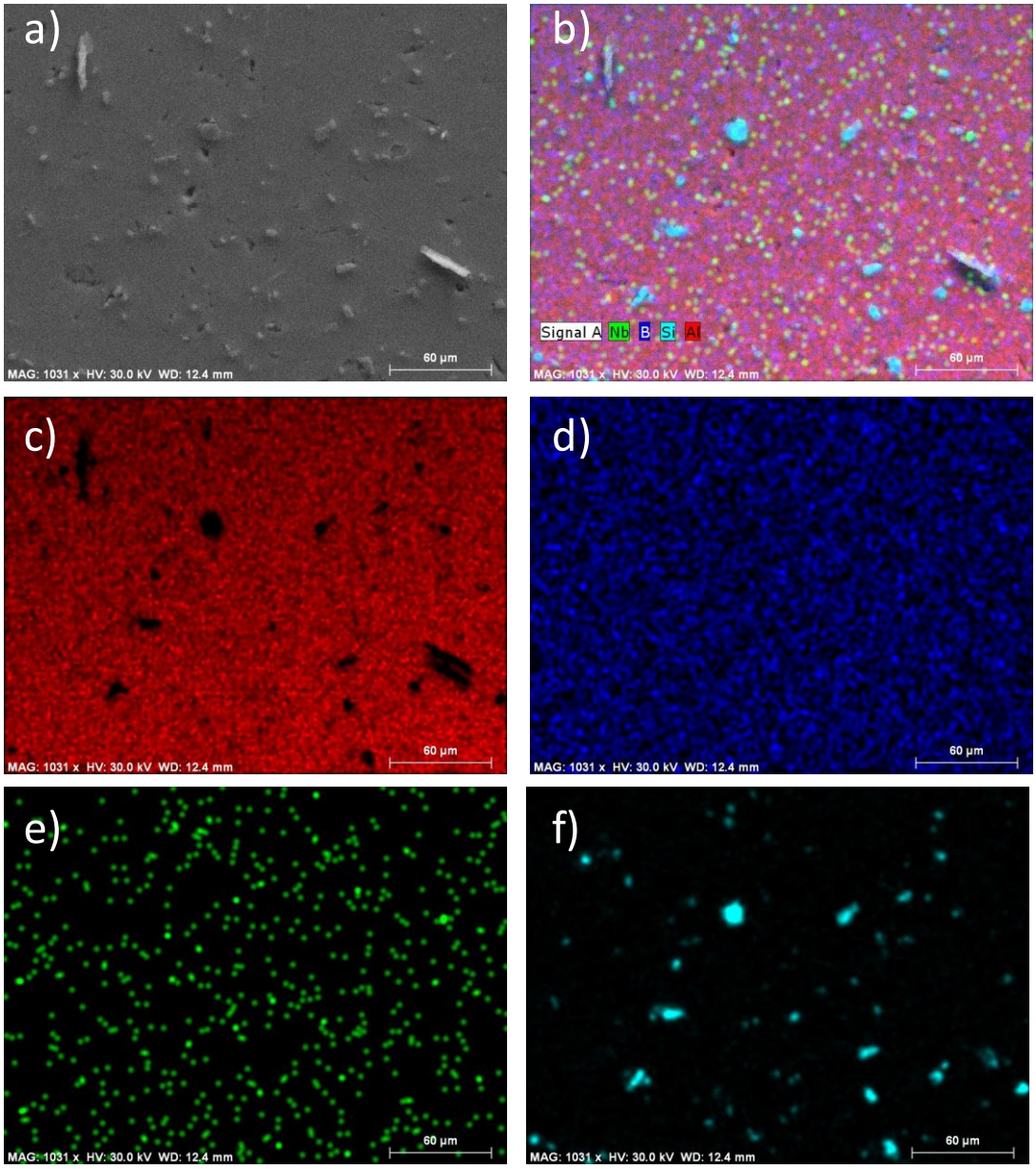

Figure 7.13 The SEM pictures of Al-5NbB_2 master alloy a) microstructure of the sample b) back scattering of the sample with the signals of elements present in the alloy (Nb, B, Si and Al); c) Al matrix; d) Boron particles e) Niobium particles; f) Silicon particles.

The figure 7.13 d and e are showing the single-phase matrix and homogeneously distributed spherical phases of Nb and B. Figure 7.14 (a) shows the cluster particles and the line scan with the signals (proportional to mass of element) of the chemical elements across the clustered particles.

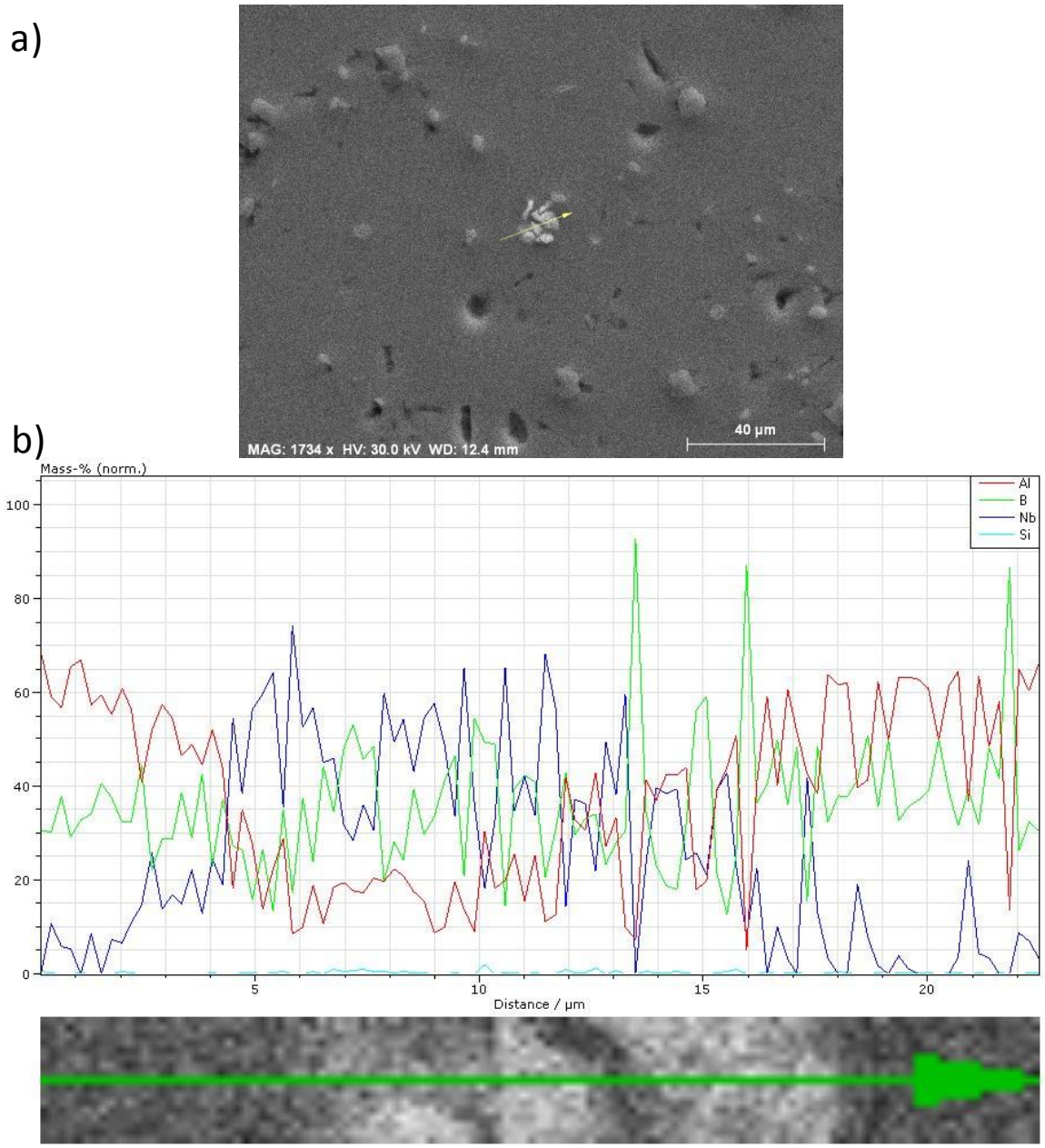

Figure 7.14 The chemical mass analysis of the particle in Al-5NbB_2 master alloy. a) The microstructure of the sample with the chosen particle cluster; b) the composition signals detected in the positions on the line. There is a strong Nb and B signal from the middle of particle suggesting that these are NbB_2 particles.

As it can be seen from Fig. 7.14b, the signals at the middle of the particle are very strong from Niobium and Boron. The atomic mass of Nb in this particle is about 70% whereas B is 55%. Based on this mass ratio, the assumption can be made that these particles are the NbB_2 phase

and these are responsible for enhanced nucleation. However more detailed analysis of Electron Probe Micro Analysis needs be performed to confirm the phases in the master alloy. In Figure 7.15 larger particles of potential nucleation sites are presented. The particles size is about 10 μm, however smaller particles were also found in the sample, that will be discussed in section 7.4.

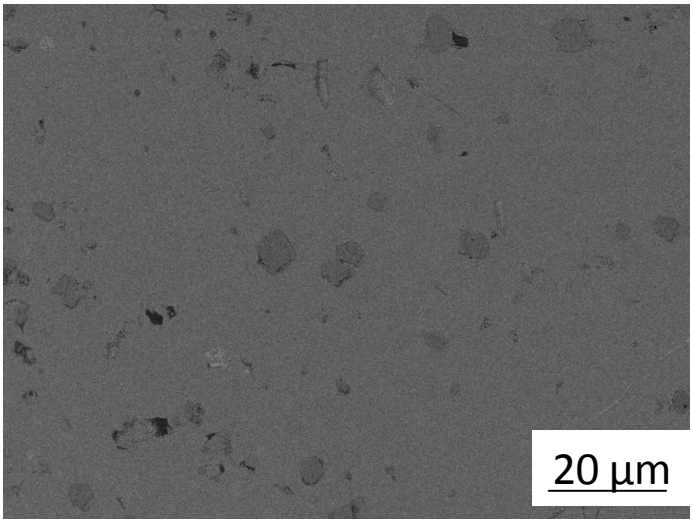

Figure 7.15 The microstructures of the NbB_2 particles in the Aluminium Matrix.

Figure 7.16 shows different types of particles in the Al-1Nb-1B master alloy.

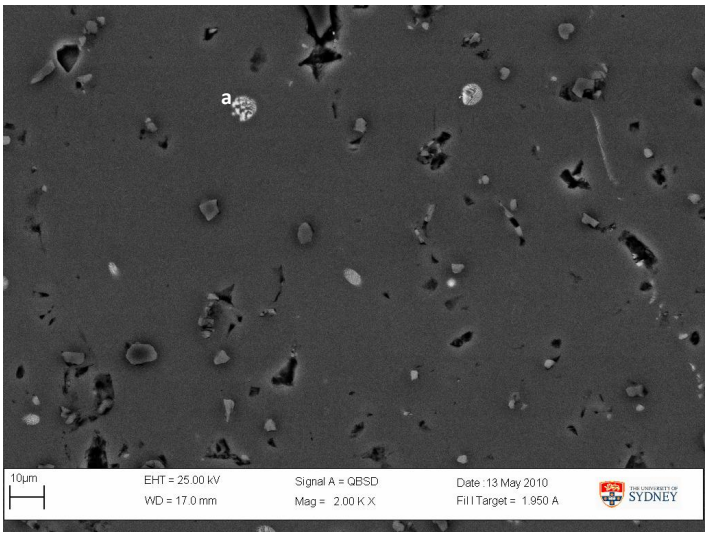

Figure 7.16 The microstructure of Al-1Nb-1B master alloy with the particles which were analysed.

The figure below presents the EDX pattern obtained at ‘a’ marked locations.

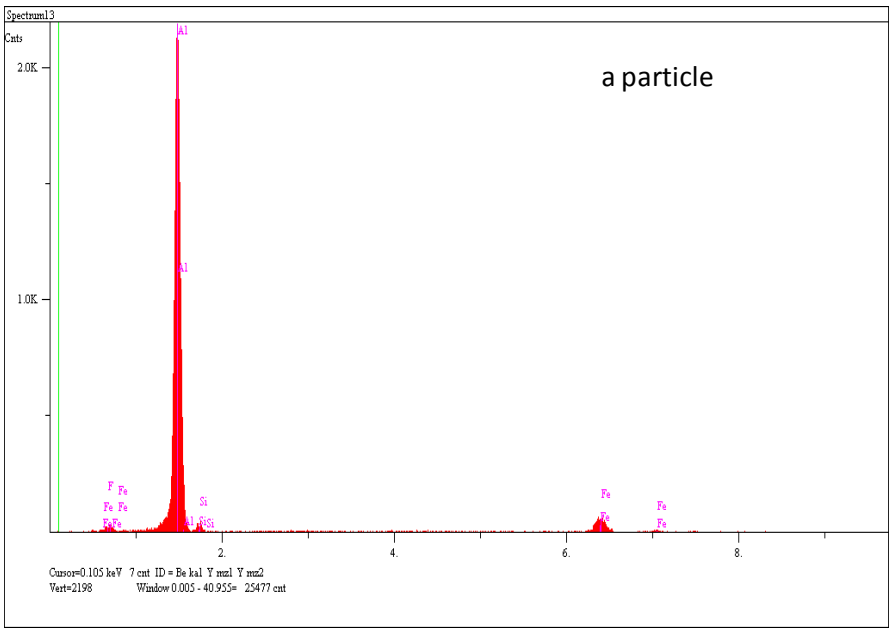

Figure 7.17 The signals of the 'a' particle in the above microstructure of master alloy Al-1Nb-1B. The data suggest that there is Iron and Silicon in the master alloy. The Fe and Si are believed to originate from the Fe/Si presence in the commercial pure Aluminium used to produce master alloy.

This backscattering image with corresponding EDX pattern identifies the presence of iron and silicon. Compositional analysis of the commercial Al was done to find the source of iron. Results suggest that the commercial Al contains Iron, Si and Ti as impurity elements.

Master alloy produced from starting composition of Al-5wt% (Nb:2B) resulted in Nb based particles embedded in Al matrix. The particles found in the master alloy could be in the form of NbB_2 or Al_3Nb. Differentiating between these phases using current methods is not possible and further work needed to identify the exact phases in the mater alloy.

7.4 Transmissions Electron Microscope Analyses of the Master Alloy

TEM analyses were done for the Al-5NbB_2 to investigate the phase contrast between the Al and NbB_2 or Al_3Nb. Phase contrast results whenever electrons of different phase are allowed to pass through the objective aperture. Since most electron scattering mechanisms involve a phase change then that some sort of phase contrast is presents every image. The most useful type of phase contrast image is formed when more diffracted beams are used to form the image. Selecting several beams allows a structure image, often called as a high-resolution

electron microscope (HREM) image, to be formed. The many lattice fringes intersect and give a pattern of bright spots corresponding to atom columns as it seen at the Figure 7.18.

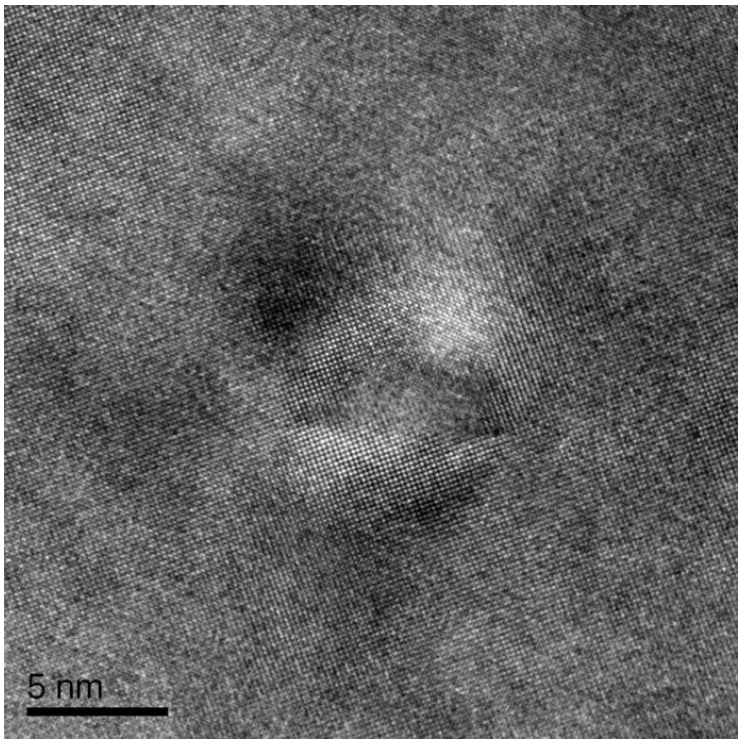

Figure 7.18 Nano-scale precipitates observed in Al-1Nb-1B (Al-5NbB$_2$) master alloy

Figure7.19 shows the interface between Nb based particles and Al.

Figure 7.19 Precipitates of NbB_2 or Al_3Nb phase with Al phase.

As it was mentioned in Chapter 4, a foreign solid phase to act as effective grain refiner it needs to have a good lattice match with the Al. Figure 7.19 shows the coherent interface between the precipitate of Nb based particles and Al. The NbB_2 or Al_3Nb phases have a good lattice match with aluminium lattice structure.

From the calculations of d-spacing between the atoms the lattice parameters can be calculated using of the equation:

$$d = \frac{a}{\sqrt{h^2+k^2+l^2}} \quad \textbf{(7.4)}$$

Where d is spacing between the atoms, a lattice parameter, h,k,l are directions of the crystal.

After the calculations of the particle at the TEM image we can assume that he lattice is Al_3Nb with the lattice parameter of 0.3732 nm compared with the literature value 0.384 nm.

7.5 Fading studies

Grain size varies with contact time, which is the time beyond between addition of master alloy and casting as seen on Figure 7.20.

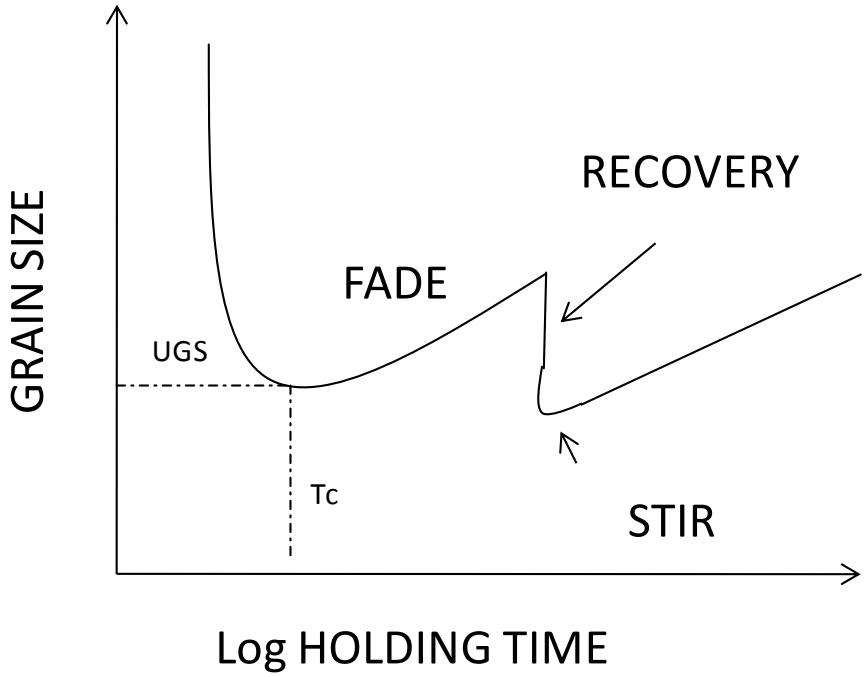

Figure 7.20 Schematic plot of grain size as a function of contact time showing fade and effect of stirring (UGS-ultimate grain size; Tc- optimum contact time); from (Kearns M.A. 1996)

In Direct Chill ingots the actual contact time for Al-5Ti-B is typically few minutes and in shape castings it is more variable - up to few hours. The grain size initially decreases as a function of contact time: this is distributed to a dispersion of boride particles, is promoter by dissolution of the Al_3Ti phase. However, an increase in grain size known as fade is observed at long holding times. The majority of fade can be attributed to particle settling which is why stirring of the melt restores grain refinement to its optimum level (Bunn A.M. 1998, Kearns M.A. 1996). The non- recovered fade is ascribed to particles forming sludge at the bottom of the crucible (Kearns M.A. 1996). Fade can also be caused by solute poisoning of inoculants

particles (Bunn A.M., Schumacher P., Kearns M.A., Boothroyd C.B., Greer A.L.,; 1999), and agglomeration of inoculants particles into clusters (Schaffer P.L. 2001).

Several experiments were carried to investigate the fade in Al-Si alloys with the addition of Nb-B. The experiments were done for LM6 with addition of 0.1 wt% Nb-0.1 wt% B (KBF_4) with a holding time up to 4 hours. The stirring was introduced in one case in other one the melt was not disturbed before casting. Figure 7.21 shows the LM6 with additional stirring before casting. All the samples were cast into TP-1 mould with the pouring temperature of 680 °C.

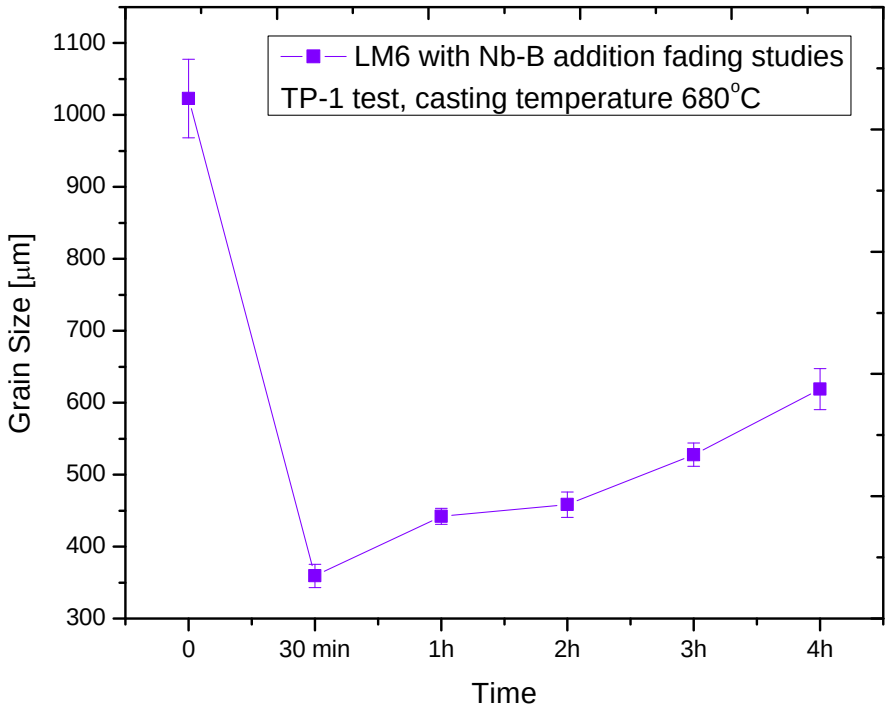

Figure 7.21 The fading studies of LM6 with addition of Nb-B. The samples were melted at 800 °C and cast into TP-1 mould at the pouring temperature of 680 °C.

Although there is a sign of fading, the grain sizes are smaller for post casting times of up to 4 h. Experiments were also done to investigate the dissolution of Nb and B and formation of the Nb-based particles. It is known that dissolution rate of Al_3Ti in liquid aluminium unsaturated with titanium is high. For a typical inoculation procedure all Al_3Ti particles introduced with the master alloy will have dissolved in a matter of few minutes. In contrast to above case, it

was found by Clyne (Clyne T.W. 1980) that dissolution rate of Al_3Nb particles suspended in an aluminium melt is very low. The majority of such a particles introduced by inoculation with the Al-Nb master alloy would survive the holding stage and be available to act as nuclei in Al. The experiment was done for LM6 with the addition of 0.1 wt% Nb-0.1 wt% B (KBF_4), the melting temperature was 800 °C and the pouring temperature into TP-1 mould 680 °C. The results are shown on Figure 7.22.

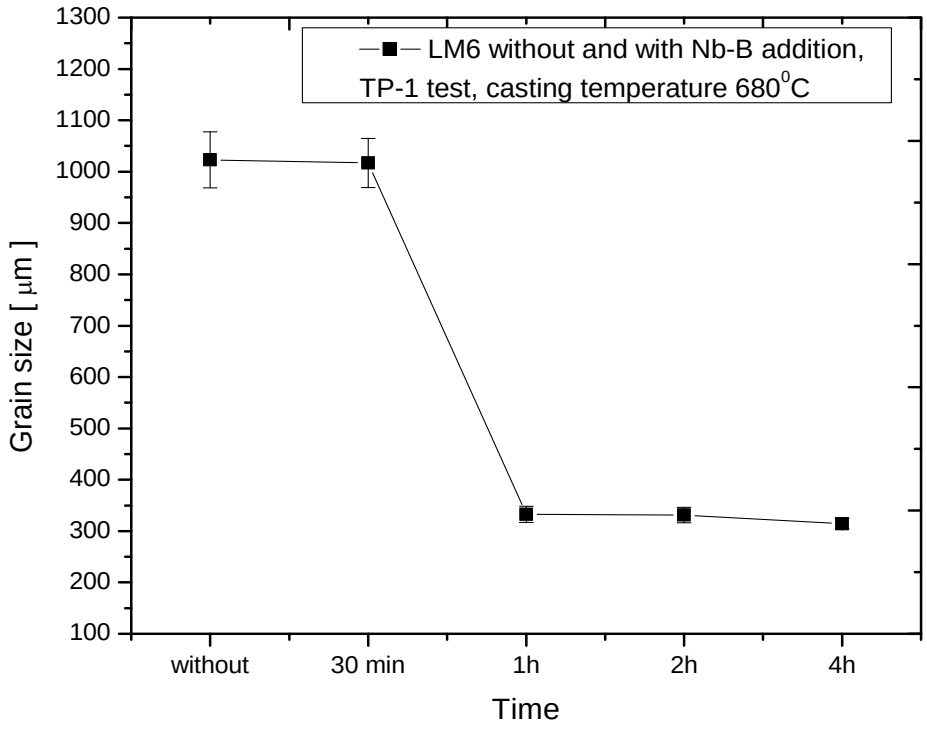

Figure 7.22 The LM6 alloy with addition of 0.1 wt% Nb- 0.1 wt% B. The melt was held from 30 min to 4 h, at a temperature of 800 °C and cast into TP-1 mould with a temperature of 680°C.

The grain size is unaffected after 30 minutes of Nb and B powder addition. After an hour of holding, the grain size decreased rapidly suggesting that enough time is required to dissolve Nb and B to form new Nb-based compounds in the liquid. By further increasing the holding time, no further improvement in grain refinement is observed, suggesting that the NbB_2 or Al_3Nb particles are stable in the melt even after long holding time of 4 h. From both

experiments we can assumed that stirring will help with particles dissolution. That's why after 30 min with stirring the grain sizes are smaller than without any mechanical interaction.

The casting industry needs refiner which survives the long holding times for example the casting of engines with the cosworth method (Campbell John G. 1987). In this process, the Al-Si alloy with a weight of 4 tonnes is melted in the large furnace and the melt is continuously transferred to the cosworth mould to cast the engine. Production takes about 5 hours. If the grain refiner has fast dissolution time it will not be useful in this operation. The Nb-B addition can survive in the melt which means that it can be helpful in cosworth method, which is commonly used to produce bulk shape castings for automotive applications

7.6 Recycling of the Al-Si

Recycling of return process scraps is a general practice in aluminium foundries. Each time return scrap is usually grain refined using well known Al-5Ti-B grain refiner. As a result, concentration of Ti and B can be found to be high even without any addition of Al-Ti-B in the latter melt treatment. Many foundries rely on the chemical analysis of Ti and B to decide whether or not additional grain refiner needs to be added. The Nb-B addition to the aluminium melt is novel and the recycling of this alloy need to be investigated. The experiments were done for LM6 aluminium alloys. 1 kg of melt was produced with 0.1 wt% Nb- 0.1 wt% B addition. The sample was cast into the cylindrical mould preheated to 200 °C with the pouring temperature of 680 °C. The sample then was cut and the microstructure analyses were done. The rest of the metal was melted again without any additional Nb-B. The procedure was repeated 4 times. Figure 7.23 shows the grain sizes for the different recycling steps.

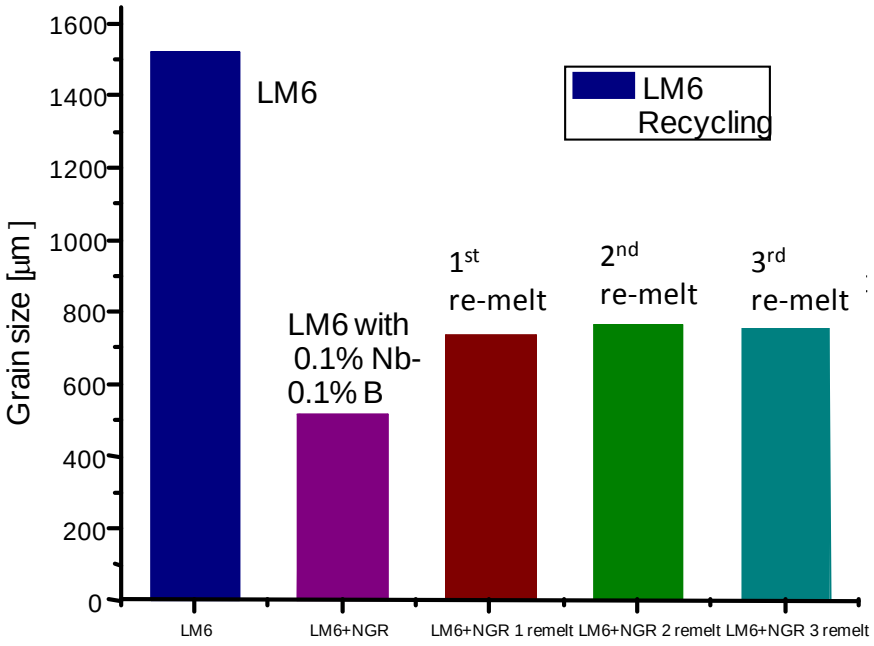

Figure 7.23 The recycling of LM6 with the addition of 0.1 wt% Nb -0.1wt% B. The samples were melted at 800 °C and cast into the steel mould, preheated to 200 °C.

The grain sizes are smaller after first casting then slightly increased after the first re-melt. The second and third re-melt have still show positive grain refinement sign. The nucleation sites are still active in the melt which will be beneficial for the recycling of the alloys after Nb-B grain refiner addition. It is possible to obtain smaller grains with additional levels of Nb and B to the melt and this study will be important from an industrial application view point.

7.7 Conclusion

The master alloy development presented in this chapter has shown that it is very difficult to optimize the suitable composition of Nb and B. The alloys with higher concentration of alloying elements need excess of boron to form NbB_2. The TEM and SEM analyses conform that in the master alloy there are potentional nucleation sites of Al_2Nb, Al_3Nb or NbB_2. The experiments conform that stirring has influence on faster particles dissolution into the melt. In addition the recycling properties of LM6 alloy with Nb-B master alloy is possible.

Chapter 8. Conclusion and Future work

8.1. Outline

This thesis describes the development of a novel grain refiner for Al alloys. The grain refiner comprises of Niobium and Boron elements. The combination of these two chemicals had previously never been used in testing the grain refinement characteristics of aluminium alloys. Chapter 4 describes the progressive development of an effective grain refiner, and in Chapter 5 the influence of the Nb-B grain refiner on grain size of Al-Si alloys is presented in detail. Mechanical properties and other microstructural features are highlighted in Chapter 6. Development of a practical method of introducing the Nb-B chemicals into liquid metal, via synthesising the Al-Nb-B master alloy, is described in Chapter 7.

8.2. Conclusions

8.2.1. Development

As described in Chapter 2, solid particles in liquid metal reduce the energy barrier during the solidification process. A crystallographic phase with good lattice matching with that of α-Al will have a lower wetting angle which has the effect of reducing the energy barrier for the formation of heterogeneous nucleation. As a result of heterogeneous nucleation, a finer grain structure can be obtained. It is known that a good heterogeneous nucleation site need to have good lattice matching with α-Al, a higher melting temperature than α-Al and phase stability of liquid Al. The research confirms that refractory alloys like Mo, Nb, Ta and W have potential to be grains refiners. However the newly developed Nb-B grain refiner with appropriate chemical concentration and conditions could be a competitor for the well known Ti-B grain refiner. The research results presented here could have a significant input to solidification science. The thermal analysis of cooling curves confirms that Al_3Nb or NbB_2 are potential heterogeneous nucleation sites as the undercooling of the melt is reduced when the Nb-B grain refiner is added. The TEM and SEM analyses describe the potential nucleation sites. Nevertheless, the phase or the mechanism responsible for grain refinement is yet to be identified.

Although it is demonstrated that Nb-B is a potential grain refiner for commercial pure Al or dilute alloys, the research in this thesis is concentrated on Al-Si alloys as the titanium based master alloy addition to Al-Si alloys is not effective in higher silicon concentration because of the poisoning effect. The titanium is consumed by silicon and forms Ti-Si silicides. The phase diagram analysis show that Nb silicides form at much higher temperatures than Ti silicides. Based on this phase diagram analysis, the Nb-B grain refiner will be highly effective for refining Al-Si alloys grain size and we confirmed the same through extensive experimental work. The Chapter 5 shows the comparison of microstructures and grain sizes of Al-Si alloys without any addition, with commercially known Al-5Ti-B and with Nb-B addition. The results achieved and described in this chapter are outstanding and exciting. The α-Al grains are refined in Al-Si alloys with the use of Nb-B addition even in higher silicon concentration. It is shown that with higher concentration of silicon the α-Al grains are larger without any addition and with Al-5Ti-B addition. The grain sizes are almost constant as a function of Si content and the overall grain size is decreased by 80% as shown in Chapter 5 (Figure 5.5). The Nb-B is chemically stable with alloying elements and the grain refinement is still noticeable in commercial alloys. We have shown that Nb-B is highly effective for commercial Al-Si alloys such as LM6, LM25 or LM24. The experiments also confirm that the Nb-B addition is very effective at a wide range of cooling rates (0.03 °C/s to 100 °C/s) that take place in various practical casting processes. Different moulds were used to achieve different cooling rates. The major discovery in this thesis is that the grain refiner is very effective in very slow cooling rates of about 0.03 °C/s. This research shows that for the first time we can chemically refine the α-Al grains of high silicon containing Al alloys under cooling conditions provided by the sand casting process. The grain sizes are less sensitive to the cooling rates. This discovery is very significant for utilization in industry especially in casting Al-Si engine blocks or large single component structures with various thicknesses.

The hyper-eutectic Al-Si alloys were also refined by Nb-B. The outstanding result was noticed in Al-14 Si with Nb-B addition. The primary silicon and eutectic size was significantly reduced.

The new master alloy was produced to facilitate the practical addition of Nb-B to the melt. The Al-Nb-B master alloy is simply highly concentrated NbB_2 and Al_3Nb phases in Al matrix. Different molar ratios were used to optimize the ideal composition of the master alloy. Initial

results suggest that a Nb:B weight ratio of 1:1 is desirable to produce refined Al-Si alloys. It is suggested that the presence of excess boron is needed to form NbB_2. The experiments also suggest that the presence of the NbB_2 phase in the liquid metal is essential for enhancing the grain refinement and the potential nucleation site would be NbB_2 for the grain refinement of α-Al containing Si as a solid solution.

Fading studies show that the particles are recovering in the melt after mixing the metal. The dissolution studies presented in Chapter 6 prove that the Al_3Nb or NbB_2 particles are stable in the melt and have longer dissolution rate if they are not disturbed. Experimental simulation of recycling of scrap show that after several re-melts of the grain refined Al-Si alloys with Nb-B, grain refinement is still observed to take place. It means that the nucleation sites of Al_3Nb or NbB_2 are stable in the material and further addition of the grain refiner is not necessary.

8.2.2. Improving the properties of the Al-Si Alloys

It is well known that fine grain structure will have better mechanical properties. The LM6, LM25, LM24 alloys were analysed. The different moulds with different cooling rates were used to produce the tensile bars. Also the HPDC (High Pressure Die Casting) was used to achieve a very fast cooling rate. The results show that the tensile strength and elongation of Al-Si alloys are improved with use of Nb-B grain refiner. The data of pure samples (i.e; without additiom) was compared with real data provided by the casting company (Norton Aluminium) and the results were very similar.

Mechanical properties of the aluminium alloys are strongly dependent on the effect of dendrite arm spacing (DAS). As it is known with smaller DAS the mechanical properties of Al-Si alloys should be improved. The analyses of DAS confirm that for alloys with smaller DAS the elongation is significantly better in Al-Si alloys with Nb-B addition. Intermetallic particles are smaller in samples with Nb-B addition. Reduced macro porosity is noticeable in alloys with the addition of Nb-B. This reduced porosity could be due to KBF_4 salt addition; however with the usage of Al-Nb-B master alloy the fraction of porosity is still lower, also the shrinkage porosity is minimized. Vickers hardness was improved for the alloys with Nb-B addition.

Based on the findings in this thesis, the Nb-B grain refiner can have a positive influence on casting and the automotive industry. The majority of aluminium and magnesium alloy component manufacturers currently produce a limited range of components, but without grain

refinement, since there are no known commercially viable grain refiners. The Nb-B grain refiner offers the end user the various benefits. The Nb-B grain refiner:

- enables castings to have fine uniform grain structure, fine eutectic structure, fine intermetallics and reduced defects.
- is potentially applicable to castings produced at a wide range of cooling rates. The industry can apply this method in various processes such as investment casting, high pressure die casting, low pressure die casting, permanent mould casting and sand castings.
- improves castability of a wide range of aluminium alloys.
- eliminates hot-tearing, a common problem in castings.
- improves much needed tensile strength and ductility.
- improves homogeneity in mechanical properties across the component.
- has the potential to tolerate high impurity levels of Fe and Si. (aluminium scrap can now be manufactured with superior properties).

Additionally, it is expected to:

- enable the casting of large structures using sand moulds.
- reduce the rejection rate during manufacture of high value components. Current reject rate ranges from 20-40% for high value castings for structural applications. Considering that the measured porosity in BGR is negligible (<0.02%), the reject ratio is expected to be very significantly reduced.

8.3. Suggestions for future work

The thesis presents the development of a novel grain refiner that is highly effective for Al-Si cast alloys. However, there is little understanding on the underlying mechanisms of grain refinement with the addition of Nb-B to Al-Si alloys. The potential chemical phases that are responsible for the observed grain refinement could be NbB_2 and Al_3Nb. Focus on understanding the nucleation mechanism that is operative during the solidification process of Al-Si alloys containing Nb and B would be highly valuable for further improving the

efficiency of the grain refiner. In order to establish orientation relationships between (i) Al_3Nb and α-Al (ii) NbB_2 and α-Al and (iii) Al_3Nb and NbB_2, investigation of interface between these phases using high resolution TEM is vital. The analysis of the nucleation sites present in the grain refined Al-Si samples are also to be investigated.

The following future experimental work is important from a practical view point to enable application of Nb-B in foundries.

- Further optimization of the master alloy process and its composition.
- The optimization of the master alloy addition method to the Al-Si alloys.
- Develop trials with potential commercial master alloy producers.
- Testing of the Nb-B grain refiner in the industrial environment should be performed for different alloys and in different processing methods (investment casting, high pressure die casting, low pressure die casting, permanent mould casting and sand castings).
- Since Nb-B addition reduces the intermetallic particle size significantly, this will enable more impure elements in Al scrap such as Fe and Si to be tolerated. Demonstrate the applicability of the Nb-B grain refiner to the recycling of aluminium casting scrap.
- Extend development work to explore related alloy systems e.g. magnesium, titanium and nickel
- In addition to laboratory produced grain size, porosity, and mechanical property measurements, end users require additional physical property data. These measurements include fatigue, creep, thermal conductivity, coefficient of thermal expansion, high temperature mechanical properties and corrosion properties.

References

Arjuna Rao A., Murty B.S., Chakraborty M., Metall. Trans. (1996): 791.

Arnberg L., Bäckerud L., Klang H., Met.Technol. 9 (1982).

Ashby M.F., Jones D.R.H., Engineering Materials 2. Pergamon, 1994.

Bäckerud L., Chai G., Tamminem J., Solidification Characterisitics of Aluminium Alloys. Vol. 2. Des Plaines, IL, USA: American Foundry Society Inc., 1990.

Bäckerud L., Gustafson P., Johnsson M., Aluminium 67 (1991): 910.

Bamberger M., Weiss B.Z., Stupel M.M., Materials Science and Technology (1987): 49-56.

Battle T.P., Int. Mat. Rev. 37 (1992): 249.

Becker R., Doring W., Ann. Phys 24 (1935): 719.

Bell J.A.E., and Winegard W.C., J. Inst. Met. 93 (1963): 357-359.

Bewlay B.P., Lipsiy H.A., Jackson M.R., Reeder W.J., Sutliff J.A., Mater. Sci. Eng. (1995): 534-543.

Bramfitt B.L., Metallurgical and Materials Transactions (1970): 2958 .

Brauer G., Anorg Z., Chem. (1939): 242.

Bunn A.M., Grain refinement in aluminium alloys. Vol. PhD Thesis. University of Cambridge, 1998.

Bunn A.M., Schumacher P., Kearns M.A., Boothroyd C.B., Greer A.L., Mater. Sci. Technol. 15 (1999): 1115-1123.

Burke J.E. and Turnbull D., Progress in Metal Physics (1952): 220-244.

Campbell F.C., Elements of Metallurgy and Engineering Alloys. ASM International, 2003.

Campbell John G. Cosworth Research & Development. Patent US 4693292. September 1987.

Cantor B., "Microstructure development during rapid solidification ." Proceedings of the 22nd Risø International Symposium on Materials Science: Science of Metastable and Nanocrystalline Alloy Structure, Properties and Modelling. 2001. 483–493.

Ceylan M., Aksoy I., Kuzuzu V., Balo N., J. of Materials Processing Technology 65 (1997): 41-51.

Christian J.W., The Theory of Transformations in Metals and Alloys. Pergamon, 1965.

Cibula A., J. Inst. Metals 76 (1949-1950): 321.

Clyne T.W., Robert M.H., Metals Technology (1980): 177-185.

Cornish A.J., Met.Sci 9 (1975): 477-484.

Dahle A.K., Nogita K., Zindel J.W., Mcdonald S.D., Hogan L.M., Metal. Mater. Trans. 32A (2001): 949.

Davies G.J., Solidification and Casting. London: Applied Science Publishers LTD, 1973.

Day M.G., Hellawell A., J. Inst. Met. 95 (1967): 337.

Degarmo, Paul E, Black, Kohser, Ronald A., Materials and Processes in Manufacturing . Wiley, 2003.

Delamore G.W. and Smith R.W., Metall. Trans. 2 (1971): 1733-1738.

Di Sabatino M., Shankar M., Apelian D., Arnberg L., "Shape Casting: The Jhon Campbell Symposium." TMS. San Francisco: TMS, 2005. 193-202.

Easton M., Davidson C., St John D., Metall. and Mater. Trans. (2010): 1528-1538.

Easton M., StJohn D., Metall. Mater. Trans 30A (1999): 1613.

Easton M.A., StJohn D.H., Materials Science and Engineering 486 (2008): 8-13.

Flemings M.C., Solidification Procedings. New York, London, Sydney: McGraw-Hill Book Co., 1974.

Frank F.C. and Van der Merwe J.H., Proce. Roy. Soc. (1949): 205-225.

Gayler M.L.V., J. Inst. Met. 10 (1927): 157.

Glicksman M.E., Koss M.B., Phys. Rev. Let. 73(4) (1994): 573-576.

Granger D.A., Light Metals 1998 (1998): 991-52.

Greer A.L., Bunn A.M., Tronche A., Evans P.V., Bristow D.J, Acta Mater. 48 (2000): 2823-35.

Gruzelski J.E. and Closset B.M., "The Treatment of Liquid Aluminium-Silicon Alloys." American Foundarymen's Society. Illinois, 1990. 19.

Guo E. and Ma F., Superalloys (1980): 431-438.

Guzowski M.M., Sigworth G.K., Sentner D.A., Metal. Trans. 18A (1987): 603-619.

Hanna M.D., Lu S.Z., Hellawell A., Metall. Trans 15A (1984)459.

Hellawell A. and Herbert P.M., Proc.Roy.Soc. 269 (1962): 560.

Hellawell A., Prog. Mater. Sci 15 (1968): 3.

Hollman J.H.and Turnbull D., Progress Met. Physics 4 (1953): 333.

Hunt J.D., Mat. Sci. Eng. 65 (1984): 75.

Jackson K.A, Hunt J.P., Acta Met. 13 (1965): 1212.

Johnsson M., Z.Metallk 85 (1994): 781.

Johnsson M. and Bäckerud L., Z. Metallk. 87 (1996): 216-220.

Johnsson M., Bäckerud I., Sigworth G.K., Metall. Trans. A 24A (1993): 481-491.

Johnsson M., Bäckerud L., Z.Metallkd. 83 (1992): 774-780.

Johnsson M., Jansson K., Metall.Trans. 89 (1998): 394-398.

Jones G.P and Pearson J., Metall. Trans. (1976): 223.

Jones G.P., Solidification processing. London: The Institute of Metals, 1987.

Jones H., Mater. Lett 26 (1996): 133-136.

Kaptay G., Kuznetsov S.A., Plasmas & Ions (1999): 45-56.

Kearns M.A., Thistlewaite S.R., Cooper P.S., Light Metals 1996. Warrendale P.A.: TMS, 1996.

Kobayashi K., Shingu P.H., Ozaki R., Scripta Mater 10 (1976): 525.

Laio H., Sun G.,. Mater. Sci. Technol. 20 (2004): 521.

Lo K., Bevk J.,Turnbull D., J. of Applied Physics 48 (1977): 2597.

Lu S., Hellawell A., Metall. Trans. A18 (1987): 1721-1733.

Man H., Fan Z., Acta Mater. 59 .2011 (2010): 2704-2712.

Marcantonio J.A., Mondolfo L.F., Metall.Trans. 2 (1971): 465-71.

Maxwell I., Hellawell A., Acta Metal. 23 (1975): 229.

Mayes C.D., MaCartney D.G., Tatlock J., Mater. Sci.Technol. 9 (1993): 97.

McCartney D.G., Int .Mater. Rev. 34 (1989): 247.

McDonald S.D., Eutectic solidification and porosity formation in unmodified and modified hypoeutectic aluminium-silicon alloys. PhD Thesis. Brisbane: The University of Queensland, 2002.

Mendiratta M.G., Dimiduk D.M., Scripta Metall. Mater. 25 (1991): 237-242.

Mihaichuk W., Modern casting (1981): 39.

Mohanty P.S., Gruzelski J.E., Acta Metall. Mater. 43 (1995): 2001-12.

Mohanty P.S., Samuel F.H., Gruzelski J.E., Acta Metall. Trans. B 26B (1995): 103-10.

Mohanty P.S., Samuel F.H., Gruzelski J.E., Kosto T.J., Light metals U.Manweiler ed.TMS (1994): 1039-45.

Mondolfo F., Aluminium Alloys: Structure and Properties. Boston: Butterworths, 1976.

Morris L.R, Winegard W.C., J. Crystal Growth 1 (1967): 245.

Munitz A., Gokhale A.B., Abbaschian R., Journal of Materials Science 35 (2000): 2263-2271.

Murray J.L., Binary Alloys Phase Diagrams second edition. Materials Park OH: ASM International, 1990.

Murty B.S, Kori S.A, Chakraborty M., International Materials Reviews 47 (2002).

Norman F., Prangnell B., Mcewen S.R., Acta Mater 46 (1998): 5715.

Okabayashi K., Nakatani Y., Notani H., Jpn. Inst. Light Metals 14 (1964): 415.

Oscar Frech GmbH., Operating instruction. Schorndorf: Frech, 2010.

Pearson J., Kearns M.A., "Aluminium Cast House Tech- nology: Theory & Practice." Gold Coast, Australia: 5th Australio-Asian Pacific Conf., 1997. 74.

Polmear I.J., Light Alloys. London: Arnold Press, 1995.

Pontes P.S., De Galiza J.A., Robert M.H., Cupini N.L., Mech. Eng. Thesis. Brazil: State University of Campinas, 1979.

Porter D.A., Easterling K.E., Phase Transformations in Metals and Alloys,. Van Nostrand Reinhold Co.Ltd, 1981.

Quested T.E. and Greer A.L. Acta Mater. 53 (2005): 4643-4653.

Quested T.E., Dinsdale A.T., Greer A.L., Materials Science and Technology 22 (2006): 1126.

Ravi M., Pillai U.T.S, Pai B.C., Damodran A.D., Dwarakadas E.S., Metal. Trans. 27A (1996): 1283.

Rooy E.L., "Elements of Metallurgy and Engineering Alloys." F.C., Campbell. ASM International, 2003.

Rooy E.R., "Metals handbook." Casting ASM International. Ed. ASM International Hanbook Committe. 1989. 743-70.

Schaffer P.L., Dahle A.K., and Zindel W., Light Metals 2004. Warrendale, PA: TMS, 2001.

Schumacher P. and Greer A.L., "Light Metals,." Ed. J. Evans ed TMS. Warrendale, PA, 1995. 869-77.

Schumacher P., Greer A.L., Mater. Sci. Eng. A181-182 (1994): 1335-39.

Schumacher P., Greer A.L., WorthJ., Evans P.V., Kearns M.A., Fisher P., Green A.H., Material Science Technology 14 (1998): 394-404.

Seifert H.J, Lukas H.L., Petzow G., Z. Metallkde 87 (1996): 2-13.

Shein R., Ivanovskii A.L., J. Phys. Condens Matter 20 (2008): 415218-9.

Shlesinger M.E., Okamoto H., Gokhale A.B., Abbashian R., Phase Equilib. 14 (1993): 502.

Sigworth G.K and Guzowski M.M., AFS Trans 93 (1985): 907.

Sigworth G.K,. Met. Trans. 15.A (1989): 277-282.

Slama G. and Vignes A., J. Less Common Metals 23 (1971): 375-393.

Spittle J.A., Keeble J.M., The Grain Refinement of Al-Si foundry alloys. Meshedani M,A.,: Light Met., 1997.

Sritharan T. and Li H., Mater. Process. Technol. 83 (1997): 585.

Suarez M.A., Alvarez O., Alvarez M.A., Journal of Alloys and Compounds, 492 (2010): 373-377.

Takeuchi T., Kosuge M., Banno N.,Kikuchi A.,Iijima Y., Superconductor Science Technology 18 (2005): 985.

Taylor, J. A.,"The effect of iron in Al-Si Casting Alloys." 35th Australian Foundry Institute National Conference. Adelaide, South Australia, 2004. 148-157.

Tiller W.A., Rutter J.W., Jackson K.A., Chalmers B., Acta Met. 1 (1953): 428.

Triverdi R., Kurz W., Int. Mat. Rev. 39 (1994): 129.

Turnbull D., J.Chem.Phys 18 (1950): 198.

Turnbull D., Fisher J.C., Jurnal of Chemical Physis 17.71 (1948): 71-73.

Tzamtzis S., "Solidification Behaviour and Mechanical Properties of Cast Mg-alloys and Al-based Particulate Metal Matrix Composites Under Intensive Shearing." PhD Thesis. 2011.

Wang L., Bian X., Mater. Sci. Techn 16 (2000): 517.

Wang L., Makhlouf M., Apelian D., Int. Mater. Rev. 40 (1995): 221.

Wang X., J.Alloys Compd. 403 (2005): 283.

Winkelman G.B., Chen Z.W., StJhon D.H., Jahedi M.Z., J. Mater. Sci. 39 (2004): 519.

Woodruff D.P., The solid liquid interface. London: Cambridge University Press, 1973.

Ye B.J., Loper C.R., Lu D.Y., Kang C.S., AFS Trans (1985): 533.

Yeremenko V.N., Natanzon Ya.V., Dybkov V.I., Journal of Materials Science 16 (1981): 1748-1756.

Yeremenko V.N., Natanzon Ya.V., Dybkov V.I., Journal of Less Common Metals 50 (1976): 29-48.

Young D.K., "Light metals." TMS, 1991. 1115.

Zhao J.C., Bewlay B.P., Jackson M.R., Peluso L.A.,in: Hemker K., Dimiduk D.M., Clemens H., Darolia R., Inui H., Larsen J.M, Sikka V.K., Thomas M., Whittenberger J.D., "Light Metals." TMS. Warrendale PA, 2001. 483-491.

Zhao J.C., Jackson M.R., Peluso L.A., Materials Science and Engineering A372 (2004): 21-27.